LNGS - s.s. 17 bis km 18,910 67010 ASSERGI (AQ) ITALY
tel.+39 0862 4371 fax +39 0862 437559
email: document@lngs.infn.it
http://www.lngs.infn.it

ANNUAL REPORT 2012

LNGS/EXP-01/13
June 2013

INFN

Annual Report 2012

Laboratori Nazionali del Gran Sasso

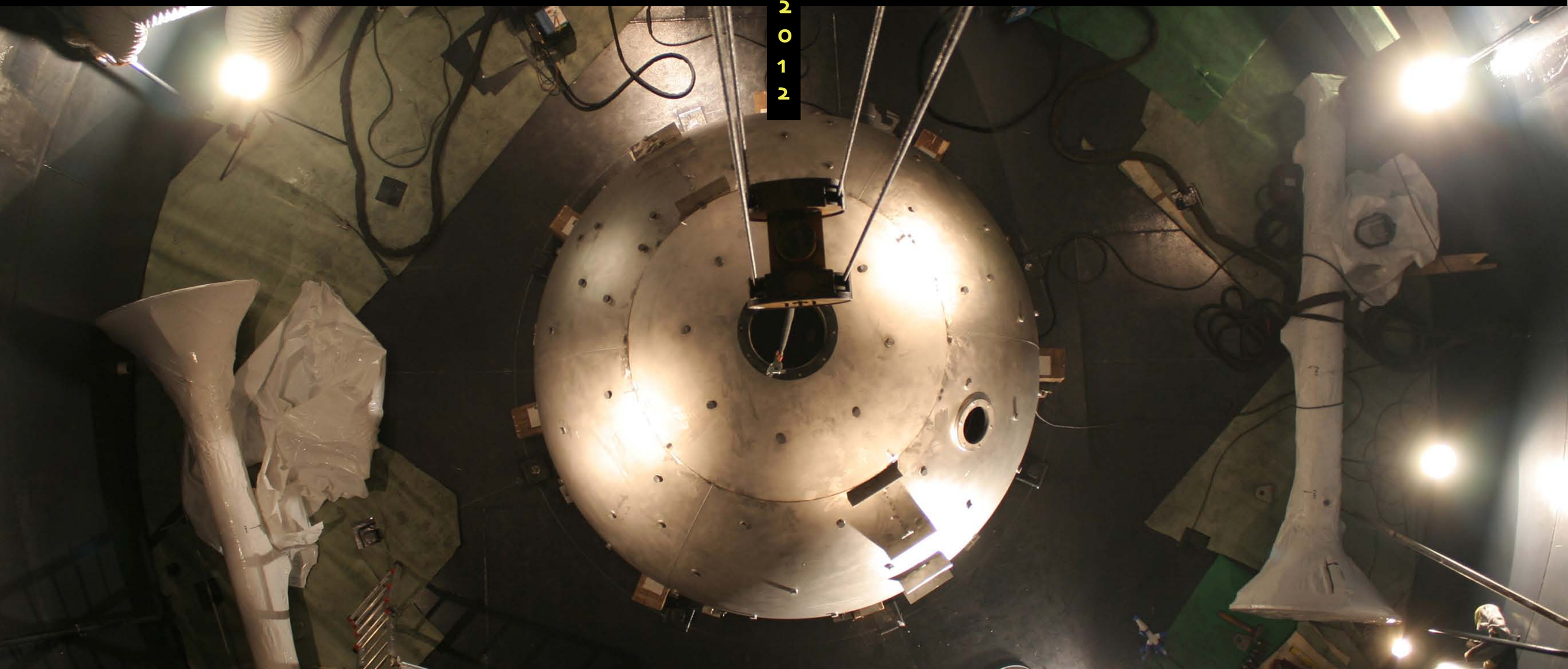

Codice ISBN
ISBN-978-88-907304-9-8

Annual Report 2012

LNGS Director — Prof. Stefano Ragazzi

Editor — Dr. Roberta Antolini

Technical Assistants — Dr. Adriano Di Giovanni
Mr. Marco Galeota

LNGS/EXP-01/13
June 2013

INFN

Laboratori Nazionali del Gran Sasso

Annual Report 2012

Contents

THE BOREXINO EXPERIMENT

The Borexino collaboration

G. Bellini[h], J. Benziger[k], D. Bick[s], G. Bonfini[e], D. Bravo[q], A. Brigatti[h], M. Buizza Avanzini[h], B. Caccianiga[h], L. Cadonati[p], F. Calaprice[l], M. Cariello[c], P. Cavalcante[e], A. Chavarria[l], A. Chepurnov[r], D. D'Angelo[h], S. Davini[c], A. Derbin[m], G. Di Pietro[e], A. Etenko[g], K. Fomenko[b,e], D. Franco[a], F. Gabriele[l], C. Galbiati[l], S. Gazzana[e], C. Ghiano[a,e], M. Giammarchi[h], M. Göger-Neff[n], A. Goretti[l], L. Grandi[l], S. Hardy[q], Aldo Ianni[e], Andrea Ianni[l], V. Kobychev[f], D. Korablev[b], G. Korga[e], Y. Koshio[e], D. Kryn[a], M. Laubenstein[e], T. Lewke[n], E. Litvinovich[g], B. Loer[l], F. Lombardi[e], P. Lombardi[h], L. Ludhova[h], I. Machulin[g], S. Manecki[q], W. Maneschg[i], G. Manuzio[c], Q. Meindl[n], E. Meroni[h], L. Miramonti[h], M. Misiaszek[d], D. Montanari[e,l], P. Mosteiro[l], V. Muratova[m], L. Oberauer[n], M. Obolensky[a], M. Orsini[e], F. Ortica[j], K. Otis[p], M. Pallavicini[c], L. Papp[e,q], S. Parmeggiano[h], L. Perasso[h], S. Perasso[c], A. Pocar[p], G. Ranucci[h], A. Razeto[e], A. Re[h], A. Romani[j], N. Rossi[e], A. Sabelnikov[g], R. Saldanha[l], P. Saggese[h], C. Salvo[c], S. Schönert[i,n], H. Simgen[i], M. Skorokhvatov[g], O. Smirnov[b], A. Sotnikov[b], S. Sukhotin[g], Y. Suvorov[e,g], R. Tartaglia[e], G. Testera[c], D. Vignaud[a], R.B. Vogelaar[q], F. von Feilitzsch[n], J. Winter[n], M. Wojcik[d], A. Wright[l], M. Wurm[n], J. Xu[l], O. Zaimidoroga[b], S. Zavatarelli[c], and G. Zuzel[i,d]

[a] Laboratoire AstroParticule et Cosmologie, 75231 Paris cedex 13, France
[b] Joint Institute for Nuclear Research, Dubna 141980, Russia
[c] Dipartimento di Fisica, Università e INFN, Genova 16146, Italy
[d] M. Smoluchowski Institute of Physics, Jagellonian University, Krakow, 30059, Poland
[e] INFN Laboratori Nazionali del Gran Sasso, Assergi 67010, Italy
[f] Kiev Institute for Nuclear Research, Kiev 06380, Ukraine
[g] NRC Kurchatov Institute, Moscow 123182, Russia
[h] Dipartimento di Fisica, Università degli Studi e INFN, Milano 20133, Italy
[i] Max-Plank-Institut für Kernphysik, Heidelberg 69029, Germany
[j] Dipartimento di Chimica, Università e INFN, Perugia 06123, Italy
[k] Chemical Engineering Department, Princeton University, Princeton, NJ 08544, USA
[l] Physics Department, Princeton University, Princeton, NJ 08544, USA
[m] St. Petersburg Nuclear Physics Institute, Gatchina 188350, Russia
[n] Physik Department, Technische Universität München, Garching 85747, Germany
[o] Instituto de Fìsica Corpuscular, Aptdo. 22085, Valencia E-46071, España
[p] Physics Department, University of Massachusetts, Amherst MA 01003, USA
[q] Physics Department, Virginia Polytechnic Institute and State University, Blacksburg, VA 24061, USA
[r] Institute of Nuclear Physics, Lomonosov Moscow State University, 119899, Moscow, Russia
[s] Institut für Experimentalphysik, Universität Hamburg, Germany

Abstract

Borexino is a large liquid scintillator detector located under the Gran Sasso mountain. The main goal of the experiment is the study of solar neutrinos, in particular those coming from the so-called ^{7}Be reaction. The exceptionally high levels of radiopurity of the scintillator have made it possible to accomplish not only its primary goal, but also produce a number of other significant results. Among these, we are going to discuss those published in 2012, regarding, in particular, the study of the Day/Night rate of ^{7}Be neutrinos, the first observation of pep neutrinos, the limits on solar axions, the measurement of the speed of ν_μ's from the CNGS beam, the study of seasonal modulations of the cosmic muon flux and the description of the Borexino calibration system.

1 Introduction

Neutrinos from the Sun have been studied by several experiments in the past 40 years. These studies have led to the discovery of solar neutrino oscillations and to the determination of the oscillation parameters $\Delta m^2_{12} = 7.6 \cdot 10^{-5}\text{eV}^2$ and $\sin^2 2\theta_{12} = 0.87$ [1]. However, the investigation of the solar neutrino spectrum is far from being complete, especially in the energy region below 1 MeV where experiments can be severely affected by background due to natural radioactivity. The Borexino experiment has been specifically designed to study the low energy solar neutrinos, in particular those coming from the so-called ^{7}Be reaction. The success of Borexino comes as a result of a 15-year long R& D study carried out by the collaboration to develop the best techniques of purification to reach the required levels of radiopurity.

2 The Borexino detector

The Borexino detector is located under the Gran Sasso mountain in the Laboratori Nazionali del Gran Sasso, Italy. It detects solar neutrinos via their elastic scattering on the electrons of 300 tons of liquid scintillator. The scintillator (PC + 1.5 g/l of PPO) is contained in a large spherical nylon vessel (R=4.25m). The scintillation light is viewed by 2214 photomultiplier tubes mounted on a Stainless Steel Sphere (SSS) concentric with the vessel at a radius of 6.85 m (see Fig. 1). In order to reduce external background, the design of Borexino is based on the principle of graded shielding, with the inner core scintillator at the center of a set of concentric shells of increasing radiopurity. Besides keeping external backgrounds at a low level, the key requirement for measuring low energy neutrinos with Borexino is the exceptional radiopurity of the scintillator itself. Based on extensive R&D studies, the Borexino collaboration developed a successful purification strategy which proved to be effective in removing the most dangerous contaminants from the scintillator. In particular, the contamination due to ^{238}U and ^{232}Th was brought to the unprecedented levels of $(1.6 \pm 0.1)\ 10^{-17}$g/g and $(6.8 \pm 1.5)\ 10^{-18}$g/g, respectively, one order of magnitude better than the designed goal of 10^{-16}g/g. The Inner Detector (ID) described above is contained in a tank filled with 2000 m^3 of ultra-pure water which provides further shielding from background from the rocks and also acts as a Cerenkov

muon detector (Outer Detector, OD) to tag residual cosmic muons. For more details concerning the Borexino detector see [3], [4].

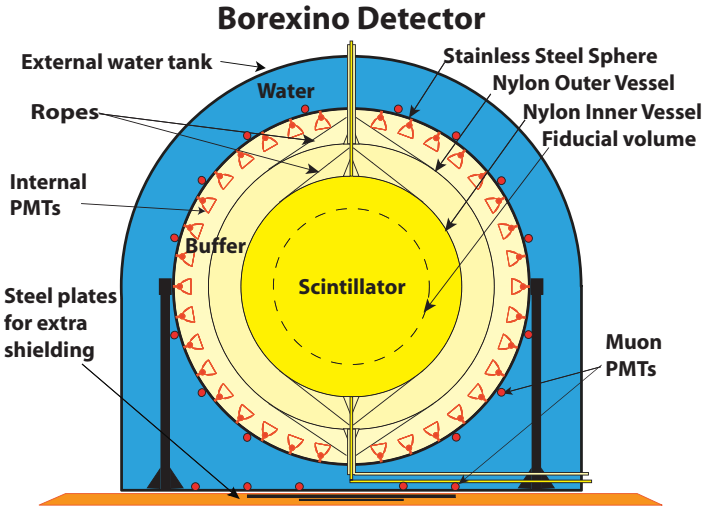

Figure 1: Schematic view of the Borexino detector

3 Status of the project

The Borexino experiment started taking data in 2007. Since then, it has produced a considerable amount of results which include the precision measurement of the ^{7}Be solar neutrino rate (with a total error of less than 5% [2]), which was the primary goal for which it had been built. It also performed the measurement of the ^{8}B solar neutrino rate with an unprecedented low energy threshold [10]. Borexino has also published significant results on non-solar neutrino physics, such as the first observation of anti-neutrinos from the Earth [11] and several limits on rare or forbidden processes [12], [13]. These important results have been discussed in previous reports and won't be adressed here. In this report we are going to focus on the articles published in year 2012.

3.1 Absence of a day-night asymmetry of the ^{7}Be neutrinos

The high precision measurement of the ^{7}Be neutrino rate has been followed by a precision study of its day rate versus its night rate. For oscillation parameter values typical of the so-called Large Mixing Angle solution there should be no measurable asymmetry (<0.1%) between the rate during day and during night, while in other regions of the oscillation parameters space, such as the so-called LOW region, there would be a significant asymmetry (between 10% and 80%) due to coherent regeneration of ν_e's as they cross the Earth.

Fig. 2 shows the energy spectrum obtained during days (red curve) superimposed to the one obtained during nights (black curve) normalized to the same experimental

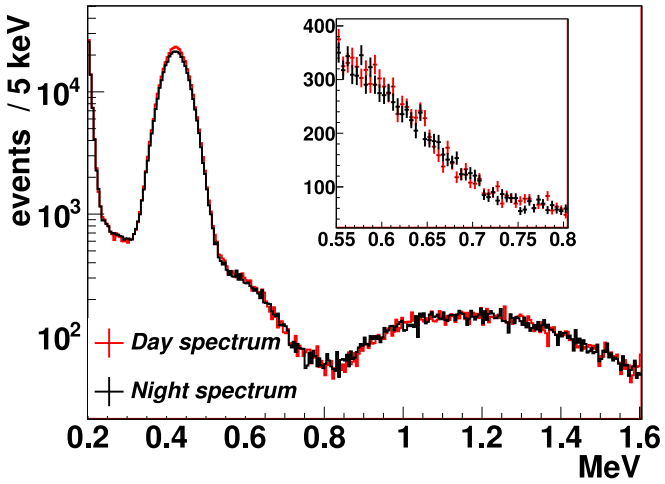

Figure 2: Event spectrum during day (red curve) and during night (black curve) normalized to the same live time. The spectrum is obtained by applying the same cuts of the standard ^{7}Be analysis, except for the Fiducial Volume which is bigger than the standard one.

live-time. In order to extract the day-night asymmetry we subtract the day spectrum from the night one and fit the difference as the sum of a constant + ^{7}Be, assuming that backgrounds are constant between day and night. The fit shows no excess of ^{7}Be signal during night which yields to a day-night asymmetry consistent with zero within errors, $A_{dn} = 0.001 \pm 0.0012(\text{stat}) \pm 0.007(\text{sys})$. This tight contraint confirms the LMA solution based on solar data only and allows to reject at more than 8.5 σ the LOW region of oscillation parameter space. This result is also potentially sensitive to new physics affecting low energy electron neutrino interaction. As an example, we are able of excluding at more than 10 σ the set of parameters chosen in [9] for the mass varying neutrino oscillation scenario.

3.2 First observation of pep neutrinos

The main result published by Borexino in 2012 concerns the first observation of neutrinos from the pep reaction. These neutrinos belong to the pp-cycle and are monocromatic (E=1.44 MeV). They have never been observed directly before, given their tiny flux and low energy. Borexino has been able to observe for the first time this class of neutrinos, thanks to its exceptional radiopurity and to its capability to exploit new analysis techniques to reject the main residual background: the cosmogenic ^{11}C. The *Three-Fold-Coincidence* (TFC) technique exploits the fact that in at least 95% of the cases the cosmic muon which produces ^{11}C by spallation in the scintillator also produces a neutron. This makes it possible to correlate in space and time the muon signal, the neutron capture gamma signal and the positron emitted as ^{11}C decays (with a half-life of 20 minutes). The TFC technique is very effective in removing ^{11}C as can be seen in Fig. 3 (upper

panel). The second technique exploits the difference in the emitted photon time distribution in case of an electron (from the scattering of neutrinos, i.e., the signal) and a positron (from the decay of ^{11}C, i.e., the background). By combining the discriminating power of these two techniques and also other information, like the spectral shape and the radial distribution of events into a multivariate analysis fit, it was possible to extract for the first time a measurement of the pep rate:

$$\text{Rate}\,(\text{pep}) = 3.1 \pm 0.6(\text{stat}) \pm 0.3(\text{sys})\ \text{counts/day} \cdot 100\ \text{tons}$$

From this analysis it was also possible to obtain the strongest constraint to date on the CNO flux

$$\text{Rate}\,(\text{CNO}) < 7.9\ \text{counts/day} \cdot 100\ \text{tons}\ (95\%\text{C.L.})$$

The Borexino results on solar neutrinos have been important to probe the ν_e survival probability P_{ee} at different energies (Fig. 4). In particular Borexino is the only experiment which has been able of probing solar neutrino oscillations both in the vacuum dominated region (low energies) and in the matter dominated region (high energies).

More details on the pep analysis and results can be found in [17].

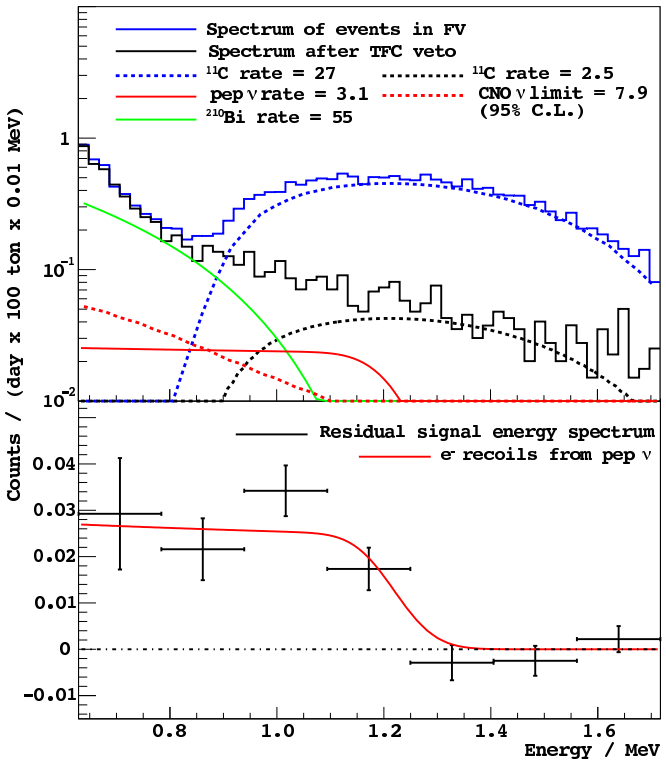

Figure 3: Top: energy spectra of the events in the FV (blue line) before and after the TFC veto is applied (black line). Bottom: residual energy spectrum after best-fit rates of all considered backgrounds are subtracted. The e^- recoil spectrum from scattering with pep-ν at the best-fit rate is superimposed (red line).

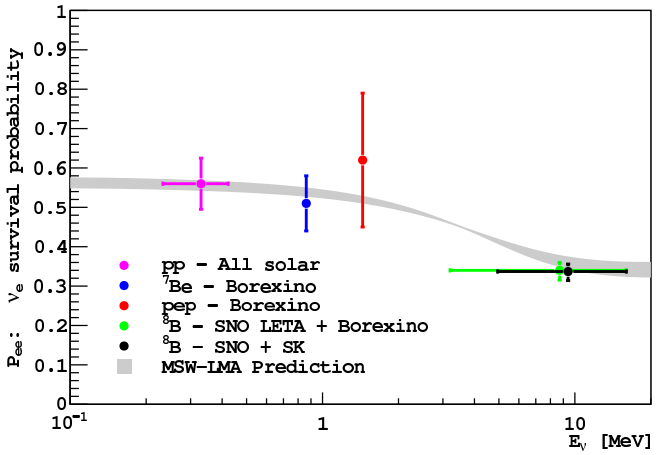

Figure 4: Survival ν_e probability P_{ee} as a function of energy for the current best-fit oscillation parameters [1] allowed to vary within 1σ band (grey band). The blu, red and green points represent the Borexino results on ^{7}Be, pep and ^{8}B neutrino rate, respectively, assuming the solar fluxes from the high-metallicity hypothesis ([8]). The purple point is the result obtained for pp neutrinos combining Borexino and all other solar neutrino experiments.

3.3 Velocity of ν_μ neutrinos from CNGS

Borexino is located in Hall C, next to the OPERA experiment. It is therefore in the best position to verify the anomaly in the time-of-flight measurement for neutrinos from the CNGS beam claimed by OPERA in September 2011 that pointed towards a superluminous velocity [14]. The ν_μ's from the CNGS beam have an average energy of 17 GeV/c and travel 730 Km from CERN to Gran Sasso with one of the highest relativistic γ factors ever produced artificially (given the low neutrino mass, in fact, γ is $> 10^{11}$). Even though the claim by OPERA has been more recently withdrawn (see [15]), a test of Special Relativity with neutrinos from the CNGS beam is nevertheless interesting. Besides, the measurement may also put an upper limit on the effect of non-standard propagation of neutrinos in matter.

Borexino is able of detecting ν_μ's which interact in the rock upstream the detector and produce a muon. The muons can be detected by Borexino since they produce scintillation light and/or Cerenkov light. In order to perform a precision measurement of the time of flight of the ν_μ coming from CERN, a new system, the High Precision Timing Facility (HPTF), has been installed and operated in Gran Sasso by the Borexino collaboration. The HPTF is a GPS based timing facility with a calibrated time-link to the CERN GPS receiver and with continual real time monitoring of the time delay to the underground laboratory. A dedicated geodetic survey at Gran Sasso Laboratories has been performed in May 2012 in order to improve the precision on the distance between the Borexino reference point at LNGS and the target at CERN. In May 2012 a two-week long dedicated run with a "short-bunched" CNGS beam (2 nsec width) was performed. The result obtained on

this set of data is consistent with the expectations, i.e., the time-of-flight difference with respect to the speed of light is found to be $\delta t = 0.8 \pm 0.7\,(\text{stat}) \pm\ 2.9\,(\text{sys})$ ns, consistent with zero.

For more details on the neutrino velocity measurement performed by Borexino see [19].

3.4 Search for solar axions

Axions could be produced in the Sun via the reaction $p + d \rightarrow^3 He + A$. The energy of the emitted particle would be monochromatic and equal to 5.5 MeV. Borexino has searched for these axions in the following reactions: Compton conversion of axions to photons ($A + e \rightarrow e + \gamma$), axioelectric effect $A + e + Z \rightarrow e + Z$, decay of axions into 2 photons $A \rightarrow 2\gamma$ and inverse Primakoff conversion on nuclei $A + Z \rightarrow Z + \gamma$. The expected signal which Borexino would see in case these reactions occurred is shown in Fig. 5 (left panel), based on "Monte Carlo" simulations. The actual Borexino spectra obtained after applying a proper set of cuts is shown in Fig. 5 (right panel): no signal is present and thanks to the very low count rate due to the excellent radiopurity, it was possible to set very stringent limits on the axion-electron, axion-photon, and isovector axion-nucleon couplings: $|g_{Ae} \times g_{3AN}| \leq 5.5 \times 10^{-13}$ and $|g_{A\gamma} \times g_{3AN}| \leq 4.6 \times 10^{-11}\text{GeV}^{-1}$ at $m_A < 1$ MeV (90% c.l.).

For more details on the search of solar axions in Borexino refer to [18].

3.5 Modulation of cosmic muon flux

Cosmic muons are secondary particles produced as cosmic rays interact in the atmosphere. Cosmic muons arrive at ground level with slightly different energies depending on the season. This is due to the fact that muons are mainly produced in the atmosphere by decaying charged pions and/or kaons. A competing process to pion/kaon decay is pion/kaon interaction. If the temperature of the atmosphere is higher (like in summer), its density is lower and the probability that pions interact before decaying is lower. Therefore the energy of the produced muon is in average larger than in winter. Borexino is located under 3800 meters of water equivalent which block most part of the cosmic rays. Only the most energetic muons survive and therefore we expect more muons in summer than in winter. Borexino has the capability to clearly identify/tag the residual muons by combining the information coming from the Inner Detector and the dedicated Outer Detector. It is therefore ideal to study in detail the phenomenon of seasonal modulations of the muon flux. Fig. 6 shows the flux of muons observed by Borexino as a function of time (upper panel) and the time evolution of atmospheric temperature over the same time span for comparison (lower panel). A correlation between the two curves is evident by eye. By fitting the time evolution of the muon flux with a sinusoidal function

$$I_\mu = I_\mu^0 + \Delta I_\mu = I_\mu^0 + \delta I_\mu \cos\left(\frac{2\pi}{T}(t - t_0)\right) \tag{1}$$

we find an average intensity $I_\mu^0 = (3.414 \pm 0.002_{\text{stat}}) \cdot 10^{-4}\text{m}^{-2}\text{s}^{-1}$, a period $T = (366 \pm 3)$ days, and a percentage modulation amplitude $(1.29 \pm 0.07)\%$. The maximum is reached on the 28^{th} of June (error $\pm$ 6 days).

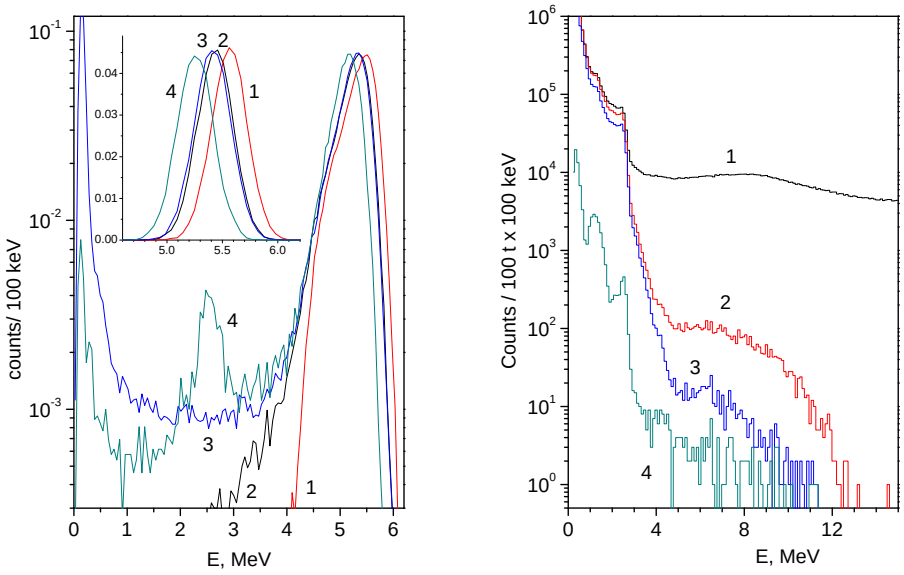

Figure 5: Left panel: simulated responses to axion interactions in the Borexino IV: (1) axioelectric effect, (2) Compton axion to photon conversion, (3) Primakoff conversion (4) decay A$\rightarrow \gamma\gamma$. Right panel: energy spectra of the events and effect of the selection cuts. (1) raw spectrum; (2) with 2 ms muon veto cut; (3) with events within 6.5 s of a muon crossing the SSS removed; (4) events inside FV.

The correlation between muon flux and atmospheric temperature has been studied and the effective temperature coefficient has been measured to be $\alpha_T = 0.93 \pm 0.04$, where α_T is defined as

$$\frac{\Delta I_\mu}{I_\mu^0} = \alpha_T \frac{\Delta T_{\rm eff}}{T_{\rm eff}^0} \tag{2}$$

This result is compatible with theoretical expectations. Fig. 7 shows the Borexino result together with all the results on α_T obtained by different experiments, at different locations (and therefore at different depths).

3.6 Calibration paper

All the results previously discussed take advantage of the detailed knowledge of the Borexino detector response, which has been achieved through several calibration campaigns performed between 2009 and 2011. In 2009, two internal calibration campaigns took place, in which radioactive sources of different types were inserted in different positions in the scintillator volume. These campaigns were meant to provide the energy calibration and to study possible systematics of the position reconstruction alghorithm. A list of the radioactive sources used in the internal calibration campaign is shown in table 1.

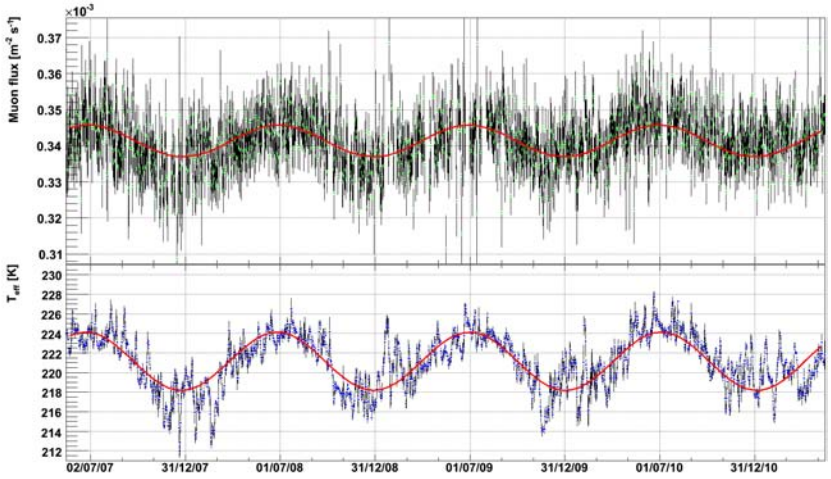

Figure 6: Upper panel: cosmic muon signal measured by Borexino as a function of time. Lower panel: effective temperature, $T_{\rm eff}$, obtained from a weighted average over atmospheric depth. Daily binning is used in both panels. The curves show the sinusoidal fit to the data.

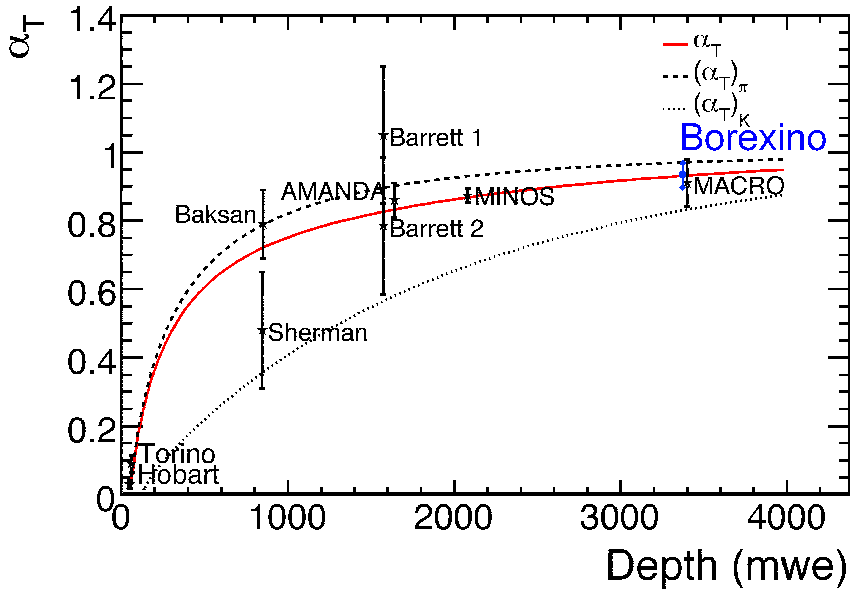

Figure 7: Measured values for the effective temperature coefficient, α_T, at varying site depths. The result from Borexino is the blue point. The red line is the value predicted including muon production by pions and kaons.

The internal calibration campaigns were extremely successful and allowed to reduce significantly the systematic error associated to the Fiducial Volume determination and to the energy scale. This allowed for example to measure the ^{7}Be rate with high precision [2].

Source	Type	E [MeV]	Position	Motivations
^{57}Co	γ	0.122	in IV volume	Energy scale
^{139}Ce	γ	0.165	in IV volume	Energy scale
^{203}Hg	γ	0.279	in IV volume	Energy scale
^{85}Sr	γ	0.514	z-axis + sphere R=3 m	Energy scale + FV
^{54}Mn	γ	0.834	along z-axis	Energy scale
^{65}Zn	γ	1.115	along z-axis	Energy scale
^{60}Co	γ	1.173, 1.332	along z-axis	Energy scale
^{40}K	γ	1.460	along z-axis	Energy scale
^{222}Rn+^{14}C	β,γ	0-3.20	in IV volume	FV+uniformity
	α	5.5, 6.0, 7.4	in IV volume	FV+uniformity
^{241}Am^{9}Be	n	0-9	sphere R=4 m	Energy scale + FV
394 nm laser	light	-	center	PMT equalization

Table 1: Radioactive sources used during the Borexino internal calibration campaigns. The radionuclides, energies and emitted particle types are shown in the first three columns. The fourth column indicates the positions where the sources were deployed within the scintillator. The main purposes for the individual source measurements are summarized in the fifth column.

In 2010 and 2011 two external calibration campaigns have been performed in which a dedicated ^{232}Th source (γ emitter) was located in different positions in the buffer region close to the stainless steel sphere to simulate background induced in the scintillator by the external contaminants. A schematic view of the external calibration setup is shown in Fig. 8.

These calibration campaigns were very successful and were crucial to understand details of the contribution of external background to the solar neutrino analysis. A thorough discussion of the hardware of both internal and external calibration systems, of the calibraton campaigns and of their main achievements has been published in [21].

4 Conclusions and perspectives

The first phase of Borexino started in 2007 and ended in 2010. Between 2010 and 2011 several purification cycles using the water extraction technique have been performed in order to increase even further the scintillator radiopurity. These purification campaigns have brought the ^{85}Kr content to values consistent with zero, and have significantly reduced the ^{210}Bi content (by a factor of ~ 3). In October 2011, after the last water extraction cycle was completed, the Phase 2 of Borexino started. The program of this new phase of the experiment is challenging and covers a broad range of fields from stellar and solar physics to particle physics. The main goal of Borexino Phase 2 is the detection of neutrinos from the solar CNO fusion cycle. This would be a major breakthrough for stellar evolution theories, since the CNO cycle is believed to be the main mechanism of hydrogen burning in stars more massive than our Sun. Although it should be present in the sun at a compar-

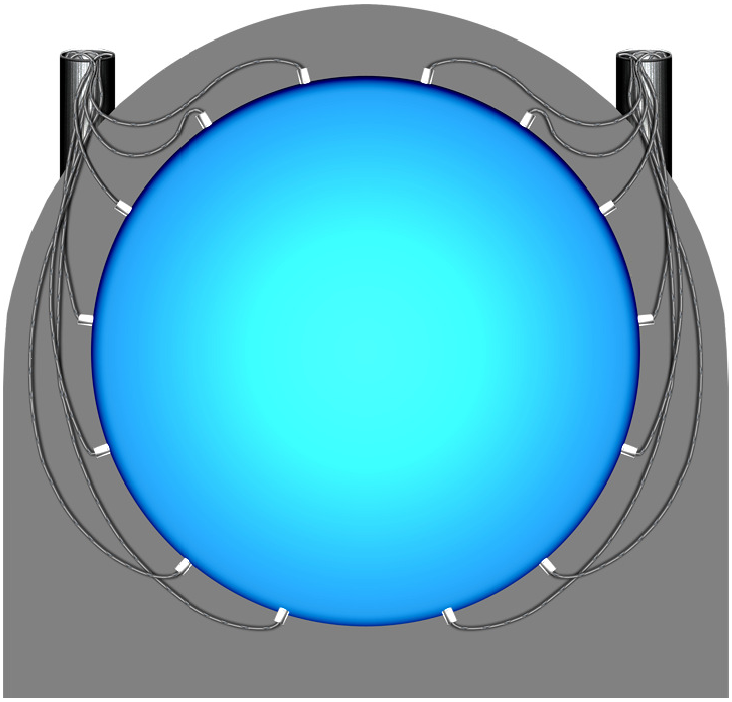

Figure 8: Schematic view of the external calibration system.

atively small level, it has never been observed. Also, the determination of the CNO flux could help disentangling between the so-called low and high metallicity hypothesis for the Sun as the reaction strongly depends on the abundances of carbon, oxygen and nitrogen at the solar center. CNO neutrino detection is very challenging especially because of the degeneracy of their spectral shape with that of the radioactive contaminant ^{210}Bi. The content of ^{210}Bi in the scintillator should be known precisely in order to disentangle its contribution from the CNO rate. A big effort is currently devoted to developing analysis techniques to determine the content of ^{210}Bi by studying the evolution in time of ^{210}Po (which is the ^{210}Bi daughter). This analysis is made difficult by disuniformities of the contaminants in the scintillator volume and variation in time of the content of ^{210}Po and ^{210}Bi due to operations and convective motions.

An other important goal for the second phase of Borexino is the direct observation of solar neutrinos from the *pp* reaction. These neutrinos stem from the most basic solar fusion reaction and are responsible for most of the solar luminosity, but have never been observed in real-time because of their low energies (E <420 keV). The main source of background for a measurement in Borexino is the high decay rate of ^{14}C and its pile-up. Detailed simulations of these backgrounds (and possibly a direct study of them with CO_2 in gaseous form dissolved in the scintillator at the end of Phase 2) are important to perform a spectral fit to disentangle the *pp* signal. The already achieved reduction of ^{85}Kr which also affects the low energy portion of the spectrum is an important progress with respect to Phase 1.

Further important results which we expect from the new data of Borexino are the improvement in the precision of the ^{7}Be rate measurement (possibly down to 3%) and

of the shape of the electron recoil spectrum. This would be an important achievement "per se" and would also help evidentiating possible effects due to neutrino Non Standard Interactions.

In general, in order to probe possible non-standard effects, it would be important to increase the amount of information in the so-called transition region from vacuum to matter dominated oscillations, by improving the precision on the pep neutrino rate and on the ^{8}B neutrino rate (in the region between 3 and 5 MeV).

4.1 The SOX project

The Borexino detector offers a unique opportunity to perform a short-baseline neutrino oscillation test, which will be able of exploring the sterile neutrino hypothesis in the range of ($\sin^2\theta_{14}$, Δm^2_{14}) currently allowed by several experimental anomalies. The idea is to place a 10 MCi ^{51}Cr neutrino source below the detector, in the so-called Icarus pit and search for a possible suppression of the neutrino flux. Since the currently preferred value for Δm^2_{14} is of the order of 1 eV^2, and the neutrino energies are of the order of $\sim$1 MeV the resulting oscillation lengths is of the order of meters. In this case, it would be even possible to observe a spatial oscillation pattern emerging inside the target volume. In its current form, the SOX project doesn't require any modifications of the Borexino experimental apparatus. Data-taking will start tentatively at the end of 2014 and will last for approximately 3 months. The project has recently received a European grant.

5 List of Publications in 2012

1. Borexino collaboration *Absence of a day-night asymmetry in the ^{7}Be solar neutrino rate in Borexino*, Phys. Lett.B 707 (2012), pp. 22-26.

2. Borexino collaboration *First evidence of pep solar neutrinos by direct detection in Borexino*, Phys.Rev.Lett.108 051302.

3. Borexino collaboration *Search for solar axions produced in the p(d,^{3}He)A reaction with Borexino detector*, Phys.Rev.D 85, 092003 (2012).

4. Borexino collaboration *Measurement of CNGS muon neutrino speed with Borexino* Phys.Lett.B 716 (2012) 401-405.

5. Borexino collaboration, *Cosmic-muon flux and annual modulation in Borexino at 3800 m water-equivalent depth*, JCAP05 (2012) 015.

6. Borexino collaboration, *Borexino calibrations: hardware, methods and results*, 2012 JINST 7 P10018.

References

[1] Nakamura K *et al* 2010 *Review of Particle Physics J.Phys* G **37** 075021.

[2] Bellini G *et al.* (Borexino coll.) 2011 *Phys.Rev.Lett.* **107** 141302.

[3] Alimonti G *et al.* (Borexino coll.) 2009 *Nucl. Instrum. Methods Phys. Res.* A **600** 568.

[4] Bellini G *et al.* (Borexino coll.) 2011 *JINST* **6** P5005.

[5] Arpesella C *et al.* (Borexino coll.) 2008 *Phys.Lett.* B **658** 101.

[6] Arpesella C *et al.* (Borexino coll.) 2008 *Phys.Rev.Lett.* **101** 091302.

[7] Haxton W, Serenelli A M and Pena-Garay C *Ap.J.* **743** 24; arXiv:1104.1639 [astro-ph].

[8] Grevesse N and Sauval A J 1998 *Space Sci.Rev.* **85** 161.

[9] De Holanda P C 2009 *JCAP* 24.

[10] Bellini G *et al.* (Borexino coll.) 2010 *Phys.Rev.* D **82** 033006.

[11] Bellini G *et al.* (Borexino coll.) 2010 *Phys.Lett.B* **687** 299-304.

[12] Bellini G *et al.* (Borexino coll.) 2010 *Phys.Rev.* C, **81** 034317.

[13] Bellini G *et al.* (Borexino coll.) 2011 *Phys.Lett.* B, **696** 191.

[14] Adams T *et al.* (OPERA coll.) 2011 arXiv:1109.4897v2 [hep-ex].

[15] Adams T *et al.* (OPERA coll.) 2011 arXiv:1109.4897v4 [hep-ex], JHEP, in press.

[16] Bellini G *et al.* (Borexino coll.) 2012 *Phys.Lett.* B **707** 22.

[17] Bellini G *et al.* (Borexino coll.) 2012 *Phys.Rev.Lett.* **108** 051302.

[18] Bellini G *et al.* (Borexino coll.) 2012 *Phys.Rev.* D **85**, 092003.

[19] Alvarez Sanchez P *et al.* (Borexino coll.) *Phys.Lett.* B **716** 401-405.

[20] Bellini G *et al.* (Borexino coll.), *JCAP05* 015.

[21] Back H.*et al.* (Borexino coll.) 2012 *JINST* **7** P10018.

COBRA Annual Report 2012

A. Bakst[a], J. Durst[a], M. Filipenko[a], T. Gleixner[a], T. Michel[a],
B. Biskup[b], V. Bocarov[b], P. Cermak[b], J. M. Jose[b], I. Stekl[b],
O. Civitarese[c],
C. Disch[d], A. Fauler[d]. M. Fiederle[d],
M. Beilicke[e], F. Kislat[e], H. Krawczynski[e], A. Zajcyk[e],
M. Fritts[f], D. Gehre[f], T. Göpfert[f], O. Reinecke[f], T. Wester[f], S. Zatschler[f], K. Zuber[f,*]
C. Gößling[g], M. Homann[g], R. Klingenberg[g], T. Köttig[g], T. Neddermann[g], S. Rajek[g],
J. Tebrügge[g], T. Quante[g],
V. Braunert[h], J. Ebert[h], C. Hagner[h], N. Heidrich[h], C. Oldorf[h], H. Rebber[h], J. Timm[h],
B. Wonsak[h],
M. Junker[i], F. Simkovic[j], J. Suhonen[k],

[a] *Universität Erlangen–Nürnberg* – Germany
[b] *Technical University of Prague* – Czech Republic
[c] *University of La Plata* – Argentina
[d] *Freiburg Materials Research Center* – Germany
[e] *Washington University in St. Louis* – USA
[f] *Technische Universität Dresden* – Germany
[g] *Technische Universität Dortmund* – Germany
[h] *Universität Hamburg* – Germany
[i] *Laboratori Nazionali del Gran Sasso* – Italy
[j] *University of Bratislava* – Slovakia
[k] *University of Jyvaskyla* – Finnland
(* Spokesperson)

Abstract

The aim of the COBRA-Experiment (**C**admium Zinc Telluride **0**-Neutrino Double-**B**eta **R**esearch **A**pparatus) is to prove the existence of neutrinoless double beta decay ($0\nu\beta\beta$-decay) and to measure its half life.

For this purpose a detector array made of Cadmium-Zinc-Telluride detectors (CZT) is operated at LNGS in Italy. This demonstrator setup is used to investigate the experimental issues of operating CZT detectors in low background mode and identify potential background components, whilst additional studies are proceeding in surface laboratories. The experiment currently consists of monolithic, calorimetric prototype-II detectors in a coplanar grid design (CPG detectors). These detectors are 1x1x1 cm^3 and will be operated in a 4x4x4 detector array.

Additionally, pixelated CZT detectors are under investigation to check their properties to distinguish the different background contributions. Based on pattern recognition in combination with energy resolved measurements it could be possible to directly image the $0\nu\beta\beta$-decay by particle identification.

1 Activities with the detector array at LNGS

In March 2012 a second layer of 16 prototype-II detectors was added to the array. Since then the 32 detector array has been collecting low-background data. Frequent calibrations with gamma radiation sources allow for the calculation of the detectors' amplification and resolution properties, which vary slowly over constant running conditions within a few percent. 51.1 kg·days of high-quality, well-calibrated data were accumulated as of December 2, with a current accumulation rate of approximately 5 kg·days per month.

1.1 Experimental upgrades

The electronics required to operate the two layers emit several hundred watts of waste heat. Currently there is no air exchange system in the lower hut which houses the COBRA setup, resulting in operating temperatures near 30 °C. Such high temperatures are undesirable for both the electronics and the CZT detectors themselves, whose resolutions are known to improve at cooler temperatures. With the planned installation of two more layers to complete the array, this situation would only get worse.

To improve the operating temperature, part of the data aquisition and electronics chain was moved into the hut above the detector array in December. The operating temperature has fallen by 4 °C and continues to decrease as the lead shielding slowly cools. This move required routing of the differential-signal cables from the lower hut to the upper hut. Although this could in principle increase the sensitivity to electromagnetic interference (EMI), the rate of EMI events was actually significantly reduced after the move. This reduction is probably the result of moving electronic components farther from the detectors and preamplifiers themselves, as well as improvements to the EMI shielding of several components. Although pulse shape analysis effectively removes EMI events, a reduction in the EMI event rate is important to reduce data storage and to allow the detectors to be run at lower trigger thresholds.

In December a pulser was installed to send fixed-amplitude, simultaneous signals to the 64 preamplifiers (two per detector, for the two anode signals of CPG detectors). By sending these signals to the preamplifiers the full readout chains can be characterized. The signals are sent in a regular pattern during low-background runs for two purposes. The first purpose is

to monitor the amplification characteristics (gain and resolution) in real time, independently of the calibration runs. The second purpose is to synchronize the clocks of the eight different ADC modules (one ADC module for every four detectors). The clock speeds of the modules differ slightly, so that for a typical four-hour run the disagreement can be larger than a tenth of a second. The synchronization possible due to the simultaneous pulser signals allows for event coincidence studies across the full array with a time resolution smaller then one millisecond. Such coincidence studies are key both for characterizing and identifying certain backgrounds and for searching for certain complex $0\nu\beta\beta$ decay modes. The pulser can be controlled remotely so that it can be configured off-site.

2 CPG activities

2.1 Reduction of surface background

Intrinsic to the coplanar grid detector design is the ability to extract well-calibrated energy and depth (distance from anode plane) information for each event [1]. The COBRA collaboration has continued to explore detailed understanding of event reconstruction and in 2012 contributed new insights to the existing literature for CPG detectors, detailing a new method for depth calculation and several effects that can influence event reconstruction [2].

With 51.1 kg·days of low-background exposure, a thorough characterization of the background in the LNGS setup is possible. Figure 1 shows the distribution of the accumulated background events in both energy and interaction depth. The depth dependence of several categories of background can be readily exploited to reduce the background for the $0\nu\beta\beta$ search.

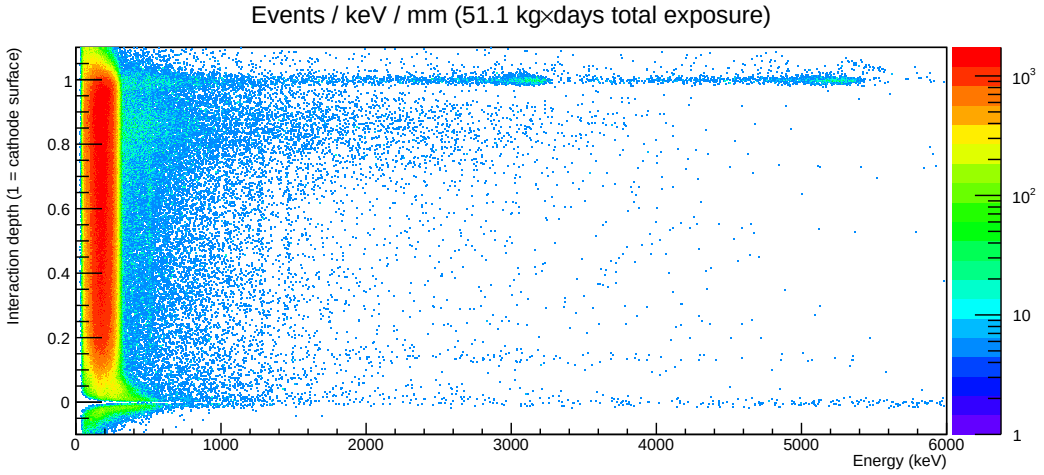

Figure 1: Distribution of events from 51.1 kg·days in interaction depth and energy. Two high energy regions on the cathode surface are identified as alpha contaminants. Three gamma lines are also visible. The region below 400 keV is dominated by the β-decay of ^{113}Cd. At low depths well-understood detector distortions and reconstruction artifacts can be seen.

Figure 2 depicts the background rate in standardized units for three different depth ranges. The largest depth range also has the smallest background in the primary region of interest, near the 2.8 MeV Q-value of ^{116}Cd $0\nu\beta\beta$ decay.

The background peaks seen near 3 and 5 MeV at depths near 1.0 have been identified as alpha contamination on the cathode surfaces. In particular the 5 MeV peak is likely due to

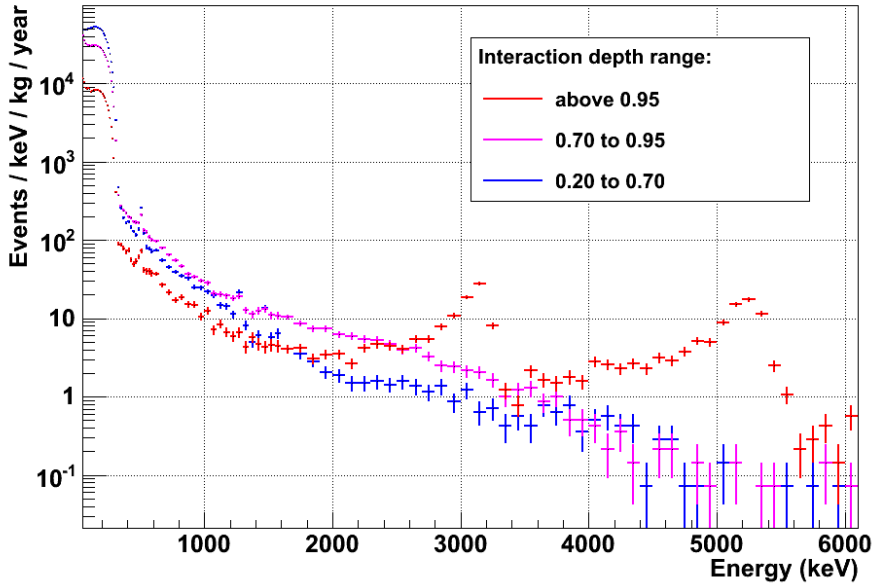

Figure 2: Background rate spectrum in three different interaction depth ranges.

low-level contamination by the long-lived radon daughter ^{210}Pb occurring during the handling and testing of the detectors before installation in the radon-free LNGS setup. It is a reasonable assumption that ^{210}Pb contamination exists on the other surfaces of the detector as well, so that much of the mid-depth background above 2 MeV may also be attributable to alpha interactions. Interactions very near the lateral surfaces of the detector produce signature distortions in the pulses as shown in Figure 3. These distortions can be characterized by pulse shape analysis. This powerful tool can reduce our backgrounds even further. Figure 4 shows that 80% of the mid-depth background above 2 MeV can be identified as surface events. The effective background rate based on an optimized sensitivity calculation at 2.8 MeV can thus be reduced to approximately 0.4 events keV^{-1} kg^{-1} year^{-1}. Ongoing studies are being performed to improve the identification of lateral-surface events as described in Section 2.2.

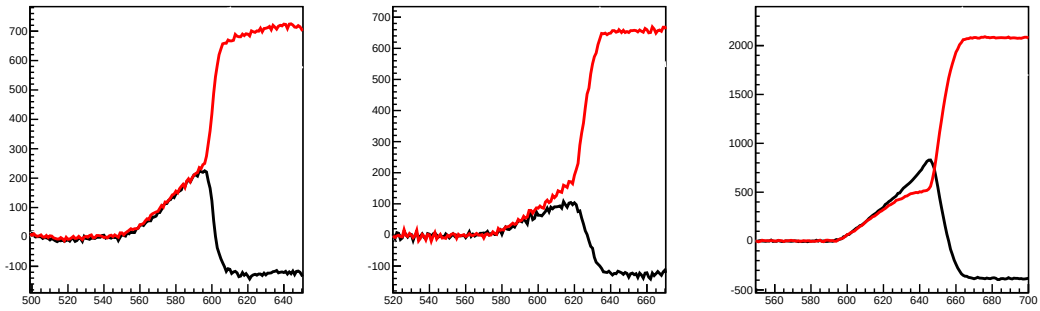

Figure 3: Pulses characteristic of lateral surface events. Right: central event, undistorted. Center and left: surface events showing distortions.

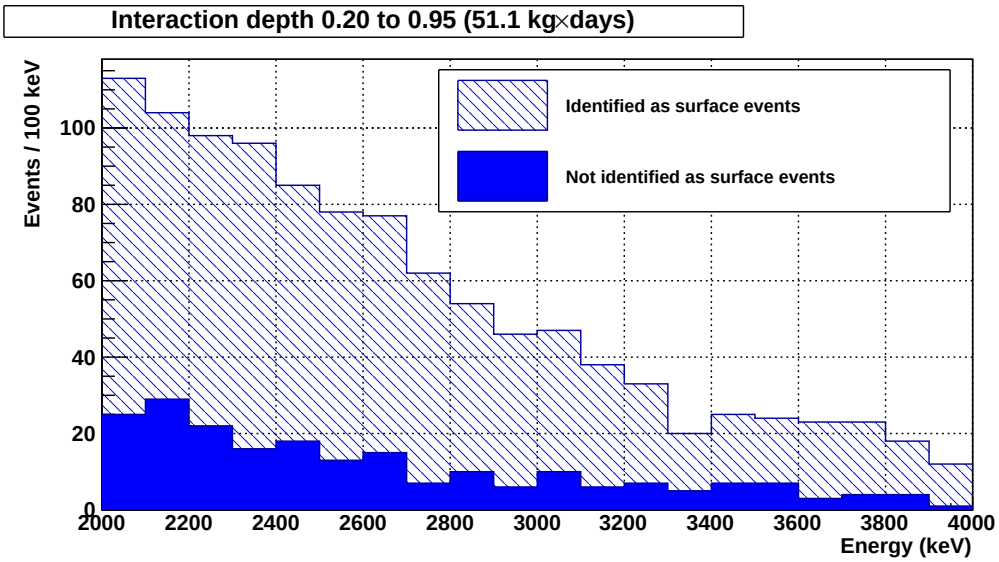

Figure 4: Remaining background in the region of interest after identification of lateral surface events through pulse shape analysis.

2.2 Laboratory tests at Dortmund

As backround reduction is one of the most challenging and crucial issues for the COBRA-Experiment, dedicated CPG tests relating to pulse shape analysis have been performed at Dortmund under controlled laboratory conditions.

Each detector signal has its own channel in the electronic read-out system. Due to the manufacturing tolerance of the electronic components used, which can be as high as 20% for some parts, the amplification of the different channels is not exactly the same. This effect cancels for the energy calculation, but not for the interaction depth calculation. To investigate this, the amplifications of three different preamplifiers were tested, in total 66 channels, using a pulse generator. These results were used to compute the spread of the calculated interaction depth. The results show that this effect is small but that nevertheless it can be corrected in the analysis. Such correction techniques are now implemented for the CPG array at LNGS.

The identification of lateral surface events in the LNGS data through pulse shape analysis must be experimentally verified. An experimental setup has been built to scan the detector with a collimated ^{241}Am alpha source. A detector is glued to a rod, so that five sides can be reached by the alpha source. The source itself and the collimator can be adjusted very precisely using micrometer screws. A light source (LED) is placed behind the source location in the collimator apparatus to identify the irradiation point on the detector. This experimental setup can be seen in Figure 5. The penetration depth of alpha radiation is only some tens of μm, i.e. surface events. In contrast to that, gamma radiation of ^{137}Cs with 662 keV penetrates the detector completely, so the events are homogeneously distributed in the detector. If the method to identify lateral surface events works, it should clearly seperate these two types of radiation in terms of their interaction locations in the detector.

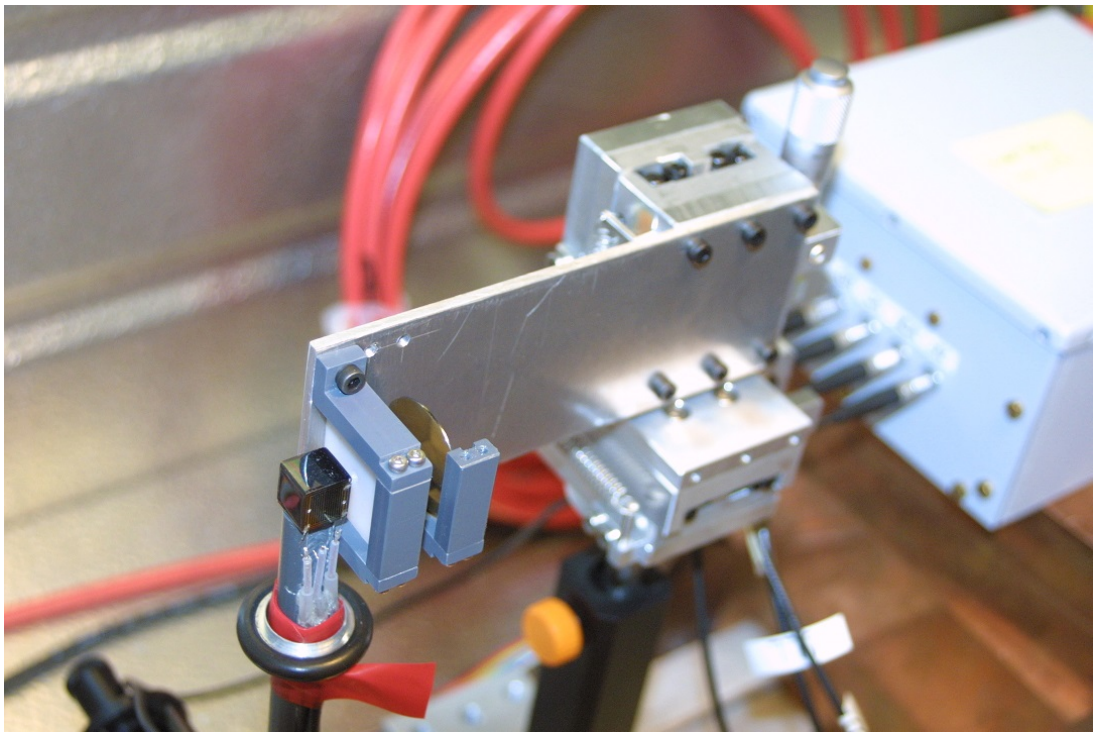

Figure 5: Experimental setup for testing detector response to surface events using a collimated alpha radiation source.

3 Pixel detector activities

3.1 Background Study for a Large Volume Pixel Detector

In collaboration with the Z. He group from the University of Michigan a large volume pixel detector system (Polaris System [3]) was tested at LNGS as described in [4]. Even though the detector system was not optimized with respect to low-background measurements the results obtained were very promising. By applying fiducial cuts, all events in COBRA's region of interest at 2.8 MeV could be discarded and an upper limit on the achieved background level of 4 events $\mathrm{keV}^{-1}\,\mathrm{kg}^{-1}\,\mathrm{year}^{-1}$ was estimated.

To further investigate the potential of large volume pixel detectors with a pixel pitch on the order of millimeters and to determine the major remaining background sources, Geant4 simulations were produced and evaluated. ^{232}Th, ^{238}U and ^{40}K were simulated in the components (PCB board, detector passivation and surrounding air) and the shielding of a Polaris-like system surrounded by 10 cm of lead. The composition of the background sources was adjusted to match the measured background.

Afterwards the same fiducial cuts that were chosen for the measured data were applied to the simulated data. The results are shown in Figure 6. The simulated background agrees well with the measurement. The simulation and the measurement are also consistent after the fiducial cuts are applied.

^{116}Cd has a high Q-value of 2813 keV, which is higher than the highest naturally occurring γ-line with noticeable emission probability (the 2.6 MeV line from the ^{208}Tl decay in the ^{232}Th decay chain). There is also only one β-decay with an energy release that is high enough to mimic a double beta event in COBRA's region of interest (the β-decay of ^{214}Bi of the ^{238}U decay chain).

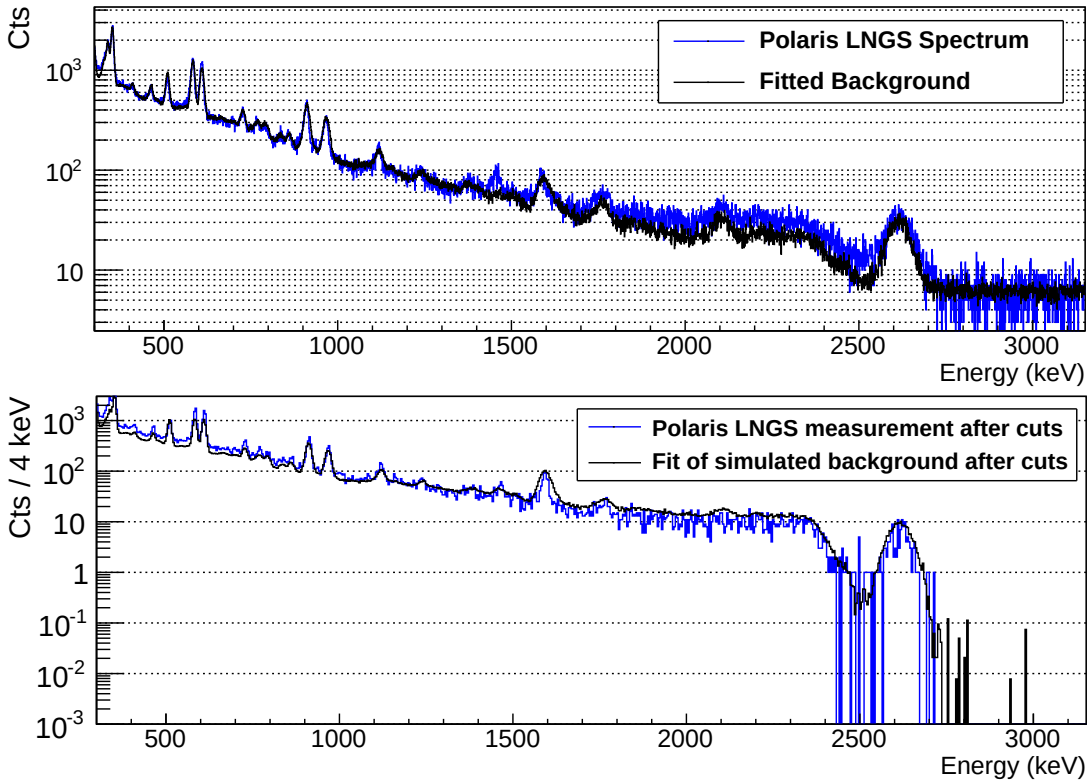

Figure 6: Simulation and measurement for a large volume detector system. The measurement is described well by the simulation, and the background reduction by applying fiducial cuts can be reproduced. As the main background at COBRA's region of interest at 2.8 MeV derives from energy depositions from α-decays, with these cuts the background level can be reduced by several orders of magnitude.

Isotope	E_γ [keV]	Intensity [%]	Isotope	E_γ [keV]	Intensity [%]
^{214}Bi	2770.0	0.024	^{208}Tl	2614.5 + 583.2	49
^{214}Bi	2880.4	0.010	^{208}Tl	2614.5 + 583.2+277.4	6
^{214}Bi	2922.1	0.017	^{208}Tl	2614.5 + 860.6	12
^{214}Bi	2978.8	0.015	^{208}Tl	2614.5 + 510.7 + 583.2	23
^{214}Bi	3000.0	0.010			
^{214}Bi	3053.9	0.020			

Table 1: High energetic γ-particles and cascades from ^{214}Bi (^{238}U chain) and ^{208}Tl (^{232}Th chain) decays. Listed are the lines with the highest intensity for the ^{214}Bi decay and the most significant cascades for the ^{208}Tl line. Data taken from [5].

The main source of background in COBRA's region of interest therefore derives from α-particles that lose energy while passing through thin material layers such as the detector passivation or air surrounding the detectors. These events can be rejected efficiently by exploiting the spatial resolution of a pixel detector and discarding events close to the surface of the detector. The simulations show that the remaining background derives from rare γ-particles from the ^{214}Bi decay and summing of γ-cascades from the ^{208}Tl decay (see Table 1). The expected background level with a Polaris-like system that has not been optimized for low-background was estimated to be at about 0.3 events keV^{-1} kg^{-1} year^{-1}. This result clearly shows the high potential of this type of pixel detector.

3.2 Installation of a CdTe stack at LNGS

By the end of 2012, a CdTe pixel detector unit was fabricated and installed at LNGS. The setup consists of two CdTe pixel detectors (matrix size 128x128 pixels, 110 μm pitch, 2 mm thickness) on a high purity base using CuFlon PCB. The unit holder is made of Delrin. The detectors were provided by Freiburger Materialforschungszentrum (FMF), University of Freiburg.

The setup was installed inside a lead shield (thickness 10 cm on all sides). Figure 7 shows the lead shield. The detectors were observed to heat up during operation, so active cooling using a fan was applied. Figure 8 shows the pixel detector unit including the Delrin support structure.

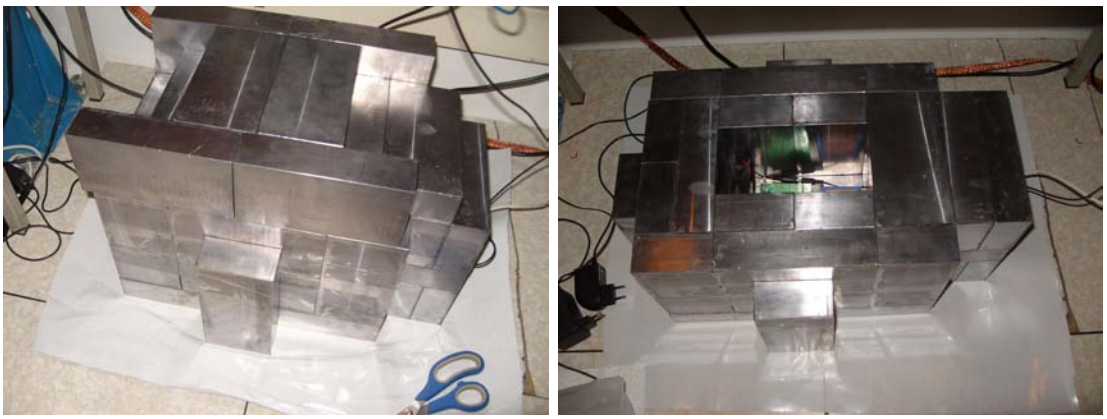

Figure 7: Lead shield for CdTe pixel detector setup. Left: outer view. Right: Pixel stack inside shield.

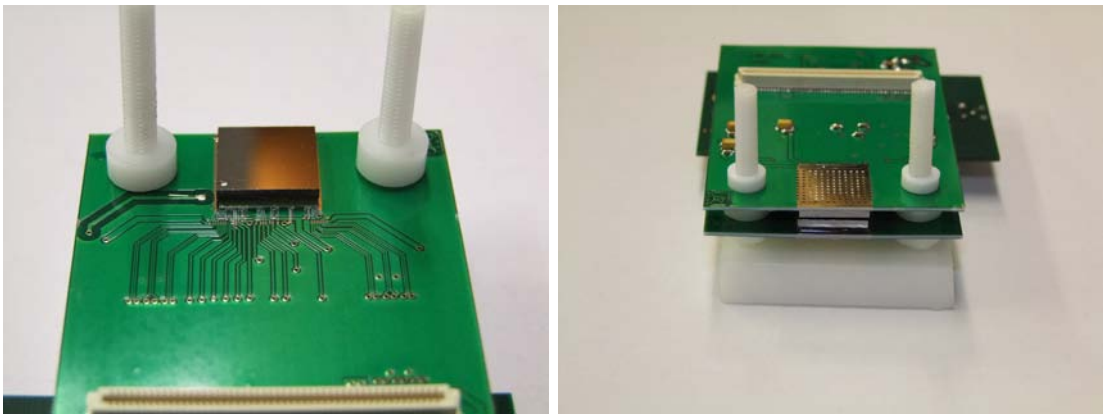

Figure 8: CdTe pixel detector setup. Left: single pixel detector. Right: entire unit, including Delrin support structure.

Figure 9 shows a very preliminary energy spectrum from 12 days of data taking. No cluster analysis has been performed yet. In total about 25000 events have been collected in the energy range up to 10 MeV. One can see two peaks in the high energy region corresponding to radon daughter isotopes.

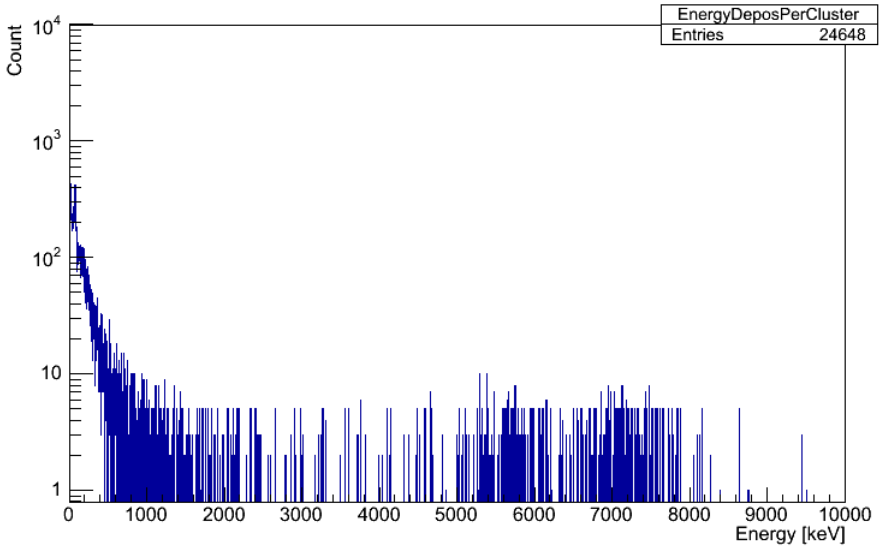

Figure 9: Spectrum from 12 days of data from the CdTe pixel detector setup.

4 List of Publications

1. *Analytical model for event reconstruction in coplanar grid CdZnTe detectors* - M. Fritts, J. Durst, T. Göpfert, T. Wester, K. Zuber (Nuclear Instruments and Methods in Physics Research A 708 (2013) 1-6)

2. *Sensitivity Studies of CdZnTe Semiconductor Detectors for the COBRA Experiment* - T. Köttig (Technische Universität Dortmund, 2012)

3. *Experimental Investigation of Pixelated Semiconductor Photodetectors with CdTe Sensor Material for the Search for the Neutrinoless Double Beta Decay* - M. Filipenko (Erlangen Centre for Astroparticle Physics, 2012)

4. *Simulation and Data-Analysis for Background Reduction for the COBRA-Experiment* - M. Homann (Technische Universität Dortmund, 2012)

5. *Upgrade of the Active Muon Veto and Software Development for the DLB Facility* - T. Quante (Technische Universität Dortmund, 2012)

6. *Ortsaufgelöste Effizienzbestimmung von CdZnTe Halbleiterdetektoren mit kollimierter Gammastrahlung für das C0BRA-Experiment* - A. Sörensen (Technische Universität Dresden, 2012)

7. *New read-out electronics and pulse shape analysis for the COBRA experiment* - J. Tebrügge (Technische Universität Dortmund, 2012)

References

[1] Z He, G.F Knoll, D.K Wehe, J Miyamoto, *Position-sensitive single carrier CdZnTe detectors.* Nuclear Instruments and Methods in Physics Research Section A **388(1-2)** (1997), pp. 180-185

[2] M Fritts, J Durst, T Göpfert, T Wester, K Zuber, *Analytical model for event reconstruction in coplanar grid CdZnTe detectors.* Nuclear Instruments and Methods in Physics Research Section A **708** (2013), pp. 1-6

[3] F. Zhang and Z. He and C.E. Seifert, *A Prototype Three-Dimensional Position Sensitive CdZnTe Detector Array.* IEEE Transactions on Nuclear Science **54(4)** (2007), pp. 843-848

[4] O. Schulz *Exploration of new Data Acquisition and Background Reduction Techniques for the COBRA Experiment.* Technische Universität Dortmund, 2011.

[5] Richard B. Firestone, *Table of Isotopes*, John Wiley & Sons, Inc. 1998.

The CRESST Dark Matter Search

G. Angloher [a], M. Bauer [e], C. Bucci [d], C. Ciemniak [c], F. von Feilitzsch [c], D. Hauff [a], P. Huff [a], C. Isaila [c], J. Jochum [e], M. Kiefer [a], C. Kister [a], H. Kraus [b], J.C. Lanfranchi [c], A. Mnster [c], F. Petricca [a], W. Potzel [c], F. Pröbst [a], F. Reindl[a], S. Roth [c], K. Rottler [e], C. Sailer[e], K. Schäffner[a], S. Scholl [c], J. Schmaler [a], W. Seidel [a, +], M. von Sivers[c], C. Strandhagen [e], L. Stodolsky [a], R. Strauss[c], A. Tanzke[a], I. Usherov[e], S. Wawoczny[c], M. Willers[c], A. Zöller[c]

[a] *MPI für Physik, Föhringer Ring 6, 80805 Munich, Germany*
[b] *University of Oxford, Department of Physics, Oxford OX1 3RH, U.K.*
[c] *Technische Universität München, Physik Department, D-85747 Garching, Germany*
[d] *Laboratori Nazionali del Gran Sasso, I-67010 Assergi, Italy*
[e] *Eberhard-Karls-Universität Tübingen, D-72076 Tübingen, Germany*
[+] *Spokesperson E-mail address: seidel@mppmu.mpg.de*
[*] *present address: University of Warwick, Coventry CV4 7AL, U.K.*

Abstract

The aim of CRESST (**C**ryogenic **R**are **E**vent **S**earch with **S**uperconducting **T**hermometers) is to search for particle Dark Matter and to contribute to the elucidation of its nature. The experiment is located at the 'Laboratori Nazionali del Gran Sasso' (LNGS), Italy, and it uses low background cryogenic detectors with superconducting phase transition thermometers for the direct detection of WIMP-nucleus scattering events.

1 Dark Matter

There is strong evidence for the existence of dark matter on all astronomical scales, ranging from dwarf galaxies, through spiral galaxies like our own, to large-scale structures. The history of the universe is difficult to reconstruct without dark matter, be it Big Bang Nucleosynthesis or structure formation.

Despite this persuasive indirect evidence for its existence, the direct detection of dark matter remains one of the outstanding experimental challenges of present-day physics and cosmology.

A plausible candidate for the dark matter is the Weakly Interacting Massive Particle (WIMP) and it is possible that it can be detected by laboratory experiments, particularly using cryogenic methods, which are well adapted to the small energy deposit anticipated. Supersymmetry provides a well-motivated WIMP candidate in the form of the Lightest Supersymmetric Particle. WIMPs are expected to be gravitationally bound in a roughly isothermal halo around the visible part of our galaxy with a density of about $0.3\,\mathrm{GeV/cm^3}$ at the position of the Earth.

Interaction with ordinary matter is expected via elastic scattering on nuclei. This elastic scattering can occur via coherent ("spin-independent") and spin-dependent interactions. For the coherent case, a factor A^2 is expected in the cross-section, favouring heavy nuclei.

Conventional methods for direct detection rely on the ionisation or scintillation caused by the recoiling nucleus. This leads to certain limitations connected with the low ionisation or scintillation efficiency of the slow recoil nuclei. The cryogenic detectors developed for CRESST measure the deposited energy calorimetrically, independent of the type of interaction, and allow for the detection of much smaller recoil energies. When such a calorimetric measurement of the deposited energy is combined with a measurement of scintillation light, an extremely efficient discrimination of the nuclear recoil signals from radioactive background signals can be obtained. These type of detectors are being used in the present phase CRESST-II.

2 Detection Principle

The low-temperature calorimeters consist of a target crystal with an extremely sensitive superconducting phase transition thermometer on its surface. A weak thermal coupling to a heat bath restores again the equilibrium temperature after an interaction. The thermometer is made of a tungsten film evaporated onto the target crystal. Its temperature is stabilised within the transition from the superconducting to the normal conducting state, which occurs at temperatures of about 10 mK. A typical width of the transition is about 1 mK. A small temperature rise e.g. from a WIMP–nucleus scattering event (typically some μK), leads to an increase of resistance, which is measured with a SQUID (**S**uperconducting **Qu**antum **I**nterference **D**evice). For the first phase of CRESST, which ended in 2001, 262 g sapphire detectors had been developed at MPI. These detectors provided an excellent energy resolution of 133 eV at 6 keV and a very low energy threshold of 600 eV.

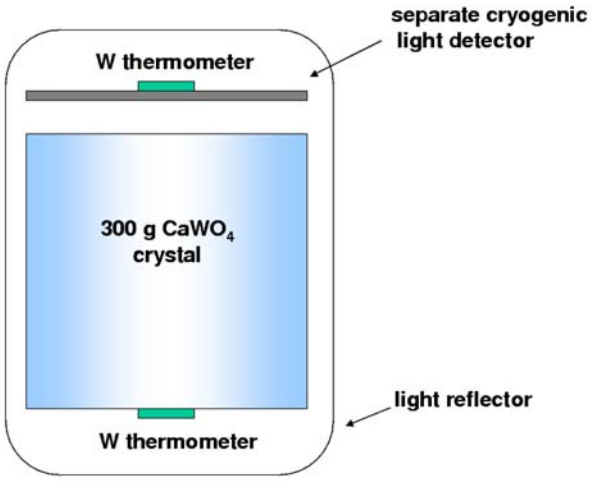

Figure 1: Schematic representation of the detector for simultaneous phonon and light measurement. It consists of two separate cryogenic detectors enclosed in a highly reflective housing, read out by tungsten superconducting phase-transition thermometers. This concept, developed by scientists of the institute, is used in CRESST-II. It allows a very efficient discrimination of the searched nuclear recoil signals from the dominant radioactive β- and γ-backgrounds.

In the second phase, CRESST-II, we are using 300 g scintillating $CaWO_4$ target crystals. The scintillating crystal is equipped with a superconducting tungsten phase-transition thermometer for the detection of the phonons created by a particle interaction in the scintillating crystal. A small fraction of $\sim 1\%$ of the deposited energy is emitted as scintillation light, which is measured with a separate cryogenic detector, optimised for light detection. Fig. 1 shows a scheme of this composite detector.

Starting with a proof-of-principle experiment in 1998, the technique of simultaneous measurement of phonons and scintillation light has been developed at the Max-Planck-Institute. The important advantage of this technique is that it offers an extremely efficient suppression of the radioactive background down to very low recoil energies of about 10 keV. While the phonon signal measures the deposited energy, the amplitude of the corresponding light signal depends on the type of interaction. Nuclear recoils, such as WIMP or neutron scattering events, emit substantially less scintillation light than fully ionising interactions, e.g. γ or β interactions, do. As the overwhelming part of the background consists of β and γ interactions, this phonon/light technique provides a very effective method of background suppression. Fig. 2 illustrates this detection method.

Compared with the alternative approach of simultaneous measurement of phonons and charge in a semiconductor crystal, which is applied in the experiments CDMS-II and Edelweiss-II, the method developed for CRESST-II has the important advantage that it does not suffer from dead layers at the surface. A reduced charge collection for ionising events occurring close to the surface in semiconducting crystals may lead to a false identification of low energetic γ's and β's as nuclear recoils. The result in Fig. 2, which was obtained with a gamma and beta source, confirms that the suppression also works for low-energy electrons impinging onto the crystal surface.

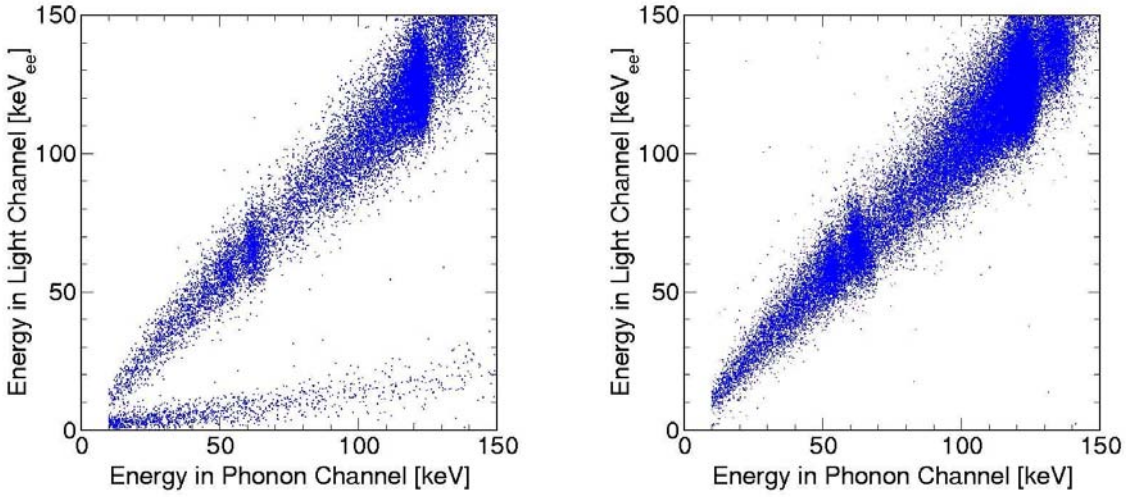

Figure 2: Coincident detection of phonons and scintillation light with a $CaWO_4$ detector. Left: The upper band of events is due to irradiation of the $CaWO_4$ crystal with electrons and gammas, whereas the lower band with lower light yield, is from nuclear recoils caused by a neutron source. Right: Removing the neutron source confirms that there is no leakage of ionising events into the nuclear recoil region.

3 The CRESST Setup in Gran Sasso

The central part of the CRESST installation at Gran Sasso is the cryostat. The low temperature which is generated in the mixing chamber of the dilution refrigerator is transferred into the radio-pure cold box, via a 1.5 m long cold finger. The cold finger is protected by thermal radiation shields, all fabricated of low-background copper. The detectors are mounted inside the cold box at the end of the cold finger. Two internal cold shields consisting of low-level lead are attached to the mixing chamber and to a thermal radiation shield at liquid N_2 temperature, respectively, in order to block any line-of-sight from the non-radio-pure parts of the dilution refrigerator to the detectors inside the cold box. The design completely avoids potentially contaminated cryogenic liquids inside the cold box.

An extensive passive shielding of low-background copper and lead surrounds the cold box and serves to shield radioactivity from the surrounding rock. The entire shielding is enclosed inside a gas-tight radon box that is flushed with boil of N_2 gas and maintained at a small overpressure. Special care was taken to minimise above-ground exposure of the construction materials of the cold box and the shielding to cosmic rays, in order to avoid activation.

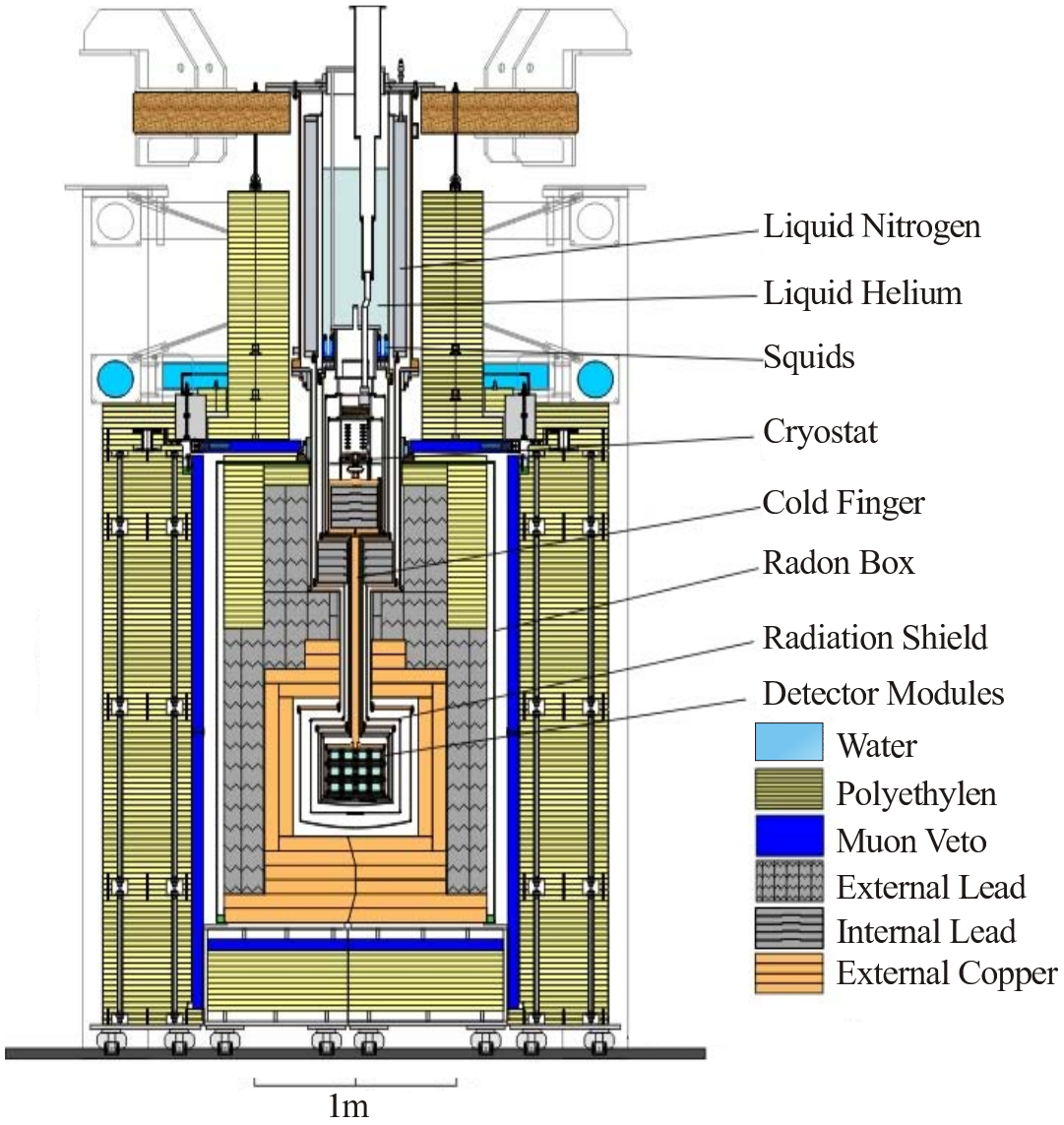

Figure 3: Dilution refrigerator and low-background cold box with its shielding upgraded for CRESST-II. The gas-tight radon box enclosing the Cu (shown in gray) and Pb (blue) shielding is completely covered by a plastic scintillator μ-veto (pink) and 40 cm of polyethylene (red).

4 2009/2010/2011 Data Taking

The latest run of CRESST took place between June 2009 and April 2011. It included a neutron test and γ-calibrations with ^{57}Co and ^{232}Th sources. Out of the 18 detector modules installed in the cryostat only 8 were used for the Dark Matter analysis. One was excluded due to its unusually poor energy resolution and an additional one was excluded being equipped with a test $ZnWO_4$ crystal. The remaining ones mainly had difficulties in cooling the light detectors and could therefore not provide the full information needed for Dark Matter analysis, but still were used to tag coincident events with signals in more

than one detector module.The validity of events which are considered for analysis is ured with few basic quality cuts applied to the raw data [1]. The data set discussed here was collected by eight detector modules, between July 2009 and March 2011, corresponding to a total net exposure after cuts of 730 kg days.

4.1 Acceptance region

As any of the nuclei in $CaWO_4$ can be the relevant target for WIMP scattering depending on the mass of a possible WIMP, the acceptance region is chosen such that it extends between the upper boundary of the oxygen band and the lower boundary of the tungsten band and that implicitly includes the calcium band. Since, as a result of the incoming WIMP velocities and nuclear form factors, no significant WIMP signal is expected at energies above 40 keV, the accepted recoil energies are limited by this value. The lower energy bound, in each detector module, is chosen such that the expected e/γ-leakage into the acceptance region is one event in the whole data set of that module. Due to the different resolutions (width of the bands) and levels of e/γ-background in the crystals, this value is different for each module.
A typical acceptance region is shown in orange in Figure 4 which presents in the light yield-energy plane the data set collected with one detector module (Ch51). The calculated bands for α's, oxygen recoils, and tungsten recoils shown in the figure are determined as described in [1].
With this definition of the acceptance region we find 67 accepted events in the sum over the eight detector modules used for Dark Matter analysis.

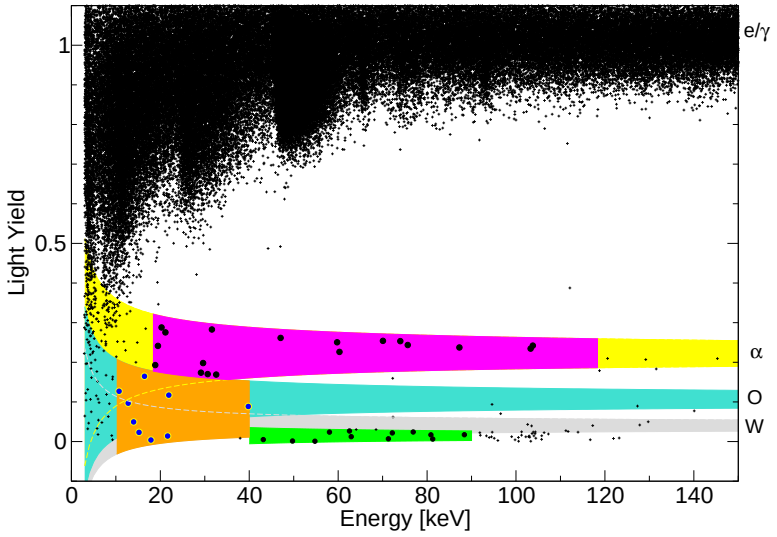

Figure 4: The data of one detector module (Ch51), shown in the light yield vs. recoil energy plane. The large population around a light yield of 1 is due to e/γ-background events. The shaded areas indicate the bands, where alpha (yellow), oxygen (turquoise), and tungsten (grey) recoil events are expected. Additionally highlighted is the acceptance region of this detector (orange) and the reference regions in the α-band (magenta) and in the ^{206}Pb-recoils band (green).

5 Background in the acceptance region

In Figure 4, next to the dominant e/γ-background, which is observed around a light yield of 1, we identify other background sources which could contribute events into the acceptance region. The scope of the analysis is to estimate the contribution of each of the identified backgrounds and to investigate a possible excess above the expectation. This is done using a maximum likelihood analysis which is thoroughly discussed in [1]. Here only its final results will be presented together with a qualitative discussion of the backgrounds in order to clarify the basic arguments and assumptions used in the analysis.

5.1 Alpha Background

In the data (see Figure 4 as an example) we observe low-energy α's with energies down to few keV. We understand these events to be due to α particles which have lost most of their energy before reaching the target crystals (for details on the housing of the detector modules see [1]). The presence of these events in our data is a consequence of the contamination with α emitters of the non-scintillating clamps holding the crystals. These events are present in all detectors, though the rates vary among modules.
Since the acceptance region has some overlap with the α-band, low energy α-events may be misidentified, leading to a certain number of background events in the acceptance region. In order to estimate this background contribution we select a reference region of the alpha band (highlighted in magenta in Figure 4) which is free of overlap with any other band. For this reference region we use an energy range of 100 keV whose low-energy bound is chosen in each detector module such that the expected e/γ-leakage is 0.1 event in the whole reference region of that module [1]. For each module we estimate in the reference region the energy spectrum dN_α/dE of the low-energy α-events. Using this spectrum we calculate for each individual module the ratio of α-events expected in the reference region and of α-events expected in the acceptance region. This ratio is then used to estimate the expected α-events in the whole acceptance region from the number of events observed in the reference region.

5.2 Lead Recoil Background

In Figure 4 we also identify an event population in and below the tungsten band around 100 keV. This population is caused by the lead nuclei from the α-decays of ^{210}Po present on the surface of the holding clamps and is present, though with different intensities, in all detector modules.
The event distribution of the ^{206}Pb recoils peaks at the full recoil energy of 103 keV but it exhibits a decreasing low-energy tail which, in some detectors, reaches the energy range of interest for Dark Matter. Since this lead-recoil band and the acceptance region overlap considerably, a leakage of some ^{206}Pb events into the acceptance region cannot be excluded.
For an estimate of this background, we follow a similar strategy as for the α background. We define a reference region for each detector module which contains predominantly ^{206}Pb recoils. As a reference region, we choose the low-energy tail of the distribution ($\leq$90 keV)

at energies above the acceptance region ($\geq$40 keV), where a possible WIMP signal cannot contribute. An example is highlighted in green in Figure 4. In this region we model the spectral energy density dN_{Pb}/dE of the ^{206}Pb events and then extrapolate the fit function into the energy range of the acceptance region to estimate the number of ^{206}Pb events expected there [1].

5.3 Neutron Background

Neutron scatterings, which mainly induce oxygen recoils in the energy range of interest, could -if neutrons are present- also contribute to events observed in the acceptance region. Differently from WIMPs, neutrons can cause coincident events in more than one detector module and this characteristic feature was exploited to estimate the contribution of neutrons to the background.
Two classes of neutron production mechanisms are identified as possibly relevant sources of background:

1. neutrons emitted by radioactive processes inside the neutron shielding (for a detailed description of the CRESST-II setup see [2, 3]);

2. neutrons produced by muons in the lead or copper shielding where the muon is missed by the veto.

For each of the two production mechanisms we used a corresponding calibration to infer the characteristic ratio between singles and coincident scatterings and to estimate from the observed coincidences the expected number of single neutron events [1].

6 Likelihood Analysis Results

The maximum likelihood fit, described in detail in [1], is based on a parameterized model of the background sources discussed in Section 5 and of a possible signal. The final results are summarized in Table 1. The total likelihood function has two maxima in the parameter space. M1 is the global maximum, but M2 is only slightly disfavored with respect to M1. The background contributions are very similar for M1 and M2 and in both cases the largest contribution is assigned to a possible WIMP signal. The possibility of two different solutions for the WIMP mass is a consequence of the different nuclei present in our target material. The given shape of the observed energy spectrum can be explained by two sets of WIMP parameters. In the case of M1, the WIMPs are heavy enough for the recoils of tungsten nuclei to appear in the energy range of the acceptance region and the possible signal is composed of 69 % of recoils on tungsten, 25 % on calcium and 7 % on oxygen. In the case of M2 tungsten recoils appear below the low-energy bound of the acceptance region. The observed signal constitutes of 52 % oxygen and 48 % calcium recoils.
Figure 5 illustrates the fit result, showing an energy spectrum of all accepted events together with the expected contributions of backgrounds and a possible WIMP signal.
The leakage of e/γ-events is the only contribution whose energy spectrum resembles that of a possible WIMP signal. A severe underestimation of this contribution could therefore

Table 1: Results of the maximum likelihood fit. The expected contributions from the considered backgrounds and from a possible WIMP signal are listed for the two solutions together with the corresponding WIMP masses and interaction cross sections. The small statistical error given for the e/γ-background reflects the large number of observed events in the e/γ-band. The other listed errors correspond to a 1σ confidence interval.

	M1	M2
e/γ-events	8.00 ± 0.05	8.00 ± 0.05
α-events	$11.5\,^{+2.6}_{-2.3}$	$11.2\,^{+2.5}_{-2.3}$
neutron events	$7.5\,^{+6.3}_{-5.5}$	$9.7\,^{+6.1}_{-5.1}$
Pb recoils	$14.8\,^{+5.3}_{-5.2}$	$18.7\,^{+4.9}_{-4.7}$
signal events	$29.4\,^{+8.5}_{-7.7}$	$24.2\,^{+8.1}_{-7.2}$
m_χ [GeV]	25.3	11.6
σ_{WN} [pb]	$1.6 \cdot 10^{-6}$	$3.7 \cdot 10^{-5}$

explain the energy spectrum of the observed excess. However, in addition to the energy spectrum, we have to take into account the information coming from the distribution in the light-yield parameter. Figure 6 shows the corresponding light-yield spectrum of the accepted events (grey) and of all events in the energy range of the acceptance region (brown), together with the expectations from all considered background sources, as inferred from the likelihood fit. The leakage of events from the e/γ-band is naturally expected to be close to the band itself. For this reason the light-yield distribution of the e/γ contribution is expected to rise towards high light yields. However, Figure 6 clearly shows that the distribution of the total accepted events does not allow a relevant increase of the e/γ contribution.

The statistical significance at which we can reject the background-only hypothesis, determined with the likelihood ratio test, is 4.7σ for M1 and 4.2σ for M2, meaning that the backgrounds which have been considered are alone insufficient to explain the data. The properties of the additional source of events indicated by the result could be satisfied by Dark Matter particles, in the form of coherently scattering WIMPs. The background contributions are nonetheless still relatively high, therefore a reduction of the overall background rate is necessary to reduce the uncertainties in the modeling of it and to clarify the observation.

Despite the fact that we have an unfavorable situation in terms of background, it is still interesting to study the WIMP parameter space compatible with our observations. Figure 7 shows the location of the two likelihood maxima in the $(m_\chi, \sigma_{\mathrm{WN}})$-plane, together with the 1σ and 2σ confidence regions. The latest result is consistent with the data of an earlier CRESST run [2] where only tungsten nuclei were considered as a possible target for WIMP scatterings and the 1σ region of M1 is slightly disfavored. The same data of [2] have been reanalyzed considering all three nuclear recoil bands like it is done in the analysis of the present data [1] to increase the sensitivity for light WIMPs. The resulting exclusion limit, which is above the 2σ regions of [1], is shown in Figure 7.

The parameters derived from our observation are in tension with the limits published by

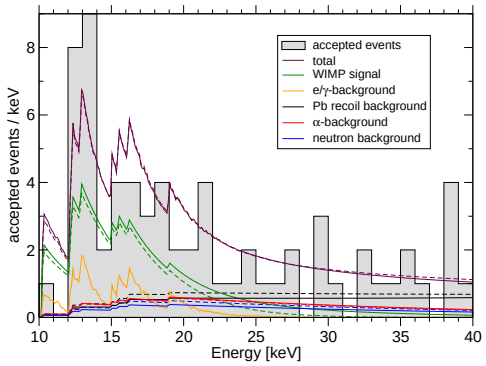

Figure 5: Energy spectrum of the accepted events from all detector modules, together with the expected contributions from the considered backgrounds and a possible WIMP signal, as inferred from the likelihood fit. The solid and dashed lines correspond to the fit results for M1 and M2, respectively.

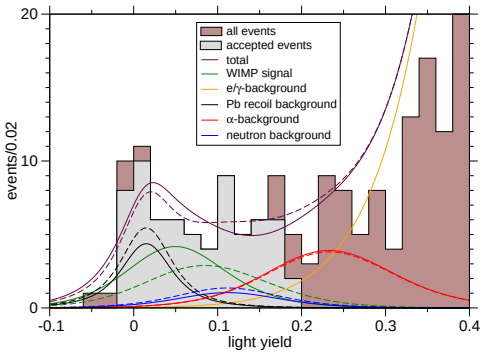

Figure 6: Light-yield distribution of all events in the energy range of the acceptance region (brown) and of the accepted events (grey). The expected contributions of background and of a possible WIMP signal from the likelihood fit are calculated for the fixed yield range of the plot. Outside the (energy dependent) yield boundaries of the acceptance region they are extrapolations of the fit. The solid and dashed lines correspond to the parameter values in M1 and M2, respectively.

other experiments [4, 5, 6]. Furthermore, the parameter regions compatible with the observation of DAMA/LIBRA (regions taken from [8]) and CoGeNT [7] are located outside the 2σ CRESST region.

7 Preparations for the next run

In the reporting period a new run has been prepeared with modificatons of detectors and setup aiming at a significant reduction of the overall background level. The most important modification addresses the reduction of the α and ^{206}Pb-recoil backgrounds. Another modification addresses the neutron background. Our main goal for the next run is to either confirm or reject the presence of a low mass WIMP signal with high confidence and negligible systematic uncertainties due to the modeling of backgrounds. In the following sections we will briefly describe the measures for the reduction of background.

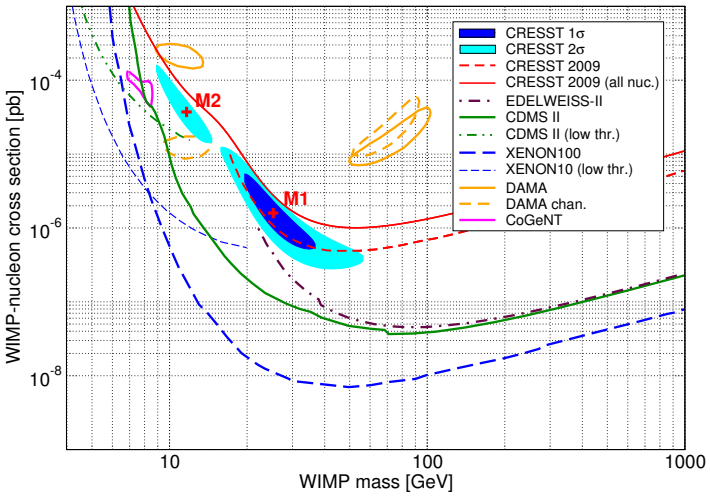

Figure 7: The WIMP parameter space compatible with the latest CRESST results. The CRESST contours have been calculated with respect to the global likelihood maximum M1. In addition the exclusion limits from CDMS-II [4], XENON100 [5], and EDELWEISS-II [6] are shown as well as the 90% confidence regions favored by CoGeNT [7] and DAMA/LIBRA [8]. For comparison we also show the CRESST limit obtained in an earlier run [2] in 2009 and the results of the reanalysis of the same run which takes into account all three nuclei in the target material.

7.1 Measures for reduction of background

7.1.1 Neutron background

The neutron shielding in the last run consisted of ∼40 cm of polyethylene (PE) surrounding the Pb/Cu shielding. The remaining neutron background in the data was most likely from neutrons in the Pb/Cu shielding, either generated by radioactive processes in the shielding material or by muons penetrating the Pb/Cu shielding without triggering the muon veto. Such neutrons inside the Pb/Cu shileding have relatively low kinetic energies and can effectively be moderated already by a relatively thin plastic layer placed inside the Pb/Cu shield. In the next run we will therefore install a 5 cm thick polyethylene layer inside the Pb/Cu shield. It is expected to reduce the background from neutrons originating in the Pb/Cu shield by more than an order of magnitude. Part of this shielding will be placed in vacuum inside the cold box, and another overlapping part outside. The outside part may be removed to still allow a neutron test with an external neutroun source during the run.

7.2 Degraded α's and ^{206}Pb nuclear recoil background

The silver coated bronze clamps holding the target crystal, which provide the only non scintillationg surface inside the detector housing, were identified as the source of these two types of backgrounds in the last run. The degraded α-particles observed at low energies can be attributed to a significant ^{210}Pb contamination in the bulk material (Cu-Sn bronze) of the clamps, while the ^{206}Pb recoil background was from ^{210}Po or ^{210}Pb atoms deposited

at the surface of the silver coated clamps. The range of the 103 keV Pb recoils in silver is just a few tens of atomic layers, and it is only the contamination of the surface which matters here.

The ^{210}Pb atoms may have been deposited during an exposure to radon in air after production of the clamps, e.g. while mounting of detectors in the cold box at Gran Sasso. The cool down of the last run was interrupted by the L'Aquila earthquake and detectors had to be repaired and remounted again underground after the earthquake, before the successful cool down took place. This resulted in a prolonged exposure of about 6 weeks to radon in the air of the underground laboratory.

On the other hand, a very rapid deposition of ^{210}Po may have occurred at the end of the electrolytic silver coating process in the moment, when the voltage was disconnected [9]. Both types of initial deposits, ^{210}Po or ^{210}Pb, can be distinguished via the resulting time dependence of the rate of ejected ^{206}Pb recoils. When ^{210}Pb is deposited, the rate will *increase* with the 138 days half life of ^{210}Po. However, when ^{210}Po is deposited the rate will decrease with the same half life. An analysis of the data of the last run indicates a rise of the rate and and suggests that it is 210Pb freshly deposited just before the start of the run, which is responsible for most of the events in the Pb reference region. This supports the hypothesis that exposure of the clamps to radon in air may have contributed a significant fraction of the low energetic ^{206}Pb recoil background observed in the last run and preventing radion exposure of the clamps may significantly reduce this background.

7.2.1 Radon prevention during assembly and mounting of detectors

Originally we planned to assemble detectors for next run in the clean room at MPI and use radon reduced air for mounting of detector modules in the cryostat. The clean room ventilation in Munich was modified to get fresh air with a high flow from about 15 m above ground, where we expected the radon level to be relatively low. First tests in early spring 2012 gave radon levels below $\sim$5 Bq/m^3. However, with rising temperatures outside, the overall level increased and sometimes peaks well above 10 Bq/m^3 were measured. This forced us to give up the plan of conveniently assembling detector modules in the clean room at MPI. An intermediate attempt of mounting in an existing glove box under N_2 atmosphere proved to be too slow and too difficult.

In autumn 2012 we finally decided to build a tight metallic housing around our already existing laminar flow area at the top floor of the CRESST building at Gran Sasso and supply it with deradonized (¡5[mBq/m^3]) air. This setup for assembling detectors has been completed in January 2013.

Additionally, a space around the coldbox of the cryostat was prepared, which can be flushed with deradonized air to avoid radon during the phase of mounting of detectors in the cold box.

7.2.2 New clamps

We made a new bronze material from selected Cu and extremely high purity tin and fabricated new clamps from this material. A small tin sample was converted into a cryogenic calorimeter to measure the rate of alpha decyas occurring in the volume. In this measurement no ^{210}Po decay was observed, which translates into an upper limit of the

^{210}Po activity of ¡ 28 mBq/kg. With this type of measurement were able to improve the limit which can be obtained with a conventional low background Ge detector by almost two orders of magnitude. All production steps from the starting material to the final clamps were carefully controlled with mass spectrometry measurements of iostopes in the natural decay chains.

We are very confident that the background of degraded alphas with this new clamps will practically disappear. Instead of using a problematic silver coating, the surface of the clamps is sputter etched and then sputter coated with aluminum. After sputter coating clamps were stored in containers continuously flushed with N^2 gas.

7.3 Schedule and perspectives of next run

We expect to be ready to mount 18 detector modules in the CRESST setup at Gran Sasso. All modules will be equipped with new clamps and more than half of them with new light detectors. Those light detectors with poor performance in the last run and those which had a transition temperature too low to be reached by the cryostat have been replaced. Six of these 18 detector modules will have design modifications to allow active discrimination of recoil nuclei from alpha decays, while the remaining detector modules will rely on radon prevention.

The main physics goal of next run is to either confirm or reject the low mass WIMP hypothesis with high confidence. With the larger number of detector modules and the experience gained during last run we aim to collect more then 2000 kg-days of data in two years.

References

[1] Godehard Angloher et al. Results from 730 kgdays of the CRESST-II dark matter search. *Eur. Phys. J. C*, 72(4), 2012.

[2] Godehard Angloher et al. Commissioning run of the CRESST-II dark matter search. *Astropart. Phys.*, 31:270, 2009.

[3] G. Angloher et al. Limits on WIMP dark matter using scintillating $CaWO_4$ cryogenic detectors with active background suppression. *Astropart.Phys.*, 23:325, 2005.

[4] Z. Ahmed et al. Dark matter search results from the CDMS II experiment. *Science*, 327:1619, 2010.

[5] E. Aprile et al. Dark matter results from 100 live days of xenon100 data. 107:131302, 2011.

[6] E. Armengaud et al. Final results of the EDELWEISS-II wimp search using a 4-kg array of cryogenic germanium detectors with interleaved electrodes. *Phys. Lett. B*, 702:329, 2011.

[7] C. E. Aalseth et al. Search for an annual modulation in a *p*-type point contact germanium dark matter detector. *Phys. Rev. Lett.*, 107:141301, 2011.

[8] Christopher Savage et al. Compatibility of DAMA/LIBRA dark matter detection with other searches. *JCAP*, 0904:010, 2009.

[9] F.L.Romines S.C.Ehinger, R.A.Pacer. Separation of the radionuclides ^{210}Pb-^{210}Bi-^{210}Po by spontaneous deposition onto noble metals and verification by cherenkov and liquid scintillation counting. *Journal of Radioanalytical and Nuclear Chemistry*, 98(1):39, 1986.

CUORE
2012 LNGS Report

F. Alessandria,[1] R. Ardito,[2] D. R. Artusa,[3, 4] F. T. Avignone III,[3] O. Azzolini,[5] M. Balata,[4] A. Bau,[6,7] T. I. Banks,[4, 8, 9] G. Bari,[10] J. Beeman,[11] F. Bellini,[12, 13] A. Bersani,[14] M. Biassoni,[6, 7] T. Bloxham,[9] C. Brofferio,[6, 7] C. Bucci,[4] X. Z. Cai,[15] L. Canonica,[4] X. Cao,[15] S. Capelli,[6, 7] M. Capodiferro,[13] L. Carbone,[7] L. Cardani,[12, 13] M. Carrettoni,[6, 7] N. Casali,[4] D. Chiesa,[6, 7] N. Chott,[3] M. Clemenza,[6, 7] C. Cosmelli,[12, 13] O. Cremonesi,[7] R. J. Creswick,[3] I. Dafinei,[13] A. Dally,[16] V. Datskov,[7] A. De Biasi,[5] M. M. Deninno,[10] S. Di Domizio,[14, 17] M. L. di Vacri,[4] L. Ejzak,[16] R. Faccini,[12, 13] D. Q. Fang,[15] H. A. Farach,[3] M. Faverzani,[6, 7] G. Fernandes,[14, 17] E. Ferri,[6, 7] F. Ferroni,[12, 13] E. Fiorini,[6, 7] M. A. Franceschi,[18] S. J. Freedman,[8, 9, ‡] B. K. Fujikawa,[9] R. Gaigher,[7] A. Giachero,[6, 7] L. Gironi,[6, 7] A. Giuliani,[19] J. Goett,[4] P. Gorla,[4] C. Gotti,[6, 7] E. Guardincerri,[4, 9, *] T. D. Gutierrez,[20] E. E. Haller,[11, 21] K. Han,[9] K. M. Heeger,[16] H. Z. Huang,[22] M. Iannone,[13] R. Kadel,[23] K. Kazkaz,[24] G. Keppel,[5] L. Kogler,[8, 9, †] Yu. G. Kolomensky,[8, 23] D. Lenz,[16] Y. L. Li,[15] C. Ligi,[18] X. Liu,[22] Y. G. Ma,[15] C. Maiano,[6, 7] M. Maino,[6, 7] M. Martinez,[25] R. H. Maruyama,[16] R. Mazza,[7] Y. Mei,[9] N. Moggi,[10] S. Morganti,[13] T. Napolitano,[18] S. Newman,[3, 4] S. Nisi,[4] C. Nones,[26] E. B. Norman,[24, 27] A. Nucciotti,[6, 7] T. O'Donnell,[8] F. Orio,[13] D. Orlandi,[4] J. L. Ouellet,[8, 9] M. Pallavicini,[14, 17] V. Palmieri,[5] A. Passerini,[6,7] L. Pattavina,[7] M. Pavan,[6, 7] M. Pedretti,[24] A. Pelosi,[13] M. Perego,[7] G. Pessina,[7] G. Piperno,[12, 13] S. Pirro,[7] E. Previtali,[7] V. Rampazzo,[5] F. Rimondi,[10, 28, ‡] C. Rosenfeld,[3] C. Rusconi,[7] E. Sala,[6, 7] S. Sangiorgio,[24] N. D. Scielzo,[24] M. Sisti,[6, 7] A. R. Smith,[29] F. Stivanello,[5] L. Taffarello,[30] M. Tenconi,[19] F. Terranova,[7] W. D. Tian,[15] C. Tomei,[13] S. Trentalange,[22] G. Ventura,[31, 32] M. Vignati,[13] B. S. Wang,[24, 27] H. W. Wang,[15] T. Wise,[16] A. Woodcraft,[33] L. Zanotti,[6, 7] C. Zarra,[4] B. X. Zhu,[22] S. Zucchelli[10, 28]

(The CUORE Collaboration)

[1]INFN - Sezione di Milano, Milano I-20133 - Italy
[2]Dipartimento di Ingegneria Strutturale, Politecnico di Milano, Milano I-20133 - Italy
[3]Department of Physics and Astronomy, University of South Carolina, Columbia, SC 29208 - USA
[4]INFN - Laboratori Nazionali del Gran Sasso, Assergi (L'Aquila) I-67010 - Italy
[5]INFN - Laboratori Nazionali di Legnaro, Legnaro (Padova) I-35020 - Italy
[6]Dipartimento di Fisica, Università di Milano-Bicocca, Milano I-20126 - Italy
[7]INFN - Sezione di Milano Bicocca, Milano I-20126 - Italy
[8]Department of Physics, University of California, Berkeley, CA 94720 - USA
[9]Nuclear Science Division, Lawrence Berkeley National Laboratory, Berkeley, CA 94720 - USA
[10]INFN - Sezione di Bologna, Bologna I-40127 - Italy
[11]Materials Science Division, Lawrence Berkeley National Laboratory, Berkeley, CA 94720 - USA
[12]Dipartimento di Fisica, Sapienza Università di Roma, Roma I-00185 - Italy
[13]INFN - Sezione di Roma, Roma I-00185 - Italy
[14]INFN - Sezione di Genova, Genova I-16146 - Italy

[15]Shanghai Institute of Applied Physics (Chinese Academy of Sciences), Shanghai 201800 - China
[16]Department of Physics, University of Wisconsin, Madison, WI 53706 - USA
[17]Dipartimento di Fisica, Università di Genova, Genova I-16146 - Italy
[18]INFN - Laboratori Nazionali di Frascati, Frascati (Roma) I-00044 - Italy
[19]Centre de Spectrométrie Nucléaire et de Spectrométrie de Masse, 91405 Orsay Campus - France
[20]Physics Department, California Polytechnic State University, San Luis Obispo, CA 93407 - USA
[21]Department of Materials Science and Engineering, University of California, Berkeley, CA 94720 - USA
[22]Department of Physics and Astronomy, University of California, Los Angeles, CA 90095 - USA
[23]Physics Division, Lawrence Berkeley National Laboratory, Berkeley, CA 94720 - USA
[24]Lawrence Livermore National Laboratory, Livermore, CA 94550 - USA
[25]Laboratorio de Fisica Nuclear y Astroparticulas, Universidad de Zaragoza, Zaragoza 50009 - Spain
[26]Service de Physique des Particules, CEA / Saclay, 91191 Gif-sur-Yvette - France
[27]Department of Nuclear Engineering, University of California, Berkeley, CA 94720 - USA
[28]Dipartimento di Fisica, Università di Bologna, Bologna I-40127 - Italy
[29]EH&S Division, Lawrence Berkeley National Laboratory, Berkeley, CA 94720 - USA
[30]INFN - Sezione di Padova, Padova I-35131 - Italy
[31]Dipartimento di Fisica, Università di Firenze, Firenze I-50125 - Italy
[32]INFN - Sezione di Firenze, Firenze I-50125 - Italy
[33]SUPA, Institute for Astronomy, University of Edinburgh, Blackford Hill, Edinburgh EH9 3HJ - UK
*Presently at: Los Alamos National Laboratory, Los Alamos, NM 87545 - USA
†Presently at: Sandia National Laboratories, Livermore, CA 94551 - USA
‡Deceased

Abstract

The Cryogenic Underground Observatory for Rare Events (CUORE) is an experiment designed to exploit the cryogenic bolometer technique to reach a sensitivity of the order 10^{26} years on the $\beta\beta(0\nu)$ half-life of ^{130}Te, thus approaching the inverted hierarchy region of the neutrino masses. The detector will consist of a close-packed array of TeO_2 crystals containing $\sim$ 206 kg of ^{130}Te in total and cooled to an operating temperature of $\sim$ 10 mK inside a large, dedicated cryostat. We report on activities carried out in 2012 for the CUORE neutrinoless double beta decay experiment.

1 Introduction

The Cryogenic Underground Observatory for Rare Events (CUORE) [1] is a cryogenic bolometer experiment designed to search for $\beta\beta(0\nu)$ in the isotope ^{130}Te. The CUORE detector will consist of a close-packed array of 988 TeO_2 crystals containing $\sim$ 200 kg of ^{130}Te and cooled inside a large cryostat to 10 mK. At this low temperature the crystals function as highly sensitive calorimeters, converting the relatively small energies deposited inside them by particles into measurable rises in temperature. The expected signature of $\beta\beta(0\nu)$ in ^{130}Te is a peak in the measured energy spectrum at 2527 keV, the Q value for the transition $^{130}\text{Te} \rightarrow ^{130}\text{Xe} + 2\beta^-$. The current best limit on $\beta\beta(0\nu)$ in ^{130}Te, $\tau_{1/2}^{\beta\beta(0\nu)} > 2.8 \times 10^{24}$ y (90% C.L.), comes from CUORE's predecessor, the Cuoricino experiment [2]. The Cuoricino detector was comprised of a tower of 62 TeO_2 crystal bolometers containing 11 kg of ^{130}Te and operated in a cryostat at the underground Laboratori Nazionali del Gran Sasso (LNGS), Italy, from 2003–2008.

The goal of CUORE is to built off the experience and results obtained with Cuoricino to search for the $\beta\beta(0\nu)$ decay mode by making a low-background, high-precision measurement of the spectrum in a narrow energy window around the Q value of the decay. The experiment will improve upon the Cuoricino results by two orders of magnitude and be sensitive to an effective Majorana neutrino mass of the order of 50 meV, better than any previous experiment. While the primary focus of the experiment is to search for $\beta\beta(0\nu)$, the technique can also make extremely sensitive measurements of other tellurium decay modes [3, 4], and other rare processes, such as searches for dark matter [5] and axions [6].

The experiment is now in the construction phase in Hall "A" of Laboratori Nazionali del Gran Sasso (LNGS) where the rock overburden provides 3650 m.w.e. of shielding against cosmic rays, while the cryostat has numerous internal and external lead shields to block natural environmental radiation.

2 Detector components

The CUORE array of 988 TeO_2 crystals will be arranged in a cylindrical matrix of 19 identical towers each containing 52 crystals held securely inside a copper structure by specially designed PTFE brackets (Fig. 1). After a tower is assembled, wires are bonded directly from the thermistor temperature sensor and Joule heater glued to each crystal to readout ribbons held in specially designed copper trays fixed to the tower structure. A complex procedure for cleaning the tower's copper parts—the so-called "TECM" process, based on a sequence of mechanical, electro-chemical, chemical, and magneto-plasma treatments—has been developed in order to guarantee that background contributions from radioactive surface contaminants are reduced to an acceptable level. However, due to concerns about the slow pace of this cleaning process we are also exploring alternative methods for shielding the crystals from copper surface contaminants—namely, by coating the copper parts in parylene or by wrapping them with polyethylene.

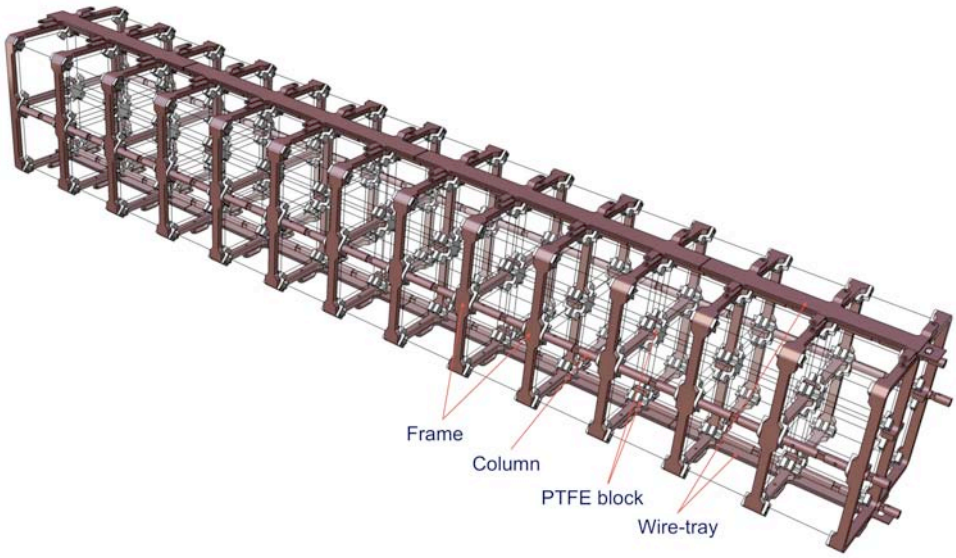

Figure 1: Detailed view of the components of a single CUORE tower.

2.1 Crystals

The $5 \times 5 \times 5$ cm^3 TeO_2 crystals are being produced at the Shanghai Institute of Ceramics, Chinese Academy of Sciences (SICCAS). Crystal production has been steadily ongoing since 2009 at a dedicated clean room facility in Jiading, China, and batches of finished crystals are shipped to LNGS every 1–2 months, traveling by sea to limit cosmogenic activation. By mid-2013, all the crystals will have been delivered to LNGS, where they are stored in nitrogen-fluxed cabinets in CUORE's underground Parts Storage Area (PSA).

All materials used in crystal production are independently checked by high-sensitivity ICPMS measurements in China (SINAP), the US (LBNL), and Italy (Milano/LNGS). This quality assessment ensures that bulk radioactive contaminations in the finished crystals are below acceptable levels. If a failure is detected, the corresponding batch is reprocessed. Indeed, earlier this year ICPMS analysis on a batch of Te and TeO_2 revealed Bi contamination levels 50 times above the contract limit. Although this created a 3-month interruption in crystal production, it prevented the situation from developing into something far worse. To eliminate possible radioactive surface contaminations, the crystals are lapped with specially selected, radiopure SiO_2 powders at SICCAS immediately before being vacuum-packed in a triple-layered PET bag.

Approximately 4% of the delivered crystals are tested as cryogenic bolometers to verify their radiopurity and to check overall performance. In these so-called CUORE Crystal Validation Runs (CCVRs), four crystals are randomly selected from the most recent shipments, assembled into a detector module, and cooled to 10 mK inside the CUORE R&D cryostat in Hall C at LNGS. Each CCVR typically lasts for ~ 1 month to acquire sufficient statistics needed to verify that the crystals meet contract specifications. All of the tested crystals have met or exceeded the desired energy resolution and the contract specifications for bulk radioactivity and dimensional tolerances. Based on this, we expect all crystals to meet the requirements for CUORE. We are actively pursuing

an arrangement with SICCAS to bring workers to LNGS for a brief period in 2013 to reprocess the surfaces of former CCVR crystals for inclusion in CUORE, in order to arrive at our target of 988 crystals.

2.2 NTD thermistors

Each CUORE crystal will be instrumented with a neutron-transmutation-doped (NTD) Ge thermistor for temperature readout. These devices are produced by irradiating pure Ge wafers in a research reactor at MIT for precise lengths of time and then sending the wafers to LBNL to be cut into thermistors. Thus far, more than 1000 thermistors have been prepared to the desired doping level in this manner. Two backup wafers were doped to the nominal level and are now being processed and tested in a cryostat at Berkeley. We have enough thermistors to implement the 988 crystals in CUORE.

2.3 Copper parts

The copper parts that will form the scaffolding for the CUORE detector towers are fabricated in the Milano and Legnaro workshops, cleaned at LNL (Laboratori Nazionali di Legnaro) according to a special protocol, and then placed in underground storage at LNGS until the time comes for assembly. Both the design of the tower structure and the surface cleaning methods are rather different with respect to those used in Cuoricino. A complete test of the copper fabrication, cleaning, and assembly sequence was possible only via the construction and operation of the CUORE-0 tower.

A first attempt at assembling the CUORE-0 tower was carried out in October 2011 and revealed two serious problems: Some of the frames had not been machined to specification, and much of the copper had been rendered too soft by the plasma cleaning. Both issues were immediately investigated and quickly resolved. It was determined that anomalous consumption of machining tools was to blame for the out-of-spec frames. A new protocol was developed and tested and will be applied to all future production. Frames that had already been produced but not yet cleaned were remachined to specification. A stricter quality check has also been implemented in which the copper components for each tower will first be individually measured and then assembled immediately after fabrication, prior to cleaning. The excessively soft copper was determined to have resulted from excessive heating during the plasma cleaning. A three-month R&D campaign was conducted to develop and test a new optimized protocol for this particular step of the cleaning process. A batch of newly machined copper parts for CUORE-0 were cleaned starting in the latter half of February 2012 and delivered to LNGS on March 20. A test assembly of the new parts indicated they were satisfactory, and the CUORE-0 tower was successfully assembled shortly thereafter.

Production of copper parts for the CUORE towers has been steadily ongoing. The production process was sped up slightly to make up for the time spent replacing the flawed parts for CUORE-0 and three CUORE towers. To streamline the production line, copper parts (including frames that until now were produced only at LNL) will first be machined at the Milano-Bicocca workshop and then sent to the LNL workshop for final refinements. A recent parts inventory revealed that 150–200 replacement columns and

20 additional frames will need to be added to the production queue for CUORE. Thanks to the improved efficiency of the production line this will push back the expected end of production by no more than $\sim$ 2 months, i.e., from November 2012 to March 2013.

Regular TECM cleaning of CUORE copper parts recommenced after Easter 2012. A new, second plasma cleaning machine was recently incorporated into the cleaning line and will increase throughput. Several quality checks have been introduced at various points in the cleaning process. Samples of leftover, unused cleaning acid are regularly sent to Milano-Bicocca to be assayed for contamination. Of greater concern is the possibility of contamination *during* the plasma cleaning, as there have been indications in the past that the copper somehow collected ^{210}Pb in the course of the process. For this reason the plasma machines have been thoroughly cleaned, and samples of plasma-cleaned copper pieces are regularly sent to Milano-Bicocca to be checked for evidence of alpha contamination. Recently a problem was found in the sample pieces produced with the second plasma cleaning machine. The machine was briefly taken out of service and thoroughly cleaned. New samples produced with the recleaned plasma machine are currently being measured, and first results on the alpha spectroscopy chain indicate no contamination. Despite this problem, TECM cleaning remains on schedule.

TECM cleaning requires a large amount of specialized manpower and time. For this reason two alternative approaches are being considered:

- **Polyethylene wrapping of the copper parts** — This is a well-tested technique that has exhibited reproducible results in previous cryogenic studies, both in regards to radioactivity and detector performance. Covering the copper with polyethylene results in background levels in the $\beta\beta(0\nu)$ region comparable with TECM-cleaned copper. The main difficulty in applying this technique to CUORE lies in making it compatible with the assembly line. Namely, the wrapping must be performed inside glove boxes in an efficient manner, and the wrapping musn't interfere with the tight mechanical tolerances for the assembled towers. Effort was made this year in developing an optimal procedure for polyethylene wrapping. The procedure consists in wrapping the parts followed by a heating of the assembled copper structure to about 80 C. Heating shrinks the film, which both improves its adhesion to the copper and reduces its profile, making it easier to handle the parts during detector assembly. Before the end of 2012 all of the copper parts used in the CUORE mockup tower will be wrapped with polyethylene and then assembled to check the procedure and identify any problems.

- **Parylene coating of the copper parts** — Parylene is a commonly used coating obtained by sublimating a dimer and allowing it to deposit on the surface of an item as a polymer film. The coating is performed at room temperature in a vacuum chamber that yields uniform deposition on all exposed surfaces, regardless of shape. With this procedure the copper can be efficiently covered with a film of the desired thickness. There are many advantages to this procedure: the coating process is relatively fast and easy; parylene adheres to copper better than polyethylene; the parylene film is very thin and so the copper parts can be handled in the same way as the TECM-cleaned parts; and the parylene powder can be purified to control its radioactivity. It is already well established that parylene film coatings maintain

their integrity at cryogenic temperatures, and we are now operating at LNGS a 12-crystal array in which both the copper and PTFE parts were coated with a 50-micron parylene film. If the background counting rate measured by this array in the $\beta\beta(0\nu)$ region is compatible with polyethylene or TECM techniques, it will only remain to validate that parylene-coated parts are compatible with the tower assembly procedure.

3 Electronics and data acquisition

The main goal of the CUORE electronics is to provide an effective low-noise system for reading out the detector and monitoring/optimizing its performance. The data acquisition system records the data and provides a link with the slow-control and analysis tools.

3.1 Front-end electronics

The design of the main CUORE board was completed at INFN Milano-Bicocca. It consists of 8 layers of 233×280-mm^2 PCB that accommodates 6 channels, each consisting of a preamplifier and a second-stage PGA, the load resistors and biasing system of the detector, and a number of other features. It contains more than 1000 components and is remotely accessible via CAN-bus serial bus. Prototyping and components procurement are now ongoing at USC. The backplane board for the main CUORE board has been finished and prototyped. The design of the pulser boards is ongoing, while the design of the power supplies was recently restarted. The connecting link between the mixing chamber and room temperature is undergoing tests at Milano-Bicocca. The final phase of the characterization and calibration of the preamplifiers is underway and procedures have been established to test the Bessel boards. USC has produced the boards for the DC/DC converting system and is starting to assemble components on the pre-production batch to be tested, hopefully, on CUORE-0. A number of Bessel boards are expected from USC, for bandwidth optimization in CUORE-0. The parameters of the Bessel filters have been optimized and construction will start shortly.

3.2 Faraday cage

The design of the CUORE Faraday cage is ongoing. The cage is needed to shield the cryostat, the high-impedance electrical links, and the electronics from disturbances coming from the main power line (50 Hz), cryogenic pumps, and any other EMI interferences which may arrive from outside. The preliminary concept is to exploit the existing carpentry of the hut as a mechanical support for low-weight shielding panels and doors. The total shielding surface will be close to 150 m^2. The selected shielding material will be a flexible ferromagnetic alloy of 0.2 mm thickness.

3.3 Slow Control

The CUORE Slow Control System (SCS) will monitor and supervise several sub-systems. The study and design of the SCS was initiated at the beginning of 2012. A typical

solution is based on distributed processes (clients/servers) controlled from a central location (server) and divided into different layers. Three possible software candidates have been identified: EPICS, Tango, and Tine. Tests of these packages are ongoing.

3.4 DAQ

After a dedicated benchmark test it was decided to organize the $\sim$ 1000 CUORE data acquisition channels into six chassis, each controlled by a separate computer. In this configuration each chassis will host 10–11 NI PXI-6284 DAQ boards. This modularity was chosen as the best tradeoff between cost and computing power per channel. Because of limited funds, only a part of the necessary material has been bought this year: 6 chassis, 6 controller boards, and 42 digitizer boards. The remaining 22 digitizer boards, as well as 128 signal cables, will be purchased in 2013.

4 Cryogenics

The concluding phase of the recovery plan for the critical stainless-steel-to-copper weld on the 300K vessel was carried out during the first half of April 2012. The vessel was delivered to Camerana on April 26. X-ray inspections done after the removal of the back material again indicated no lack of fusion. Only shallow or mid-depth porosities were identified and it was therefore decided to proceed with the TIG welding of the steel flange and the cleaning of the 300K vessel. The acceptance tests were performed at the SIMIC company's construction site in Camerana. The tests, carried out by INFN personnel with local support from SIMIC, included vacuum tests of the 4K and 300K vessels, overpressure tests of the 4K and 300K vessels, cold tests with LN_2 (77 K) of the 4K vessel, and mechanical tests of the 40K vessel.

After individual vacuum and pressure tests of both the 300K and 4K vessels, a vacuum test was carried out at 77 K by inserting the 4K vessel into the 300K vessel (without the 40K vessel in between) using the same elements to be employed later at LNGS during the final commissioning.

The low-temperature test was carried out twice. Both the 300K and the 4K vessels were demonstrated to be vacuum-tight. All weldings were tested with He bags and revealed no leaks at the level $< 2\times10^{-9}$ mbar l/s.

Particular care was devoted to the critical Cu-steel weldings that caused the delay experienced in 2011. In addition, no deterioration of mechanical properties or vacuum tightness was reported after the pressure and cold tests. In the two low-temperature cycles the target temperature (about 82 K) was reached smoothly (the cooldown rate with superinsulation in the 4K vessel was 3.5 K/h) but we observed a vacuum leak below 160 K. The leak was traced to defective flanges on the fast-cooling ports, which were used to inject nitrogen in the inner vessel. This is the only anomaly reported during the tests, which otherwise showed the vessels to be well within spec. The vessels and the plates were delivered to LNGS on July 17 and Phase I of the commissioning started on July 30. The aim of Phase I is to:

- Mount the cryostat down to the 4K vessel in its near-final configuration (excepting only the bars that hold the three innermost vessels and the fast cooling ports);
- Mount the detector suspensions down to 4 K and measure their response with dummy loads in air and vacuum;
- Mount one complete DCS line and test it both at room temperature and at 4 K;
- Cool the cryostat without thermal loads down to 4 K using three pulse tubes (PTs) mounted in their final configuration.

The three plates, the suspensions, and the three vessels have been mounted inside the CUORE clean room at LNGS. In addition, one DCS line was mounted and mechanically checked. All parts needed for Phase I are either in place or available with very few exceptions. Work is in progress for the realization of the thermalizations of the PTs, the characterization and gilding of the PTs before their installation into the cryostat, and for the readout of the thermometers to be used during the first cooldown to 4 K.

In parallel to Phase I of the commissioning, we progressed in the design and procurement of the parts needed for Phase II, which aims to bring the cryostat to base temperature (10 mK) without thermal loads. Its preparation includes the standalone test of the dilution unit, the construction of the three innermost vessels, and the production of the Fast Cooling System. The startup of Phase II is scheduled for April 2013.

4.1 Cooling unit

The power to operate the CUORE detectors in the 10-mK range is provided by a cooling system based on a closed-cycle, cryogen-free, high-power ^{3}He/^{4}He dilution refrigerator system (DRS). The DRS has been completed and successfully tested in July 2011. The result in terms of cooling power, is extremely good: 8 W at 12 mK is safely larger than the 5 W requested in the specifications. The lowest base temperature obtained was about 5.26 mK. The final test dewar was then produced and the DRS completely disassembled and modified in order to meet to the CUORE cryostat specifications. At this point a frustrating leak on the ^{3}He/^{4}He circuit appeared. A number of cooling tests were then carried out to eliminate the leak, and in March 2012 Leiden Cryogenics completed a new temperature test in which no leak was observed. The final test under the supervision of the CUORE collaboration experts was successfully performed at the end of March 2012. The DRS was packed and shipped to LNGS together with the test cryostat in May 2012. Unfortunately during the shipment a bellow connection of the DRS broke. The broken part was sent back to Leiden Cryogenic, repaired, and returned to LNGS on September 18, 2012. G. Frossati from Leiden Cryogenics visited LNGS in October 2012 to reassemble the DRS and perform a complete onsite commissioning of the test cryostat. Starting from November, the test cryostat has been used for several tests (including the CUORE wiring system section from 300 K to 10 mK) before the completion of the CUORE cryostat. The fast cooling system (FCS) is a forced He gas circulation system designed to improve the conductance to the internal parts of the cryostat+detector+shield system during its initial cooldown. The FCS design, finalization, and fabrication are proceeding in parallel

in order for it to be delivered in March 2013, for the final test of the DRS inside the CUORE cryostat.

5 The Detector Calibration System (DCS)

The CUORE detector calibration system (DCS) consists of 12 radioactive source strings that are able to move, under their own weight, through a set of guide tubes that route them from outside the cryostat at 300 K to their locations between the bolometers in the detector region inside the cryostat. The DCS consists of a vacuum motion system above the 300K flange, a thermalization mechanism at the 4K stage of the cryostat, and a set of guide tubes in the lower region of the cryostat. Weak ^{232}Th radioactive sources are integrated into a Kevlar-based string with copper crimps and teflon coating to minimize friction. For the energy calibration of the CUORE detector array with radioactive sources the source strings are moved into the detector region of the cryostat, and removed during regular data taking. The calibration of the entire array of 988 crystals is expected to take about 1 day, plus about 1-2 days of insertion and retraction time. The source insertion and energy calibration with radioactive sources is expected to be performed about once a month during the regular operation of CUORE.

Recently the calibration group accomplished the following tasks:

1. We completed the fabrication of the hardware for the DCS 4K, full-scale test planned during the assembly and commissioning of the cryostat at LNGS. This includes a test beam for mounting the guide tubes, the thermalization mechanism, and guide tubes. This hardware test system continues to be tested at the University of Wisconsin until the planned 4K test at lNGS in early 2013.

2. The S-shaped guide tubes between 300K and 4K have been redesigned to accommodate a possibly larger than expected variation in the flange position during cool down. A custom design for guide tubes based on flexible vacuum bellows was developed including a custom teflon insert. The first set of these new guide tubes was fabricated and installed in the cryostat at LNGS in September 2012. Detailed motion tests with these new guide tubes have been performed at Wisconsin. All remaining S-tubes are being fabricated right now and will be installed in early 2013.

3. Production of the radioactive source strings is complete and as-built production drawings and documentation have been prepared.

4. Using a new 10K test setup at Wisconsin detailed thermal testing of the cool down of the source capsules as well as operation of the thermalization mechanism was performed. The cool down of the source strings performed as expected. Long-term motion testing with the thermalization mechanism is under way. Intermittent motion issues with the ultra-clean motion surfaces is under investigation. A possible backup for the motion design of the thermalization mechanism is being developed.

Installation of the DCS started with the successful installation of the S-tubes between the 300K and 4K flanges in September 2012. Figure 2 shows the newly designed S-

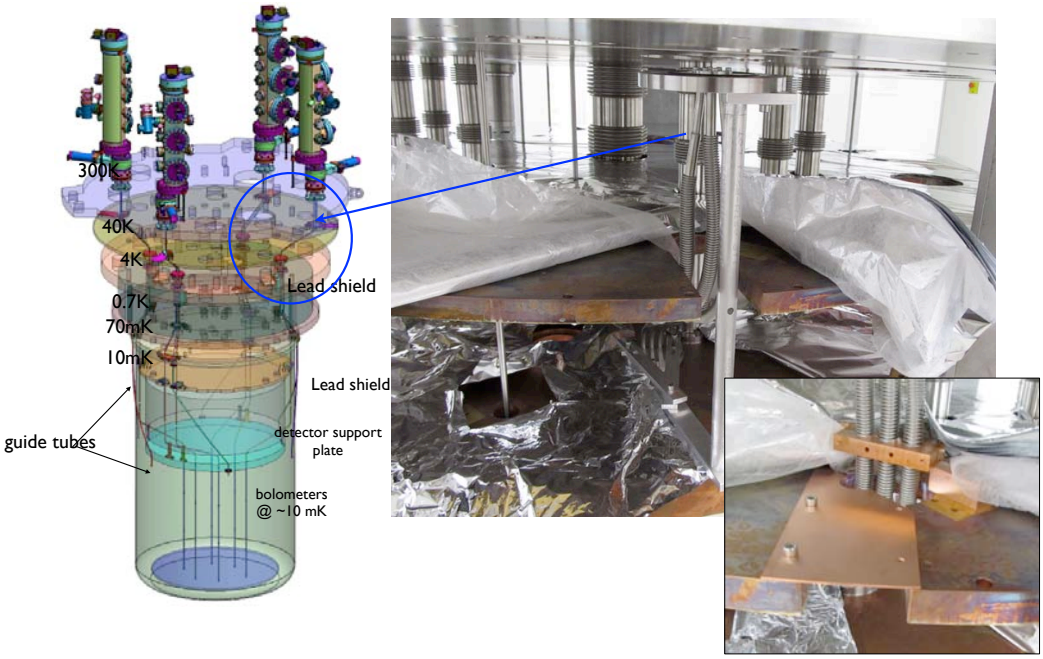

Figure 2: Installation of the newly designed S-shaped, bellow-based guide tubes in the cryostat at LNGS in September 2012. This work marked the beginning of the on-site DCS installation work.

shaped guide tube after installation in the cryostat at LNGS. All remaining S-tubes are in fabrication.

The commissioning and testing of the detector calibration system proceeds in parallel in different tests stands at the University of Wisconsin. Motion testing and characterization of the diagnostic instrumentation continued at 300K. A new 10K test setup was commissioned at Wisconsin in summer 2012. This setup is used to study and optimize the contact force, the motion of the thermalization mechanism, and the overall cool-down of the source string.

6 Radiation shields

CUORE will be equipped with two shielding structures: one external to the cryostat to absorb neutron and gamma rays from the environment, and the other inside the cryostat to shield the detectors from the radioactivity of the cryostat itself.

- **The internal lead shield**, consists of a lateral shield and an overhead disc. The lateral shield is 60-mm-thick Roman lead layered between the IVC and still vessels at 4 K. Its goal is to protect the detectors from the radioactivity of the outer vessels and the superinsulation. The overhead disc is 310-mm-thick lead (250-mm modern + 60-mm Roman) located between the mixing chamber (MC) plate and the detectors, maintained at 0.1 K. It will protect the detector from the radioactivity of all overhead cryostat components. The design of the lateral lead shield was finalized in March 2012. The shield will be produced in 8 ring-shaped sections supported by

a copper structure with lateral stainless steel bars. MTH Metalltechnik in Germany, has been identified to complete the production. A procedure to produce the first test ring with modern low-radioactivity lead is under definition and the complete production is foreseen for November 2013.

- **The external shield**, made of three layers: an outermost polyethylene layer acting as a neutron moderator; a middle layer of H_3BO_3 powder to absorb neutrons; and an innermost layer of lead to absorb photons. The shield will be held in a stainless steel structure, consisting of four rings, which is designed to satisfy mechanical and safety requirements. The rings, which will be internally faced with polyethylene, have been commissioned for production by an external company and will be delivered to LNGS at the beginning of 2013. The assembly of the entire structure, the stacking of the rings atop each other, the addition of the internal lead layer, and the filling of the hollow space between the lead and polyethylene layers with the H_3BO_3 powder will be concluded by the end of 2013.

7 Detector Assembly Plan

The construction of the 19 CUORE detector towers is one of the most critical activities in the upcoming two years, and requires availability of all the needed parts at LNGS plus a coordinated, significant effort of the entire collaboration, together with a sizable technical support from external companies.

A dedicated clean room was installed in 2011 at the second floor of the underground CUORE building (Fig. 3). It was designed to host the three major detector assembly activities: sensor coupling, mechanical assembly, and wire bonding. A set of dedicated, N_2-fluxed glove boxes were built to provide a Rn-free environment for all assembly activities. A dedicated glove box hosts a semi-robotic system for coupling the NTD thermistors and Si heaters to the TeO_2 crystals, while a single workstation with four interchangeable glove boxes is used for the mechanical assembly and bonding.

8 CUORE-0

The goal of CUORE-0 is to perform a full test and debugging of the hardware and procedures specially developed in recent years for CUORE. After the successful construction of the tower in Spring 2012, the second phase of the CUORE-0 program—validation of detector performance and production of physics results—has begun.

The CUORE-0 tower was completed in the first half of April 2012. In mid-April the tower was moved from the CUORE clean room to the former Cuoricino clean room for attachment to the dilution refrigerator there. The installation was completed at the end of April (see Fig. 4). All the sensor connections were checked. Besides two sensors (an NTD and a heater) whose problems were already reported during the CUORE-0 assembly, a short to ground of one of the NTDs appeared. This was probably due to a contact of one of the gold wires with the copper cover on the wire trays.

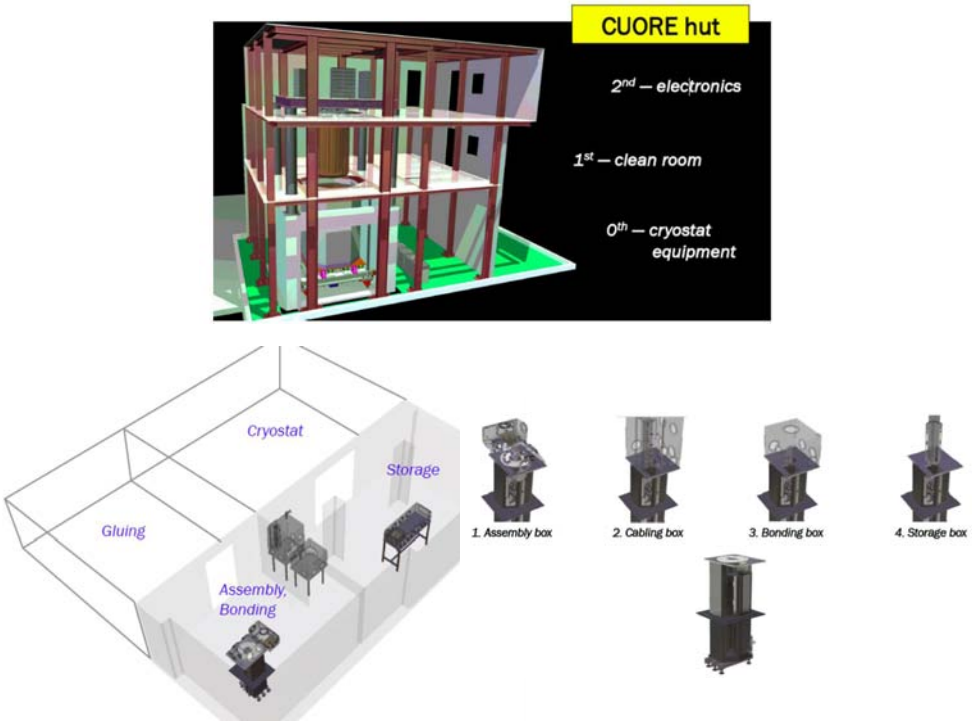

Figure 3: Scheme of the underground CUORE building, clean room, and the tower assembly line.

During the pre-cooldown tests, a leak in the dilution unit was discovered and we were forced to open the cryogenic system and disconnect the detector. Careful examination revealed the leak was in a step heat exchanger. In June a technician from Oxford Instruments, who manufactured this particular dilution refrigerator in 1989, visited LNGS and fixed the leak. The performance of the repaired refrigerator performance was tested during July, and at the end of the month we reinstalled the CUORE-0 detector (Fig. 4). In August we closed and tested the cryogenic system. During the subsequent cooldown, two problems arose that have delayed CUORE-0 data taking. The first was that the cooling power of the cryogenic system was less than expected. We believe this was due to a lack of ^{3}He in the ^{3}He-^{4}He mixture as adding 5 liters of ^{3}He solved the problem. (Indeed, during each cooldown a very small fraction of ^{3}He can get lost and no replacement had been performed since 1989.) The second problem was that despite extensive effort, we could not find a position in which the detector achieved stable operation at base temperature. We suspected the problem was due to either limitations in the so-called "verticalization system" used to align the cryostat, or to thermal shorts inside the cryostat, or possibly a combination of both. We decided to again stop operation and reopen the cryostat to investigate the situation. The problem was immediately identified: the two detector readout tapes had become detached from where they passed over the lead shield, bringing them into contact with the 50 mK shield. The cables were more firmly secured to the lead shield using strong tie. The parallelism of the cryostat flanges and the range of motion of the verticalization system were also checked and found to be satsifactory. We initiated a

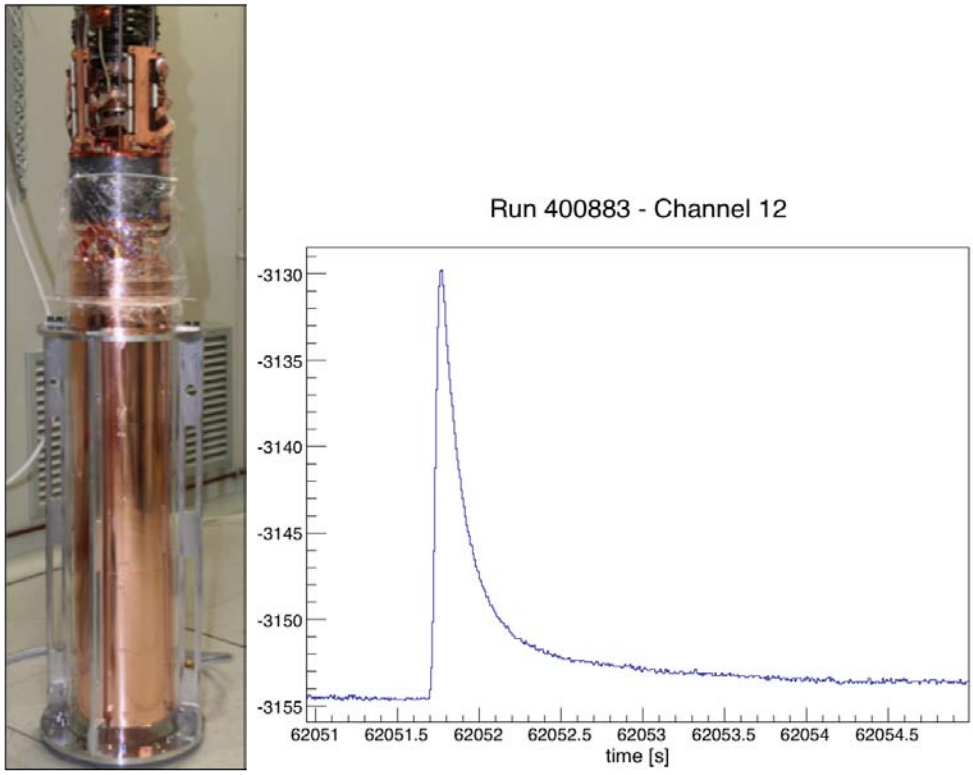

Figure 4: The CUORE-0 tower under the cryostat coldest point and a CUORE-0 detector thermal pulse.

new cooldown in mid-October.

This effort yielded important information on the system performance. In particular, we verified that no sensor connections were lost during cooldown, meaning that the new bonding system can tolerate the thermal contractions of both the copper and wiring system. We also observed thermal pulses on the detectors (Fig. 4) showing the expected behavior.

The completion of CUORE-0 has been a full test of the full assembly procedure that will be used for CUORE. It was determined that the repeatability of the strip gluing and the overconstrained design of hte cable rail made some of the mechanical coupling difficult between the tower and the cable rail. An updated set of procedures have been developed and successfully tested. A new simplified version of the cable rails have been produced and its assembly, handling, and coupling tested with a mock-up tower. A team of operators has been trained on the assembly operation in November 2012 and currently 10 operators are now sufficiently experienced to be able to bond a CUORE tower.

We look forward to an exciting and productive year for CUORE-0 and CUORE in 2013.

9 Publications in 2012

1. F. Alessandria *et al.*, "CUORE crystal validation runs: Results on radioactive contamination and extrapolation to CUORE background", Astroparticle Physics **35**, 839 (2012).

2. E. Andreotti *et al.*, "Search for double-beta decay of ^{130}Te to the first 0^+ excited state of ^{130}Xe with the CUORICINO experiment bolometer array", Physical Review C **85**, 045503 (2012).

3. E. Andreotti *et al.*, "Production, characterization, and selection of hte heating elements for the response stabilization of the CUORE bolometers", Nuclear Instruments and Methods in Physics Research Section A **664**, 161 (2012).

4. C. Mancini-Terracciano and M. Vignati, "Noise correlation and decorrelation in arrays of bolometric detectors", Journal of Instrumentation **7**, P06013 (2012).

5. J. W. Beeman *et al.*, "Discrimination of α and β/γ interactions in a TeO_2 bolometer", Astroparticle Physics **35**, 558 (2012).

6. L. Gironi, "CUORE: The challenge of a 988 bolometer array", Journal of Low Temperature Physics **167**, 1015 (2012).

7. A. Nucciotti *et al.*, "Status of the cryogen-free cryogenic system for hte CUORE experiment", Journal of Low Temperature Physics **167**, 528 (2012).

References

[1] C. Arnaboldi *et al.*, Astropart. Phys. **20**, 91 (2003).
C. Arnaboldi *et al.*, Nucl. Instr. Meth. A **518**, 775 (2004).
R. Ardito *et al.*, CUORE: A cryogenic underground observatory for rare events, arXiv hep-ex/0501010 (2005).

[2] C. Arnaboldi *et al.*, Phys. Rev. Lett. **95**, 14501 (2005).
E. Andreotti, *et al.*, Astropart. Ph. 34 **34**, 822 (2011).

[3] E. Andreotti *et al.*, Astropart. Phys. **34**, 643 (2011).

[4] E. Andreotti *et al.*, Phys. Rev. C **85**, 045503 (2012).

[5] F. Alessandria *et al.*, J. Cosmology Astropart. Phys. **1**, 038 (2013).

[6] F. Alessandria *et al.*, arXiv:1209.2800.

DAMA

Collaboration:

P. Belli[a], R. Bernabei[a,@], A. Bussolotti[a,*], S. d'Angelo[a], A. Di Marco[a], F. Emiliani[a], F. Montecchia[a], A. d'Angelo[b], F. Cappella[b], A. Incicchitti[b], A. Mattei[b,*], O.G. Polischuk-Shkulkova[b,g], R. Cerulli[c], V. Caracciolo[c], S. Castellano[c], C.J. Dai[d], H.L. He[d], H.H. Kuang[d], X.H. Ma[d], X.D. Sheng[d], R.G. Wang[d], Z.P. Ye[d,e]

in some detector developments, by-product results and small scale experiments: A.S. Barabash[r], R.S. Boiko[g], V.B. Brudanin[h], M. Casalboni[a], D.M. Chernyak[g], F.A. Danevich[g], M.L. di Vacri[c], E. Galenin[n], E.N. Galashov[l], A. Gektin[n], V. Isaienko[i], V.V. Kobychev[g], S.I. Konovalov[r], G.P. Kovtun[m], N.G. Kovtun[m], V.M. Kudovbenko-Mokina[g], M. Laubenstein[c], S.S. Nagorny[g], S. Nisi[c], C. Palazzesi[a], P. Prosposito[a], D.V. Poda[c,g], R. B. Podviyanuk[g], A.P. Shcherban[m], V.N. Shlegel[l], D.A. Solopikhin[m], Yu.G. Stenin[l], J. Suhonen[o], A.V. Tolmachev[q], S. Tkachenko[n], V.I. Tretyak[g], V.I. Umatov[r], Ya.V. Vasiliev[l], I.M. Vyshnevskyi[g], R.P. Yavetskiy[q]

in some studies on $\beta^+\beta^+$, EC/β^+, EC/EC decay modes (under the joint Indo-Italian DST-MAE project and inter-universities agreement): P.K. Raina[p], A.K. Singh[p], P.K. Rath[p], S. Ghorui[p]

[a]Dip. Fisica, Univ. Roma "Tor Vergata" and INFN Tor Vergata, 00133 Roma, Italy.
[b]Dip. Fisica, Univ. Roma "La Sapienza" and INFN-Roma, 00185 Roma, Italy.
[c]Laboratorio Nazionale del Gran Sasso, INFN, 67010 Assergi (Aq), Italy.
[d]IHEP, Chinese Academy, P.O. Box 918/3, Beijing 100039, China.
[e]Physics Dept, Jing Gangshan University 343009, Jiangxi, China.
[g]Institute for Nuclear Research, MSP 03680, Kiev, Ukraine.
[h]Joint Institute for Nuclear Research, 141980 Dubna, Russia.
[i]National University of Kyiv-Mohyla Academy, 04655 Kyiv, Ukraine
[l]Nikolaev Institute of Inorganic Chemistry, 630090 Novosibirsk, Russia.
[m]National Science Center Kharkiv Institute of Physics and Technology, Kharkiv, Ukraine.
[n]Institute for Scintillation Materials, 61001 Kharkiv, Ukraine.
[o]Dep. of Physics, University of Jyvaskyla, P.O. Box 35, FIN-40351, Jyvaskyla, Finland
[p]Indian Institute of Technology, Kharagpur, India.
[q]Institute for Single Crystals, 61001 Kharkiv, Ukraine
[r]Institute of Theoretical and Experimental Physics, 117259 Moscow, Russia
[@] Spokesperson; [*] technical staff.

Abstract

DAMA is as an observatory for rare processes located deep underground at the Gran Sasso National Laboratory of the I.N.F.N. (LNGS) that develops and exploits low background scintillators. In 2012 the main experimental activities have been performed with: i) the second generation DAMA/LIBRA set-up (sensitive mass: $\simeq$ 250 kg highly radiopure NaI(Tl)) (upgraded in 2008, 2010 and at the end of 2012); ii) the DAMA/LXe set-up (sensitive mass: $\simeq$ 6.5 kg liquid Kr-free Xenon enriched either in ^{129}Xe or in ^{136}Xe); iii) the DAMA/R&D set-up (a facility dedicated to perform relatively small scale experiments, mainly investigating double beta decay modes in various isotopes); iv) the DAMA/Ge set-up (mainly dedicated to sample measurements and to specific measurements on rare processes); v) a small set-up (named DAMA/CRYS) in preparation for prototype tests and detectors' qualification. The main DAMA activities during 2012 are summarized in the following.

1 DAMA/LIBRA

DAMA/LIBRA (Large sodium Iodide Bulk for Rare processes) is an unique apparatus for its sensitive mass, target material, intrinsic radio-purity, methodological approach and all the controls performed on the experimental parameters (c.f.r. [1, 2, 3, 4, 5] and the 2012 publication list). It is the successor of DAMA/NaI[6, 7, 8, 9, 10, 11, 12, 13, 14, 15, 16, 17, 18], with a higher exposed mass, higher duty cycle, higher granularity (25 detectors in a matrix 5×5) and increased sensitivity. The apparatus has also the unique feature (as well as DAMA/NaI) that routine calibrations are regularly performed down to the energy threshold in the same conditions as the production runs, without any contact with the environment and without switching-off the electronics. The high light yield: 5.5 – 7.5 photoelectrons/keV, and all the features of the detectors have allowed the analyses of the data down to 2 keV software energy threshold (each PMT works at single photoelectron level) in the already published exposure. After the upgrade at fall 2010 when all the PMTs have been substituted with new ones having higher quantum efficiency, the feasibility to decrease the software energy threshold down to 1 keV has been demonstrated (see in the 2012 publication list) and the set-up is running in the new configuration (named DAMA/LIBRA-phase2) with the aim to collect a very large exposure in order to reach the goals of this upgrade. Among the scientific goals of this set-up we mention: i) further investigation with high sensitivity of the Dark Matter (DM) particle component(s) in the galactic halo by the model independent approach known as DM annual modulation signature, and determination of all the modulation parameters with very high precision (e.g. a possible behaviour of the phase value with energy could give information on some aspects of the galactic halo); ii) corollary investigations on the nature of the candidate(s) and on the many possible astrophysical, nuclear and particle physics scenarios with the new potentiality offered by the lower software energy threshold; iii) investigations of other model dependent and/or model independent approaches to investigate DM particles, and of second order effects; iv) new studies of possible exotic scenarios (as SIMPS, neutral nuclearities, Q-balls, etc.); v) improved search for processes violating the Pauli exclusion principle in ^{23}Na and ^{127}I; vi) new search for possible electric charge non-conserving (CNC) processes, as the electron decay into invisible channels and

in the $e^- \to \nu_e + \gamma$ channel, excitations of nuclear levels of ^{23}Na and ^{127}I after CNC electronic capture, etc., with increased sensitivity; vii) search for possible nucleon, di-nucleon and tri-nucleon decay into invisible channels in ^{23}Na and ^{127}I; viii) new search for solar axions by Primakoff effect in NaI(Tl) with increased sensitivity; ix) search for nuclear rare decays in ^{23}Na, ^{127}I and Tl isotopes (as e.g. superdense states, cluster decay), etc.. The most of such investigations require dedicated data taking and high exposure to reach competitive sensitivities.

Some further improvements of the set-up have occurred at the end of 2012; some other ones are in preparation.

The main goal of DAMA/LIBRA is the investigation of the DM particles in the galactic halo by exploiting the DM model independent annual modulation signature[19, 20]. In fact, as a consequence of its annual revolution around the Sun, which is moving in the Galaxy traveling with respect to the Local Standard of Rest towards the star Vega near the constellation of Hercules, the Earth should be crossed by a larger flux of Dark Matter particles around $\sim$ 2 June (when the Earth orbital velocity is summed to the one of the solar system with respect to the Galaxy) and by a smaller one around $\sim$ 2 December (when the two velocities are subtracted). Thus, this signature has a different origin and specific peculiarities e.g. than those effects correlated with seasons.

The contribution of the signal to the counting rate in the k–th energy interval can be written as: $S_k = S_{0,k} + S_{m,k} \cos \omega(t - t_0)$, where: i) $S_{0,k}$ is the constant part of the signal; ii) $S_{m,k}$ is the modulation amplitude; iii) $\omega = \frac{2\pi}{T}$ with period T; iv) t_0 is the phase.

The DM annual modulation signature is very distinctive since it requires the simultaneous satisfaction of all the following peculiarities: the rate must contain a component modulated according to a cosine function (1) with one year period (2) and a phase that peaks roughly around $\simeq 2^{nd}$ June (3); this modulation must only be found in a well-defined low energy range, where DM particle induced events can be present (4); it must apply only to those events in which just one detector of many actually "fires" (*single-hit events*), since the DM particle multi-interaction probability is negligible (5); the modulation amplitude in the region of maximal sensitivity must be $\lesssim$7% for usually adopted halo distributions (6), but it can be larger in case of some possible scenarios.

Thus, when exploiting such a DM annual modulation signature the experimental observable is not the constant part of the signal S_0 (as in other approaches), but its modulation amplitude, S_m, as a function of energy. This has several advantages; in particular, in this approach the only background of interest is that able to mimic the signature, i.e. able to account for the whole observed modulation amplitude and to simultaneously satisfy all the many specific peculiarities of the signature. No background of this sort has been found or suggested by anyone over more than a decade. Thus, the DM annual modulation model-independent approach does not require any identification of S_0 from the total *single-hit* counting rate, in order to establish the presence of DM particles in the galactic halo. The S_0 value can be worked out by a maximum likelihood analysis which also takes into account the energy behaviour of each detector (see literature) for each considered scenario. Thus, the DM annual modulation signature allows one to avoid *a priori* assumptions on the nature and interaction type of the DM particle(s) and to overcome the large uncertainties associated to the exploitation of many data selections/subtractions/statistical-discrimination procedures, to the modeling of surviv-

ing background in keV region, etc. pursued in approaches trying to extract S_0 in case some candidates and/or interaction types are a-priori assumed.

In conclusion, only systematic effects or side reactions simultaneously able to fulfil all the specific requirements of the DM annual modulation signature and to account for the whole observed modulation amplitude could mimic this signature; thus, no other effect investigated so far in the field of rare processes offers a so stringent and unambiguous signature.

At present status of technology the DM annual modulation is the only model independent signature available in direct dark matter investigation that can be effectively exploited.

So far the results on the first six annual cycles have been released. A peculiar annual modulation of the single-hit events in the (2—6) keV energy region satisfying all the many requests of the DM annual modulation signature has been confirmed.

The total exposure already released by the former DAMA/NaI experiment and by the present DAMA/LIBRA in its first six annual cycles is 1.17 ton $\times$ yr. In particular, as required by the DM annual modulation signature: (1) the single-hit events show a clear cosine-like modulation as expected for the DM signal; (2) the measured period is equal to (0.999$\pm$0.002) yr, a value well compatible with the 1 yr period expected for the DM signal; (3) the measured phase (146 $\pm$7) days is well compatible with about 152.5 days, as expected for the DM signal; (4) the modulation is present only in the low energy (2—6) keV interval and not in other higher energy regions, consistently with expectation for the DM signal; (5) the modulation is present only in the single-hit events while it is absent in the multiple-hit ones, as expected for the DM signal; (6) the measured modulation amplitude in NaI(Tl) of the single-hit events in the (2—6) keV energy interval is: (0.0116$\pm$0.0013) cpd/kg/keV (8.9σ C.L.). No systematics or side processes able to simultaneously satisfy all the many peculiarities of the signature and to account for the whole measured modulation amplitude is available (see e.g. in Refs. [2, 3, 9, 10, 11, 21, 22, 23, 24, 25, 26] and in the 2012 publication list).

No other experiment exists, whose result can be directly compared in a model independent way with those by DAMA/NaI and DAMA/LIBRA. It is also worth noting that in the DM field DAMA/LIBRA is the set-up still having the highest intrinsic radiopurity, the largest exposed sensitive mass, the largest collected exposure, the deepest controlled running condition and stability, and the only one with highly sensitive ULB (Ultra-Low Background) NaI(Tl) detectors.

The DAMA obtained model independent evidence is compatible with a wide set of scenarios regarding the nature of the DM candidate and related astrophysical, nuclear and particle Physics. For example, some of the scenarios available in literature and the different parameters are discussed in Ref. [10, 11, 7, 12, 13, 14, 15, 16, 17, 5, 27, 28] and in Appendix A of Ref. [2]. A further large literature is available on the topics; many possibilities are open. Finally, as regards model dependent results by indirect and direct experiments actually they are not in conflict with the DAMA model independent result considering both their experimental and theoretical uncertainties.

The DAMA/LIBRA experiment is continuously running. Moreover, it is foreseen to complete in 2013 the results of DAMA/LIBRA-phase1 by including also the exposure collected during the 7th annual cycle (the latter before the 2010 upgrade).

1.1 Upgrades

A first upgrade of the DAMA/LIBRA set-up was performed in September 2008. A more important upgrade was performed at the end of 2010, when all the low background PMTs have been replaced with new ones having higher quantum efficiency (see Fig.1), realized with a special dedicated development by HAMAMATSU co..

The feasibility to decrease the software energy threshold down to 1 keV has been demonstrated and a scientific paper has been published (see in the 2012 publication list). This upgrade has improved the set-up performance and increases its sensitivity in particular as regards deeper corollary information on the nature of the DM candidate particle(s) and on the various related astrophysical, nuclear and particle Physics scenarios.

Since January 2011 the DAMA/LIBRA experiment is again in data taking in the new configuration (DAMA/LIBRA-phase2).

We remind that up to October 2010 low background PMTs, developed by EMI-Electron Tubes with dedicated R&D, were used; those PMTs had Q.E. 30% at λ=380 nm; the light yield and other response features already allowed a software energy threshold of 2 keV in the data analysis.

A detailed analysis of all the features of the new high quantum efficiency PMTs and related implications has been carried out and a dedicated paper has been published where all the details can be found (see in the 2012 publication list). Just as example in Fig. 1 we show the values of the Q.E. of the new 50 HAMAMATSU PMTs installed in DAMA/LIBRA both at peak and at the λ of the NaI(Tl) scintillation light.

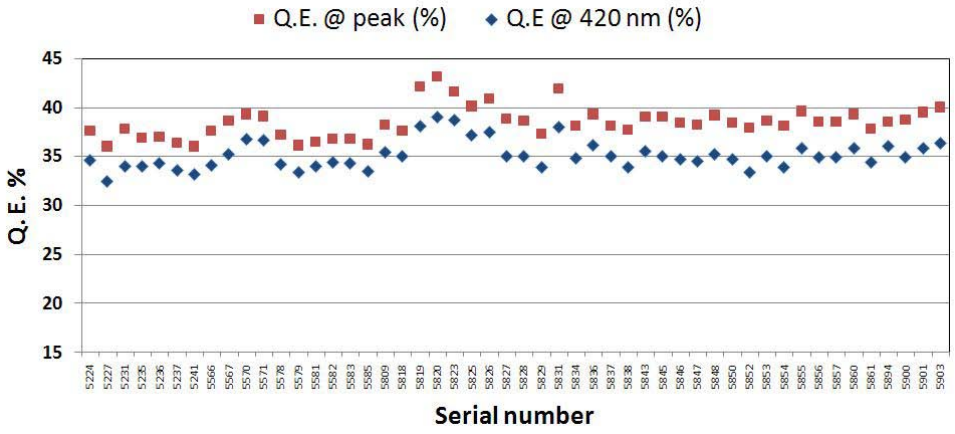

Figure 1: The Q.E. at peak and at 420 nm of each one of the 50 high Q.E. PMTs, installed in DAMA/LIBRA. The averages (RMS) are 38.5% (1.6%) and 35.1% (1.4%), respectively; the RMS show that the Q.E. spread in the PMTs production is well limited.

At the end of the year 2012, new-concept preamplifiers were installed and some new trigger modules prepared. Developments of some new electronic modules are planned.

1.2 No role for muons in the DAMA annual modulation result

Sometimes naive statements were put forward as the fact that in nature several phenomena may show some kind of periodicity. The point is whether they might mimic the DM annual

modulation signature in DAMA/LIBRA (and former DAMA/NaI), i.e. whether they

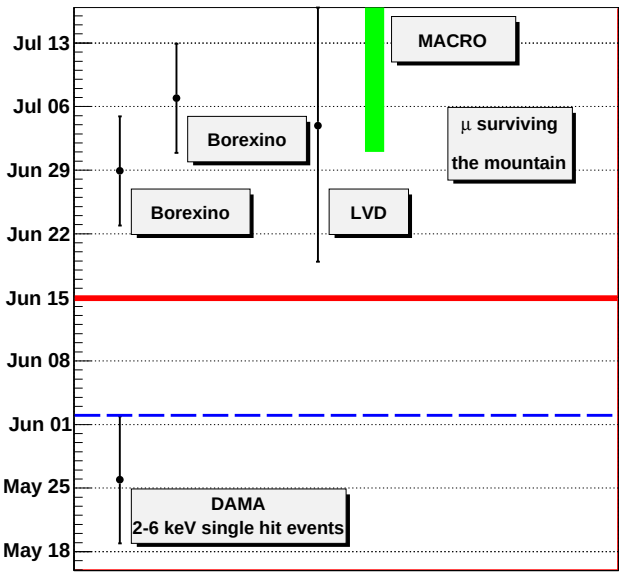

Figure 2: The phase of the DAMA annual modulation signal [3] and the muon phases quoted by Borexino in two analyses (May 2007 – May 2010 [29], and May 2007 – May 2011 [30]), by LVD (January 2001 – December 2008 [31]), and by MACRO (January 1991 – December 1994 [32]). The muon phases quoted by those three experiments have to be regarded as mean values among the muon phases in all the considered years since the muon phase depends on the temperature of the outer atmosphere and, thus, it changes each year. The phase of the DAMA observed effect has instead a stable value in the different years [2, 3]. The horizontal dashed line corresponds to 2nd June (date around which the phase of the DM annual modulation is expected). The middle of June is also marked as an example; in fact, the maximum effective temperature at the LNGS location cannot be as early as the middle of June (and for several years), date which is still 3 σ far away from the phase of the DAMA observed effect. For more arguments and details see in the 2012 publication list: EPJC 72 (2012) 2064.

might be not only quantitatively able to account for the observed modulation amplitude but also able to simultaneously satisfy all the requirements of the DM annual modulation signature; the same is also for side reactions.

Careful investigations on absence of any significant systematics or side reaction able to account for the measured modulation amplitude and to simultaneously satisfy all the requirements of the signature have already been quantitatively carried out (see e.g. Ref. [9, 10, 11, 2, 3, 21, 22, 23, 24, 25, 26], refs therein). In 2012 a paper with all arguments further excluding any role of muons in the the DAMA annual modulation result has been published (see in the 2012 publication list); it shows the many reasons which exclude any possibility for muons or muons induced process to mimic the DM annual modulation signature. Fig. 2, as an example, shows the inconsistency between the high energy muon phases measured at Gran Sasso by some experiments having different aims, and the phase

measured by DAMA investigating in the keV region the DM annual modulation signature. Many arguments and details are reported in the dedicated paper.

1.3 Search for charge non-conserving processes in ^{127}I by coincidence technique

New lifetime limits on the charge non-conserving (CNC) electron capture with excitation of the 417.9 keV nuclear level in the ^{127}I were established by using the coincidence technique on an exposure of 0.87 ton $\times$ yr, collected by DAMA/LIBRA (see 2012 publication list).

The usual approach to investigate CNC electron capture processes is to search in the experimental energy distribution for the peaks due to the γ rays induced by possible de-excitation processes in the ^{127}I nuclei which might follow the CNC electron capture. In the present case an alternative experimental approach was followed. The idea is that each CNC electron capture decay produces an excited level and the relaxation of the atomic shells. In a multi-detector set-up the products of the atomic relaxation are contained in the source = detector releasing a total energy of 33.2 keV, considering only ^{127}I K-shell electrons involved in the process. The γ quanta emitted in the nucleus de-excitation may escape from the source = detector and then interact with one of the surrounding detectors, giving events in coincidence with multiplicity two (two detectors fire). The search for events with multiplicity two – in the particular energy interval of interest for the process searched for – offers both a peculiar signature for this process and a significant reduction of the background. The analysis was focused on the case of the 417.9 keV excited level of ^{127}I, since it offers the largest efficiency for the detection of double-coincidence from the CNC electron capture searched for, and the lowest background.

The new obtained limit on the mean life is $\tau > 1.2\times10^{24}$ yr (90 % C.L.), about one order of magnitude larger than those previously available for CNC electron capture involving nuclear level excitations of ^{127}I. The obtained limit is also very close to the best limit available in literature for CNC-EC processes $\tau > 3.7\times10^{24}$ yr (90 % C.L.) in ^{129}Xe [33].

1.4 Conclusions and perspectives

The model independent positive evidence for the presence of DM particles in the galactic halo is supported at 8.9σ C.L. (on a cumulative exposure of 1.17 ton$\times$yr i.e. 13 annual cycles of DAMA/NaI and DAMA/LIBRA). Corollary analyses in some of the many possible scenarios for DM candidates, interactions, halo models, nuclear/atomic properties, etc. have been carried out in the past and are in progress as well as analyses/data taking to investigate other rare processes. The analysis of the seventh annual cycle (the last one of DAMA/LIBRA-phase1, that is before the installation of the high quantum efficiency PMTs at the end of 2010) will be released in 2013. Other analyses on DM features are also in progress.

Various preliminary analyses on possible rare processes have been carried out (see Ref. [4] and the 2012 publication list) and will be continued in future as also the former

DAMA/NaI apparatus did [18]. In particular a search for charge non-conserving processes in ^{127}I by coincidence technique has been published in 2012.

The further upgrade was successfully concluded in fall 2012, while further improvements are planned for the electronics. DAMA/LIBRA is continuously running in the new configuration, named DAMA/LIBRA-phase2. Other DM features, second order effects, and several other rare processes will be investigated with high sensitivity.

The strictly quality control allows DAMA/LIBRA to be still the highest radiopure set-up in the field with the largest exposed sensitive mass, the full control of running conditions, the largest duty-cycle and an exposure orders of magnitude larger than any other activity in the field.

2 DAMA/LXe

We pointed out since 1990 [34] the possible interest in using the liquid Xenon as target-detector material for particle DM investigations. Since the end of 80's (former Xelidon experiment of the INFN) we have realized several liquid Xenon (LXe) prototype detectors. In 1996 we pointed out to the INFN-CSN2 the intrinsic problems of this detector medium for large scale experiments dedicated to DM investigation and agreed to pursue the activity by exploiting Kr-free enriched Xenon gases in limited volume.

The presently running set-up (with a Cu inner vessel filled by $\simeq$ 6.5 kg – $\simeq$2 l – of liquid Xenon) can work either with Kr-free Xenon enriched in ^{129}Xe at 99.5% or Kr-free Xenon enriched in ^{136}Xe at 68.8% [35, 36, 37]. Many competing results were achieved on several rare processes [35, 36, 37, 40]. It is worth noting that e.g. the mass exposed when using the Xenon enriched in ^{129}Xe corresponds for spin-dependent coupled particles to expose 24.5 kg of natural Xenon, while the exposed mass when using the Xenon enriched in ^{136}Xe correspond for spin-independent coupled particles to an exposed mass of 50.4 kg of natural Xenon.

For completeness we remind that the set-up had a long stop because of the forbiddeness of using cryogenic liquids in the LNGS underground laboratories; we profited from this long period to perform several upgrades. Then, the DAMA/LXe set-up restarted the data taking following regular maintenance schedules. In 2011 the old compressor went out of order and several months were necessary to provide and install a new one able to contemporaneously drive two cold-heads as necessary in some phases of the purification/liquefaction procedures.

In the recent period, data are collected by using Kr-free Xenon enriched in ^{136}Xe and focusing the high energy region to study rare processes. Various efforts and data analyses are in progress.

3 DAMA/R&D

The DAMA/R&D installation is a low-background set-up dedicated to relatively small scale experiments [41, 42, 43, 44]. The measurements mainly investigate 2β decay modes in various isotopes; both the active and the passive source techniques have been exploited as well as sometimes the coincidence technique, with particular attention to $2\beta^+$ processes.

In the $2\beta^+$ investigations a gap of several orders of magnitude between theoretical expectations and experimental results is the usual situation and the better achieved sensitivities do not exceed the level of $T_{1/2} \simeq 10^{21}$ yr. It should be stressed that the searches for $2\beta^+$ processes are interesting not so much for the neutrino mass, but rather to study the contribution of right-handed currents in weak interaction. Studies of the neutrinoless double electron capture (2ϵ) and electron capture with positron emission ($\epsilon\beta^+$) decays could help to understand a contribution of the right-handed admixtures in weak interaction to the neutrinoless $2\beta^-$ decay [45].

Even more important motivation to search for double electron capture appears from a possibility of a resonant process thanks to energy degeneracy between initial and final state of mother and daughter nuclei. Such a resonant process could occur if the energy of transition ($Q_{2\beta}$) minus the energies of two bounded electrons on K or/and L atomic shells of daughter nucleus is near to the energy of an excited level (E_{exc}) of the daughter isotope.

Therefore developments of experimental technique to improve the reachable sensitivity in the searches for 2ε, $\varepsilon\beta^+$, and $2\beta^+$ processes are strongly required.

Finally, investigations on various kinds of new scintillators and preliminary works for the future measurements are also in progress.

Some of the main 2012 results are listed in the following, with more details on the works published in 2012.

- The final results on double beta decay modes in Zn and W isotopes with the $ZnWO_4$ crystal scintillators have been published in 2011 and new efforts for more radio-pure detectors have been started in 2012 to further increase the experimental sensitivity in the future. A new $ZnWO_4$ detector of 1 kg mass is now at hand. Measurements with neutrons to investigate anisotropy of the response to heavy particles in the keV region are also under consideration for other kind of investigation (see also Sect. 5.1).

- The results on double beta decay modes obtained by using enriched $^{106}CdWO_4$ detector in DAMA/R&D have been published (see Sect. 3.1) and efforts for the new set-up in GeMulti, exploiting the coincidences between the $^{106}CdWO_4$ detector and four HP-Ge detectors, have been completed with the installation of the experimental set-up (see Sect. 4).

- The data taking with the detectors system housing two enriched $^{116}CdWO_4$ detectors is continued. New efforts to further reduce the background have been performed by exploiting various modifications of the experimental set-up. Preliminary results have been presented at NPAE2012 and LUMDETR-2012 conferences.

- The work for lowering the background and for the future (some years from now) installation of the $^{116}CdWO_4$ detectors in the low-background 4 HP-Ge detectors facility has started. The aim is to investigate the $2\nu2\beta$ transitions of ^{116}Cd to the excited states of ^{116}Sn at level of sensitivity $T_{1/2} = 10^{22}$ yr, as expected by the theoretical predictions.

- The preparation of other future measurements is in progress.

3.1 Search for 2β processes in ^{106}Cd with enriched $^{106}CdWO_4$ crystal scintillator.

The isotope ^{106}Cd is one of the most promising candidates for $2\beta^+$ decay because: 1) of its natural isotopic abundance (1.25 ± 0.06)% and of the possibility to achieve samples enriched up to 100%; 2) of its rather large $Q_{2\beta}$= (2775.39±0.10) keV and of the possibility to study all the various $2\beta^+$, $\epsilon\beta^+$ and 2ϵ decay modes; 3) the favorable theoretical estimates of the half-lives. Thus, with the $CdWO_4$ crystal scintillator (215 g) enriched in ^{106}Cd to 66%, described in details in a previous paper [44], high sensitivity measurements of $2\beta^+$ processes in ^{106}Cd have been published (see 2012 publication list and e.g. Fig. 3).

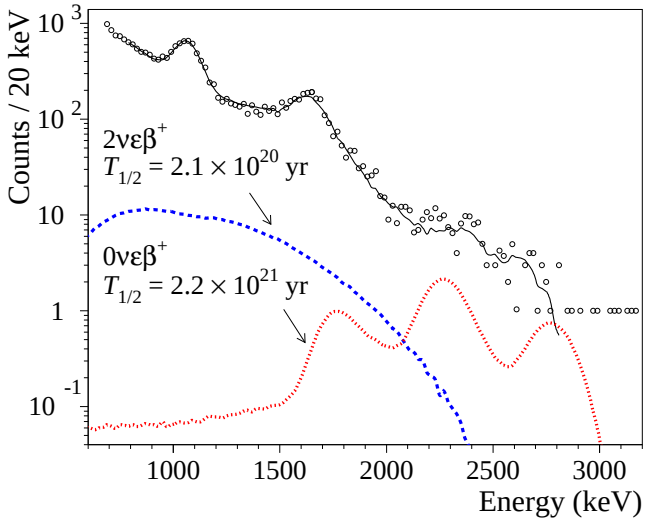

Figure 3: Part of the energy spectrum of γ and β events accumulated with the $^{106}CdWO_4$ detector over 6590 h (circles) and its fit in the energy interval $780 - 2800$ keV (solid line) together with the excluded distributions of $2\nu\varepsilon\beta^+$ and $0\nu\varepsilon\beta^+$ decay of^{106}Cd.

After 6590 h of data taking new improved half-life limits on the double beta processes in ^{106}Cd have been established at the level of 10^{19} - 10^{21} yr; in particular, $T_{1/2}$ $(2\nu\epsilon\beta^+)$ $\geq 2.1 \times 10^{20}$ yr, $T_{1/2}$ $(2\nu 2\beta^+) \geq 4.3 \times 10^{20}$ yr, and $T_{1/2}$ $(0\nu 2\epsilon) \geq 1.0 \times 10^{21}$ yr. The resonant neutrinoless double electron capture to the 2718 keV, 2741 keV, and the 2748 keV excited levels of ^{106}Pd has been restricted to $T_{1/2}(0\nu 2K) \geq 4.3 \times 10^{20}$ yr, $T_{1/2}$ $(0\nu KL_1)$ $\geq 9.5 \times 10^{20}$ yr, and $T_{1/2}$ $(0\nu KL_3) \geq 4.3 \times 10^{20}$ yr, respectively (all limits at 90% C.L.). The radioactive contamination of the $^{106}CdWO_4$ crystal scintillator has also been quoted. A new more sensitive data taking has been set in a different set up (see Sect. 4) and is running in 2013.

3.2 Low background detector with enriched $^{116}CdWO_4$ crystal scintillators to search for double β decay of ^{116}Cd

The ^{116}Cd isotope is a very interesting candidate for the neutrinoless $2\beta^-$ decay because of: 1) its natural isotopic abundance is comparatively high (7.49%) and of the possibility

to achieve samples enriched up to 100%; 2) its rather large $Q_{2\beta}$ value (2809 keV); 3) the favorable theoretical estimates of the half-lives and nuclear matrix elements.

A cadmium tungstate crystal boule enriched in ^{116}Cd to 82% with mass of 1868 g was grown by the low-thermal-gradient Czochralski technique. This is the second boule never produced of $^{116}CdWO_4$. The isotopic composition of cadmium and the trace contamination of the crystal boule were estimated by High Resolution Inductively Coupled Plasma Mass-Spectrometry.

Thus, two $^{116}CdWO_4$ crystal scintillators (586 g and 589 g; see Table 1) have been realized from the boule and the set-up was running firstly over 1727 h deep underground at the Gran Sasso National Laboratories of the INFN, which allowed to estimate the radioactive contamination of the enriched crystal scintillators [46]. After an annealing procedure the two detectors were running for a total of 7593 h (paper in press), see Table 1 and Fig. 4. The radioactive contamination of a 3rd $^{116}CdWO_4$ sample (326 g) cut from the same boule and the scraps (264 g) after the crystal growth were also checked with the help of ultra low background γ spectrometry at LNGS.

Table 1: Some information about the data takings with the $^{116}CdWO_4$ detectors.

Run	Detector mass (g)	Life time (hours)	Some features
1	586.2	1727	Detectors inside a plastic veto wrapped by PTFE
	589.3		Light guides also wrapped by PTFE
			Liquid scintillator LS-221 (ISMA, Kharkiv)
			DAQ: sampling rate 20 MSa/s; energy threshold $\simeq$ 20 keV
2	579.8	7593	After crystals' annealing
	582.4		Detectors inside a plastic veto wrapped by Tyvek
			Light guides wrapped by Mylar
			Liquid scintillator LS-Ultima Gold.
			DAQ: sampling rate 50 MSa/s; energy threshold $\simeq$ 300 keV
3	579.8	continuously	Active veto substituted by
	582.4	running	OFHC low radioactive Cu bricks completely surrounding each detector

The low background measurements to search for double β decay of ^{116}Cd with the help of the enriched cadmium tungstate crystal scintillators are in progress. In October 2012 the active veto has been substituted by OFHC low radioactive Cu bricks completely surrounding each detector, in order to further decrease the background. This set-up is now in data taking.

At the end of the present data taking in DAMA/R&D (some years from now), the $2\nu2\beta$ transitions of ^{116}Cd to the excited states of ^{116}Sn is planned to be investigated at level of sensitivity expected by the theoretical predictions also installing the enriched scintillators in the the low-background 4 HPGe detectors facility.

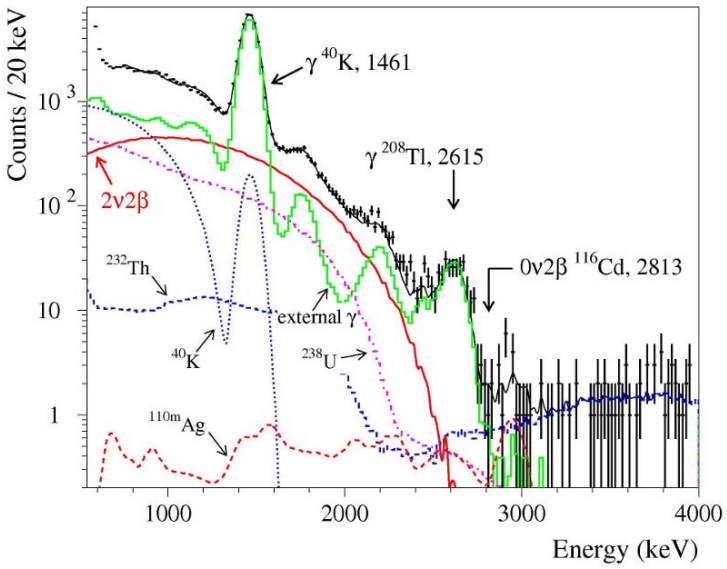

Figure 4: The energy spectrum of the $\gamma(\beta)$ events measured with the $^{116}CdWO_4$ scintillation detector over 7593 h in the low-background set-up (points) together with the fit (solid black line). The $2\nu2\beta$ decay of ^{116}Cd and the main components of the background are also shown: the distributions of internal ^{40}K, ^{232}Th, ^{238}U, and cosmogenic ^{110m}Ag, the contribution from external γ quanta. The energies are in keV.

4 Measurements with DAMA/Ge and LNGS Ge facility

The measurements on samples and on various R&D developments are performed by means of the DAMA low background Ge detector, specially realized with a low Z window; it is operative deep underground in the low background facility of the LNGS. Some selected materials are in addition measured with high sensitivity ICP-MS and mass spectrometers. Also other Ge detectors (in particular, GeMulti) are used for some peculiar measurements.

In particular, the main data takings/results during year 2012 with DAMA/Ge and LNGS Ge facility are summarized in the following.

- The radioactive contamination of ^{7}LiI(Eu) crystal scintillators was studied and a paper was submitted (published in 2013).

- New measurements with the purified $\simeq$1 kg of Ru, in order to investigate the 2β processes of ^{96}Ru and ^{104}Ru isotopes with higher sensitivity, have been carried out. Preliminary results were presented at conference and paper is in press on Phys. Rev. C in 2013. A new set-up schema is ready for new measurements; all needed materials are at hand. The main aim is to investigate the $\epsilon\beta^{+}2\nu$ channel whose theoretical $T_{1/2}$ estimate is in the range 10^{21}—10^{22} yr, which is not very far from the presently reached sensitivity.

- Efforts to obtain larger amounts of natural Pt or Pt samples enriched in ^{190}Pt isotope

for new measurements on double β decay processes with improved sensitivity are in progress.

- The purification of the 3.16 kg of Nd_2O_3 has been completed. The preparation of new measurements with additional $\simeq$ 1.5 kg of metallic Nd to test a result that declared the observation of the $2\nu2\beta$ decay of the ^{150}Nd to the first excited level 0^+_1 of ^{150}Sm is in progress.

- The first experimental investigation of the 2β decay of ^{184}Os and ^{192}Os was performed using a sample of ultra-pure osmium and the paper was submitted (published in 2013). New measurements are foreseen to assess with high C.L. the presence of the rare α decay of ^{184}Os to the first excited level 103.5 keV of ^{180}W, for which preliminary indication has been presented at NPAE2012 conference.

- A more sensitive measurement with the $^{106}CdWO_4$ crystal scintillator inside the 4π low-background HPGe detectors facility (the GeMulti ultralow-background set-up with four 225-cm^3 HPGe detectors) started in October 2012. In particular a special light guide for the $^{106}CdWO_4$ in this configuration was built; it is made of $PbWO_4$ from archaeological Pb. Such a set-up configuration will be effective to investigate 2ν mode of $\epsilon\beta^+$ and $2\beta^+$ decays, and also 2ϵ transitions of ^{106}Cd to excited states of ^{106}Pd, at the level of sensitivity of the theoretical predictions: $T_{1/2} = 10^{20}$ - 10^{22} yr. The sensitivity of the experiment, in particular to the two neutrino $\varepsilon\beta^+$ decay of ^{106}Cd, is expected to be enhanced thanks to the high energy resolution of the GeMulti detector and to the improvement of the background conditions in coincidence mode. Moreover, the development of a $^{106}CdWO_4$ crystal scintillator depleted in $^{113/113m}$Cd isotopes is also foreseen in future.

- Continuing the developments for the future data taking.

The future measurements on all other topics for incoming years are in preparation. In the following just the results of the measurements published in 2012 are summarized.

4.1 Radioactive contamination of SrI_2(Eu) crystal scintillator

The interest in strontium iodide crystal (SrI_2(Eu)) increased in the last few years because of its high light output (>100000 γ/MeV) and its good energy resolution ($\simeq$ 3% at 662 KeV). An important advantage of SrI_2(Eu) in comparison to other high resolution scintillators, like for instance $LaCl_3$(Ce), $LaBr_3$(Ce), Lu_2SiO_5(Ce), LuI_3(Ce), is the absence of natural long-living radioactive isotopes (as ^{138}La in lanthanum and ^{176}Lu in lutetium). It makes SrI_2(Eu) scintillators promising in various applications, in particular for low counting experiments as e.g. those searching for double β decay. A SrI_2(Eu) crystal doped by 1.2% europium was produced by using the Stockbarger growth technique and characterised studing the relative photoelectron output and energy resolution for γ quanta (see Fig.5 and 2012 publication list). The intrinsic radioactivity of the SrI_2(Eu) crystal scintillator was tested both by using it as scintillator at sea level and by ultra-low background HPGe γ spectrometry deep underground (see Fig.6).

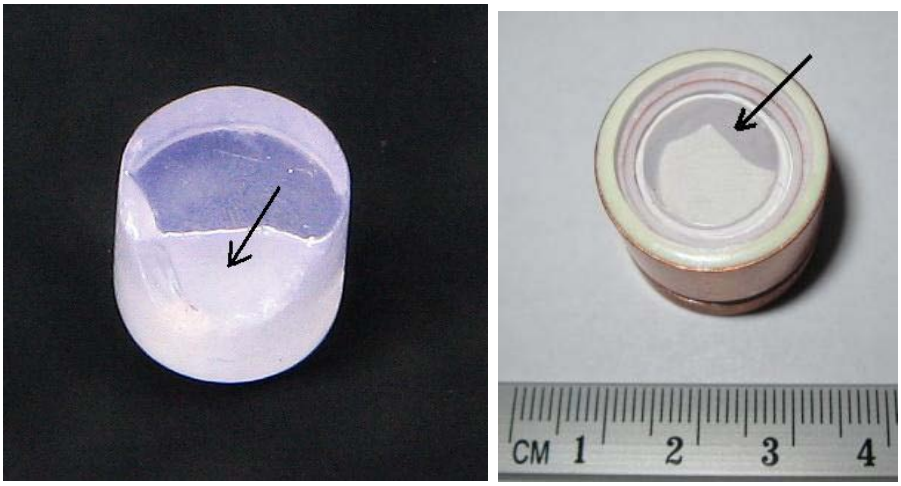

Figure 5: Left: $SrI_2(Eu)$ crystal before encapsulation. Right: Low background $SrI_2(Eu)$ scintillation detector. Arrows show irregularity of the crystal shape.

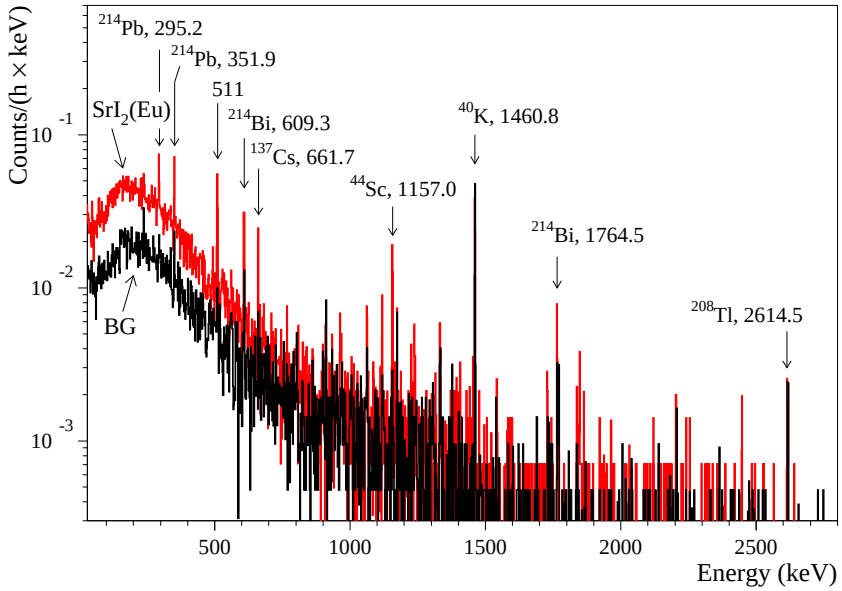

Figure 6: Energy spectra accumulated with the $SrI_2(Eu)$ sample over 706 h, and without sample over 1046 h (BG) by ultra-low background HPGe γ spectrometer deep underground. The energies of the γ lines are in keV. The background was accumulated before the contamination of the HPGe set-up by ^{44}Ti.

The response of the $SrI_2(Eu)$ detector to α particles (α/β ratio and pulse shape) was estimated by analysing the ^{226}Ra internal trace contamination of the crystal. The measured α/β ratio was 0.55 at E_α = 7.7 MeV, and no difference in the time decay of the scintillation pulses induced by α particles and γ quanta was found. The potentiality of such a scintillator in the search for the double electron capture and electron capture

with positron emission in ^{84}Sr has been pointed out. These studies have demonstrated the potentiality of this material for a variety of scintillation applications, including low-level counting experiments. An R&D of SrI_2(Eu) crystal scintillators is in progress.

4.2 Search for ^{7}Li solar axions using resonant absorption in LiF crystal

If axions exist, they could be intensively born inside the Sun. They could be produced: (1) in the interaction of the thermal γ quanta with the solar electromagnetic fields due to the Primakoff effect; the energy spectrum of these axions is continuous up to ~ 20 keV with the mean value of ~ 4.2 keV. Their flux is related with value of coupling constant $g_{a\gamma}$; (2) axions can be emitted instead of γ quanta in deexcitations of excited nuclear levels in magnetic transitions; their spectrum is quasi-monoenergetic, and the flux is related with g_{aN}. Nuclei can be excited due to the thermal movement (in the center of the Sun the temperature is $\simeq 1.3$ keV); evidently, nuclei with excited levels at low energies E_{exc} are preferable (^{57}Fe: $E_{exc} = 14.4$ keV, ^{83}Kr: $E_{exc} = 9.4$ keV). Also, the nuclear levels can be populated in the nuclear reactions inside the Sun, e.g. in the main *pp* cycle: $^7\mathrm{Be} + e^- \rightarrow {}^7\mathrm{Li} + \nu_e$ with 10.52% population of the ^{7}Li level with 477.6 keV energy. In spite of a great theoretical interest in axions (which also could constitute a part of dark matter, see e.g. [47]), intensive experimental searches up to now gave no direct evidences of their existence. Indirect cosmological and astrophysical arguments prefer the axion mass in the range of $10^{-6} - 10^{-2}$ eV.

The resonant excitation of nuclei as an experimental scheme of searching for quasi-monoenergetic solar axions was proposed in [48]. Quasi-monoenergetic axions emitted in magnetic transitions instead of γ quanta by excited nuclei (^{7}Li, ^{57}Fe, ^{83}Kr or others) in the Sun could resonantly excite corresponding levels of the same nuclei on the Earth. ^{7}Li, as a favorable target to search for hadronic solar axions, was discussed at the first time in [49]. Due to the motion of ^{7}Li nuclei in the Sun core with high temperature (near 1.3 keV in the center), the axion 478 keV line is symmetrically Doppler broadened with width $\simeq 0.5$ keV that is much bigger than the energy of the nuclear recoil ($\simeq 1.8 \times 10^{-2}$ keV), than the redshift due to the gravitation of the Sun ($\simeq 5 \times 10^{-3}$ keV), and than the decay width of the 478 keV excited level ($\simeq 6 \times 10^{-6}$ keV). Because of the thermal broadening, the 478 keV axions could be resonantly absorbed by ^{7}Li nuclei in a laboratory at the Earth [49].

Gamma quanta (and/or conversion electrons) emitted in the subsequent deexcitation processes can be observed with the help of detectors located near a sample with ^{7}Li, ^{57}Fe, ^{83}Kr (or incorporating these nuclei).

In 2008, we performed preliminary studies [50] of a few LiF samples (LiF powders and LiF crystals) to investigate the possibilities to improve the best ^{7}Li limit: $m_a < 16.0$ keV, which existed at that time [51].

The final results of a new experiment performed with a radiopure LiF crystal (553 g) during 4044h of measurements were published in 2012 (see Fig.7 and 2012 publication list). The data were collected with a LiF crystal[1] $\oslash 89 \times 40$ mm having a mass of 552.6

[1]Produced by the Czochralski method in the Institute for Scintillation Materials (Kharkiv, Ukraine).

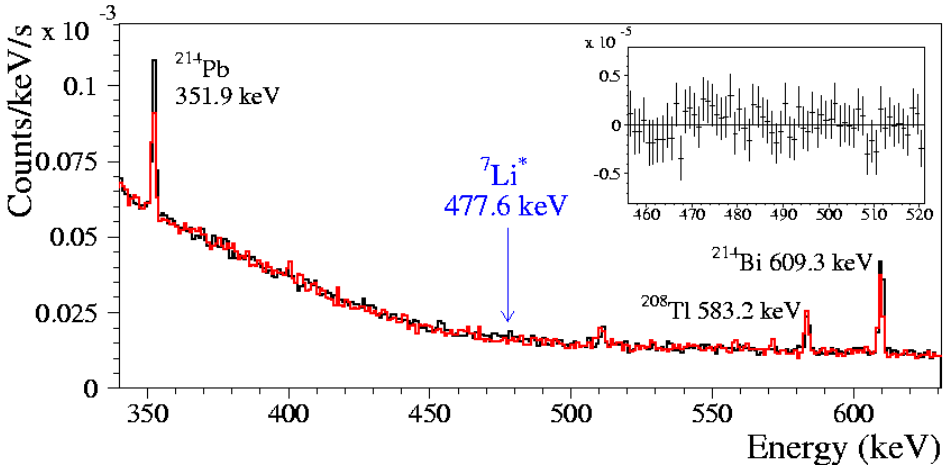

Figure 7: Energy spectrum measured with the LiF crystal (553 g) during 4044 h (black histogram). The background spectrum (red histogram) practically coincides with the LiF data. The expected ^{7}Li peak at 477.6 keV is shown. Difference between the rates with and without the LiF target is shown in Inset.

g and with DAMA ultra-low background HP Ge detector. These measurements lead to a new limit on the mass of the monochromatic axions coupled to nucleons, which could be emitted in the Sun in the deexcitation of the ^{7}Li nuclei and which, coming to the Earth, could excite the corresponding ^{7}Li 477.6 keV level: $m_a < 8.6$ keV at 90% C.L. This is the best limit obtained in the experiments with resonant absorption in ^{7}Li nuclei. In the used approach, the axions are coupled to nucleons both at the production and at the absorption processes, and thus the m_a limit is related only to the axion-nucleon coupling constant g_{aN}; uncertainties related with $g_{a\gamma}$ and g_{ae} disappear. Hence, this experiment is sensitive to a coupling constant different than the one investigated e.g. by the CAST experiment.

The obtained limit improves the value $m_a < 13.9$ keV set in our preliminary measurements [50]. Joining the determined limit with the results of similar experiments with ^{57}Fe nuclei, one can extend a window in the excluded axion masses to the limits [477.6, 0.145] keV.

5 Other activities

Other two activities performed in 2012 will be briefly summarized in the following.

5.1 On the potentiality of the $ZnWO_4$ anisotropic detectors to measure the directionality of Dark Matter

In recent years we have made extensive efforts and measurements with $ZnWO_4$ crystal scintillators, in particular to investigate double beta decay of Zn and W isotopes [42].

The crystal was doped by W on the level of $\simeq 1\%$ with an aim to improve its scintillation properties.

These scintillators (see e.g. Fig. 8) have the particular feature to be anisotropic in the light output and in the pulse shape for heavy particles (p, α, nuclear recoils) depending on the direction with respect to the crystal axes. The response to γ/β radiation is isotropic

Figure 8: Three of the $ZnWO_4$ crystal scintillators recently developed [43]. Two $ZnWO_4$ samples (left and middle pictures) have been grown in the Institute of Scintillation Materials (Kharkiv, Ukraine). The crystal in the right picture has been produced in the Nikolaev Institute of Inorganic Chemistry (Novosibirsk, Russia); it is $\simeq$ 8 cm in diameter and $\simeq$ 15 cm length of cylindrical part.

instead. This feature offers the possibility to study the directionality approach, which is applicable in the particular case of those DM candidate particles inducing just nuclear recoils. Among the anisotropic scintillators, the $ZnWO_4$ has unique features, which make it an excellent candidate for this type of research, and there is still plenty of room for the improvement of its performances. In 2012 the possibility of a low background pioneer experiment (named ADAMO, Anisotropic detectors for DArk Matter Observation) to exploit deep underground the directionality approach by using anisotropic $ZnWO_4$ scintillators has been explored; for details see in the 2012 publication list.

For completeness, we mention that another interesting idea about a detector with anisotropic response is put forward by us and some external collaborators; it is based on the use of Carbon Nanotubes (CNT).

5.2 Nemesis

In the period of interest here, the results of the NEMESIS experiment which has operated at sea-level in the Physics Department of the Roma "Tor Vergata" University have also been published (see 2012 publication list). The measurements obtained in the investigation of possible exotic components in cosmic rays by exploiting the delayed coincidence technique have been presented; no excess was found in the experimental data. These results restrict the DAEMONs (DArk Electric Matter Objects), suggested as a possible exotic component in cosmic rays able to contribute to the Dark Matter) flux to be less than 0.32 DAEMONs/$(days \times m^2 \times sr)$ at 90% C.L.. In particular, this upper limit does not support the possible positive hint previously reported by the sea-level St. Petersburg experiment, considering the same approach and physical scenario. Details can be found in the 2012 publication list.

6 Conclusions

The positive model independent evidence for the presence of DM particles in the galactic halo is now supported at 8.9σ C.L. (on a cumulative exposure of 1.17 ton×yr i.e. 13 annual cycles of DAMA/NaI and DAMA/LIBRA) and is compatible with a wide set of scenarios regarding the nature of the DM candidate and related astrophysical, nuclear and particle Physics. The last upgrade of DAMA/LIBRA, occurred in fall 2012, was successfully concluded; further improvements are planned. The results, obtained by analysing the data of the last (seventh) annual cycle of DAMA/LIBRA-phase1, will be released soon, giving the final DM model independent result of DAMA/LIBRA-phase1.

DAMA/LIBRA-phase2 – started after the replacement of all the PMTs with new ones having higher quantum efficiency – is continuously in data taking. The strictly quality control allows DAMA/LIBRA to be still the highest radiopure set-up in the field with the largest exposed sensitive mass, the full control of running conditions, the largest duty-cycle and an exposure orders of magnitude larger than any other activity in the field.

Finally, in 2012 all the DAMA/set-ups have regularly been in data taking and various kinds of measurements are in progress and planned for the future. Several competing results on developments and rare processes have been published.

7 List of Publications during 2012

1. P. Belli, R. Bernabei, R.S. Boiko, V.B. Brudanin, F. Cappella, V. Caracciolo, R. Cerulli, D.M. Chernyak, F.A. Danevich, S. d'Angelo, A. Di Marco, M.L. Di Vacri, E.N. Galashov, A. Incicchitti, V.V. Kobychev, G.P. Kovtun, N.G. Kovtun, V.M. Mokina, M. Laubenstein, S.S. Nagorny, S. Nisi, D.V. Poda, R.B. Podviyanuk, O.G. Polischuk, D. Prosperi, A.P. Shcherban, V.N. Shlegel, D.A. Solopikhin, Yu.G. Stenin, J. Suhonen, A.V. Tolmachev, V.I. Tretyak, Ya.V. Vasiliev, R.P. Yavetskiy, *Searches for neutrinoless resonant double electron captures at LNGS*, J. of Physics: Conf. Ser. 375 (2012) 042024.

2. R. Cerulli, R. Bernabei, P. Belli, F. Cappella, C.J. Dai, A. d'Angelo, A. Di Marco, H.L. He, A. Incicchitti, X.H. Ma, F. Montecchia, X.D. Sheng, R.G. Wang, Z.P. Ye, *Technical aspects in dark matter investigations*, J. of Physics: Conf. Ser. 375 (2012) 012006.

3. P. Belli, R. Bernabei, R.S. Boiko, V.B. Brudanin, F. Cappella, V. Caracciolo, R. Cerulli, D.M. Chernyak, F.A. Danevich, S. d'Angelo, E.N. Galashov, A. Incicchitti, V.V. Kobychev, M. Laubenstein, V.M. Mokina, D.V. Poda, R.B. Podviyanuk, O.G. Polischuk, V.N. Shlegel, Yu.G. Stenin, J. Suhonen, V.I. Tretyak and Ya.V. Vasiliev, *Search for double decay of* ^{106}Cd *by using isotopically enriched* $106CdWO_4$ *crystal scintillator*, J. of Physics: Conf. Ser. 375 (2012) 042021.

4. R. Bernabei, P. Belli, F. Cappella, V. Caracciolo, R. Cerulli, C. J. Dai, A. d'Angelo, A. Di Marco, H. L. He, A. Incicchitti, X. H. Ma, F. Montecchia, X. D. Sheng, R. G. Wang and Z. P. Ye, *DAMA/LIBRA results and perspectives*, J. of Physics: Conf. Ser. 375 (2012) 012002.

5. R. Bernabei, P. Belli, A. Di Marco, F. Montecchia, F. Cappella, A. d'Angelo, A. Incicchitti, V. Caracciolo, R. Cerulli, C.J. Dai, H.L. He, X.H. Ma, X.D. Sheng, R.G. Wang, Z.P. Ye, *DAMA/LIBRA at Gran Sasso*, Phys. Proc. 37 (2012) 1095-1104.

6. R. Bernabei, P. Belli, A. Di Marco, F. Montecchia, F. Cappella, A. d'Angelo, A. Incicchitti, D. Prosperi, R. Cerulli, C.J. Dai, H.L. He, X.H. Ma, X.D. Sheng, R.G. Wang, Z.P. Ye, *Particle dark matter signal in DAMA/LIBRA*, Nucl. Inst. and Meth. A 692 (2012) 120-122.

7. P. Belli, R. Bernabei, R. Cerulli, F.A. Danevich, E. Galenin, A. Gektin, A. Incicchitti, V. Isaienko, V.V. Kobychev, M. Laubenstein, S.S. Nagorny, R.B. Podviyanuk, S. Tkachenko, V.I. Tretyak, *Radioactive contamination of SrI_2(Eu) crystal scintillator*, Nucl. Inst. and Meth. A 670 (2012) 10-17.

8. R. Bernabei, P. Belli, A. Bussolotti, F. Cappella, V. Caracciolo, M. Casalboni, R. Cerulli, C.J. Dai, A. d'Angelo, A. Di Marco, H.L. He, A. Incicchitti, H.H. Kuang, M. Laubenstein, X.H. Ma, A. Mattei, F. Montecchia, C. Palazzesi, P. Prosposito, X.D. Sheng, R.G. Wang, Z.P. Ye, *Performances of the new high quantum efficiency PMTs in DAMA/LIBRA*, Journal of Instrumentation 7 (2012) P03009.

9. R. Bernabei, P. Belli, F. Cappella, V. Caracciolo, R. Cerulli, C. J. Dai, A. d'Angelo, A. Di Marco, H. L. He, A. Incicchitti, X. H. Ma, F. Montecchia, X. D. Sheng, R. G. Wang, Z. P. Ye, *Particle Dark Matter in the galactic halo: results from DAMA/LIBRA*, Int. J. of Modern Physics (Conf. Ser.) 12 (2012) 37.

10. R. Bernabei, P. Belli, F. Cappella, R. Cerulli, C.J. Dai, A. d'Angelo, S. d'Angelo, A. Di Marco, H.L. He, A. Incicchitti, X.H. Ma, F. Montecchia, X.D. Sheng, R.G. Wang, Z.P. Ye, *Search for charge non-conserving processes in ^{127}I by coincidence technique*, Eur. Phys. J. C 72 (2012) 1920.

11. P. Belli, R. Bernabei, F. Cappella, R. Cerulli, F.A. Danevich, A. d'Angelo, A. Incicchitti, V.V. Kobychev, M. Laubenstein, O.G. Polischuk, V.I. Tretyak, *Search for ^7Li solar axions using resonant absorption in LiF crystal: final results*, Physics Letters B 711 (2012) 41.

12. P. Belli, R. Bernabei, R.S. Boiko, V.B. Brudanin, F. Cappella, V. Caracciolo, R. Cerulli, D.M. Chernyak, F.A. Danevich, S. d'Angelo, E.N. Galashov, A. Incicchitti, V.V. Kobychev, M. Laubenstein, V.M. Mokina, D.V. Poda, R.B. Podviyanuk, O.G. Polischuk, V.N. Shlegel, Yu.G. Stenin, J. Suhonen, V.I. Tretyak, Ya.V. Vasiliev, *Search for double beta decay processes in ^{106}Cd with the help of $^{106}CdWO_4$ crystal scintillator*, Phys. Rev. C 85 (2012) 044610.

13. R. Bernabei, P. Belli, F. Cappella, V. Caracciolo, R. Cerulli, C. J. Dai, A. d'Angelo, A. Di Marco, H. L. He, A. Incicchitti, X. H. Ma, F. Montecchia, X. D. Sheng, R. G. Wang, Z. P. Ye, *No role for muons in the DAMA annual modulation results*, Eur. Phys. J. C 72 (2012) 2064.

14. R. Bernabei, *Dark matter particles in the galactic halo: DAMA/LIBRA results and perspectives*, Ann. Phys. 524 (2012) 497.

15. A.S. Barabash, P. Belli, R. Bernabei, F. Cappella, V. Caracciolo, S. Castellano, R. Cerulli, D.M. Chernyak, F.A. Danevich, E.N. Galashov, A. Incicchitti, V.V. Kobychev, S.I. Konovalov, M. Laubenstein, D.V. Poda, R.B. Podviyanuk, O.G. Polischuk, V.N. Shlegel, V.I. Tretyak, V. I. Umatov, Ya. V. Vasiliev, *First results of the experiment to search for double beta decay of* ^{116}*Cd with the help of enriched* ^{116}*CdWO4 cystal scintillators*, to appear in the Proceed. of the 4-th Int. Conf. on Current Problems in Nuclear Physics and Atomic Energy (NPAE2012), September 2012, Kiev, Ukraine.

16. P. Belli, R. Bernabei, F. Cappella, R. Cerulli, F.A. Danevich, S. d'Angelo, A. Di Marco, A. Incicchitti, G.P. Kovtun, N.G. Kovtun, M. Laubenstein, D.V. Poda, O.G. Polischuk, A.P. Shcherban, V. I. Tretyak, *First search for double beta decay of Osmium by low background HPGe detector (preliminary results)*, to appear in the Proceed. of the 4-th Int. Conf. on Current Problems in Nuclear Physics and Atomic Energy (NPAE2012), September 2012, Kiev, Ukraine.

17. R. Bernabei, P. Belli, F. Cappella, V. Caracciolo, R. Cerulli, C. J. Dai, A. d'Angelo, A. Di Marco, H. L. He, A. Incicchitti, X. H. Ma, F. Montecchia, X. D. Sheng, R. G. Wang, Z. P. Ye, *DAMA/LIBRA results and perspectives*, Bled workshop in Physics vol. 13 n.2 (2012),1 - ISSN 1580-4992.

18. R. Bernabei, P. Belli, F. Cappella, R. Cerulli, A. d'Angelo, F. Emiliani, A. Incicchitti, *Search for DAEMONS with NEMESIS*, Mod. Phys. Lett. A 27 (2012) 1250031.

References

[1] R. Bernabei et al., Nucl. Instr. and Meth. A 592 (2008) 297.

[2] R. Bernabei et al., Eur. Phys. J. C 56 (2008) 333.

[3] R. Bernabei et al., Eur. Phys. J. C 67 (2010) 39.

[4] R. Bernabei et al., Eur. Phys. J. C 62 (2009) 327.

[5] P. Belli et al., Phys. Rev. D 84 (2011) 055014.

[6] P. Belli, R. Bernabei, C. Bacci, A. Incicchitti, R. Marcovaldi, D. Prosperi, DAMA proposal to INFN Scientific Committee II, April 24^{th} 1990.

[7] R. Bernabei et al., Phys. Lett. B 389 (1996) 757; R. Bernabei et al., Phys. Lett. B 424 (1998) 195; R. Bernabei et al., Phys. Lett. B 450 (1999) 448; P. Belli et al., Phys. Rev. D 61 (2000) 023512; R. Bernabei et al., Phys. Lett. B 480 (2000) 23; R. Bernabei et al., Phys. Lett. B 509 (2001) 197; R. Bernabei et al., Eur. Phys. J. C 23 (2002) 61; P. Belli et al., Phys. Rev. D 66 (2002) 043503.

[8] R. Bernabei et al., Il Nuovo Cim. A 112 (1999) 545.

[9] R. Bernabei et al., Eur. Phys. J. C18 (2000) 283.

[10] R. Bernabei el al., La Rivista del Nuovo Cimento 26 n.1 (2003) 1-73.

[11] R. Bernabei et al., Int. J. Mod. Phys. D 13 (2004) 2127.

[12] R. Bernabei et al., Int. J. Mod. Phys. A 21 (2006) 1445.

[13] R. Bernabei et al., Eur. Phys. J. C 47 (2006) 263.

[14] R. Bernabei et al., Int. J. Mod. Phys. A 22 (2007) 3155.

[15] R. Bernabei et al., Eur. Phys. J. C 53 (2008) 205.

[16] R. Bernabei et al., Phys. Rev. D 77 (2008) 023506.

[17] R. Bernabei et al., Mod. Phys. Lett. A 23 (2008) 2125.

[18] R. Bernabei et al., Phys. Lett. B408 (1997) 439; P. Belli et al., Phys. Lett. B460 (1999) 236; R. Bernabei et al., Phys. Rev. Lett. 83 (1999) 4918; P. Belli et al., Phys. Rev. C60 (1999) 065501; R. Bernabei et al., Il Nuovo Cimento A112 (1999) 1541; R. Bernabei et al., Phys. Lett. B 515 (2001) 6; F. Cappella et al., Eur. Phys. J.-direct C14 (2002) 1; R. Bernabei et al., Eur. Phys. J. A 23 (2005) 7; R. Bernabei et al., Eur. Phys. J. A 24 (2005) 51; R. Bernabei et al., Astrop. Phys. 4 (1995) 45.

[19] K.A. Drukier et al., Phys. Rev. D 33 (1986) 3495.

[20] K. Freese et al., Phys. Rev. D 37 (1988) 3388.

[21] R. Bernabei et al., *AIP Conf. Proceed.* **1223**, 50 (2010) (arXiv:0912.0660).

[22] R. Bernabei et al., J. Phys.: Conf. Ser. **203**, 012040 (2010) (arXiv:0912.4200); http://taup2009.lngs.infn.it/slides/jul3/nozzoli. pdf, talk given by F. Nozzoli.

[23] R. Bernabei et al., in the volume *Frontier Objects in Astrophysics and Particle Physics* (Vulcano 2010), S.I.F. Ed. (2011), 157 (arXiv:1007.0595).

[24] R. Bernabei et al., Can. J. Phys. 89 (2011) 11.

[25] R. Bernabei et al., to appear on Proceed. of the Int. Conf, TIPP 2011.

[26] R. Bernabei et al., arXiv:1210.6199; arXiv:1211.6346

[27] A. Bottino et al., Phys. Rev. D 85 (2012) 095013.

[28] A. Bottino et al., arXiv:1112.5666.

[29] Borexino coll., D. D'Angelo talk at the Int. Conf. Beyond the Desert 2010, February 2010, Cape Town, South Africa; G. Bellini, talk at the Scientific Committee II of INFN, sept. 2010, available on the web site of the Committee: http://www.infn.it/

[30] Borexino coll., Proceed. of Int. Cosmic Ray Conference (ICRC 2011) Beijing, China, 2011, in press [arXiv:1109.3901]; Borexino coll., [arXiv:1202.6403] submitted for publication.

[31] M. Selvi on behalf of the LVD coll., Proceed. of The 31st Int. Cosmic Ray Conference (ICRC 2009) Lodz, Poland, 2009, in press.

[32] M. Ambrosio et al., Astropart. Phys. 7 (1997) 109-124.

[33] P. Belli et al., Phys. Lett. B 465, 315 (1999).

[34] P. Belli et al., Il Nuovo Cim. 103A (1990) 767.

[35] P. Belli et al., Phys. Lett. B 387 (1996) 222 and Phys. Lett. B 389 (1996) 783 (erratum); R. Bernabei et al., New J. Phys. 2 (2000) 15.1; Eur. Phys. J.-direct C11 (2001) 1; Phys. Lett. B 436 (1998) 379; R. Bernabei et al., in the volume "Beyond the Desert 2003", Springer (2003) 365.

[36] R. Bernabei et al., Nucl. Instr. & Meth. A482 (2002) 728.

[37] R. Bernabei et al., Phys. Lett. B 546 (2002) 23; F. Cappella, PhD Thesis, Università di Roma "Tor Vergata", 2005.

[38] P. Belli et al., Il Nuovo Cim. C 19 (1996) 537; Astrop. Phys. 5 (1996) 217.

[39] R. Bernabei et al., Phys. Lett. B 527 (2002) 182.

[40] P. Belli et al., Phys. Rev. D 61 (2000) 117301; Phys. Lett. B 465 (1999) 315; R. Bernabei et al., Phys. Lett. B 493 (2000) 12; Eur. Phys. J. A 27 s01 (2006) 35.

[41] R. Bernabei et al., Astropart. Phys. 7 (1997) 73; R. Bernabei et al., Il Nuovo Cim. A 110 (1997) 189; P. Belli et al., Astropart. Phys. 10 (1999) 115; P. Belli et al., Nucl. Phys. B 563 (1999) 97; R. Bernabei et al., Nucl. Phys. A 705 (2002) 29; P. Belli et al., Nucl. Instr. Meth. A 498 (2003) 352; R. Cerulli et al., Nucl. Instr. Meth. A 525 (2004) 535; R. Bernabei et al., Nucl. Instr. Meth. A 555 (2005) 270; R. Bernabei et al., Ukr. J. Phys. 51 (2006) 1037; P. Belli et al., Nucl. Phys. A 789 (2007) 15; P. Belli et al., Phys. Rev. C 76 (2007) 064603; P. Belli et al., Eur. Phys. J. A 36 (2008) 167; P. Belli et al., J. Phys. G 38 (2011) 015103.

[42] P. Belli et al., Nucl. Phys. A 826 (2009) 256; P. Belli et al., Phys. Lett. B 658 (2008) 193.

[43] P. Belli et al., Nucl. Instrum. Meth. A 626-627 (2011) 31.

[44] P. Belli et al., Nucl. Instr. Meth. A 615 (2010) 301.

[45] M. Hirsch et al., Z. Phys. A 347 (1994) 151.

[46] A.S. Barabash, et al., J. of Instr. 6 (2011) P08011.

[47] L.D. Duffy, K. van Bibber, New J. Phys. 11 (2009) 105008.

[48] S. Moriyama, Phys. Rev. Lett. 75 (1995) 3222.

[49] M. Krcmar et al., Phys. Rev. D 64 (2001) 115016.

[50] P. Belli et al., Nucl Phys. A 806 (2008) 388.

[51] A.V. Derbin et al., JETP Lett. 81 (2005) 365.

DarkSide-50 Annual Report - 2012

D. Akimov[j],T. Alexander[c], D. Alton[a], K. Arisaka[w], H.O. Back[l], P. Beltrame[w], J. Benziger[k], A. Bolozdynya[j], G. Bonfini[h], A. Brigatti[r], J. Brodsky[l], S. Bussino[u], L. Cadonati[z], F. Calaprice[l], A. Candela[h], H. Cao[l], P. Cavalcante[h], A. Chavarria[l], A. Chepurnov[i] S. Chidzik[l],D. Cline[w], A.G. Cocco[s], C. Condon[l], D. D'Angelo[r], S. Davini[y],M. De Vincenzi[u], E. De Haas[l], A. Derbin[m], G. Di Pietro[r], I. Dratchnev[m], D. Durben[b], A. Empl[y], A. Etenko[j], A. Fan[w], G. Fiorillo[s], K. Fomenko[h], G. Forster[z], F. Gabriele[l], C. Galbiati[l],S. Gazzana[h], C. Ghag[p], C. Ghiano[h], A. Goretti[l], L. Grandi[l],M. Gromov[l], M. Guan[d], C. Guo[d], G. Guray[l], E. V. Hungerford[y], Al. Ianni[h], A. Ianni[l], A. Kayunov[m], K. Keeter[b], C. Kendziora[c], S. Kidnera[a], R. Klemmer[l], V. Kobychev[e], G. Koh[l], M. Komor[l], D. Korablev[g], G. Korga[y], E. Shields[l], P. Li[d], B. Loer[c], P. Lombardi[r], C. Love[o], L. Ludhova[r], S. Luitz[n], L. Lukyanchenko[l], A. Lund[z], K. Lung[w], Y. Ma[d], I. Machulin[j], S. Mari[u], J. Maricic[x], C.J. Martoff[o], Y. Meng[w], E. Meroni[r], P. Meyers[l] T. Mohayai[l], D. Montanari[c], M. Montuschi[h], M.E. Monzani[n], P. Mosteiro[l], B. Mount[b], V. Muratova[m], A. Nelson[l], A. Nemtzow[z], N. Nurakho[v], M. Orsini[h], F. Ortica[t], M. Pallavicini[q], E. Panti[c] S. Parmeggiano[r],R. Parsells[l], N. Pelliccia[t], L. Perasso[q], F. Perfetto[s], A. Pocar[z], S. Pordes[c], K. Randle[z], G. Ranucci[r], A. Razeto[h], A. Romani[t], B. Rossi[l], N. Rossi[h] S.D. Rountree[a], P. Saggese[h], R. Saldanha[h], C. Salvo[q], W. Sands[l], M. Seigar,[v], D. Semenov[m], M. Skorokhvatov[j], O. Smirnov[g], A. Sotnikov[g], S. Sukhotin[j], Y. Suvarov[w], R. Tartaglia[h], J. Tatarowicz[o], G. Testera[q], A. Teymourian[w],J. Thompson[b], E. Unzhakov[m], R.B. Vogelaara[a], H. Wang[w], S. Westerdale[l], M. Wojcik[f], A. Wright[l], J. Xu[l], C. Yang[d], S. Zavatarelli[q], M. Zehfus[f], W. Zhong[d],G. Zuzel[f]

[a] Physics and Astronomy Department, Augustana College, Sioux Falls, SD 57197, USA
[b] School of Natural Sciences, Black Hills State University, Spearfish, SD 57799, USA
[c] Fermi National Accelerator Laboratory, Batavia, IL 60510, USA
[d] Institute of High Energy Physics, Beijing 100049, China
[e] Institute for Nuclear Research, National Academy of Sciences of Ukraine, Kiev 03680, Ukraine
[f] Smoluchowski Institute of Physics, Jagellonian University, Krakow 30059, Poland
[g] Joint Institute for Nuclear Research, Dubna 141980, Russia
[h] Laboratori Nazionali del Gran Sasso, SS 17 bis Km 18+910, Assergi (AQ) 67010, Italy
[i] Skobeltsyn Institute of Nuclear Physics, Lomonosov Moscow State University, Moscow 119991, Russia
[j] National Research Centre Kurchatov Institute, Moscow 123182, Russia
[k] Chemical Engineering Department, Princeton University, Princeton, NJ 08544, USA
[l] Physics Department, Princeton University, Princeton, NJ 08544, USA
[m] Saint Petersburg Nuclear Physics Institute, Gatchina 188350, Russia
[n] SLAC National Accelerator Center, Menlo Park, CA 94025, USA
[n] Physics Department, Temple University, Philadelphia, PA 19122, USA
[o] Department of Physics and Astronomy, University College London, London WC1E 6BT, United Kingdom
[p] Physics Department, Universit 'a degli Studi and INFN, Genova 16146, Italy
[q] Physics Department, Universit 'a degli Studi and INFN, Milano 20133, Italy
[r] Physics Department, Universit 'a degli Studi Federico II and INFN, Napoli 80126, Italy
[s] Chemistry Department, Universit 'a degli Studi and INFN, Perugia 06123, Italy
[t] Physics Department, Universit 'a degli Studi Roma Tre and INFN, Roma 00146, Italy
[u] Department of Physics and Astronomy, University of Arkansas, Little Rock, AR 72204, USA
[v] Physics and Astronomy Department, University of California, Los Angeles, CA 90095, USA
[w] Department of Physics and Astronomy, University of Hawaii, Honolulu, HI 96822, USA
[x] Department of Physics, University of Houston, Houston, TX 77204, USA
[y] Physics Department, University of Massachusetts, Amherst, MA 01003, USA
[z] Physics Department, Virginia Tech, Blacksburg, VA 24061, USA

Abstract

The DarkSide collaboration is undertaking a direct search for WIMP dark matter using a two-phase liquid-argon (LAr) Time Projection Chamber (TPC). This detector is embedded inside water and scintillator veto tanks which are used to shield and identify neutron background events. The detector is filled with LAr, depleted in the ^{39}Ar radio-isotope, as is recovered and purified from underground gas wells. The 50 kgm DarkSide detector (fiducial mass of 33 kg) has a competitive physics reach, particularly at the higher WIMP masses ($\approx 10^{-45}$ cm^2), and remains essentially background free if scaled to an approximately 5T future design. The detector and supporting systems are nearing completion and are presently being installed in Hall C at LNGS. Initial commissioning is expected to begin in late March 2013, and the first data runs are expected by Spring of 2013. The DarkSide-50 detector will acquire data using underground Argon in the Fall of 2013 and run for approximately 3 years.

1 Introduction

The existence of dark matter is inferred from gravitational effects, but its true identity remains unknown. One possibility motivated by elementary particle physics and cosmology, is that dark matter consists of elementary particles which are remnants of the creation of the universe [1]. Direct observation of these Weakly Interacting Massive Particles (WIMPs) might be observed for example, in experiments at the LHC or from radiation produced by WIMP-WIMP annihilations in galactic halos. However, it may also be possible to detect WIMPs through their collisions with atomic nuclei in a laboratory, as the earth orbits through the dark matter halo of our galaxy.

In 2009, the DarkSide Collaboration proposed to undertake a direct search for WIMPs at the LNGS facility using a 2-phase liquid-argon detector [2]. This proposal featured 1) the use of underground Ar, depleted in the radio-isotope ^{39}Ar, 2) essentially background free detection through a combination of water and scintillation shielding Vetos, and 3) careful screening and preparation using radio-pure components. A prototype 10 kg test detector was operated in Hall C at LNGS for the past year, providing information and guidance in order to complete the proposed 50 kg DarkSide-50 detector. This 50 kg detector will now be commissioned in the coming few months. The following sections develop in more detail the progress of the past year and present status of the DarkSide-50 proposal.

2 The DS-10 Experiment at LNGS

For the past 12 months the DarkSide collaboration has operated the DarkSide-10 prototype, which is a 10 kg, two-phase LAr-TPC, Figure 1. DarkSide-10 was a test apparatus for many of the innovations of the DarkSide program [3]. This prototype detector was surrounded by a 1 m-thick shield of polyethylene sheets and water tanks. The TPC was filled with atmospheric argon because it was not designed to yield physics results. The detector ran in several configurations to explore and verify various design choices for DarkSide.

Some of the technology and geometry with appropriate scaling which was explored by DarkSide-10 is incorporated in DarkSide-50. This is now discussed in the remainder of this section. The drift extraction fields required for the two-phase TPC are contained between two transparent conducting electrodes. These are constructed of an Indium-Tin Oxide (ITO) deposition on transparent windows. The initial, above-ground tests used acrylic windows, but have now been replaced with synthetic fused-silica windows. The fused silica windows are thinner, and also allow the ITO deposition to be significantly thinner. This is believed to be a major reason for the high photo-electron (pe) yields for the scintillation light as reported below [4]. Because Argon scintillation light at 128 nm does not pass through most windows, including those of of the cryogenic PMTs, the entire inner surface of the TPC including the ITO windows, is coated with a vacuum-evaporated, wave length-shifter (WLS) TetraPhenylButadiene(TPB). DarkSide-10 was used to test different reflective substrates, including 3M Vikuity and PTFE, in order to

optimize the photo-electron yield, mechanical robustness, and their radio-purity. The transparent-electrode construction is unique to DarkSide and provides near-ideal planar electrodes for terminating the TPC field, while maintaining high window transparency.

In DarkSide-10 the wavelength-shifted light illuminates two arrays of seven Hamamatsu R11065 PMT's located behind the top and bottom windows [5]. These PMTs lie outside the active detector volume but within the LAr. During the course of DarkSide-10 running, the early-production R11065's were selected for best performance at LAr temperature. This information was communicated to Hamamatsu to help guide the ongoing collaborative development of the PMTs.

n ionization charge deposited in the LAr is drifted to the top of the TPC where it is extracted into a Ar gas pocket to produce an electro-luminescence measure of the charge. This signal provides additional nuclear-recoil discrimination [6]. The extraction electrode is composed of a thin stainless steel membrane on which are etched a close-packed array of hexagonal holes. The membrane is greater than 85% transparent to scintillation light and essentially 100% transparent to ionization. The best DarkSide-10 photo-electron yield at null field was 9 p.e./keVee [4]. This high photo-electron yield was stable within a few percent for over 6 weeks.

The high voltage (HHV) for the drift field requires careful design of the feedthroughs in the TPC cryostat. A field of 150 kV is required for a ton scale detector, so a new HHV feedthrough patterned after the ICARUS 150 kV feedthrough [7], was installed last year. It uses ultra-high-molecular-weight polyethylene as an insulator and has been tested in liquid argon to 100 kV. This design held -35 kV input voltage on the first attempt, and has operated flawlessly providing the design drift field of 1 kV/cm and extraction field of 4 kV/cm for DS-10.

The DarkSide-10 detector was operated throughout the current reporting period, achieving and exceeding all its operating and design goals. These include obtaining a record-high scintillation light photo-electron yield (9 p.e./keVee), stable TPC operation at full design voltages over an approximately four month period of continuous operation.

3 The Outer Detectors

To obtain the scientific reach for a WIMP search at a sensitivity of 10^{-46} to 10^{-47} cm^2 at the Gran Sasso depth, effective neutron and muon suppression must be employed. The DarkSide experiment uses a combination of active water and scintillator Vetos.

3.1 The water veto (CTF)

DarkSide-50 is mounted within the 10m diameter, 11m tall Borexino CTF water tank, which provides an approximately 4m thick active shield of high purity water. This tank is

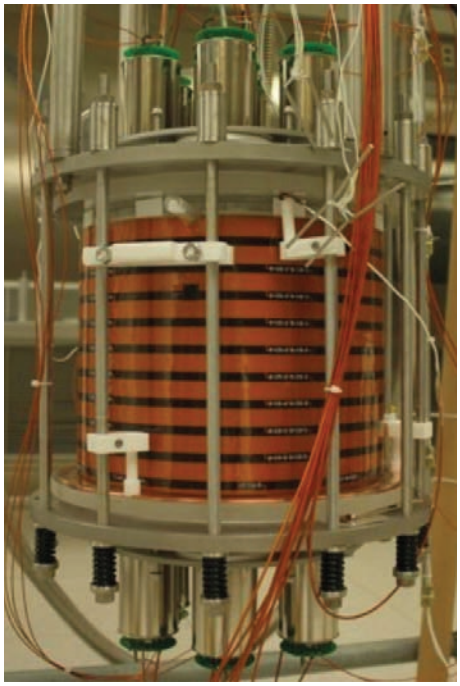

Figure 1: A photograph of the DarkSide10 detector showing the copper rings which provide the constant drift field, and the PMT located on top and bottom of the active detector region

Figure 2: A photograph of the inside of the CTF water tank showing the Stainless Steel Sphere which contains the scintillation veto

instrumented with 80 PMT which provide a Cherenkov signal for penetrating muons and charged particle showers. The interior of the walls of the CTF are covered with a Tyvek reflectance film [8]. The PMT point inward from the CTF wall and upward from the floor. All PMT have mu-metal shields. As anticipated from simulation, the PMT signals will be highly efficient in vetoing muon and muon induced showers (see the simulation section below).

3.2 The scintillation veto (LSV)

A 4m stainless steel sphere contains 15T of a purified 50-50 mixture of TriMethylBorate (TMB) and 1,3,4-TriMethylBenzene (PseudoCumene, PC), augmented with natural boron (20% ^{10}B). The Boron has a large capture cross section for ^{10}B(n, α)^{7}Li, which reduces the capture time and capture does not result in gamma emission. The TPC will be positioned at the center of the LSV, which itself is centered in the CTF water veto, Figure 2. The scintillator is viewed by 110 Hamamatsu R5912-HQE-LRI glass-bulb PMT with mu-metal shields [5]. These look inward from the interior surface of the stainless steel sphere. The interior and exterior of the LSV stainless steel sphere is covered with

Lumirror reflectance foil [8], which has up to 90/All PMT have mu-metal shields. It is anticipated that a neutron capture will produce at least 30 photo-electrons, which will be easily detectable.

All necessary scintillation efficiency, safety, and environmental tests on the main components of this mixture have been carried out at Princeton and LNGS, and safe handling procedures have been developed and written according to LNGS regulations. The scintillator thickness is not only sufficient for the background free operation of DarkSide-50, but also for a planned upgrade to a ton scale detector.

The CTF water tank was drained and an the stainless scintillation sphere installed inside the tank. The tank surfaces have been draped with the Lumirror reflector and the PMTs and cabling are in the process of being installed. Major construction of the LSV within the CTF tank has been completed.

4 The Time Projection Chamber

4.1 Underground Argon

Atmospheric argon contains ^{39}Ar which is a β-emitter (Q=565 keV, $t_{1/2}$=269 yr) [9]. It is produced by cosmic ray spallation, and nominally occurs at an activity of 1 Bq/kg. Since the identification of nuclear recoil uses the pulse shape of the scintillation light,. a clean measurement of each individual pulse out to several microseconds is required. Thus pile-up in larger, unsegmented LAr detectors can only be avoided by using a isotopically purified sample of Ar. The DarkSide group has demonstrated extraction of low radioactivity argon from underground sources of gas (UAr). With NSF funding over the past two years, DarkSide developed a source of low radioactivity argon [10]. In addition, a production plant for collecting, storing and purifying the ^{40}Ar gas was constructed. In this plant, the extracted gas is increase from 600 parts per million to a few percent (3-5%) [11]. Subsequent purification of UAr is then carried out in a cryogenic distillation plant operating at Fermilab, where the N_2/UAr ratio in the output is below the sensitivity limit of our gas analyzer. However, we believe that a purity better than 99.999% is within reach. The distillation rate is on the order of 1 kg/day, but we expect this to improve as we refine the operating conditions of the column. As of February 2013, more than 100 kg of UAR have been extracted and about 25 kg of this purified through the distillation plant. A newly designed, high-pressure pre-distillation of the gas increases the argon content and the through-put.

The ^{39}Ar content of the underground argon was recently measured by constructing a low background liquid argon scintillation detector. The detector was designed to have minimum intrinsic radioactivity, as the external background was efficiently shielded with a graded shield of low-radioactivity lead and oxygen-free, high conductivity copper. The experiment was operated underground at the Kimballton Underground Research Facility

(KURF) in order to reduce cosmogenic background. By comparing the underground argon spectrum with an atmospheric argon spectrum, Figure 3, and subtracting expected backgrounds in the detector, a 95%-C.L. upper limit of 0.65% for the ^{39}Ar concentration in UAr compared to that in the atmospheric argon was found.

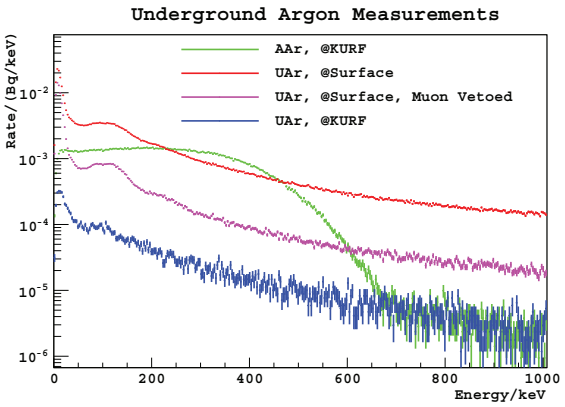

Figure 3: The figure shows the result of an attempted measurement of the ^{39}Ar content in the extracted underground Argon. It demonstrates that the measured activity in undetectable at a level of less than 0.65% of Atmospheric Ar (Blue compared to Green curves)

Figure 4: A photograph of the DarkSide50 cryostat hanging from a flange similar to the flange on top of the CTF

4.2 Construction of the TPC

Design of DarkSide-50 was developed in parallel with the DarkSide-10 prototype. The engineering design is completed, and the procurement of parts and construction of the TPC is in progress. The design features a low background stainless steel cryostat of 160 kg, active volume diameter and height each of 35.6 cm, an Ar gas pocket above the LAr of 1 cm, a total LAr mass of 145 kg, and an active LAr mass of 49.4 kg. The TPC has arrays of 19 Hamamatsu R11065 PMTs viewing the LAr from the top and bottom of the inner TPC vessel. The typical drift field is 1 kV/cm with an extraction field of 3.8 kV. The maximum applied HHV field is therefore approximately - 43 kV. The inner cylinder containing the active volume is made of high reflectivity Teflon with embedded Cu rings, (similar to the figure of DS-10, Figure **??**). The rings produce a graded potential in order to supply the constant drift field. As described in the above section on the DS-10 test facility, the internal components of the TPC are plated with a TPB wave shifter. All components for the vessel have been screened and will be properly cleaned before assembly to insure low levels of radio-activity. A sealed bellows reaching from the cryostat to the feedthrough plate in the radon-suppressed clean-room will limit the exposure of

the internal detector components to radon-bearing air. The bellows are an extension of the detector internal vacuum, and are also employed as a common cable duct and argon recirculation line. They are assembled and sealed to the detector in the clean room, and are intended to remain un-opened throughout the experiment.

The metal-bulb, low-radioactivity R11065 PMTs with new Bialkali-LT, high efficiency photo-cathodes of the TPC operate of the at LAr temperatures. Hamamatsu has developed a low temperature) photo-cathode for this purpose [5]. The PMTs have been tested at the Napoli Cryogenic test facility at room and LN temperatures, using Laser inputs. A number were found with problems and returned to the manufacturer. Another problem recently observed in DS-10 was manifested as a rapid increase in dark current. The frequency of occurrence was correlated with the illumination level. This issue could presumably be fixed in a new version of the PMTs. However, a cold preamplifier positioned on the PMT base will be installed, as discussed in the Data Acquisition section below. This will allow operating the PMTs at lower voltage and thus lower gain which would mitigate the problem.

Assembly of the TPC will begin in the clean room atop the CTF facility in February 2013. Figure 4 shows the DarkSide50 dewar hanging from a flange similar to the one which seals the top of the liquid scintillator veto.

5 Electronics and DAQ

Due to the different responses of the TPC and veto detector systems, the DAQ involves three independent data streams; 1) data from the TPC, 2) data from the Vetos (Water and Scintillator Vetos), and 3) slow control data. The data streams are independently triggered, but the TPC triggers read both TPC and Veto data, while Veto triggers read only Veto data. The triggers are generated at the physical locations of the digitizers (the TPC in the clean-room atop the CTF and the Veto in the Control Room). These are properly synchronized to prevent conflicting overlaps. The TPC signals from the 38 PMTs are read by two waveform digitizers per PMT channel, in order to accommodate a sufficient dynamic range of PMT pulse heights. The small signal channel is amplified by a factor of 8 and is sensitive down to 1 photo-electron. It is digitized by CAEN 1720, 250 MHz 12 bit digitizers. The high signal channel is attenuated by a factor of 0.2 and read by a CAEN 1724, 128 MHz 14 bit digitizers. The high signal overlaps the range of the small signal channel, but extends the linear signal to $\approx$ 1000 pe in order to provide a reliable S1/S2 signal ratio for nuclear-recoil to electromagnetic ionization, and guarantees the study alpha and gamma backgrounds with little or no ADC saturation. WIMP events are expected to be fully contained in both channels.

The TPC wave form must acquire signals for the approximate 300 μs drift time in the TPC. This results in substantial amounts of data, and limits the TPC trigger rate to no more than $\approx$ 10 Hz. On the other hand the Veto signals are only a few 10's of ns wide

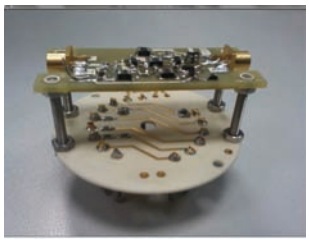

Figure 5: A picture of the cold preamp board mounted on the PMT base

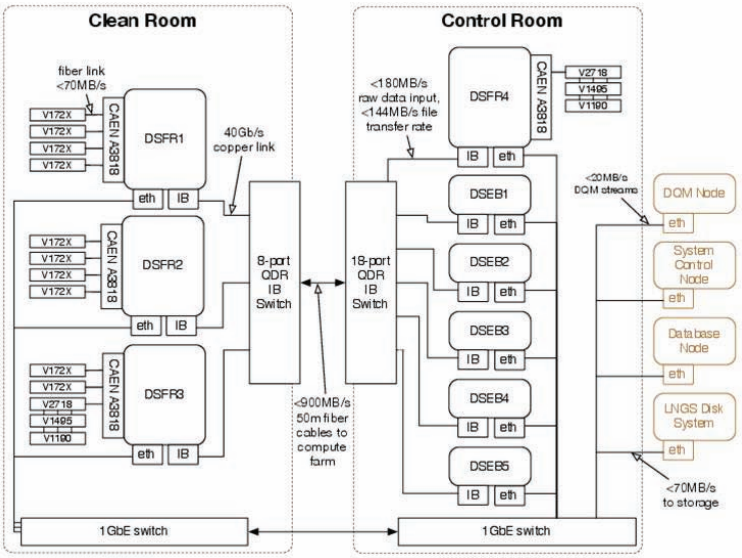

Figure 6: A block diagram of the TPC electronics.

and have limited dynamic range. They must be digitized with fast digitizers, although the data stream can be zero suppressed. The veto signals are processed by National Instruments NI-PXI 5162 1.35 GHz 10 bit digitizers. The bandwidth of all digitizers requires matching preamplifiers, and the low signal TPC channels in particular, require very low noise. A cold preamplifier placed on the TPC tube base in LAr, Figure 5 has been designed and tested, not only allowing the PMT to be run at lower high voltage, but providing an extremely low noise signal which feeds an amplification circuit prior to digitization.

Because the TPC and Veto digitization systems are physically separated by some 20-30m, the TPC digitizing system in the clean room nearer the TPC photo-tubes. Signals from both systems must be exchanged to synchronize the trigger and read out the TPC data, Figure 6. These signals are passed by optical Ethernet and 10 Gb Infiniband cables. System triggers are generated at each location by firmware encoded in CAEN 1495 logic modules, but the TPC V1495 module is the master unit and generates all trigger DAQ reads. The triggers have a unique 12-bit Trigger ID Number and 4bit trigger type. The TPC V1495 trigger module increments the Trigger Number when a trigger type is generated.

6 Cryogenics and infrastructure

There are two clean-rooms to support DarkSide-50 operations. DS-50 components will be cleaned in CR1, a completely rebuilt version of the Borexino clean room on the floor of Hall C. It is equipped with a large ultrasonic cleaner and vacuum oven. In CR1, the TPB wavelength shifter will be vacuum-deposited by 2-m-diameter evaporator which was

shipped from Princeton and rebuilt. A second similar room was constructed on top of the water tank, Figure 7, to support radon-free insertion of the TPC detector into the veto/shield systems, and for eventual detector servicing.

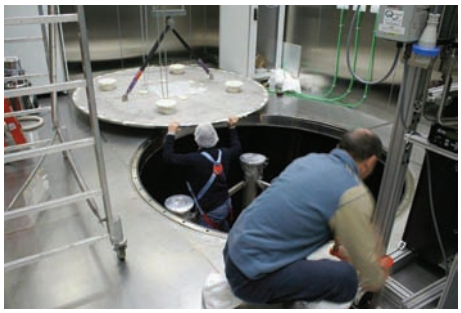

Figure 7: A picture of the clean-room mounted above the CTF which shows the insertion plate for the TPC cryostat with the Stainless Steel Scintillator vessel below.

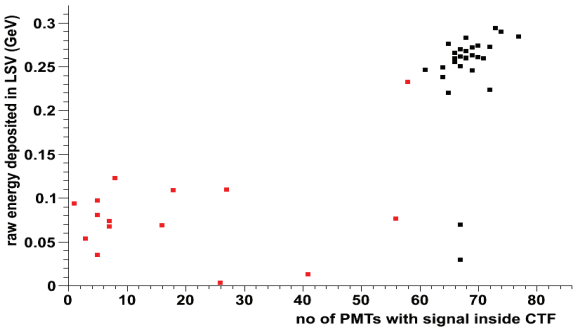

Figure 8: The result of a FLUKA simulation demonstrating that the water and scintillation Vetos result in background free operation for a 3-year run. Note that the number of PMT with signals either in the CTF or the LSV can remove by veto all background

The cooling and recirculation system for DarkSide-50 cryogens uses an external liquefaction plant based on a novel condenser. Argon gas flows out of the detector and is purified by passing through a heated getter. It is then cooled by heat exchange with a liquid nitrogen cold head located on top of the water tank, and is finally returned to the detector cryostat. Both the condenser and the associated gas/liquid handling system have passed initial operating tests. Preparation and approval of safety and operating procedures for DarkSide-50 are underway.

7 Simulations

Three independent simulation codes have been developed within the DarkSide collaboration to study and simulate the detector response and expected background. A full detector GEANT-4 simulation developed was developed in previous years to drive the TPC design and the requirements of material radio-purity [12]. In parallel with this simulation an optical Monte Carlo and a FLUKA simulation were developed to respectively study the optics and signals generated from local ionization in the TPC and a FLUKA study of cosmogenically produced backgrounds in the vetos and TPC.

In the optical study, the internal release of beta ionization at a given location in the detector generates the emission of primary scintillation light (S1). The ionization, drift and extraction of ionization electrons is followed into the gas pocket, and the production

of the secondary scintillation light (S2) produced. The code simulates the optical processes based on input obtained by analysis of experimental data. Thus photons are traced until they are absorbed or detected. The simulation is used to tune analysis algorithms developed in DarkSide10. Further improvements of this software are still being achieved.

At Gran Sasso depth, cosmic-ray muon interactions create backgrounds which can dominate experiments searching for rare events. Because of the difficulty of measuring very low-rate neutrons and other backgrounds, accurate simulations play a key role in understanding these backgrounds and designing a detector system which can eliminate them. We have undertaken a program to test and vet the accuracy of FLUKA cosmogenic background simulations through careful comparison with other simulations and available experimental data [13]. The starting point of any simulation of cosmogenic backgrounds in a specific experiment is the energy and angle dependent muon flux at the cavern wall within the Gran Sasso underground facility (LNGS.) This can be calculated from detailed information on the slant depth, overburden geometry, and composition of the surrounding rock through which the muons propagate. Details of the particular site and experimental apparatus are then required to reproduce the experimental background for a specific experiment. Our standard FLUKA results agree well with most existing data. After these checks, our simulation package was applied to predicting cosmogenic backgrounds in the DarkSide-50 detector. Simulating a 36 year exposure, we find a total of 10 neutron events which have energy deposited in the TPC. However, all of these events left sufficient energy deposition in the water and/or scintillator vetoes of the experiment to be identified and removed later in the analysis. This simulation, which is still being improved, supports the claim that the DarkSide-50 experimental design is capable of acquiring background-free data for the actual proposed 3-year run period Figure 8. Improvements in handling isotope production, which contributes to the neutron background, and the extension of the MC to implement signal response and data flows, are the next tasks of this activity.

8 Calibrations

The DarkSide detector will be calibrated using a combination of internally distributed and external point sources. The internal calibrations are undertaken by dissolving ^{83}Kr into the active argon volume. The mono-energetic electrons produced by the ^{83}Kr decay allow the uniformity of the energy response of the detector to be studied in detail. The short half-life of the isotope means that long term contamination of the detector is not a concern. A telescoping manipulator system similar to the one used by the Double Chooz experiment [14] allows neutron-and gamma-emitting point sources and a fast isotropic light source to be deployed throughout the LSV, particularly near the argon active volume. These sources are used to calibrate the energy and optical response of the LSV as a function of position and to measure the efficiency of neutron-induced recoils in the argon detector. By deploying γ-ray sources near the argon volume, the time stability of the argon energy response and be be monitored [15]. The 83Kr injection system has constructed and ^{83}Rb source been procured. Deployment of the source manipulation system for DarkSide-50 is expected in the summer 2013.

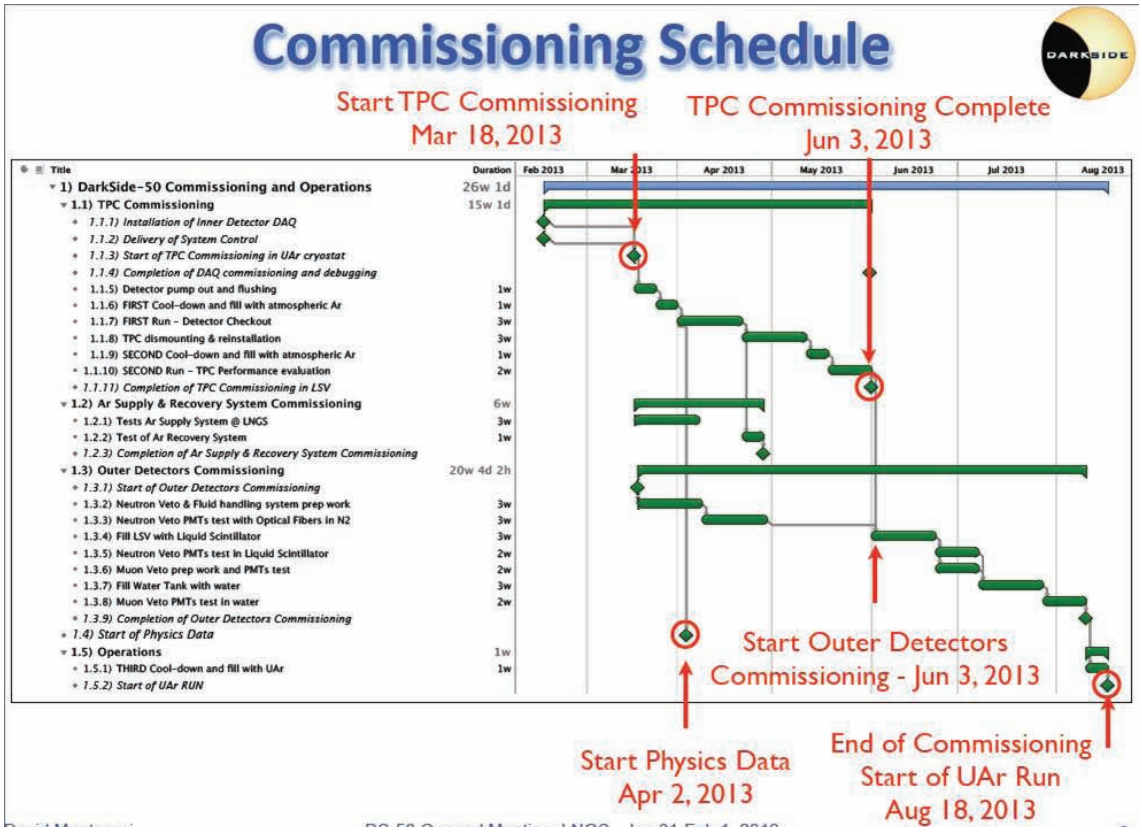

Figure 9: The construction and commissioning timeline for the DS-50 experiment

9 Summary

The DarkSide experiment has made substantial progress over the past year in all aspects of the proposal. All necessary items are now in final stages of completion in order to begin commissioning of the detector. Commissioning will begin using atmospheric argon and transition to depleted Ar in Summer 2013. Physics data would begin in Fall of 2013 and run for approximately 3 years. A timeline for activities is given in Figure 9.

10 List of Publications

1. D. Akimov, et al. (DarkSide Collaboration),Light Yield in DarkSide-10: A Prototype Two-phase Liquid Argon TPC for Dark Matter Searches arXiv:1204.6218 (2012).

2. H.O. Back, et al., First Commissioning of a Cryogenic Distillation Column for Low Radioactivity Underground Argon, arXiv:1204.6061 (2012).

3. H.O. Back, et al., First Large Scale Production of Low Radioactivity Argon From Underground Sources, arXiv:1204.6024 (2012).

4. J. Xu, et al., A Study of the Residual 39Ar Content in Argon from Underground Sources, arXiv:1204.6011 (2012).

5. P. Collon, et al., Reducing potassium contamination for AMS detection of 39Ar with an electron-cyclotron-resonance ion source, Nuclear Instruments and Methods B 283, 77 (2012).

6. T. Empl, et al, Study of Cosmogenic Neutron backgrounds at LNGS; ArXiv;2013.

References

[1] Committee on the Physics of the Universe, Board on Physics and Astronomy, Division on Engineering and Physical Sciences of the National Research Council of the National Academies, Connecting Quarks with the Cosmos: Eleven Science Questions for the New Century, http://www.nap.edu/catalog.php?record id=10079, National Academies Press (2003).

[2] The DarkSide Collaboration, http://darkside-docdb.fnal.gov/cgi-bin/ShowDocument?docid=360 (2012).

[3] //www.darkside.lngs.infn.it/ds-10

[4] D. Akimov et al. (DarkSide Collaboration), Light Yield in DarkSide-10: a Prototype Two-phase Liquid Argon TPC for Dark Matter Searches, arXiv:1204.6218 (2012).

[5] //www.hamamatsu.com

[6] A. Bolozdynya, Two-phase emission detectors and their applications, Nucl. Inst. and Meth. **A 422**(1999)314

[7] //www.ICARUS.lngs.infn.it

[8] M. Janecek and W. Moses, Optical Reflectance Measurements for Commonly used Reflectors, IEEE Transcations on Nuclear Science, **59**(2012)490

[9] Table of Isotopes, Eight Edition, R. B. Firestone, John Wiley & Sons, New York, 1996

[10] J. Xu et al., A Study of the Residual 39Ar Content in Argon from Underground Sources, arXiv:1204.6011 (2012).

[11] H.O. Back et al., First Large Scale Production of Low Radioactivity Argon From Underground Sources, arXiv:1204.6024, 2012; H.O. Back et al., First Commissioning of a Cryogenic Distillation Column for Low Radioactivity Underground Argon, arXiv:1204.6061 (2012);

[12] A. Wright, P. Mosteiro, B. Loer, and F. Calaprice, Nucl. Instr. Meth. A 644, 18 (2011).

[13] A. Empl and E. Hungerford, paper in preparation (2012).

[14] //www.doublechooz.inp3.fr

[15] W. Wilson, R. Perry, W. Charlton, T. Parish, G. Estes, T. Brown, E. Arthur, M. Bozoian, T. England, D. Madland, et al., SOURCES 4A - A Code for Calculating (γ,n) Spontaneous Fission, and Delayed Neutron Sources and Spectra LA-13639-MS, LANL (1999).

GERDA – the search for $0\nu\beta\beta$ decay

M. Agostini [n], E. Andreotti [q], A.M. Bakalyarov [l], M. Balata [a], I. Barabanov [j], N. Barros [c], L. Baudis [r], C. Bauer [f], N. Becerici-Schmidt [m], E. Bellotti [g,h], S. Belogurov [k,j], S.T. Belyaev [l], G. Benato [r], A. Bettini [o,p], L. Bezrukov [j], T. Bode [n], V. Brudanin [d], R. Brugnera [o,p], D. Budjáš [n], A. Caldwell [m], C. Cattadori [h], A. Chernogorov [k], F. Cossavella [m], V. D'Andrea [a], E.V. Demidova [k], A. Domula [c], V. Egorov [d], R. Falkenstein [q], K. Freund [q], N. Frodyma [b], A. Gangapshev [j,f], A. Garfagnini [o,p], C. Gotti [g,h], P. Grabmayr [q], V. Gurentsov [j], K. Gusev [l,d,n], K.K. Guthikonda [r], W. Hampel [f], A. Hegai [q], M. Heisel [f], S. Hemmer [o,p], G. Heusser [f], W. Hofmann [f], M. Hult [e], L.V. Inzhechik [j], L. Ioannucci [a], J. Janicskó Csáthy [n], J. Jochum [q], M. Junker [a], T. Kihm [f], I.V. Kirpichnikov [k], A. Kirsch [f], A. Klimenko [f,d], K.T. Knöpfle [f], O. Kochetov [d], V.N. Kornoukhov [k,j], V.V. Kuzminov [j], M. Laubenstein [a], A. Lazzaro [n], V.I. Lebedev [l], B. Lehnert [c], H.Y. Liao [m], M. Lindner [f], I. Lippi [p], A. Lubashevskiy [f], B. Lubsandorzhiev [j], G. Lutter [e], C. Macolino [a], B. Majorovits [m], W. Maneschg [f], G. Marissens [e], I. Nemchenok [d], S. Nisi [a], D. Paleoselitis [m], L. Pandola [a], K. Pelczar [b], G. Pessina [g,h], A. Pullia [i], M. Reissfelder [f], S. Riboldi [i], N. Rumyantseva [d], C. Sada [o,p], M. Salathe [f], C. Schmitt [q], B. Schneider [c], J. Schreiner [f], O. Schulz [m], B. Schwingenheuer [f], S. Schönert [n], H. Seitz [m], E. Shevchik [d], M. Shirchenko [l,d], H. Simgen [f], A. Smolnikov [f], L. Stanco [p], H. Strecker [f], M. Tarka [r], C.A. Ur [p], A.A. Vasenko [k], K. von Sturm [o,p], V. Wagner [f], M. Walter [r], A. Wegmann [f], T. Wester [c], M. Wojcik [b], E. Yanovich [j], P. Zavarise [a], I. Zhitnikov [d], S.V. Zhukov [l], D. Zinatulina [d], K. Zuber [c], and G. Zuzel [b].

[a] INFN Laboratori Nazionali del Gran Sasso, LNGS, Assergi, Italy
[b] Institute of Physics, Jagiellonian University, Cracow, Poland
[c] Institut für Kern- und Teilchenphysik, Technische Universität Dresden, Dresden, Germany
[d] Joint Institute for Nuclear Research, Dubna, Russia
[e] Institute for Reference Materials and Measurements, Geel, Belgium
[f] Max Planck Institut für Kernphysik, Heidelberg, Germany
[g] Dipartimento di Fisica, Università Milano Bicocca, Milano, Italy
[h] INFN Milano Bicocca, Milano, Italy
[i] Dipartimento di Fisica, Università degli Studi di Milano e INFN Milano, Milano, Italy
[j] Institute for Nuclear Research of the Russian Academy of Sciences, Moscow, Russia
[k] Institute for Theoretical and Experimental Physics, Moscow, Russia
[l] National Research Centre "Kurchatov Institute", Moscow, Russia
[m] Max-Planck-Institut für Physik, München, Germany
[n] Physik Department and Excellence Cluster Universe, Technische Universität München, Germany
[o] Dipartimento di Fisica e Astronomia dell'Università di Padova, Padova, Italy
[p] INFN Padova, Padova, Italy
[q] Physikalisches Institut, Eberhard Karls Universität Tübingen, Tübingen, Germany
[r] Physik Institut der Universität Zürich, Zürich, Switzerland

Abstract

The GERDA collaboration is performing a search for neutrinoless double beta decay of ^{76}Ge with the eponymous detector. The experiment has started operation in November 2011 and is taking data since. The performance of the system and the background reduction achieved are described. In parallel, the preparation of Phase II is ongoing. New material enriched in ^{76}Ge has been purified, crystals have been pulled and new detectors of BEGe type have been produced.

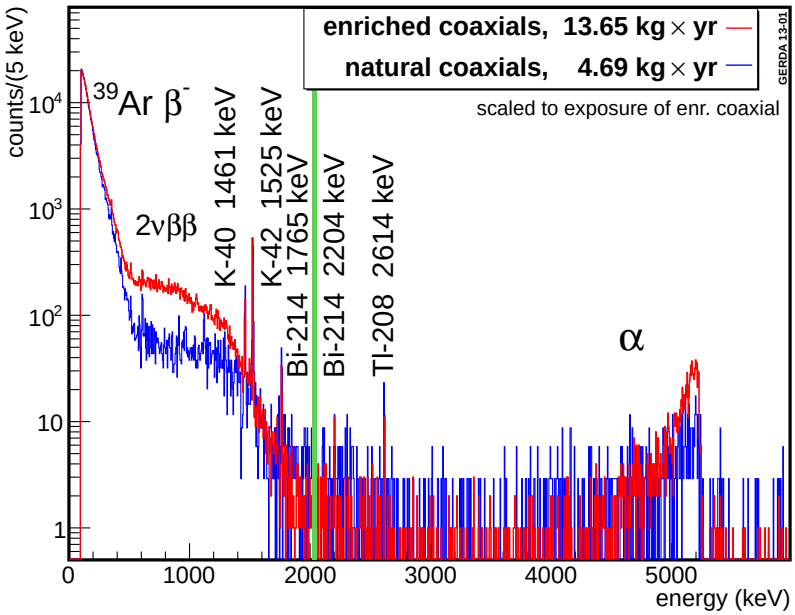

Figure 1: Spectra taken with enriched (red) and non-enriched (blue) detectors during 2012. The $^{\text{nat}}$Ge spectrum has been normalized to match the exposure of $^{\text{enr}}$Ge. The blinding window of $Q_{\beta\beta}$±20 keV is indicated as green bar. Identified γ lines are indicated.

1 Introduction

The GERmanium Detector Array (GERDA) experiment at the Laboratori Nazionali del Gran Sasso of INFN searches for the $0\nu\beta\beta$ decay of ^{76}Ge. High-purity germanium (HPGe) detectors isotopically enriched in ^{76}Ge are operated bare and immersed in liquid argon (LAr) in order to reduce backgrounds external to the HPGe detectors. Neutrinoless double beta decay of atomic nuclei $(A, Z) \rightarrow (A, Z+2) + 2\,e^-$ is a forbidden process in the Standard Model (SM) of particle physics because it violates lepton number by two units. An observation of such a decay would demonstrate lepton number violation in nature and would prove that neutrinos have a Majorana component. The GERDA experiment proceeds in a staged implementation: In Phase I, an exposure of 20 kg·yr is being acquired mainly with the re-processed enriched Heidelberg-Moscow and IGEX detectors. A background index of approximately $2 \cdot 10^{-2}$ cts/(keV·kg·yr) and an average energy resolution of 4.5 keV (FWHM) at $Q_{\beta\beta}$ has been acchieved which translates to a sensitivity for the half-life of $\approx 2 \cdot 10^{25}$ yr (90% C.L.) after an exposure of 20 kg·yr. Additional 20 kg of new enriched thick-window Broad Energy Germanium (BEGe) detectors will be deployed in Phase II. The goal is then to probe half-lifes up to $2 \cdot 10^{26}$ yr with a background index of 10^{-3} cts/(keV·kg·yr) after an exposure of 100 kg·yr. Novel background reduction methods will be used to reduce the background index by one order of magnitude with respect to that achieved in Phase I. This will be achieved by detecting the liquid argon scintillation

light as a veto signal, as developed in the GERDA-LARGE facility, in combination with the powerful pulse shape discrimination performance of the novel BEGe detectors.

2 GERDA Phase I: data taking

After the commissioning the GERDA experiment, the data taking period started on November 9th 2011 with 8 enriched detectors and 3 of natural isotopic composition. Having verified a smooth operation, data blinding was implemented on January 11, 2012. The properties of the inserted detectors are summarized in Table. 1.

Table 1: Characteristics of the Phase I enriched and natural detectors. The isotopic abundances for ^{76}Ge, f_{76}, of the ANG-type detectors are taken from Ref. [2]; those for RG-type detectors are from Ref. [3]; the natural abundance [4] is taken for GTF detectors. The numbers in parentheses in the last column give the 1σ-uncertainties.

detector name	serial nr. ORTEC	diam. (mm)	length (mm)	total mass (g)	operat. bias (V)	abundance f_{76}
ANG 1	*)	58.5	68	958	3200	0.859 (13)
ANG 2	P40239A	80	107	2833	3500	0.866 (25)
ANG 3	P40270A	78	93	2391	3200	0.883 (26)
ANG 4	P40368A	75	100	2372	3200	0.863 (13)
ANG 5	P40496A	78.5	105	2746	1800	0.856 (13)
RG 1 †)	28005-S	77.5	84	2110	4600	0.855 (1)
RG 2 †)	28006-S	77.5	84	2166	4500	0.855 (1)
RG 3 †)	28007-S	79	81	2087	3300	0.855 (1)
GTF 32	P41032A	89	71	2321	3500	0.078 (1)
GTF 42	P41042A	85	82.5	2467	3000	0.078 (1)
GTF 44	P41044A	84	84	2465	3500	0.078 (1)
GTF 45	P41045A	87	75	2312	4000	0.078 (1)
GTF 110	P41110A	84	105	3046	3000	0.078 (1)
GTF 112	P41112A	85	100	2965	3000	0.078 (1)

*) produced by Canberra, serial nr. b 89002.
†) as different types of measurements vary, an uncertainty of 2 % is taken in evaluations.

Unfortunately, two of the enriched detectors, ANG 1 and RG 3, developed high leakage currents soon. Thus, they were turned off. The remaining total mass for analysis is 14.6 kg with an average enrichment of 86% in ^{76}Ge corresponding to 165 moles. The active masses of the detectors were assessed at typically $\sim$87 % by comparing γ-ray detection efficiencies to Monte Carlo simulations of the diodes with dead layer thicknesses varied [1]. This assessment will be refined with in-situ GERDA data. The energy spectra of the six remaining taken from a calibration run with ^{228}Th are shown in Fig. 2.

Energy calibrations are performed on a (bi)weekly basis with the ^{228}Th sources. Spectra of the six active enriched detectors are shown in Fig. 2, including scaled subplots for

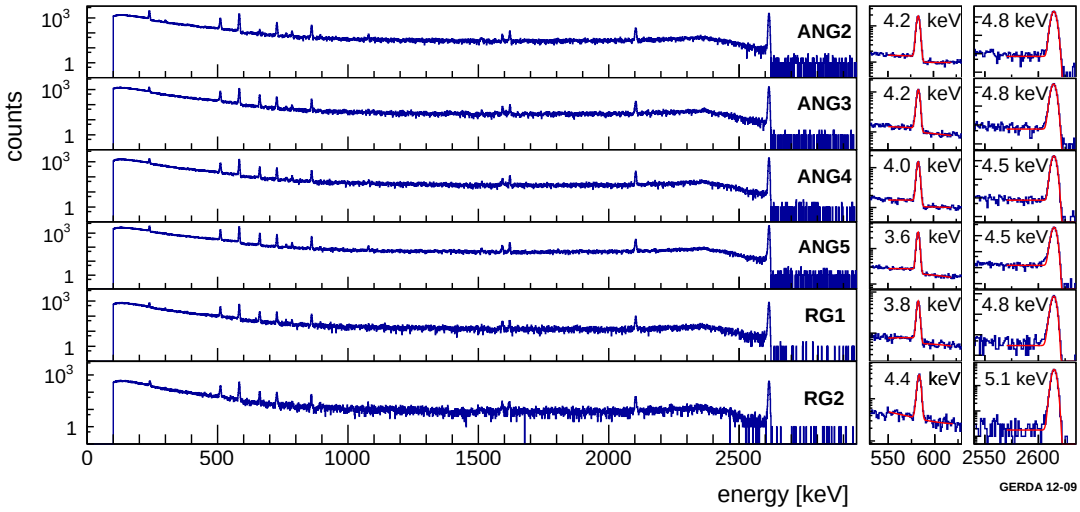

Figure 2: The energy spectra of the six enriched germanium detectors are plotted for a calibration with ^{228}Th. The blow-ups on the right show the fit results for the 583.2 keV and the 2614.5 keV lines including the values for a Gaussian FWHM.

the 583.2 and the 2614.5 keV lines. The high count rates cause pile up that would manifest itself in tails on the low energy side of the peaks. Proper pile up rejection algorithms and further data quality cuts have been applied before the fitting. The peaks are fitted well by a Gaussian and an error function representing the background. The results are shown by the red lines and the FWHM of the Gaussian is given in keV. Values between 4.2 to 5.3 keV (FWHM) at 2614 keV have been obtained. These can be translated to a mass weighted average of 4.5 keV (FWHM) at $Q_{\beta\beta}$=2039.01(5) keV [5]. The resolution of the 2614.5 keV line for all detectors during the first months of data taking is shown in Fig. 3. The energy resolution is stable with time.

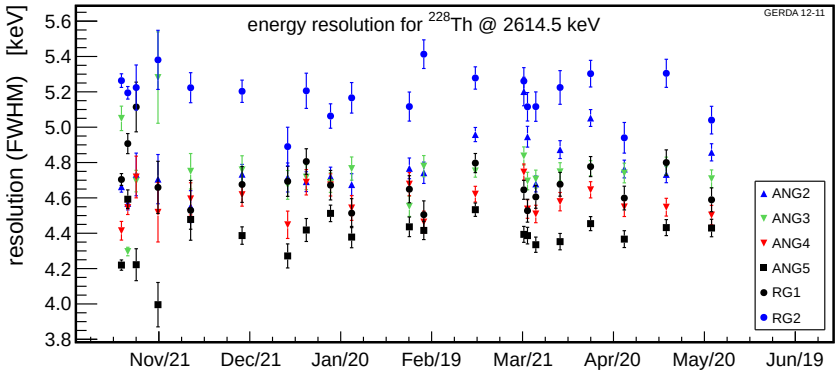

Figure 3: The energy resolution of the germanium detectors is plotted for several energy calibrations with the ^{228}Th source.

The same is also true for the gain, which show changes normally only after power

failures or temperature drifts. The 2614.5 keV γ-line positions in the calibration spectra are stable in time as shown in Fig. 4 as they fall into a range of $\pm$1.3 keV. The shifts observed between two calibrations can be scaled linearly to the interesting energy at $Q_{\beta\beta}$. The two lines at $\pm$1.3 keV shown in Fig. 4 correspond to $\pm$1 keV at $Q_{\beta\beta}$. The gain shifts within the ROI thus are typically less than 1 keV. This value is small compared to the average FWHM of 4.5 keV and shows that the data from all periods can be added in the search for the peak of the $0\nu\beta\beta$ decay.

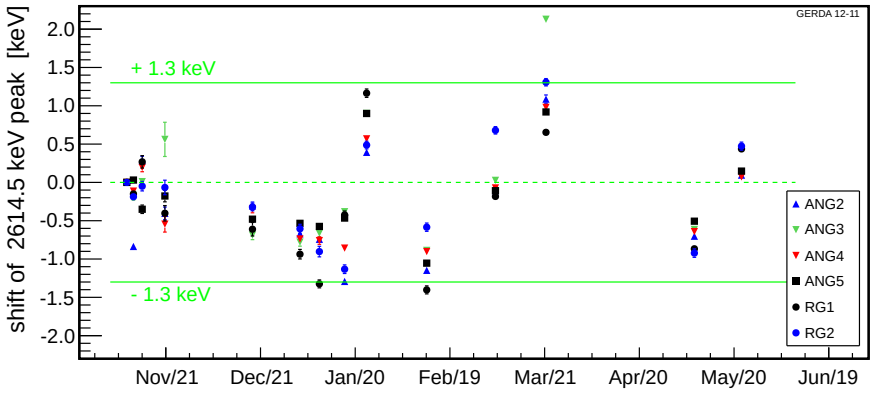

Figure 4: Variations of the 2614.5 keV γ line between successive calibrations. The green lines indicate $\pm$1 keV variations at $Q_{\beta\beta}$ if scaled linearly in energy.

The PMTs of the muon veto have been checked for pulse height stability for more than one year. A satisfying individual stability is reflected in the constant average light output

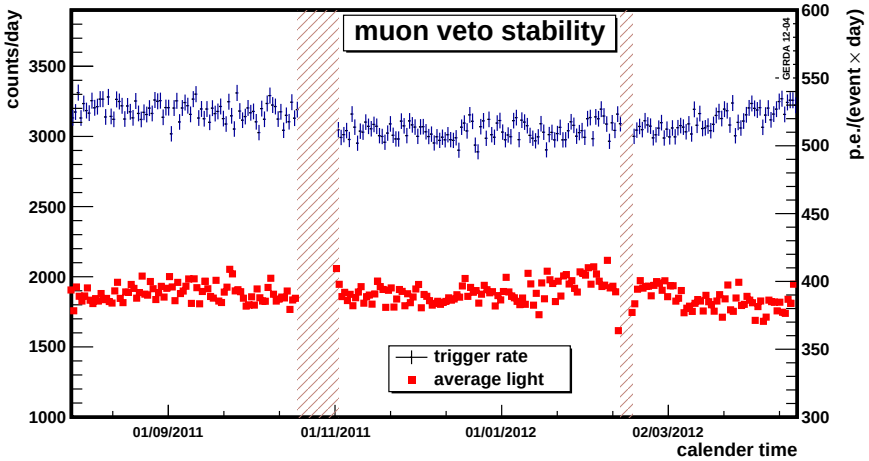

Figure 5: The average light output per event and day (squares, right scale) of the Cherenkov muon veto. The daily rates (crosses, left scale) are rather constant.

per muon event per day (Fig. 5, squares and right scale). This constancy is mandatory

for a reliable determination of the muon rate that is shown by the crosses in Fig. 5 (left scale). Except for short term fluctuation the rate is consistent with a 2 % sinusoidal variation with a period of about one year. This is a well-known phenomenon [7] that will be verified when a longer period of data is available. The observed muon rate in GERDA results in a preliminary value of $(3.42\pm0.03)\cdot10^{-4}$ cts/(m^{2}s) which compares very well with the recent BOREXINO result of $(3.41\pm0.01)\cdot10^{-4}$ cts/(m^{2}s) [7].

Table 2: Counts and rates of background lines for the enriched and natural detectors in GERDA in comparison to the enriched detectors of HDM [9]. Upper limits correspond to 90 % credibility interval. The central value is the mode of the posterior probability distribution function and the error bars account for the smallest interval containing 68% probability.

		^{nat}Ge (3.17 kg·yr)		^{enr}Ge (6.10 kg·yr)		HDM (71.7 kg·yr)
isotope	energy	tot/bck	rate	tot/bck	rate	rate
	[keV]	[cts]	[cts/(kg·yr)]	[cts]	[cts/(kg·yr)]	[cts/(kg·yr)]
^{40}K	1460.8	85 / 15	$21.7^{+3.4}_{-3.0}$	125 / 42	$13.5^{+2.2}_{-2.1}$	181 ± 2
^{60}Co	1173.2	43 / 38	< 5.8	182 / 152	$4.8^{+2.8}_{-2.8}$	55 ± 1
	1332.3	31 / 33	< 3.8	93 / 101	< 3.1	51 ± 1
^{137}Cs	661.6	46 / 62	< 3.2	335 / 348	< 5.9	282 ± 2
^{228}Ac	910.8	54 / 38	$5.1^{+2.8}_{-2.9}$	294 / 303	< 5.8	29.8 ± 1.6
	968.9	64 / 42	$6.9^{+3.2}_{-3.2}$	247 / 230	$2.7^{+2.8}_{-2.5}$	17.6 ± 1.1
^{208}Tl	583.2	56 / 51	< 6.5	333 / 327	< 7.6	36 ± 3
	2614.5	9 / 2	$2.1^{+1.1}_{-1.1}$	10 / 0	$1.5^{+0.6}_{-0.5}$	16.5 ± 0.5
^{214}Pb	352	740 / 630	$34.1^{+12.4}_{-11.0}$	1770 / 1688	$12.5^{+9.5}_{-7.7}$	138.7 ± 4.8
^{214}Bi	609.3	99 / 51	$15.1^{+3.9}_{-3.9}$	351 / 311	$6.8^{+3.7}_{-4.1}$	105 ± 1
	1120.3	71 / 44	$8.4^{+3.5}_{-3.3}$	194 / 186	< 6.1	26.9 ± 1.2
	1764.5	23 / 5	$5.4^{+1.9}_{-1.5}$	24 / 1	$3.6^{+0.9}_{-0.8}$	30.7 ± 0.7
	2204.2	5 / 2	$0.8^{+0.8}_{-0.7}$	6 / 3	$0.4^{+0.4}_{-0.4}$	8.1 ± 0.5

In July two natural detectors were removed and a string of five enriched BEGe detectors were inserted on the one-string arm. This increased the total mass by about 3 kg. Except for the low energy part due to ^{39}Ar, the spectra from the BEGe and the coaxial enriched detectors are the same within statistics. The energy resolution of the BEGe detectors increased with respect to the vacuum cryostat measurements to about 3 keV (FWHM) at 2.6 MeV in GERDA.

The blinded region amounts to 40 keV around $Q_{\beta\beta}$. It is the aim to analyze and to describe the background first, to define the background index (BI) at $Q_{\beta\beta}$, before opening the window. The opening will take place after reaching the targeted exposure of 20 kg·yr and after having the analysis procedures defined. Events with an energy close to $Q_{\beta\beta}$ are not exported to TIER1 but are saved in the backup of the raw data.

3 Phase II

3.1 Phase II detector characterization

During 2012 all ^{enr}BEGe slices were turned into working BEGe detectors at Canberra-Olen, in Belgium. The diodes were mounted in a vacuum cryostat, assembled in conventional dewars and transported to the HADES Underground Laboratory in SCK-CEN, in Mol (Belgium), to perform acceptance tests. The aims of these tests were to verify the detector specifications given by Canberra, to determine the optimal operational conditions and to fully characterize the detectors and their performance.

Figure 6: Setups used for the characterization measurements. Left: Setup for static source measurements. Right: Automated scanning tables.

In order to perform the measurements two different types of setups were used: a measurement table that allows to place a calibration source at a set of fixed positions from the top of the cryostat (optionally with a collimator); and a setup with a movable arm controlled by a series of motors, that allowed to perform top and lateral surface scans with a collimated source. Pictures from both designs can be seen in Figure 6.

The fixed calibration setup was used with several different sources (^{228}Th, ^{241}Am, ^{60}Co and ^{133}Ba) and was used to measure the standard performance of the detectors such as depletion voltage, energy resolution, average dead-layer thickness and pulse shape performance. The tables were designed to facilitate the placement and removal of the cryostat in order to minimize the time spent in switching detectors to be tested. The automated scanning tables were designed to move a collimated 5 MBq ^{241}Am source around the detector cryostat, allowing to sample the detector top and lateral surfaces. These tables were used to study the charge collection efficiency of the diode by looking at the detector response to the source placed in different positions on the top and lateral surfaces of the diode. Measurements were performed on both setups for each diode. The duration of each measurement varied with the source, its activity and the objective of the

the measurement. There were a total of five setups (two fixed measurement tables and three scanning tables), allowing to simultaneously characterize up to five detectors.

At present the production of 30 operational diodes is complete, as well as the standard measurements planned for the characterization campaign. The detectors have a mass of $0.5 - 0.8$ kg and exhibit energy resolutions of $1.64 - 1.86$ keV (FWHM) for 1.332 MeV γ from ^{60}Co, being in good agreement with reference values specified by Canberra, and below the specification value of 2.3 keV. At the 2.614 MeV γ of ^{208}Tl the energy resolution was found to be $2.20 - 2.73$ keV. The dead-layer was estimated using data from measurements with , ^{241}Am, ^{60}Co and ^{133}Ba sources. The diodes present an average dead-layer of ~ 0.8 mm, which is in agreement with the specifications. The active volume is estimated from measurements with a ^{60}Co source and yielded an average value of $\sim$88 %. For tests of pulse-shape performance both fixed measurements with a ^{228}Th source and scanning measurements with a ^{241}Am were carried out. The A/E resolution was found to be $0.4 - 3.0$ %, varying substantially from detector to detector. This effectss could be traced back to surface charges on the passivation layer which is required for operating them in the vacuum cryostat, which however will be removed for the final detector configuation. At the end of the characterization campaign of the first batch of seven diodes, five were deployed in the GERDA detector.

3.2 Preparation of LAr instrumentation for Phase II

It has been demonstrated in the LARGE facility that background in the Ge-detectors can be suppressed efficiently by applying an anti-coincidence cut on argon scintillation signals. Therefore, the collaboration pursued several design options for an instrumentation of the GERDA cryostat to read out the scintillation light in Phase II.

Table 3: Results obtained with MC and LARGE.

source	LARGE	MC
internal sources		
^{228}Th	1180 ± 250	909 ± 235
^{226}Ra	4.6 ± 0.2	3.8 ± 0.1
^{60}Co	27 ± 1.7	16.1 ± 1.3
external sources		
^{228}Th	25 ± 1.2	17.2 ± 3.2
^{226}Ra	3.2 ± 0.2	33.2 ± 0.4

A Monte Carlo (MC) simulation infrastructure was developed in order to assess the expected performance in GERDA. Using the data from LARGE the MC was optimized. In Table 3 a comparison of the suppression factors obtained with MC and LARGE data are shown. A general good agreement was obtained. A discrepancy was observed for the ^{60}Co source, which after posterior tests was demonstrated to be due to missing information concerning the design of the source, leading to a discrepancy in the amount of β escaping the source into the LAr. A spectrum measured with an internal ^{228}Th source is shown in Figure 7.

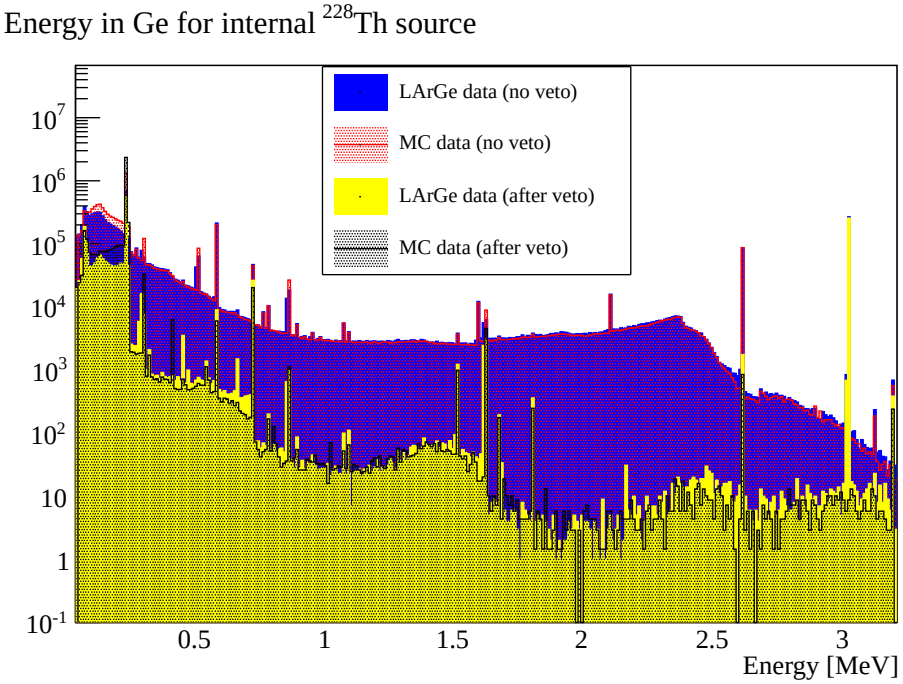

Figure 7: Energy spectrum measured in a depleted BEGe in LArGe using a ^{228}Th source close to the detector. In blue and yellow are, respectively, the energy spectra before and after LAr scintillation veto measured in LArGe. In red and black the corresponding spectra obtained from MC are shown.

After the validation of the MC with LArGe data, a simulation campaign was carried on testing the performance of the different proposed designs. From the results of this campaign, the collaboration pursues a hybrid design, combining a PMT readout, similar to the one deployed in LArGe, together with wavelength shifting (WLS) fibers coupled to SiPM's. The hybrid design is composed by a cylindrical shroud with a diameter of 500 mm that is deployed through the cryostat neck assuming a single arm lock that handles up to seven detector strings. The shroud is composed of three parts, being the uppermost an lowermost made of copper, while the central one is lined with wavelength shifting fibers readout by SiPMs. The copper surfaces are lined with VM2000 reflector foil and a wavelength shifter (Tetra Phenyl Butadiene). The light within this volume is shifted in the coated copper surfaces and in the fiber surface and then either guided towards PMTs at the top and bottom, or guided in the fiber towards the SiPMs. Figure 8 shows a schematic of the hybrid design.

MC simulations of the hybrid design for the most dangerous backgrounds (^{208}Tl and ^{214}Bi) were performed. Some of the most relevant results are listed in Table 4.

Two types of low-background R11065 3" PMTs were purchased from Hamamatsu A dedicated test stand for full characterization in LAr is operational at MPIK. These tests comprise the integration of the full system, including mechanical PMT support, custom made voltage dividers (VD), cabling, and the DAQ. Radiopurity assays of PMTs and VDs demonstrated activities of $\leq$ 1.94 mBq/PMT of ^{228}Th and $\leq$ 1.7 mBq/PMT of ^{226}Ra. Preliminary estimates indicate that the instrumentation induced background is $< 10^{-4}$

Figure 8: Schematic of the hybrid design for the LAr scintillation veto. The central cylinder (in gray) is composed of scintillating fibers.

Table 4: Expected suppression factors for some backgrounds in GERDA using the hybrid design.

background	location	suppression factor
^{208}Tl	holders	320 ± 34
	external	112 ± 39
^{214}Bi	holders	10.3 ± 0.3
	surface of detectors	3.5 ± 0.1
	homogeneous in LAr	54.8 ± 7.9

cts/(keV·kg·yr) including self-vetoing. A mockup for mechanical tests of the shroud was built and the tests were successful.

As mentioned previously the central part of the shroud is composed of wavelength shifting (WLS) fibers. The fibers are sensitive to scintillation light from all sides and guide the shifted light to silicon photomultipliers (SiPMs). The total mass of fibers necessary is estimated in 1 kg. Samples of fibers were screened with ICPMS at LNGS. The estimated activity for both Th and U is in the range of 5×10^{-5} Bq/kg. Preliminary estimates indicate that the fibers fibers would cause a background of $< 10^{-3}$ cts/(keV·kg·yr), excluding self-vetoing. One hundred pieces of 3 mm×3 mm SiPMs in 'die' were purchased from Ketek GmbH. Most of the hardware components for the production of a full setup with fibers is available. A setup with one ton of LAr was built in the TUM underground laboratory and tests with a full size prototype will be performed soon.

One of the challenges for GERDA Phase II are the background signals created by ^{42}K decays on the detector surfaces. Pulse shape discrimination for both p^+ and n^+ surface events is highly efficient for this class of events, provided that A/E resolutions are achieved which are similar to those found in measurements with vacuum cryostats [8]. As this might not be achievable in the GERDA experimental environment, additional measures are required. Following the experiences of Phase I, modified mini-shrouds are considered to reduce the attraction of ^{42}K towards the detectors. A division into optical sub-volumes however would reduce the background suppression factors by detecting the liquid argon scintillation light to intolerable levels.

Presently several options with transparent or optically active mini-shrouds are being tested: *i*) a mesh mini-shroud biased with positive high voltage, *ii*) hermetically closed mini-shrouds made from nylon coated with a TBP/polystyrene wave length shifter or from pure polystyrene or polyvinyl toluene, and *iii*) a mini-shroud made from Cuflon which is lined inside with a TBP covered reflective foil. While the first option is transparent for the primary liquid argon scintillation light, it does not provide a convective barrier for ^{42}Ar or neutral ^{42}K. The second design option shifts the XUV scintillation light to the visible spectrum which then can penetrate the transparent mini-shroud and propagate to the SiPM curtain and PMTs. The third option relies on the detection of the shifted scintillation light by large area SiPMs mounted inside the Cuflon mini-shroud, close to the detectors. All solutions are undergoing experimental verifications and tests in the LARGE test stand. For this purpose, a new batch of ^{42}Ar had been produced at the TUM-MLL accelerator laboratory and inserted into the liquid argon of LARGE in order have high-statistic ^{42}K data.

3.3 BEGe Detector Integration

In order to reach the background requirements of Phase II, a new design for the detector holders was developed. In order to lower further the background contribution from the holders, the new design has substantially less mass and uses cleaner materials. To minimize the backgrounds from ^{228}Th and ^{226}Ra, the holders are made mostly of silicon (upper and lower plates), with vertical supports made of copper. Aluminium contacts are evaporated on the germanium diodes and signal and high-voltage contacts done by wire bonding. For Phase II of GERDA the existing holders in the current HPGe detectors will also be replaced by the new model. A Phase II prototype detector assembly was produced and is currently being tested at the GDL, in order to optimize and test the handling of the mounted detector-holder pair and the integration with the front-end electronics. Studies of Aluminium evaporation on BEGe detectors and bonding of the contacts have been completed successfully. The dedicated evaporation machine was moved to Canberra, Olen (Belgium) and the Al-evaporation process integrated into the final detector processing, which is currently ongoing at the manufacturer.

3.4 Other activities

The unblinding at the end of Phase I is planned for early summer 2013. For the transition to Phase II several maintenance and inspections of the cryogenic systems are planed.

Other activities of the collaboration comprise preparations for the installation of the new lock system, the new version of the preamplifier (CC3 and GEFRO), the screening and weaving of new cables.

4 Conclusions

GERDA Phase I data taking is close to its completion and a sensitivity of approximately $2 \cdot 10^{25}$ yr for the half-life will be reached. The transition towards Phase II is under preparation and will start subsequently.

5 List of Publications

1. *Isotopically modified Ge detectors for GERDA: from production to operation*
   J. of Instrumentation (JINST), 8 (2013) P104018
   D. Budjas, M. Agostini, L. Baudis, E. Bellotti, L. Bezrukov, R. Brugnera, C. Cattadori, A. di Vacri, R. Falkenstein, A. Garfagnini, S. Georgi, P. Grabmayr, A. Hegai, S. Hemmer, M. Hult, J. Janicsko Csathy, V. Kornoukhov, B. Lehnert, A. Lubashevskiy, S. Nisi, G. Pivato, S. Schönert, M. Tarka and K. von Sturm

2. *The GERDA experiment for the search of $0\nu\beta\beta$ decay in ^{76}Ge*
   Eur. Phys. J. C 73 (2013) 2330
   The GERDA collaboration, K.-H. Ackermann *et al.*

3. *Measurement of the half-life of the two-neutrino double beta decay of ^{76}Ge with the GERDA experiment*
   J. Phys. G: Nucl. Part. Phys. 40 (2013) 035110
   The GERDA collaboration, M. Agostini *et al.*

4. *The slow control system of the GERDA double beta decay experiment at Gran Sasso*
   J. of Instrumentation (JINST), 7 (2012) P10017
   R. Brugnera, F. Costa, A. Garfagnini, G. Gigante, S. Hemmer, I. Lippi, M. Michelotto, C. Ur and D. Zinato

References

[1] M. Barnabé Heider, PhD thesis, U. Heidelberg, May 2009; GSTR-12-008.

[2] H.V. Klapdor-Kleingrothaus *et al.*, Nucl. Instrum. Methods **A522**, 371 (2004).

[3] V. Khournoukov, priv. communication; measurements performed by the Botchvar Institute, Moscow, Russia.

[4] J. R. De Laeter *et al.*, Pure Appl. Chem. **75**, 683 (2003).

[5] G. Douysset *et al.*, Phys. Rev. Lett.**86**, 4259 (2001).

[6] M. Agostini *et al.*, J. Phys., Conf. Ser. **375**, 042027 (2012).

[7] B. Bellini *et al.*, submitted to JCAP, arXiv:1202.6403

[8] D. Budjas *et al.*, *Isotopically modified Ge detectors for Gerda: from production to operation*, J. of Instrumentation (JINST), 8 (2013) P104018

[9] O. Chkvorets, PhD Thesis, U. Heidelberg, 2008.

The ICARUS Experiment

The ICARUS Collaboration

M. Antonello[a], B. Baiboussinov[b], P. Benetti[c], F. Boffelli[c], E. Calligarich[c], N. Canci[a], S. Centro[b], A. Cesana[e], K. Cieślik[f], D.B. Cline[g], A.G. Cocco[d], A. Dabrowska[f], D. Dequal[b], A. Dermenev[h], R. Dolfini[c], C. Farnese[b], A. Fava[b], A. Ferrari[i], G. Fiorillo[d], D. Gibin[b], S. Gninenko[h], A. Guglielmi[b], M. Haranczyk[f], J. Holeczek[m], A. Ivashkin[h], J. Kisiel[m], I. Kochanek[m], J. Lagoda[l], S. Mania[m], A. Menegolli[c], G. Meng[b], C. Montanari[c], S. Otwinowski[g], A. Piazzoli[c], P. Picchi[n], F. Pietropaolo[b], P. Plonski[o], A. Rappoldi[c], G.L. Raselli[c], M. Rossella[c], C. Rubbia[1,a,i], P. Sala[e], A. Scaramelli[e], E. Segreto[a], F. Sergiampietri[p], D. Stefan[a], J. Stepaniak[l], R. Sulej[a,l], M. Szarska[f], M. Terrani[e], F. Varanini[b], S. Ventura[b], C. Vignoli[a], H.G. Wang[g], X. Yang[g], A. Zalewska[f], K. Zaremba[o], A. Zani[c]

[a]INFN - Laboratori Nazionali del Gran Sasso, Assergi, Italy
[b]Università di Padova e INFN, Padova, Italy
[c]Università di Pavia e INFN, Pavia, Italy
[d]Università Federico II di Napoli e INFN, Napoli, Italy
[e]Politecnico di Milano e INFN, Milano, Italy
[f]H.Niewodniczański Institute of Nuclear Physics, Kraków, Poland
[g]Department of Physics, UCLA, Los Angeles, USA
[h]Institute for Nuclear Research of the Russian Academy of Sciences, Moscow, Russia
[i]CERN, Geneva, Switzerland
[l]Nuclear Center for Nuclear Research, Warszawa, Poland
[m]Institute of Physics, University of Silesia, Katowice, Poland
[n]INFN Laboratori Nazionali di Frascati, Frascati, Italy
[o]Institute for Radioelectronics, Warsaw Univ. of Technology, Warsaw, Poland
[p]Università di Pisa e INFN, Pisa, Italy

Abstract

In 1977 C.Rubbia [1] conceived the idea of a LAr-TPC (Liquid Argon Time Projection Chamber). The ICARUS T600 cryogenic detector, installed in the Gran Sasso underground laboratory, demonstrates an industrial scale realization of this idea. In 2012, the ICARUS T600 experiment has continued the collection of CNGS neutrino interactions, has performed a precision measurement of the neutrino velocity and has been searching for the LSND anomaly in the CNGS neutrino beam. Also, tools for reconstruction and analysis have been developed. This will be presented, together with discussion of detector future after the CNGS beam stop in December 2012.

[1]Spokesman of the ICARUS Collaboration

1 ICARUS T600 detector

The technical details of the ICARUS T600 detector have been described in [2], whereas its LNGS underground operation in [3]. Therefore, herein we only recall the main features of this cryogenic detector, being so far the biggest LAr-TPC realized ever. Two half-modules, each housing two TPCs separated by a centrally placed common cathode, are filled with about 760 tons of ultra-pure LAr. Electrons from ionization travel toward the three parallel planes of the TPC anode wires, inducing signals in the first two *induction* planes and being collected by the third *collection* plane. This allows to obtain: (1) a three-dimensional image of an ionizing event by exploiting the measurement of the absolute time, provided by prompt emission of scintillation light in LAr collected in photomulipliers, (2) particle identification by studying the event topology and energy deposition as a function of the particle range (dE/dx versus range), and (3) calorimetric measurements via dE/dx ionization signal. The ICARUS T600 detector performance can be summarized as follows: 1 mm^3 precision in event topology, muon momentum measurement via multiple scattering with $\Delta p/p \sim$ 15-20% depending on the track length and momentum, e/γ separation with 2% X_0 sampling, electromagnetic showers energy resolution $\sigma(E)/E = 0.03/\sqrt{E(GeV)} \oplus 0.01$, low energy electrons resolution $\sigma(E)/E = 0.11/\sqrt{E(GeV)} \oplus 0.02$ and hadronic showers resolution $\sigma(E)/E = 0.30/\sqrt{E(GeV)}$.

During 2012, like in 2011, the ICARUS experiment has been taking data on the CNGS neutrino beam with a very high detector live-time. We report, in the following, an overview of the experimental activity of the year 2012 concerning not only detector operation and upgrades but also improvements and further developments of the software tools for the analysis. The relevant scientific results obtained during this year are also reported.

2 Cryogenics and LAr purity

The whole T600 cryogenic plant has been operating for almost 3 years since the commissioning completion (Spring 2010). It has demonstrated to be safe, reliable and functional. In particular the continuous operation of the cryogenic plant and its good performances guaranteed high thermal stability, high LAr thermal uniformity (within 1 K), high argon purity with no dead time at all for the detector. The evolution of liquid argon purity is shown in Fig. 1. As one can see, electron lifetime is typically around 5-6 ms in both cryostats and it is always kept above 2 ms even after the LAr recirculation stops, usually due to pump faults. A LAr recirculation system partial upgrade is ongoing in order to test a new more reliable type of pump on one of the two cryostats.

3 Trigger System

At the end of the 2011 CNGS beam data-taking campaign, a major effort to improve the PMT readout system was started aiming at improving the cosmic ray data taking efficiency. The full HV biasing system was re-designed, integrating in each PMT channel

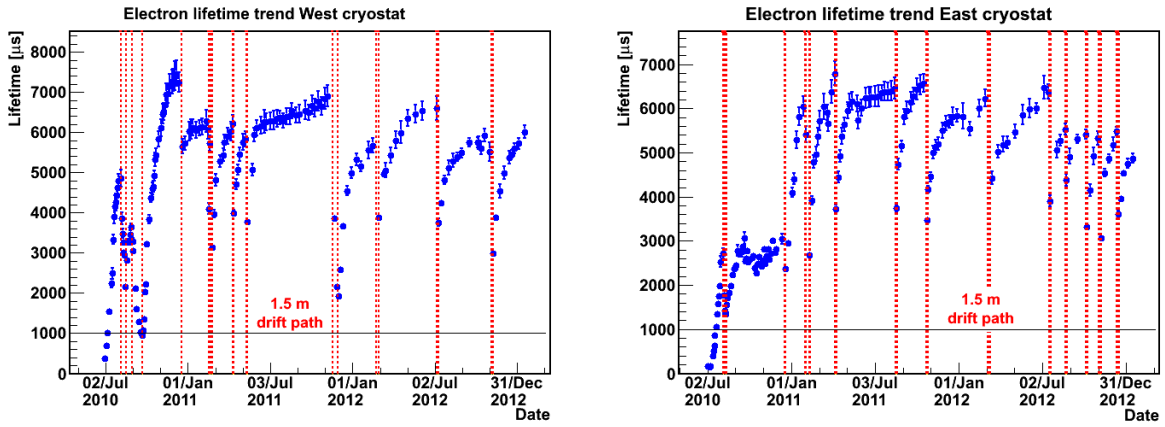

Figure 1: *Time evolution of the free electron lifetime in the West (left) and East (right) cryostats. For details see the text.*

a custom-made low-noise charge preamplifier with an external active signal adder. This allows the PMT light integration over a $RC = 10\mu$s, thus exploiting also the slow component of the light signals. For each chamber the PMT signal sum is discriminated in order to provide the trigger FPGA board with four independent trigger lines. Thresholds were set to about 100 photo-electrons for the West cryostat signals and 200 photo-electrons for the East cryostat signals in order to take into account the different number of installed devices (9+9 PMTs in the West cryostat; 27+27 in the East cryostat). A scan of the cosmic trigger rates as a function of the single PMT sum signal threshold was performed to optimize the PMT cosmic trigger efficiency. In both analyses, using the optimized thresholds, an overall trigger rate of about 35 mHz has been then achieved leading to about 130 cosmic events per hour collected on the full T600.

The PMT trigger electronics was improved with a monitoring system of the single PMT rates and was completed including the PMT waveforms in the DAQ. A total of 19 waveforms digitizers (the same model adopted for the wire signal recording) have been modified (20 Mhz sampling rate) and set up in order to accept in input the slow PMT signals coming from the preamplifiers output.

In addition to the PMT based trigger, a new algorithm (DR-slw) to detect the local Region of Interest (ROI) of each event, was implemented in a new SuperDaedalus chip, in order to perform a trigger based on local charge deposition. On each 32 wire board a Global- Trigger-Out signal (GTO) is generated if at least one of the two 16-channel blocks has reached the majority threshold. One logical board is hosted in each single crate handling the GTO signals from the 18 read-out boards (9 for Collection plus 9 for Induction view) to perform a further majority level in view of a trigger signal generation.

During December 2011 almost 800 SuperDaedalus chip have been installed in the detector, covering all the Collection views. After the successful tests, the SuperDaedalus electronic boards for the second-level trigger were put in production at the end of April 2012. From January 2012 a new bunch of production has started, covering Induction1 and Induction2 views. As a result the T600 is fully equipped with SuperDaedalus trigger system from end of August 2012. The initial tests were addressed to study the critical

issues, such as noise and PMT-induced signals on wires. After several interventions made to reduce the noise level, it has been possible to trigger on the GTO signals from Collection and Induction2 views with a trigger rate of 120 mHz, well below the DAQ limit. SuperDaedalus parameters used were: threshold on single hit 8 ADC counts; Majority of fired channels 10/16; Stretching $100 \div 125\mu$s (allowing to trigger on inclined tracks).

This new trigger system based on the charge recognition on the TPC wires has been activated for the CNGS data taking from June 2012 soon after the commissioning period. The demonstrated almost full efficiency of SuperDaedalus trigger on CNGS interactions allowed to qualify the PMT trigger efficiency after the HV system intervention. As a result an almost full PMT trigger efficiency was measured for neutrino interactions, while exceeding 99% for muons induced by neutrino interaction on the rocks.

Moreover the SuperDaedalus set-up has been gradually introduced in the data taking for cosmic rays from September 2012 (Collection view). The Induction2 view has been included in December 2012 while Induction1 is under study aiming to reduce the noise level. Preliminary results indicate a promising improvement of the cosmic event trigger efficiency in the $0.1 \div 1$ GeV energy range (see Fig. 2).

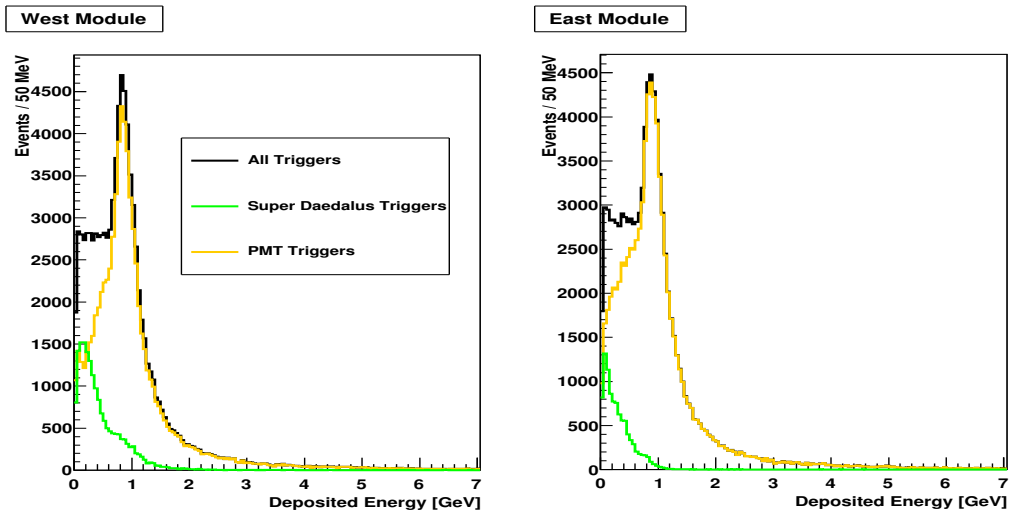

Figure 2: *Preliminary energy distribution of the c-rays triggered by PMT (yellow) and SuperDaedalus (green) for the two mdolules.*

4 DAQ System

While the reliability of the DAQ system didn't show any specific criticality, the beam shutdown period (from November 14th 2011 to March 22nd 2012) has been dedicated to rework the architecture in order to reduce possible single points of failure, to increase parallelism in the data streams from the detector to the control room and to distribute data processing task over a larger number of machines (that can backup each other in case of failures). A new storage element (50 TB) in the DAQ rack allows further buffering

before the transfer to CNAF, and will provide an high bandwidth space where to store the first double data copying. The whole network infrastructure connecting readout racks has thus been doubled (to cope with instantaneous traffic peaks during readout) with supplementary switches. This led to a significant reduction (46%) of the event build time. Four new pc's, that may operate both as building machines or as event builder nodes, have been added to the event building farm. Currently the maximum sustainable event acquisition rate is 700-800 mHz. Further optimization are in progress regarding traffic shaping and interference with the downstream data flow.

In order to participate to the campaign of measurement on the neutrino time of flight, with the CNGS beam in bunched mode, the ICARUS T600 PMT readout system, up to now used as primary trigger source, has been equipped with an additional PMT-DAQ system, derived from the DAQ developed for the WArP experiment, based on six 2-channel, 8-bit, 1-GHz AGILENT AC240 digitizer boards.

The digitizer boards are organized in two crates, connected to the event building computers and to data storage via optical link. All digitizers within the same crate are synchronized with each other at a 10 ps level.

The PMT-DAQ system continuously records the Sums of the direct PMT signals (from eight horizontal arrays) along with several TTL timing signals: the ESAT PPmS (Pulse Per milliSecond) as in 2011 set-up; a 2 kHz synchronization pulse from the White Rabbit[2] (WR) system, in phase with the related PPS; a replica of the ICARUS trigger PMT trigger signal obtained through a dedicated fan-out setup. Replicas of the same signal are also sent to High Precision Timing Facility[3] (HPTF) and to the WR facility for time stamping. All these signals allow defining an absolute time for the PMT-DAQ digitizers in the time bases related to the four different timing systems [4].

5 2012 data taking with CNGS beam

ICARUS-T600 restarted data taking with CNGS beam on March 23^{rd} 2012 and proceeded without major interruptions up to December 3^{rd}. In this period it has been possible to collect an event statistics corresponding to 3.58×10^{19} pot over the 3.83×10^{19} pot delivered by CERN, thanks to a detector live-time in excess of 93 % for CNGS exploitation (Fig. 3). The CERN-SPS accelerator was operated in bunched mode, with $\sim 10^{12}$ pot per spill, from May 10^{th} to May 24^{th} 2012, in the framework of the dedicated campaign aimed at improving the neutrino time of flight measurement significance. During this period ICARUS-T600 detector collected, with 100% duty cycle, the 1.8×10^{17} pot delivered by CERN.

[2]White Rabbit is an open source protocol for reliable, fast and deterministic transmission of control information. It intrinsically accounts for signal propagation delay.

[3]The High Precision Timing Facility[4] is a completely new and independent timing system, setup by the Borexino Collaboration, using a Rb clock combined with PolaRx4 GPS receiver.

[4]The number of concurrent timing system is four because, besides the standard ESAT system of LNGS and the HPTF, made available by the Borexino Collaboration, one has to consider the WR-2 and WR-4 systems, set up both at CERN and LNGS by CERN staff, which make use of two different and inter-calibrated GPS receivers (PolaRx2 and PolaRx4).

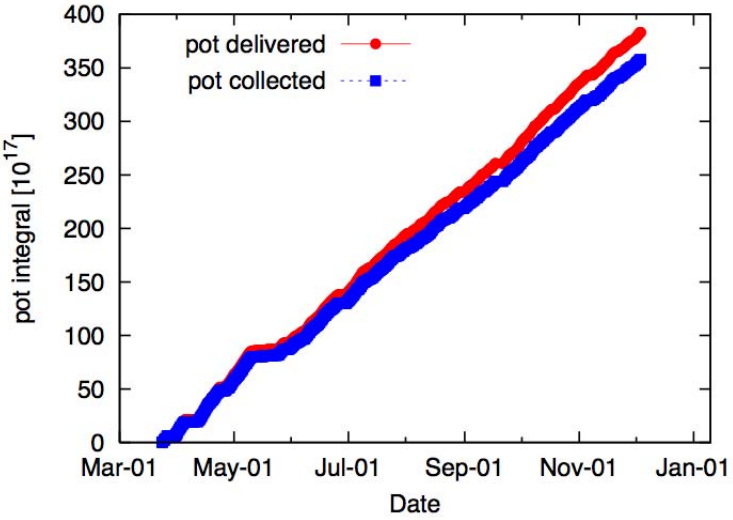

Figure 3: *Integrated proton on target delivered to CNGS in the 2012 campaign (red), starting March 23rd 2012. The beam intensity recorded by T600 is also shown (blue). The two weeks in May with low intensity beam, devoted to neutrino time of flight measurements, are clearly recognizable.*

6 Reconstruction tools for analysis

The availability of the large data sample collected so far allows for further progresses and checks of the event reconstruction tools.

With regards to 3-D reconstruction, a novel approach has been developed [P1]. It is based on the Polygonal Line Algorithm fit in the 3D space, optimized to all the available hits in the 2D wire planes and all the identified 3D reference points (interaction vertices, peculiar points like delta rays). The main advantage is that 2D hit-to-hit associations are not needed and therefore missing track parts in single view are accepted as well as horizontal tracks. The new approach, now implemented for the track reconstruction, may be used for reconstruction of cascade-like objects, as well as precise reconstruction of the vertex region and in global event reconstruction. It is the basis for the reconstruction of particle directions, for the evaluation of dE/dx and its recombination correction, and for the Particle Identification algorithm (PId). As an example, the dE/dx of muons from the CNGS 2011 event sample is shown in Fig. 4[Left], together with the expected distribution from MonteCarlo. The agreement, both in shape and in average is within 2%.

Improvements in PId allow for a reduction of the systematic effects due to trajectory and charge measurement errors. Stopping particle identification is based on the dependency of reconstructed dE/dx versus track residual range. The purity and efficiency measured on MC test sample is above 80% for tracks longer than 6 cm (p, K, π, μ). Additional observation of decay products allows for a perfect separation (close to 100%) of protons and kaons. The practical implementation of the PId algorithm is based on a neural network approach with Bayesian optimization of the structure and training parameters. To check the PId, a set of stopping particles has been visually selected. This set includes stopping negative pions and muons that can be absorbed by the Argon nuclei with a sizable probability of emitting only neutral particles, therefore they can be visually

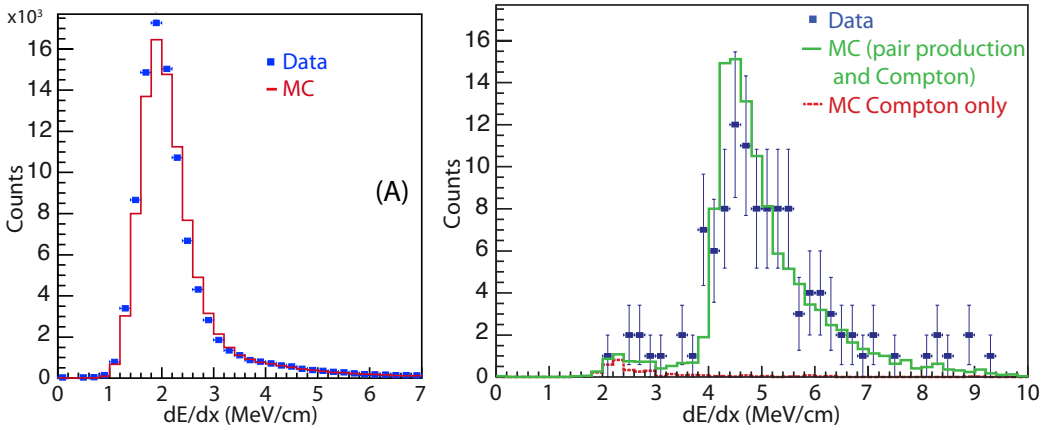

Figure 4: *[Left]: Energy deposition density distribution for muons in CNGS CC interactions, compared with Monte Carlo, normalized to the same number of entries. Each entry corresponds to one wire hit. [Right]: Average ionization in the first 8 wire hits for sub-GeV photons in the T600 data (full squares), compared to Monte Carlo expectations (solid line) normalized to the same number of events. In MC case, the Compton contribution is shown also separately (dotted line).*

misidentified as protons. Fig. 5 illustrates both the PID capabilities and the agreement of the reconstructed dE/dx with respect to theoretical and Monte Carlo values.

Reconstruction of showers from π_0 conversion is also progressing, with the aim of validating the identification capabilities. One of the selection criteria is the double ionization in showers initiated by photons. The possible photon misidentification is essentially due to photons undergoing Compton scattering, whose cross section becomes negligible with respect to the pair production above a few hundreds MeV. Monte Carlo studies indicate a residual contamination of about 0.18% for the energy spectrum of photons from pion decays in CNGS events, rising to a few % in the sub-GeV energy region. The loss in efficiency for electron showers is only 10%. First results from an ongoing study on low energy showers from isolated secondary π^0's in the T600 CNGS data confirm the MC expectation (see Fig. 4[Right]). The plot shows a good agreement between data and simulations, including the low ionisation tail due to Compton interactions.

Muon momentum reconstruction in the T600 is based on the analysis of multiple scattering. Since the muon momentum measurement dominates the accuracy in ν_μ CC event reconstruction, a thorough investigation of the statistical and systematic errors connected with the method is underway. Moreover, the already available algorithm, which is based on a Kalman filter procedure, has been complemented with a simpler one based on the "classical" formulation of the multiple scattering method [5]. This allows for cross checks and control of the systematics. Both methods have been succesfully tested on Monte Carlo events and long stopping muons from neutrino interactions in the upstream rock, as shown in Fig. 6.

Activity is also ongoing on the automation of the event reconstruction, a challenging task due to the complexity of the high-energy CNGS events. For global reconstruction, the fundamental issue has been identified as the development of a general approach for the segmentation of the event at the 2D hit level, namely the identification of tracks, cascades,

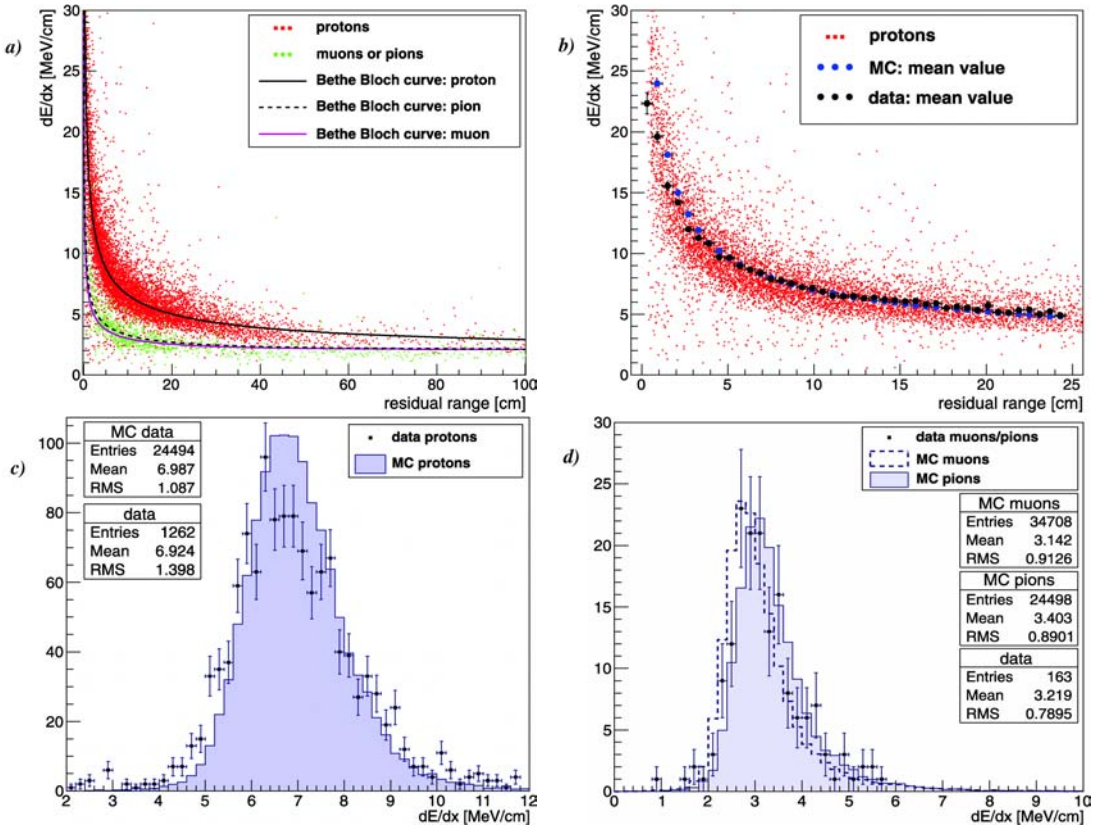

Figure 5: *a) The selected sample of data tracks identified as proton or μ/πtracks; b) mean value of dE/dx distributions in 6 mm bins of residual range: black data tracks identified as protons; blue simulated proton tracks; points in the background data tracks identified as protons; c) dE/dx in 8-12 cm residual range for tracks identified as protons, compared to simulated proton tracks; d) dE/dx in 8-12 cm residual range for tracks identified as μ/π, compared to simulated muon and pion tracks.*

vertices and their mutual relations. Work is ongoing on an algorithm that exploits iterative tracking of hit clusters and detection of vertices and track scattering/crossing points.

Completion of the data analysis will represent a major commitment for all 2013 and most likely it will continue in the following year, with involvement of all the ICARUS institutions and groups.

7 Search for the LSND anomaly in the CNGS beam

The ICARUS experiment has been visually searching for the signature of a signal due to a LSND-like anomaly in the CERN to Gran Sasso neutrino beam (CNGS) [P2]. The CNGS facility [6] provides a neutrino beam composed mainly of muon neutrinos peaked in the range $10 \leq E_\nu \leq 30$ GeV.

According to detailed Monte Carlo (MC) calculations of the neutrino beam [7], about 2850 charged current (CC) events/kt/year are expected at LNGS for a nominal proton beam intensity of 4.5×10^{19} pot/year with a spectral contamination from anti-neutrino of about 2% and an electron component of slightly less than 1%. The integral error on

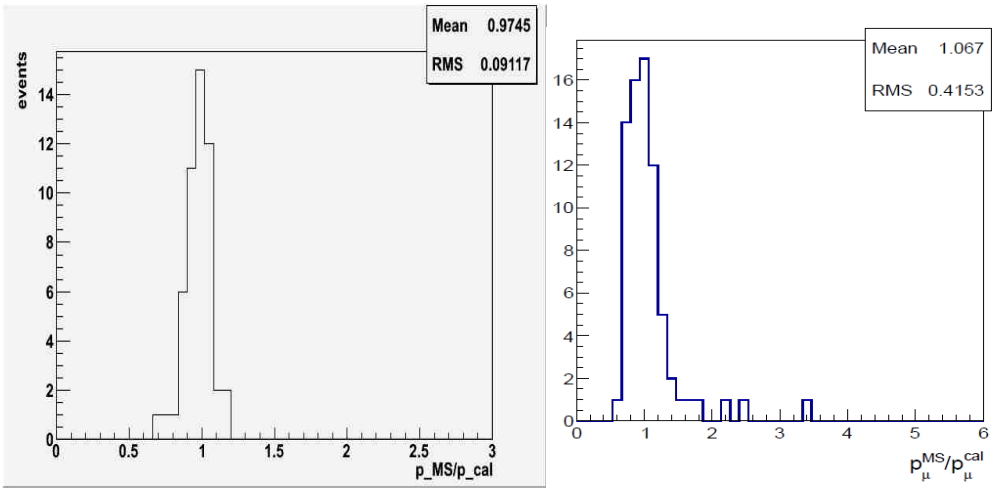

Figure 6: *Ratio between the μ momentum reconstructed via Multiple Scattering and the one reconstructed through calorimetry (p_μ^{MS}/p_μ^{cal}) for stopping muons (mainly from the upstream rock) acquired during the 2011 ICARUS T600 run. [Left]: Kalman filter; [Right]: "classical" method.*

the ν_e/ν_μ ratio is estimated to be better than 7 %.

The ICARUS experiment is operated at $L/E_\nu \approx 36.5$ m/MeV, a value much larger than the one of the experiments where anomalies appeared. In first approximation, a hypothetical $\nu_\mu \to \nu_e$ LSND-like anomaly will produce very fast oscillations as a function of the neutrino energy E_ν, averaging to $\sin^2(1.27\Delta m^2_{new} L/E_\nu) \approx 1/2$ and $\left\langle P_{\nu_\mu \to \nu_e} \right\rangle = 1/2 \sin^2(2\theta_{new})$. This signal will have to be compared with the small, but significant, backgrounds due to other and more conventional neutrino sources.

The search for $\nu_\mu \to \nu_e$ events due to a LSND-like anomaly has been performed as follows. The ICARUS experimental sample has been based on 168 neutrino events collected in 2010 (5.8×10^{18} pot) and 923 events collected in 2011 (2.7×10^{19} pot out of the 4.4×10^{19} collected in 2011), leading to a total of 1091 observed neutrino events, in good agreement, within 6%, with the Monte Carlo expectation. To this initial sample, a minimal fiducial volume cut has been applied to collect as much statistics as possible: the interaction vertex is required to be at a distance of at least 5 cm from each side of the active volume and at least 50 cm from its downstream wall. Furthermore, only events with a deposited energy smaller than 30 GeV have been included in the analysis, in order to optimize the signal over background ratio. In the analysis, the "electron signature" has been defined by the following requirements:

(a) vertex of the event inside the fiducial volume;

(b) visible event energy smaller than 30 GeV, in order to reduce the beam ν_e background;

(c) the presence of a charged track starting directly from the vertex, fully consistent over at least 8 wire hits with a minimum ionising relativistic particle, i.e. the average dE/dx must be lower than 3.1 MeV/cm after removal of visible delta rays (see Fig. 4[Left]), and subsequently building up into a shower;

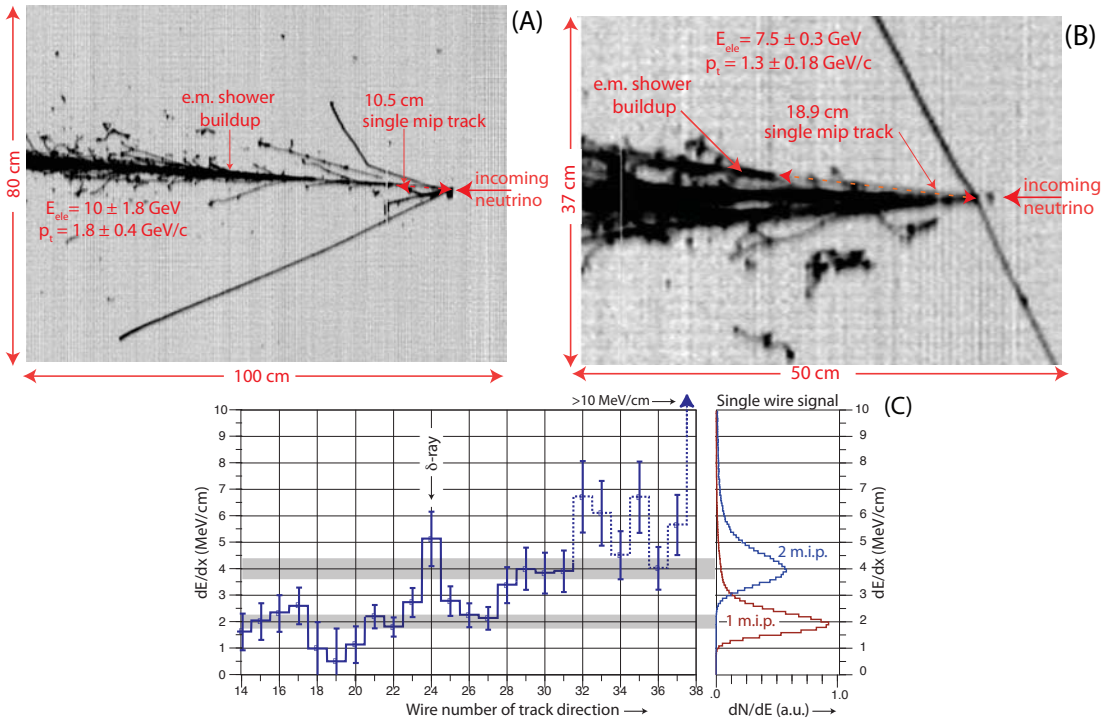

Figure 7: *The two observed events (A) and (B) with a clearly identified electron signature. Event in (A) has a total energy of* 11.5 ± 1.8 *GeV, and a transverse electron momentum of* 1.8 ± 0.4 *GeV/c. Event in (B) has a visible energy of* $\sim$*17 GeV and a transverse momentum of* 1.3 ± 0.18 *GeV/c. In both events the single electron shower in the transverse plane is clearly opposite to the remaining of the event. (C): display of the actual dE/dx along individual wires of the electron shower shown in Fig. 7(A), in the region* ($\geq$ *4.5 cm from primary vertex) where the track is well separated from other tracks and heavily ionising nuclear prongs. As a reference, the expected dE/dx distribution for single and double minimum ionising tracks (see Fig. 4[Left]), are also displayed. The dE/dx evolution from single ionising electron to shower is also shown.*

(d) visible spatial separation from other ionising tracks within 150 mrad in the immediate vicinity of the vertex in at least one of the two transverse views ($\pm 60°$), except for short proton like recoils due to nuclear interactions.

In order to determine the electron signature selection efficiency η, ν_e events have been generated with MC according to the ν_μ CC spectrum. These events have been visually and independently scanned by three different people in different locations. An excellent agreement has been found with differences in less than 3% of the sample. As a result, the average number of positively identified electron-like neutrino events is 90, corresponding to a selection efficiency $\eta = 0.74 \pm 0.05$. In a good approximation η is independent of the details of the energy spectrum.

A similar scan of 800 MC neutral current events has shown no presence of apparent $\nu_\mu \rightarrow \nu_e$ events, consistent for our sample with an estimated upper limit of 0.3 events (including possibly misidentified ν_μ CC events).

The expected number of ν_e events due to conventional sources in the energy range and fiducial volumes defined in (a) and (b) are as follows: 3.0 ± 0.4 events due to the estimated ν_e beam contamination; 1.3 ± 0.3 ν_e events due to the presence of θ_{13} oscillations

from $sin^2(\theta_{13}) = 0.0242 \pm 0.0026$ [8]; 0.7 ± 0.05 ν_τ with $\tau \to e$ from the three neutrino mixing standard model predictions [9], giving a total of 5.0 ± 0.6 expected events, where the uncertainty on the NC and CC contaminations has been included. The expected visible background is then 3.7 ± 0.6 (syst. error only) events after the selection efficiency $\eta = 0.74 \pm 0.05$ reduction has been applied. Given the smallness of the number of electron like signal expected in absence of LSND-like anomaly, the estimated systematic uncertainty on the predicted number is clearly negligible w.r.t. its statistical fluctuation.

In the recorded experimental sample, two events in which a ν_e signature have been identified, to be compared with the above expectation of 3.7 events for conventional sources. The event in Fig. 7(A) has a total energy of 11.5 ± 2.0 GeV and an electron of 10 ± 1.8 GeV taking into account a partially missing component of the e.m. shower. The event in Fig. 7(B) has 17 GeV of visible energy and an electron of 7.5 ± 0.3 GeV. In both events the single electron shower in the transverse plane is opposite to the remaining of the event, with the electron transverse momentum of 1.8 ± 0.4 GeV/c and 1.3 ± 0.18 GeV/c respectively. Fig. 7(C) displays the actual dE/dx along individual wires of the electron shower shown in Fig. 7(A), in the region (≥ 4.5 cm from primary vertex), where the track is well separated from other tracks and heavily ionising nuclear prongs.

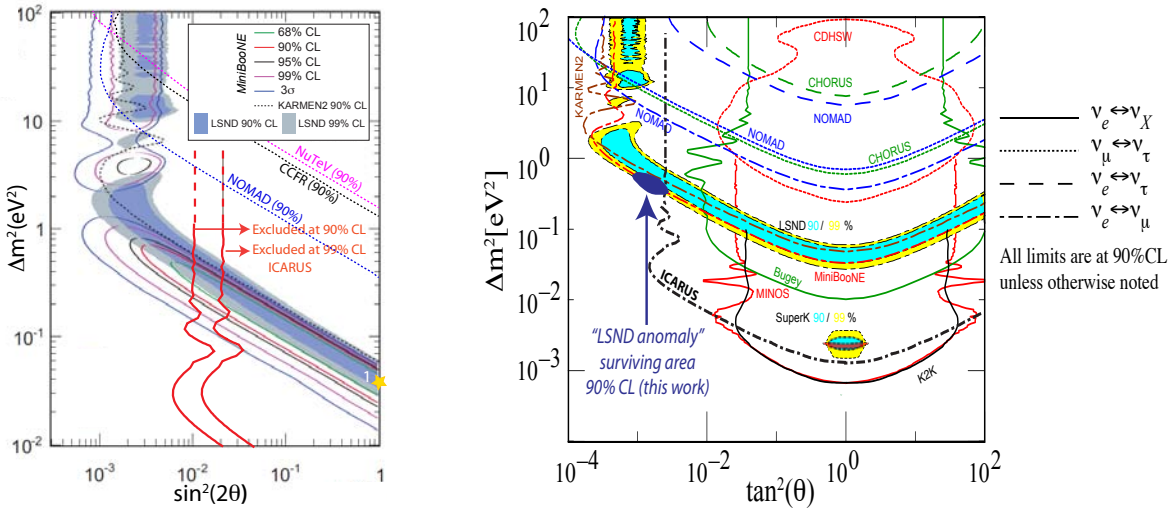

Figure 8: *[Left]: two-dimensional plot of* Δm^2 *vs* $\sin^2(2\theta_{new})$ *for the main published experiments sensitive to the* $\nu_\mu \to \nu_e$ *anomaly [10, 11, 12, 13, 14, 15] and the present ICARUS result. The ICARUS limits to the oscillation probability are* $\langle P_{\nu_\mu \to \nu_e} \rangle \leq 5.4 \times 10^{-3}$ *and* $\langle P_{\nu_\mu \to \nu_e} \rangle \leq 1.1 \times 10^{-2}$ *, corresponding to* $\sin^2(2\theta_{new}) \leq 1.1 \times 10^{-2}$ *and* $\sin^2(2\theta_{new}) \leq 2.2 \times 10^{-2}$ *respectively at 90% and 99% CL. Limits correspond to 3.41 and to 7.13 events. [Right]: regions in the* $(\Delta m^2, \tan^2(\theta))$ *plane excluded by the ICARUS experiment compared with the published results [9]. While for* $\Delta m^2_{new} \gg 1eV^2$ *there is already disagreement for* $\nu_\mu \to \nu_e$ *between the allowed regions from the published experiments, for* $\Delta m^2_{new} \leq 1eV^2$ *the ICARUS result now allows to define a much smaller, narrower allowed region centered around* $(\Delta m^2, \sin^2(2\theta))_{new} = (0.5eV^2, 0.005)$ *in which there is a 90% C.L. overall agreement.*

Within the range of our observations, our result is compatible with the absence of a LSND-like anomaly. Following Ref. [17], at statistical confidence levels of 90% and 99% and taking into account the detection efficiency η, the limits due to the LSND anomaly are respectively 3.4 and 7.1 events. According to the above described experimental sample

and the number of recorded events, the corresponding limits on the oscillation probability are $\left\langle P_{\nu_\mu \to \nu_e} \right\rangle = 5.4 \times 10^{-3}$ and $\left\langle P_{\nu_\mu \to \nu_e} \right\rangle = 1.1 \times 10^{-2}$ respectively. The exclusion area of the ICARUS experiment is shown in Fig. 8[Left] in terms of the two-dimensional plot of $\sin^2(2\theta_{new})$ and Δm^2_{new}. In most of the area covered by ICARUS and allowed by LSND and MiniBooNE, the oscillation averages approximately to a half of its highest value, $\sin^2(1.27\Delta m^2_{new} L/E_\nu) \approx 1/2$. For lower values of Δm^2_{new}, the longer baseline strongly enhances the oscillation probability with respect to the one of the short baseline experiments. In ICARUS and for instance with $\left(\Delta m^2, \sin^2(2\theta)\right)_{new} = (0.11\ \text{eV}^2,\ 0.10)$ as many as 30 anomalous $\nu_\mu \to \nu_e$ events should have been present with $E_\nu \leq 30$ GeV in the analysed sample.

A detailed comparison among the various results on different oscillation phenomena, between different pairs of neutrino flavours, each having specific mixing angles and Δm^2 is shown in Fig. 8[Right] [9]. Even if disappearance and appearance results should not be referred to a single effective θ and Δm^2, the plot allows situating the residual "LSND anomaly" in the framework of the present neutrino oscillation results. While for $\Delta m^2_{new} >> 1\ \text{eV}^2$ there is already disagreement between the allowed regions from the published experiments, for $\Delta m^2_{new} \leq 1\ \text{eV}^2$ the ICARUS result now allows to define a much smaller, narrower region centered around $\left(\Delta m^2, \sin^2(2\theta)\right)_{new} = (0.5\ \text{eV}^2,\ 0.005)$ in which there is 90% CL agreement between (1) the present ICARUS limit, (2) the limits of KARMEN and (3) the positive signals of LSND and MiniBooNE collaborations. This is the area in which the expectations from cosmology suggest a substantial contribution to the dark mass signal.

This region will be better explored by the proposed ICARUS/NESSiE dual detector experiment [18] to be performed at CERN at much shorter distances (∼300 m and ∼1.6 km) and lower neutrino energies, which increase the event rate, reduce the overall multiplicity of the events, enlarge the angular range and therefore improve substantially the ν_e selection efficiency.

8 Addressing the Superluminal neutrino problem

Beyond its initial physics program, the experiment has proved to be well suited also to address the superluminal neutrino problem firstly raised by the OPERA experiment [19]. In this section we report the results on the search for the analogue to the Čerenkov radiation in the ICARUS T600 detector and on the direct measurement of the CNGS neutrino velocity using a dedicated neutrino bunched beam.

Super-luminal muon neutrinos should lose their energy by producing photons and e^+e^- bremsstrahlung pairs, through Z^0 mediated processes analogous to Čerenkov radiation, as argued by A.G.Cohen and S.L.Glashow [20]. Both pair emission rate Γ and neutrino energy loss dE/dx are proportional to δ^3 where $\delta = (v_\nu^2 - c^2)/c^2$, being v_ν and c the neutrino and light velocity respectively.

A full Fluka Monte Carlo simulation of the CNGS neutrino propagation to Gran Sasso was performed, including the superluminal radiating process kinematics, as a function of δ. Expectations for $\delta = 5 \times 10^{-5}$, corresponding to the first OPERA claim, are: (1) full ν event suppression for $E_\nu > 30GeV$; (2) about 10^7 e^+e^- pairs/10^{19}p.o.t./kt with a very

clear signature: isolated e.m. shower ($E_{dep} > 200MeV$) within $150mrad$ from CNGS beam axis.

The raw energy deposition E_{dep} for CC and NC muon neutrino events was measured calorimetrically and its experimental distribution was compared with the MC expectations: no spectrum suppression was found in both NC and CC data (see Fig. 9) and no e^+e^- pair brehmstrahlung event candidates were found. This lack of events was translated into a 90% CL limit for $\delta < 2.5 \times 10^{-8}$ [P3].

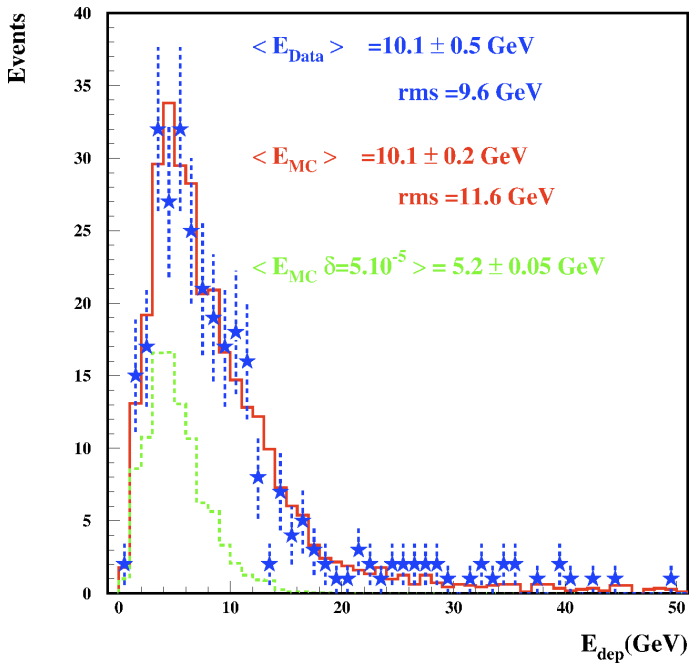

Figure 9: *Experimental raw energy E_{dep} distribution for ν_μ and $\overline{\nu_\mu}$ CC interactions in ICARUS (blue) compared with Monte Carlo expectations for an unperturbed spectrum (red), and for $\delta = 5 \times 10^{-5}$ (green). 1.53×10^{19} p.o.t. were used for the analysis.*

Any ionizing event produces in LAr abundant scintillation light ($\sim 2.5 \times 10^4 \gamma$/MeV at 128 nm) which is exploited for the direct measurement of the neutrino velocity. The 4% of the γ's are emitted within $1ns$ from the ionizing event, corresponding to about $50-100$ phe/GeV/D^2, where D is the distance from the closest PMT.

At the end of the 2011 run, the CERN CNGS neutrino beam briefly operated in lower intensity mode ($\sim 10^{12}$ p.o.t./pulse) with a proton beam structure made of narrow bunches $\sim 3ns$ wide. This very tightly bunched beam allowed a very accurate time-of-flight (tof) measurement of neutrinos on an event-by-event basis. During this period the ICARUS T600 detector collected 7 beam-associated events, consistent with 2.2×10^{16} p.o.t. The neutrino velocity measurement was performed combining the accurate determination of the baseline and of the tof. The baseline measurement was performed based on old geodetic measurement available for the OPERA detector combined with recent optical triangulations providing the distance between the OPERA origin and the ICARUS detector entry wall along the beam direction. The baseline was estimated in $731222.3 \pm 0.5m$. The origin of the neutrino tof measurement is the Beam Current Transformer (BCT) detector

(BFCTI.400344), located upstream of the CNGS neutrino target; the reference end-point is set at the upstream wall position of the ICARUS T600 active volume. The proton beam time-structure at the BCT is recorded by a 1 GS/s waveform digitizer. Every acquisition is time-tagged with respect to the SPS timing system, associating each neutrino event at LNGS to a precise proton bunch. The absolute UTC timing signal at CERN and at LNGS is provided by two identical systems: an ESAT 2000 GPS receiver coupled with a high accuracy GPS PolaRx2e receiver for time-transfer applications, operating in common-view mode, and a Cs atomic clock Symmetricom Cs4000. The systematic error for their synchronization is ~ 2.0 ns. All the timing signal transmission paths, including the $8km$ optical fiber driving the UTC time stamp from the outside LNGS buildings to the underground hall have been carefully measured ($\sim 1ns$ of accuracy). On the detector side, several corrections have been included in order to measure the neutrino arrival time. The propagation time of the scintillation light signals from the PMT window to the PMT-DAQ system has been carefully calibrated. It includes the PMT transit time, overall cabling ($\sim 44m$) and the delay through signal adders and preamplifier. The associated uncertainty is $\pm 5.5ns$, dominated by PMT transit time fluctuations due to different bias voltages. All measurements have been done directly using PMT-sum signals. In addition, the distance of each event from the closest PMT and the position of the interaction vertex inside the detector active volume have been evaluated leading to the relative time correction with $1ns$ of accuracy. The difference $\delta t = tof_c - tof_\nu$ between the expected tof based on the speed of light ($tof_c = 2439098 \pm 1.7$ ns) and the neutrino tof resulted to be, on average, $\delta t = +0.3 \pm 4.9_{stat} \pm 9.0_{syst}$ ns [P4] with an r.m.s. of $10.5ns$ (see Fig. 10*[Left]*).

With the aim of improving the neutrino tof measurement significance, in 2012 two additional weeks of bunched beam were provided. The new beam had 64 bunches with a narrow width of $4ns$ FWHM. For this measurement the four CERN-LNGS time syncronization/distribution systems described in section 4 were available.

With respect to the 2011 setup the PMT-DAQ system has been also improved by augmenting the granularity of PMT-sum signal recording (9 PMTs instead of 27). Moreover a new calibration campaign has been performed with improved accuracy allowing to infer, with the precision of $1ns$, the transit time of each single PMT as a function of the bias voltage applied.

In 2012, a high precision geodesy campaign by Politecnico di Milano re-evaluted the neutrino baseline in $731222.03 \pm 0.10m$, in agreement with the previous value.

During the 2012 bunched beam run, ICARUS T600 collected 25 beam-associated events, consistent with 1.8×10^{17} p.o.t. The final evaluation of tof_ν was obtained, event by event, as weighted average of all the available timing paths. The distribution of $\delta t = tof_c - tof_\nu$ is shown in Fig. 10*[Right]* and the resulting average value is $\delta t = +0.10 \pm 0.67_{stat} \pm 2.39_{syst}$ ns, fully compatible with the neutrino propagation at the speed of light, excluding neutrino velocities exceeding the speed of light by more than 1.35×10^{-6} c at 90% C.L. [P5]. The corresponding deviation of the neutrino velocity from the speed of light is $\delta(v/c) = (v_\nu - c)/c = (0.4 \pm 2.8_{stat} \pm 9.8_{syst}) \times 10^{-7}$.

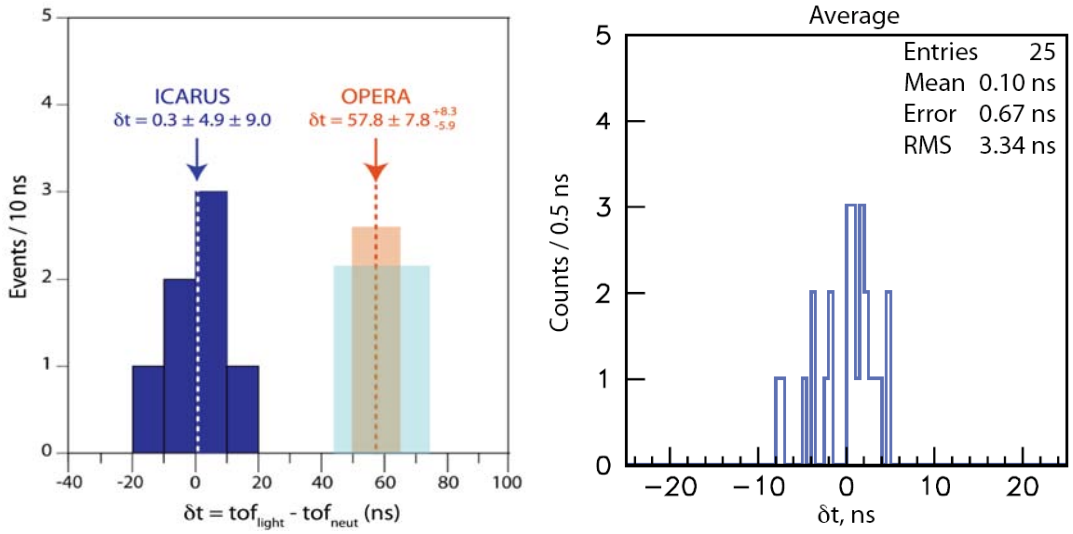

Figure 10: *[Left]: Bunched beam campaign 2011: event distribution in ICARUS T600 for* $\delta t = tof_c - tof_\nu$*. The first OPERA claim that motivated the neutrino velocity measurement with ICARUS T600 is also shown. [Right]: Bunched beam campaign 2012: event distribution in ICARUS T600 for* $\delta t = tof_c - tof_\nu$*, according to the averaging procedure of all synchronization paths.*

9 Future perspectives

For the next years, the ICARUS Collaboration is proposing a new experiment with an intense ∼2 GeV neutrino beam at CERN SPS with the aim of definitely clarifying the possible existence of additional neutrino states, as hinted by neutrino calibration source experiments, reactor and accelerator experiments, and eventually measure the corresponding oscillation parameters.

The experiment is based on two identical LAr-TPCs, complemented by magnetised spectrometers, detecting electron and muon neutrino events at Far and Near positions located at 1600 m and 300 m from the proton target respectively.

The ICARUS T600 detector, the largest LAr-TPC ever built with a size of about 600 ton of imaging mass, now running in the LNGS underground laboratory, will be moved at the CERN Far position. An additional 1/4 of the T600 detector (T150) will be constructed and located in the Near position.

Two large area spectrometers, placed downstream of the two LAr-TPC detectors, will perform charge identification and muon momentum measurements from sub-GeV to several GeV energy range, greatly complementing the physics capabilities.

This experiment will offer remarkable discovery potentialities (Fig. 11), collecting a very large number of unbiased events both in the neutrino and antineutrino channels, largely adequate to definitely settle the origin of the observed neutrino-related anomalies.

Before the transport to CERN and after three successful years of uninterrupted operation, the ICARUS detector requires an extensive re-furbishing in order to improve its performance and further continue operation.

The existing internal detector will be housed into new vessels made of extruded Aluminum profiles, instead of the Al honeycomb panels presently used. Bi-metal joints and

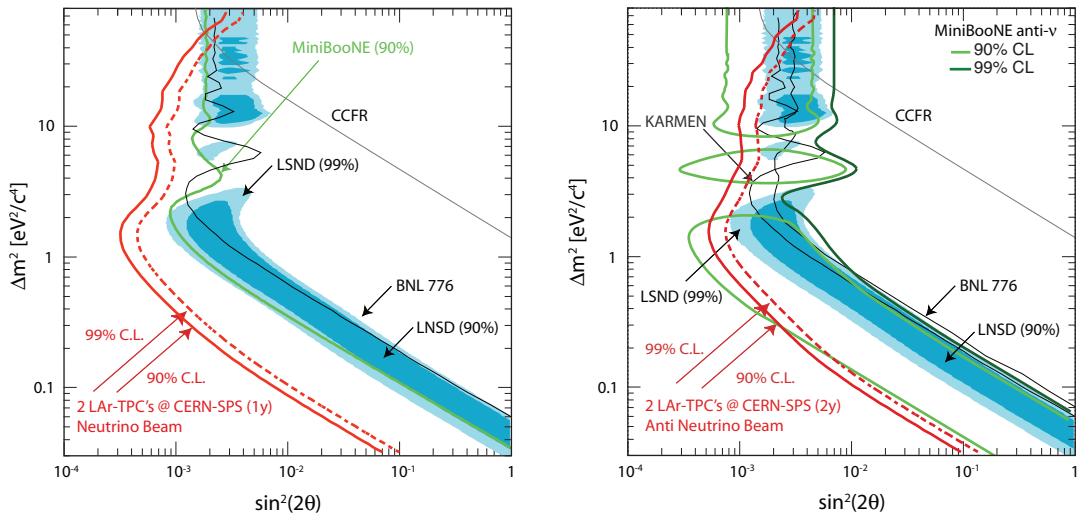

Figure 11: *Expected sensitivity for the proposed experiment exposed at the CERN-SPS neutrino beam (left) and anti-neutrino (right) for* 4.5×10^{19} *pot (1 year) and* 9.0×10^{19} *pot (2 years), respectively. The LSND allowed region is fully explored in both cases.*

flanges will be recovered from the present containers. A new external insulation based on industrial membrane tank concept, widely used for liquid natural gas storage/transport, will ensure a much better performance and full containment in case of spill from main LAr vessels. The PMT system will be completed in both modules.

The first phase of the refurbishing will take place at LNGS and is finalized to the LAr recovery and to the TPC inner detector extraction. It will require trained and expert personnel and will be staged as follows: (1) cryostat emptying (550,000 l of LAr), requiring 5 weeks operating with $\Delta p_{max} < 0.45$ bar steps, 1-2 truck / day; (2) cryostat heating, lasting up to one month proceeding by $\Delta Tmax < 50$K steps to prevent thermal shock on wire chambers; (3) activities planned in parallel to the heating phase finalized to the recovery of the cryogenic plant, DAQ/trigger electronics, TPC cabling, ancillary systems, PMT removal.

The TPCs will be transported inside clean and lightweight containers, installed on the trolleys already used for the transport from Pavia to LNGS. Feasibility study and cost estimate for T600 transport out of LNGS have been carried out in close collaboration with CERN Transport Group. No major works are foreseen for the LNGS underground Laboratory infrastructures. The detailed schedule and logistics plan are being defined together with LNGS management to take into account any possible interference with other underground activities.

List of Publications Year 2012

[**P1**] M. Antonello et al. (ICARUS Collaboration), Precise 3D track reconstruction algorithm for the ICARUS T600 liquid argon time projection chamber detector, e-Print: arXiv:1210.5089 [physics.ins-det] (2012), accepted for publication on Advances in High Energy Physics.

[P2] M. Antonello et al. (ICARUS Collaboration), Experimental search for the LSND anomaly with the ICARUS LAr TPC detector in the CNGS beam, e-Print: arXiv:1209.0122 [hep-ex] (2012), accepted for publication on European Physical Journal C.

[P3] M. Antonello et al. (ICARUS Collaboration), A search for the analogue to Cherenkov radiation by high energy neutrinos at superluminal speeds in ICARUS, Physics Letters B Volume 711, Issues 3–4, 15 May 2012, pages 270–275.

[P4] M. Antonello et al. (ICARUS Collaboration), Measurement of the neutrino velocity with the ICARUS detector at the CNGS beam, Physics Letters B Volume 713, Issue 1, 18 June 2012, pages 17–22.

[P5] M. Antonello et al. (ICARUS Collaboration), Precision measurement of the neutrino velocity with the ICARUS detector in the CNGS beam, Journal of High Energy Physics, JHEP11 (2012)049.

References

[1] C.Rubbia, CERN-EP/77-08 (1977).

[2] S. Amerio et al., Nucl. Instr. Meth. **A527**, (2004) 329.

[3] C. Rubbia et al., JINST 6 (2011) P07011. e-Print: arXiv:1106.0975 [hep-ex].

[4] B. Cacianiga et al., e-Print: arXiv:1207.0591v2 [hep-ex].

[5] A. Ferrari, C. Rubbia, Muon momentum determination by multiple scattering in liquid argon, ICARUS-TM 99/10.

[6] G. Aquistapace et al. CERN 98-02, INFN/AE-89-05 (1998); R. Bailey et al. CERN-SL/99-034 (DI), INFN/AE-99/05 Addendum (1999); E. Gschwendtner et al., CERN-ATS-2010-153 (2010).

[7] A. Ferrari et al., CERN-AB-Note-2006-038 (2006).

[8] G. L. Fogli et al. arXiv:1205.5254 [hep-ph] (2012).

[9] J Beringer et al. (Particle Data Group), Phys. Rev. D86, 010001 (2012).

[10] A. Aguilar et al. Phys. Rev. D 64, 112007 (2001).

[11] A. A. Aguilar-Arevalo et al.,arXiv:1207.4809v1 [hep-ex] 19 Jul 2012 and references therein.

[12] B. Armbruster et al.,Phys. Rev. D 65, 112001 (2002).

[13] P. Astier et al.,Phys. Lett. B 570 19 (2003).

[14] A. Romosan et al., Phys. Rev. Lett. 78 2912 (1997).

[15] S. Avvakumov et al., Phys. Rev. Lett. 89 (2002) 011804.

[16] C. Giunti and M. Laveder, Phys. Rev. D 82, 053005 (2010). And references therein.

[17] G.J. Feldman and R. D. Cousins, Phys. Rev. D 57 (1988) 3873.

[18] M. Antonello et al., SPSC-P-347 (2012); C. Rubbia et al., SPSC-P-345 (2011).

[19] OPERA collaboration, T. Adam et al., arXiv:1109.4897v1[hep-ex] (2011).

[20] A.G. Cohen and S.L. Glashow, Phys. Rev. Lett. 107 (2011) 181803 [arXiv:1109.6562].

LUNA: Laboratory for Underground Nuclear Astrophysics

M. Aliotta[a], M. Anders[b], D. Bemmerer[b], C. Broggini[c], C. Bruno[d], A. Caciolli[c], F. Cavanna[e], P. Corvisiero[e], T. Davinson[a], R. Depalo[f], A. Di Leva[g], Z. Elekes[b], A. Formicola[h], Zs. Fülöp[i], G. Gervino[j], A. Guglielmetti[d], C. Gustavino[k], Gy. Gyürky[i], G. Imbriani[g], M. Junker[h], R. Menegazzo[c], M.-L. Menzel[b], P. Prati[e], V. Roca[g], C. Rolfs[l], C. Rossi Alvarez[c], D. Scott[a], E. Somorjai[i], O. Straniero[m], F. Strieder[l], T. Szucs[i], F. Terrasi[n], H.P. Trautvetter[l], D. Trezzi[o]
Spokesperson: A. Guglielmetti

[a]University of Edinburgh, Edinburgh, United Kingdom
[b]Helmholtz-Zentrum Dresden-Rossendorf, Dresden, Germany
[c]INFN, Padova, Italy
[d]Università degli Studi di Milano and INFN, Milano, Italy
[e]Università degli Studi di Genova and INFN, Genova, Italy
[f]Università degli Studi di Padova and INFN, Padova, Italy
[g]Università degli Studi di Napoli "Federico II", and INFN, Napoli, Italy
[h]INFN, Laboratori Nazionali del Gran Sasso (LNGS), Assergi (AQ), Italy
[i]Institute for Nuclear Physics, Hungarian Academy of Sciences, Debrecen, Hungary
[j]Università degli Studi di Torino and INFN, Torino, Italy
[k]INFN, Roma, Italy
[l]Institut für Experimentalphysik III, Ruhr-Universität Bochum, Bochum, Germany
[m]Osservatorio Astronomico di Collurania, Teramo, and INFN Napoli, Italy
[n]Seconda Università di Napoli, Caserta and INFN, Napoli, Italy
[o]INFN, Milano, Italy

Abstract

Aim of the LUNA experiment is the measurement of thermonuclear fusion cross sections relevant for stellar nucleosynthesis. In the course of the year 2012, the experimental activity has been focussed on the ^{2}H(α,γ)^{6}Li and ^{17}O(p,γ)^{18}F reactions. For the former, data acquired in 2011 were analyzed, taking into account the strong beam induced background component. For the latter, the resonance at 193 keV as well as the direct capture component were deeply investigated both with the prompt-γ and with the activation techniques and data analyzed and published.

A firts set of preliminary measurements for the study of the ^{22}Ne(p,γ)^{23}Na also took place. Moreover, intense work was dedicated to the LUNA-MV project, now partly financed in the framework of the "Progetti Premiali"' of the Italian Research Ministry.

1 The $^2H(\alpha,\gamma)^6Li$ reaction and the Big Bang Nucleosynthesis

In its standard picture, the Big Bang Nucleosynthesis occurs during the first minutes of cosmic time, with the formation of light isotopes such as ^{2}H, ^{3}He, ^{4}He, ^{6}Li and ^{7}Li. Their abundance depends only on particle physics parameters, on baryon-to-photon ratio and on nuclear cross sections of involved processes. The observed abundances of ^{2}H, ^{3}He, and ^{4}He are in good agreement with calculations, confirming the overall validity of BBN theory. On the other hand, the observed abundance of ^{7}Li is a factor 2-3 lower than the predicted one, and the amount of ^{6}Li observed in metal poor stars is unexpectedly large compared to Big Bang Nucleosynthesis (BBN) predictions. Even though many of the claimed ^{6}Li detections may be in error, for a few metal-poor stars there still seems to be a significant amount of ^{6}Li [1]. The difference between observed and calculated values may reflect unknown post-primordial processes or physics beyond the Standard Model. However, the cross section of the ^{2}H(α,γ)^{6}Li reaction, i.e. the leading process to synthesize ^{6}Li, has never been measured before LUNA at BBN energies ($30 < E(keV) < 400$), making the theoretical predictions of ^{6}Li very uncertain [2].

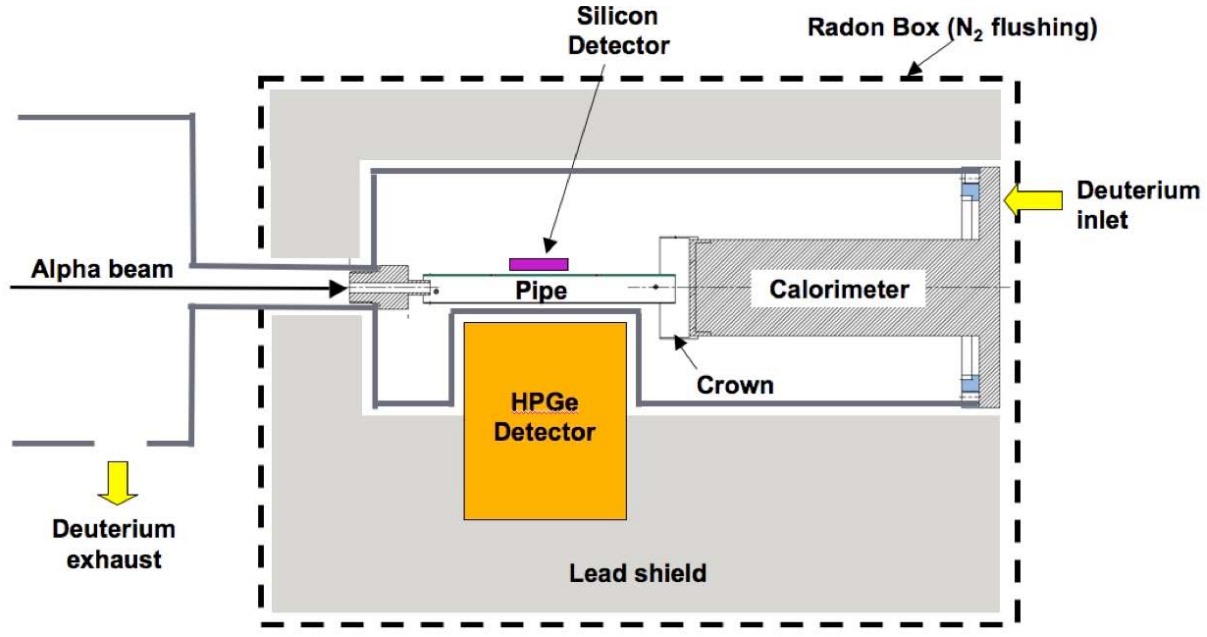

Figure 1: Experimental set-up.

Figure 1 shows the experimental set-up. The α-beam impinges on a windowless gas

target of D_2. The signal is maximized minimizing the distance between the germanium detector and the beam line. The natural background is reduced by means of a 4π lead shield and an anti-Radon box that encloses the reaction chamber and the HPGe detector. The measurement of the ^{2}H$(\alpha,\gamma)^6$Li reaction is affected by an inevitable beam induced background. In fact, the ^{2}H$(\alpha,\alpha)^2$H Rutherford scattering induces a small amount of ^{2}H$(^2H,n)^3$He reaction. The neutrons produced by the ^{2}H$(^2H,n)^3$He reaction induce $(n,n'\gamma)$ reactions in the HPGe detector and in the surrounding materials (lead, steel, copper), generating a beam-induced background in the HPGe spectrum [3].

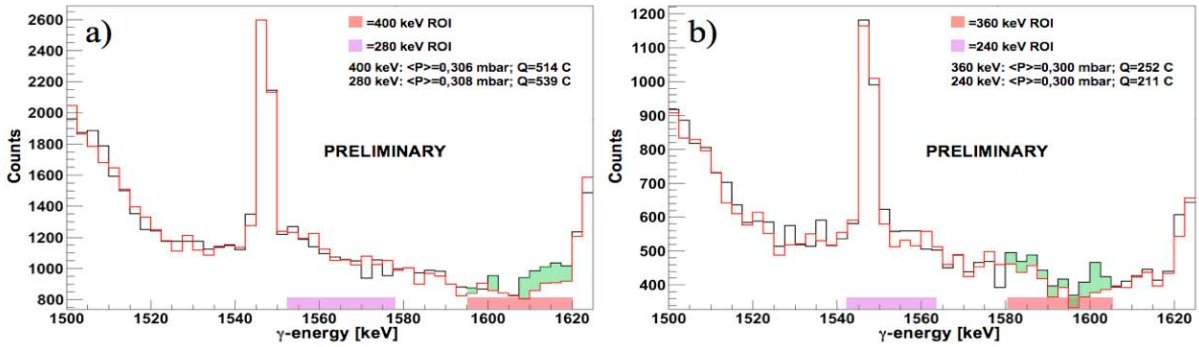

Figure 2: a) Experimental spectra for $E_\alpha = 400$ keV (black line) and for $E_\alpha = 280$ keV (red line). The red and violet bands indicate the RoI at $E_\alpha = 400$ keV RoI and $E_\alpha = 280$ keV, respectively. Note the counting excess visible (green bins) in correspondence to the 400 keV RoI. b) Experimental spectra for $E_\alpha = 360$ keV (black line) and for $E_\alpha = 240$ keV (red line). As foreseen, the counting excess shifts to the $E_\alpha = 360$ keV RoI.

To reduce the effective path for the scattered deuterons, and therefore the ^{2}H$(^2H,n)^3$He reaction yield, a 17.8 cm long tube, with a square cross section of 2x2 cm, is placed along the beam line (see figure 1). In this way, the neutron production is limited at the level of few neutrons/second. The set-up is implemented with a silicon detector faced to the gas target volume, to monitor the running conditions through the detection of protons generated in the ^{2}H$(^2H,p)^3$H reaction. The Beam Induced Background due to the $(n,n'\gamma)$ reactions weakly depends on the α-beam energy because the energy of neutrons is mainly related to the Q-value (Q=3.269 MeV) of the ^{2}H$(^2H,n)^3$He reaction [3], while the energy of γ-rays coming from the ^{2}H$(\alpha,\gamma)^6$Li reaction depends on the beam energy through the following relationship:

$$E_\gamma[keV] = 1473.48 + E_{beam}\frac{m_D}{m_D + m_\alpha} \pm \Delta E_{doppler} - E_{recoil}$$

By exploiting the energy dependence of γ-rays due to the ^{2}H$(\alpha,\gamma)^6$Li reaction, it is possible to extract the signal with a measurement performed in two steps [4]:

1. Measurement with $E_{beam} = 400$ keV on D_2 target. The Ge spectrum is mainly due to the background induced by neutrons. The ^{2}H$(\alpha,\gamma)^6$Li γ signal is expected in a well defined energy region (1587-1625 keV).

2. Same as 1, but with $E_{beam} = 280$ keV. The background is essentially the same as before, while the gammas from the ^{2}H$(\alpha,\gamma)^6$Li reaction are shifted to 1550-1580 keV.

Figure 2a shows the spectra with $E_\alpha = 400$ and 280 keV, respectively. A counting excess is visible in the $E_\alpha = 400$ keV RoI. Similarly, Figure 2b shows the spectra at $E_\alpha = 360$ and 240 keV. Although in this case the measurements are shorter with respect to the ones at $E_\alpha = 400$ and 280 keV, because of the occurrence of an accelerator failure, it can be noticed that the counting excess at $E_\alpha = 360$ is shifted to lower energy with respect to the $E_\alpha = 400$ keV one, as expected. As a preliminary result, the LUNA data exclude a nuclear solution for the ^{6}Li problem. When the analysis of data will be completed, the LUNA measurement will substantially reduce the uncertainty of the computed ^{6}Li abundance, thus making the comparison with the observed ^{6}Li abundance more constraining for the underlying physics.

2 The ^{17}O(p,γ)^{18}F reaction

Classical novae, a frequent phenomenon in our Galaxy, are explained as thermonuclear explosions on the surface of white dwarf stars accreting hydrogen-rich material from less evolved companions in binary star systems [5] and have been proposed as a key source of ^{13}C, ^{15}N, ^{17,18}O, and ^{18,19}F isotopes in the Universe [6]. In particular, the short-lived radioisotope ^{18}F ($t_{1/2} = 110$ min) may provide a signature of novae outbursts through the detection of 511 keV γ-ray emission from positron-electron annihilation following its β^+ decay. Indeed, the observation of these γ rays by satellite missions could put constraints on current nova models [7]. Hydrogen burning of ^{17}O is believed to play a key role on the destruction of ^{17}O and on the formation of ^{18}F, mainly through the competing reactions ^{17}O(p,γ)^{18}F and ^{17}O(p,α)^{14}N. Thus, the thermonuclear rates of both reactions should be determined with a high degree of accuracy directly in the energy region of hydrogen burning in classical novae. At nova temperatures, the ^{17}O(p,γ)^{18}F reaction rate is dominated by a direct-capture (DC) reaction mechanism despite the presence of two narrow resonances at $E = 66$ and 183 keV above the proton threshold in ^{18}F. In addition, non-resonant contributions arise from the low-energy tails of two broad resonances at $E = 556.7$ and 676.7 keV. A reliable determination of the total ^{17}O(p,γ)^{18}F reaction rate thus requires the accurate knowledge of the individual energy dependence of both resonant and non-resonant contributions. We report on the results of a new and improved investigation of the ^{17}O(p,γ)^{18}F reaction using both activation and prompt γ-ray detection techniques to address a key source of discrepancy in existing results.

2.1 Experimental approach and first results

The peculiarities of the 400 kV facility are particulary well suited for the study of the ^{17}O(p,γ)^{18}F reaction, where reaction γ-ray lines with very low intensities up to $\simeq 5.0$ MeV have to be measured. High beam intensities and high detection resolution have to be coupled to high target stability and purity. A proton beam, with currents up to 200 μA

on target, entered the target chamber through a liquid-nitrogen cooled copper-pipe biased to -300 V for secondary electrons suppression, see Figure 3.

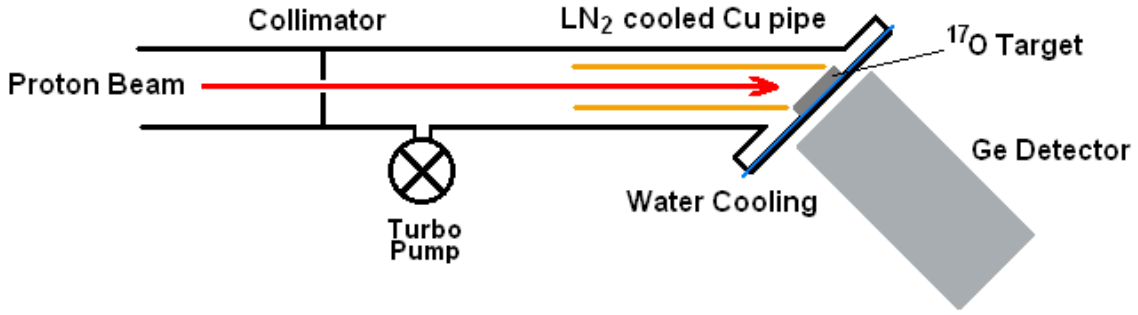

Figure 3: Schematic diagram of the experimental setup

The target was directly water cooled with de-ionised water. Targets were prepared in the LNGS chemistry service by anodization of Ta backings (0.3 mm thick disks) in isotopically enriched water (66% in ^{17}O and 4% in ^{18}O). Full details on target preparation and characterisation have been reported in [8]. The target thickness was closely monitored for signs of degradation during intense proton-beam bombardment by regularly measuring the thick-target yield profile [9] of the narrow isolated resonance at E = 143 keV in ^{18}O(p,γ)^{19}F [8]. Prompt γ rays from the ^{17}O(p,γ)^{18}F reaction were detected using a large volume (115% relative efficiency) high-purity germanium (HPGe) detector placed at 1.5 cm from the target and surrounded by 5 cm lead. Both detector and target were at an angle of 55 degrees with respect to the beam axis, with the detector's front face parallel to the target surface. The ^{17}O(p,γ)^{18}F reaction proceeds by populating several states in ^{18}F, leading to a complex decay scheme. Measurements were taken at the 183 keV resonance and at several off-resonance energies. A sample γ-ray spectrum showing the quality of our data is given in Figure 4. Independent determinations of the total S-factor were carried out for all primary and secondary transitions.

The E=183 keV resonance strength $\omega\gamma$ was determined using the thick-target yield approach [9]. Independent determinations of the total S-factor were carried out for all primary and secondary transitions. An independent determination of both resonant and non-resonant contributions to the ^{17}O(p,γ)^{18}F total cross section was also obtained with the activation technique, i.e. by detecting the 511 keV γ rays from the positron annihilation following the β^+ decay of ^{18}F. Activation spectra were recorded using the low-background facility STELLA (SubTErranean Low Level Assay) at LNGS. The weighted average of the resonance strength values from both techniques gives $\omega\gamma$=1.67$\pm$0.12 (stat+sys) μeV. The reaction rate uncertainty was reduced by a factor of 4 leading to improved constraints on classical novae nucleosynthesis [10]. The astrophysical S factor has been determined

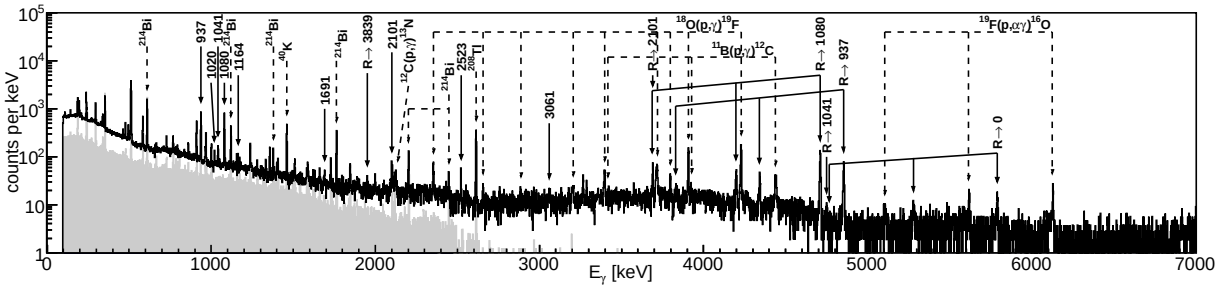

Figure 4: Sample spectrum from prompt γ-ray measurements of the ^{17}O(p,γ)^{18}F reaction at the E = 183 keV resonance. Primary transitions are labelled as $R \rightarrow E_{\rm x}$, while secondary transitions are labelled by their energies. Some of the most prominent background transitions (dashed arrows) are also shown for comparison, together with a time-normalised background spectrum (grey area).

by means of both prompt γ-rays and activation measurements: results from the two approaches are found to be in excellent agreement and a final publication is in progress [11].

This experimental project of the LUNA collaboration is also supported by C. Salvo (INFN-Ge), M. Laubenstein (INFN-LNGS), E. Napolitani (University of Padova), V.Rigato (INFN-LNL).

3 ^{22}Ne(p,γ)^{23}Na

The ^{22}Ne(p,γ)^{23}Na reaction takes place in hydrogen burning, in the neon-sodium cycle that is important in astrophysical novae. At novae temperatures, the reaction rate is dominated by a number of low-energy resonances [12]. However, for the resonances below $E_{\rm p}$ = 0.4 MeV, only upper limits exist in the literature [13]. The rate adopted in the most recent reaction rate compilation [12] uses indirect data [14] to quantify the strength of several of these resonances, adopting upper limits in several cases. The lowest-lying resonance with a directly measured strength is the one at $E_{\rm p}$ = 479 keV [15].

This lack of information makes the deduced reaction rate prone to error. There is a significant discrepancy (Figure 5) between the reaction rate shown in the NACRE compilation [17] and the rate given in the compilations by Iliadis and co-workers [18, 16]. This is mainly due to the inclusion of some low-energy resonances at E = 68 and 100 keV in the NACRE, but not in the Iliadis compilations. Therefore, both the rates and the quoted uncertainties should be taken with a grain of salt, until more experimental information is available.

A sensitivity study taking this discrepany as an uncertainty found a significant impact on the nucleosynthetic output [19]. For models of so-called CO novae, i.e. nova explosions taking place on a white dwarf consisting mainly of carbon and oxygen, the yields of the following nuclides were significantly affected by variations in the ^{22}Ne(p,γ)^{23}Na rate: ^{22}Ne (factor of 100), ^{23}Na (factor of 7), ^{24}Mg (factor of 70), ^{25}Mg (factor of 5), and even ^{26}Al (factor of 20). Therefore, a new study seems highly desirable. The previous upper limits

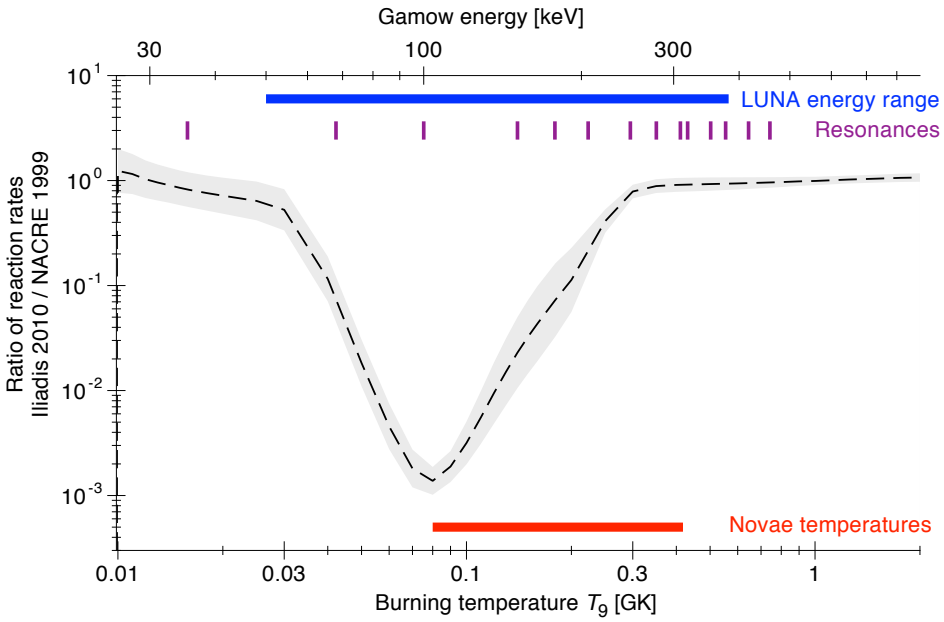

Figure 5: Astrophysical reaction rate of the ^{22}Ne(p,γ)^{23}Na reaction. The ratio of the Iliadis [16] and the previous NACRE [17] rates is plotted. The shaded area covers the nominal uncertainty range given by Iliadis.

for the low-energy resonance strengths in the ^{22}Ne(p,γ)^{23}Na reaction are in the μeV range [13, 14, 16], much higher than the typical sensitivity of LUNA experiments, which lies in the neV range.

As a first step of the study of this reaction at LUNA, some in-beam feasibility tests using neon gas of natural abundance (9% ^{22}Ne) have been conducted in the previous ^{2}H(α,γ)^{6}Li setup. Then, a setup equivalent to the planned ^{22}Ne(p,γ)^{23}Na setup has been constructed, and systematic studies on the gas density with and without beam are currently ongoing. The construction of the well-shielded final setup is planned for early summer 2013.

4 The LUNA-MV project

The LUNA-MV project foresees the realization of a worldwide unique facility inside the underground Gran Sasso Laboratory centered on a 3.5 MV single-ended accelerator for hydrogen and helium. Two different beam lines are foreseen devoted to solid and gas target experiments, respectively. This will allow us to study key reactions of the Hydrogen and Helium burning such as ^{3}He(α,γ)^{7}Be, ^{12}C(α,γ)^{16}O, ^{13}C(α,n)^{16}O and ^{22}Ne(α,n)^{25}Mg reactions. The best place inside LNGS to build such a facility has already been identified as the B node site, far away from the main experimental halls and of the needed dimensions. This site needs a complete refurbishment starting from the impermeabilization of the floor as already performed in the rest of the Laboratory, the construction of an experimental hall, the electrical and safety plants , etc. Very important steps have been performed for the LUNA-MV project during 2012. A special project ("Progetto premiale") has been

submitted to the Italian Research Ministry, after approval by INFN management, with a total request of 6,4 millions of euros in five years, 2.805 of which for the year 2012. The money for the year 2012 has been granted and will allow us to completely refurbish the node B site and buy the core of the 3.5 MV accelerator. To complete the facility with the beam lines, shielding and detectors approximately 3 more millions are requested. The funding of the first year of the "'Progetto Premiale"' has given an exceptional push to the LUNA MV project with respect to the preparation of all the technical documents and executive projects necessary for the tendering procedures, both for site preparation (including shielding) and for the machine. Moreover, given the presence of water utilities of the Teramo Aqueduct in the B node site, a few meetings of members of the LUNA collaboration, LNGS management and LNGS technical division with the Teramo aqueduct, Teramo Health Institute (ASL Teramo) and "Istituto Superiore di Sanità" (main Health Institute) took place in 2012. As a final outcome a document containing a full description of the B-node site, of the LUNA MV accelerator and shielding, of the works necessary for the preparation of the site including technical specifications of all the materials which will be used, and the risk matrices was sent to "Istituto Superiore di Sanità" on Feb 11th, 2013 for an official answer to the question if the LUNA MV project and site preparation have an impact on the water quality. The expected (positive) answer will be sent also to Teramo Health Institute and Abruzzo Region and will allow us to really start the works for the site preparation. The tendering procedure for buying the commercial accelerating machine is going to start in the next few weeks. Approximately 1,5-2 years will be necessary for the installation of the machine on site, once the ordering procedure has been completed. The LUNA collaboration has also organized a workshop at LNGS in February 2013 in order to start-up the new LUNA-MV collaboration. About 60 people were present coming mainly from Europe but also Asia and United States of America. As a final outcome, adhesions to the project will be collected in the next months. These adhesions should be intended as the willingness of the involved group to apply soon to the financing agency of the respective country. After the completion of this first phase, involved people will be called to participate to the drafting of the official Memorandum of Understanding where the agreements among financial agencies will be included, and afterward to the constitution of working groups on specific scientific/technical issues related to the LUNA MV project.

5 List of Publications

- *"Impact of a revised $^{25}Mg(p,\gamma)^{26}Al$ reaction rate on the operation of the Mg-Al cycle"*,
  O. Straniero, G. Imbriani, F. Strieder, D. Bemmerer, C. Broggini, A. Caciolli, P. Corvisiero, H. Costantini, S. Cristallo, A. DiLeva, A. Formicola, Z. Elekes, Zs. Fulop, G. Gervino, A. Guglielmetti, C. Gustavino, Gy. Gyurky, M. Junker, A. Lemut, B. Limata, M. Marta, C. Mazzocchi, R. Menegazzo, L. Piersanti, P. Prati, V. Roca, C. Rolfs, C. Rossi Alvarez, E. Somorjai, F. Terrasi, H.P. Trautvetter,
  ApJ 763 (2013) 100

- *"Neutron induced background by an α-beam incident on a deuterium gas target and*

its implications for the study of the $^2H(\alpha,\gamma)^6Li$ *reaction at LUNA"*,
M. Anders, D. Trezzi, A. Bellini, M. Aliotta, D. Bemmerer, C. Broggini, A. Caciolli, H. Costantini, P. Corvisiero, T. Davinson, Z. Elekes, M.Erhard, A. Formicola, Zs. Fulop, G. Gervino, A. Guglielmetti, C. Gustavino, Gy. Gyurky, M. Junker, A. Lemut, M. Marta, C. Mazzocchi, R. Menegazzo, P. Prati, C. Rossi Alvarez, D. Scott, E. Somorjai, O. Straniero, T. Szucs
Eur. Phys. J. 49 (2013) 28

- *"First Direct Measurement of the* $^{17}O(p,\gamma)^{18}F$ *Reaction Cross Section at Gamow Energies for Classical Novae"*,
D. A. Scott, A. Caciolli, A. Di Leva, A. Formicola, M. Aliotta, M. Anders, D. Bemmerer, C. Broggini, M. Campeggio, P. Corvisiero, Z. Elekes, Zs. Fulop, G. Gervino, A. Guglielmetti, C. Gustavino, Gy. Gyurky, G. Imbriani, M. Junker, M. Laubenstein, R. Menegazzo, M. Marta, E. Napolitani, P. Prati, V. Rigato, V. Roca, E. Somorjai, C. Salvo, O. Straniero, F. Strieder, T. Szucs, F. Terrasi, and D. Trezzi (LUNA Collaboration),
Phys. Rev. Lett. 109 (2012) 208001 Editors' Suggestion

- *"Preparation and characterisation of isotopically enriched* Ta_2O_5 *targets for nuclear astrophysics studies"*,
A. Caciolli, D.A. Scott, A. Di Leva, A. Formicola , M. Aliotta, M. Anders , A. Bellini, D. Bemmerer, C. Broggini , M. Campeggio, P. Corvisiero, R. Depalo, Z. Elekes , Zs. Fu lop, G. Gervino, A. Guglielmetti, C. Gustavino, Gy. Gyurky, G. Imbriani , M. Junker, M. Marta, R. Menegazzo, E. Napolitani, P. Prati, V. Rigato , V. Roca, C. Rolfs, C. Rossi Alvarez , E. Somorjai, C. Salvo, O. Straniero, F. Strieder, T. Szucs , F. Terrasi, H.P. Trautvetter, and D. Trezzi,
Eur. Phys. J. A 48 (2012) 144

- *"The* $^{25}Mg(p,\gamma)^{26}Al$ *reaction at low astrophysical energies"*,
F. Strieder, B. Limata, A. Formicola, G. Imbriani, M. Junker, D. Bemmerer, A. Best, C. Broggini, A. Caciolli, P. Corvisiero H. Costantini, A. DiLevab, c, Z. Elekes, Zs. Fulop, G. Gervino, A. Guglielmetti, C. Gustavino, Gy. Gyurky, A. Lemut, M. Marta, C. Mazzocchi, R. Menegazzo, P. Prati, V. Roca, C. Rolfs, C. Rossi Alvarez, E. Somorjai, O. Straniero, F. Terrasi, H.P. Trautvetter,
Phys. Lett. B 707 (2012) 60

- *"A new experiment on the* $^2H(\alpha,\gamma)^6Li$ *reaction*", M. Anders, PoS(NIC XII) 137

- *"Study of the* $^2H(\alpha,\gamma)^6Li$ *nuclear reaction producing* ^6Li *in standard Big Bang nucleosynthesis"*, M. Anders. D. Bemmerer, and C. Gustavino for the LUNA collaboration, Memorie della Società Astronomica Italiana Suppl. 22, 181 (2012)

- *"Towards a study of the* $^{22}Ne(p,\gamma)^{23}Na$ *reaction at LUNA"*, F. Cavanna, R. Depalo and M. Menzel, American Institute of Physics (AIP) Conference Series

- *"Nuclear astrophysics at LUNA: recent results"*, A. Guglielmetti, PoS(ENAS 6) 057 (2012)

- *"LUNA data on the $^2H(\alpha,\gamma)^6Li$ reaction and Big Bang Nucleosynsthesis"*, C. Gustavino, PoS(NIC XII) 074

- *"Study of the $^2H(\alpha,\gamma)^6Li$ reaction producing ^6Li in standard Big Bang Nucleosynthesis"*, C. Gustavino, PoS(ICHEP2012) 439

- *"$^{17}O(p,\alpha)^{14}N$ study at the LUNA accelerator"*, D.A. Scott, C. Bruno and A. Caciolli, Nuclear Instruments and Methods in Physics Research A

- *"Misura delle reazioni $^{17}O(p,\gamma)^{18}F$ e $^{18}O(p,\gamma)^{19}F$ nell'ambito dell'esperimento LUNA"*, M. Campeggio, Milan, 4th April 2012 - Master thesis

- *"Experimental Study of the $^{22}Ne(p,\gamma)^{23}Na$ Reaction and its Implications for Novae Scenarios"*, M. Menzel, Dresden, 21st December 2012 - Master thesis

- *"Studio del fondo di un rivelatore al germanio per misure di sezioni durto di reazioni nucleari di interesse astrofisico"*, G. Lerner, Milan, 18th October 2012 - Bachelor thesis

- *"Misure ancillari per lo studio della reazione $^{17}O(p,\alpha)^{14}N$ a LUNA"*, F. Tresoldi, Milan, 19th December 2012 - Bachelor thesis

6 Conference and seminar contributions

- M. Anders, "Direct measurement of the $d(\alpha,\gamma)^6Li$ cross-section at astrophysical energies", talk at WE-Heraeus Seminar on Astrophysics with modern small-scale accelerators, Physikzentrum Bad Honnef (Germany) 06-10.02.2012

- M. Anders, "A new experiment on the $^2H(\alpha,\gamma)^6Li$ reaction", poster at XII International Symposium on Nuclei in the Cosmos, Cairns (Australia) 05-10.08.2012

- M. Anders, "A new experiment on the $^2H(\alpha,\gamma)^6Li$ reaction", poster at XII International Symposium on Nuclei in the Cosmos, Cairns (Australia) 05-10.08.2012

- M. Anders, D. Bemmerer and C. Gustavino, "Study of the $^2H(\alpha,\gamma)^6Li$ nuclear reaction producing ^6Li in standard Big Bang nucleosynthesis, Lithium in the Cosmos, Paris (France) 27-29.02.2012

- D. Bemmerer, "Underground Laboratories", invited talk at the 496 Wilhelm und Else Heraeus - Seminar "Astrophysics with modern small-scale accelerators", Bad Honnef (Germany), 06.-10.02.2012

- D. Bemmerer and C. Gustavino, "Study of the ^{2}H(α,γ)^{6}Li nuclear reaction producing ^{6}Li in standard Big Bang nucleosynthesis" Poster presentation at Lithium in the Cosmos, Paris (France) 27.-29.02.2012

- D. Bemmerer, "Experimental study of the ^{2}H(α,γ)^{6}Li reaction and other recent progress at LUNA." Group report at German Physical Society Spring Meeting, Mainz (Germany) 19.-23.03.2012

- C. Broggini, "Luna, il Sole e l'altre stelle", invited talk at XCVIII Congresso Nazionale of Italian Physical Society, Napoli (Italy) 17.-21.09.2012

- C. Broggini, "Origin and status of Luna at Gran Sasso", lecture (invited) at International school of subnuclear physics 2012, Erice (Italy) 23.06-02.07.2012

- C. Broggini, "Luna at Gran Sasso: nuclear reactions at the energy of the stars", seminar (invited) at International school of nuclear physics 34th course, Erice (Italy) 16-24.09.2012

- C. Bruno, "Misura della reazione $^{17}O(p,\alpha)^{14}N$ alle energie di interesse astrofisico", talk at XCVIII Congresso Nazionale of Italian Physical Society, Napoli (Italy) 17.-21.09.2012

- A. Caciolli, "Measurement of $^{17}O(p,\gamma)^{18}F$ resonance at E =183.3 keV at the LUNA accelerator", talk at WE-Heraeus Seminar on Astrophysics with modern small-scale accelerators, Physikzentrum Bad Honnef (Germany) 06-10.02.2012

- A. Caciolli, "Astrophysical S factor for the 17O(p,g)18F reaction at Novae energy", talk at the 2nd European Nuclear Physics Conference 2012, Bucharest (Romania) 17-21.09.2012

- A. Caciolli, "$^{17}O(p,\alpha)^{14}N$ study at the LUNA accelerator", poster at Frontier Detectors for Frontier Physics, La Biodola, Elba Island (Italy) 20-26.05.2012

- F. Cavanna, "Towards a study of the $^{22}Ne(p,\gamma)^{23}Na$ reaction at LUNA", talk at the Carpathian Summer School of Physics 2012, Sinaia (Romania) 24.06-07.07.2012

- R. Depalo, "Towards a study of the ^{22}Ne(p,γ)^{23}Na reaction at LUNA", Poster presentation at 2nd European Nuclear Physics Conference, Bucharest (Romania), 17.-21.09.2012. Winner of the Poster Prize of the European Physical Society.

- A. Di Leva, "Determinazione del rate della $^{17}O(p,\gamma)^{18}F$ alle energie di interesse astrofisico", talk at XCVIII Congresso Nazionale of the Italian Physical Society, Napoli (Italy) 17.- 21.09.2012

- A. Formicola, "Misure dirette di reazioni nucleari di interesse astrofisico", invited talk at Incontro nazionale di fisica nucleare, Laboratori Nazionali del Sud (Italy) 12-14.11.2012

- A. Formicola, "Underground measurement of the ^{17}O+p reactions", talk at Castiglion Fiorentino Workshop New Frontiers in Nuclear Astrophysics, Castiglione Fiorentino (Italy) 18-22.06.2012

- A. Formicola, "Measurement of $^{17}O(p,\gamma)^{18}F$ resonance at E = 183.3 keV with the LUNA accelerator", talk at Workshop on Nuclear Astrophysics at the Canfranc Underground Laboratory, Canfranc (Spain) 22-23.03.2012

- A. Guglielmetti, "Luna: the experimental status of the art", invited talk at Electro-Weak Probes: from Low-Energy Nuclear Physics to Astrophysics, Trento (Italy) 25-29.06.2012

- A. Guglielmetti, "The LUNA experiment: present and future", invited talk at Workshop on Nuclear Astrophysics at the Canfranc Underground Laboratory, Canfranc (Spain) 22-23.03.2012

- A. Guglielmetti, "Status of the LUNA experiment", invited talk at the 7th Italy-Japan Symposium on nuclear physics, Milan (Italy) 20-23.11.2012

- A. Guglielmetti, "Il progetto LUNA MV ai Laboratori del Gran Sasso", talk at XCVIII Congresso Nazionale of Italian Physical Society, Napoli (Italy) 17.-21.09.2012

- C. Gustavino, "The $^2H(\alpha,\gamma)^6Li$ reaction at LUNA and Big Bang Nucleosynthesis", invited talk at Frontier Objects in Astrophysics and Particle Physics, Vulcano (Italy) 28.05-02.06.2012. Acta Polytecnica 2013 (accepted)

- C. Gustavino, "LUNA data on the $^2H(\alpha,\gamma)^6Li$ reaction and Big Bang nucleosynthesis", talk at Nuclei in the Cosmos 2012, Cairns (Australia) 5-12.08.2012

- C. Gustavino, "Study of the $^2H(\alpha,\gamma)^6Li$ reaction producing ^{6}Li in standard Big Bang nucleosynthesis", talk at ICHEP2012, Melbourne (Australia) 4-11.07.2012

- G. Imbriani, "Underground experiments and their impact on stellar modelling", invited talk at Nuclei in the Cosmos 2012, Cairns (Australia) 5-12.08.2012

- M. Junker, "Present Results and future developments in Underground Nuclear Astrophysics at LNGS", talk at 2nd European Nuclear Physics Conference, Bucharest (Romania) 17.-21.09.2012

- M. Junker, "What can be learned from 20 years of Underground Nuclear Astrophysics?", lecture (invited) at the Carpathian Summer School of Physics 2012, Sinaia (Romania) 24.06-07.07.2012

- R. Menegazzo, "A new LUNA experiment on the $^2H(\alpha,\gamma)^6Li$ reaction", talk at Castiglion Fiorentino Workshop New Frontiers in Nuclear Astrophysics, Castiglione Fiorentino (Italy) 18-22.06.2012

- M.-L. Menzel, "$^{22}Ne(p,\gamma)^{23}Na$ measurements at LUNA II and impact on astrophysical scenarios", talk at MASCHE (Massive Stars as Agents of Chemical Evolution) Collaborative Research Project within EuroGenesis, Frankfurt (Germany) 26.11.2012

- M.-L. Menzel, "Towards a measurement of the ^{22}Ne(p,γ)^{23}Na cross-section at LUNA", Poster presentation at the 496 Wilhelm und Else Heraeus - Seminar "Astrophysics with modern small-scale accelerators", Bad Honnef (Germany), 06.-10.02.2012

- D. Scott, "Underground Investigation of the ^{17}O+p reactions", talk at the Carpathian Summer School of Physics 2012, Sinaia (Romania) 24.06-07.07.2012

- D. Scott, "Underground Measurement of the $^{17}O + p$ Reactions", oral presentation at Institute Of Physics Nuclear Physics Conference, Brighton (UK) 02-04.04.2012

- D. Trezzi, "Looking the Cosmos from the LNGS deep underground laboratory: the LUNA experiment", invited talk at Current Problems in Nuclear Physics and Atomic Energy 2012, Kiev (Ukraine) 07.09.2012

- D. Trezzi, "LUNA: Laboratory for Underground Nuclear Astrophysics", talk at Direct Reactions with Exotic Beams 2012, Pisa (Italy) 26-29.03.2012

- D. Trezzi, "Misura della reazione $^2H(\alpha,\gamma)^6Li$ a LUNA", talk at XCVIII Congresso Nazionale of Italian Physical Society, Napoli (Italy) 17.-21.09.2012

- D. Trezzi, "The LUNA-MV project at Gran Sasso Laboratories", talk at Dust in EuroGENESIS environments: from primitive, massive stars to novae, Perugia (Italy) 14.11.2012

- L. Votano and A. Formicola, "LNGS, present and future of LUNA", invited talk at Nupecc Meeting, Milan (Italy) 09.03.2012

References

[1] See proceedings of "Lithium in the Cosmos", 27-29 February 2012, Paris.

[2] L. Marcucci, K. Nollett, R. Schiavilla, and R.Wiringa, Nucl. Phys. A 777, 111 (2006).

[3] M. Anders et al., 49 (2013) 28Eur.Phys.J. A.

[4] C. Gustavino: Proceedings of "XII International Symposium on Nuclei in the Cosmos", 5th-10th august 2012, Cairns, Australia; PoS(NIC XII)074.

[5] B. Paczyński *et al.*, Acta Astron. 15 (1965) 197

[6] J. José and M. Hernanz, Ap. J. 494 (1998) 680

[7] M. Hernanz *et al.*, Ap. J. 527 (1999) L97

[8] A. Caciolli *et al.*, Eur. Phys. J. A 48 (2012)144

[9] C. Iliadis, *Nuclear Physics of Stars* (Wiley-VCH, 2007)

[10] D. Scott *et al.*, PRL 109 (2012) 202501

[11] A.Di Leva*et al.* LUNA Collaboration,(2013) in preparation

[12] C. Iliadis, R. Longland, A. E. Champagne, and A. Coc, Nucl. Phys. A **841**, 251 (2010).

[13] J. Görres, C. Rolfs, P. Schmalbrock, H. P. Trautvetter, and J. Keinonen, Nucl. Phys. A **385**, 57 (1982).

[14] S. E. Hale, A. E. Champagne, C. Iliadis, V. Y. Hansper, D. C. Powell, and J. C. Blackmon, Phys. Rev. C **65**, 015801 (2002).

[15] R. Longland, C. Iliadis, J. M. Cesaratto, A. E. Champagne, S. Daigle, J. R. Newton, and R. Fitzgerald, Phys. Rev. C **81**, 055804 (2010).

[16] C. Iliadis, R. Longland, A. E. Champagne, A. Coc, and R. Fitzgerald, Nucl. Phys. A **841**, 31 (2010), 1004.4517.

[17] C. Angulo, M. Arnould, M. Rayet, P. Descouvemont, D. Baye, C. Leclercq-Willain, A. Coc, S. Barhoumi, *et al.*, Nucl. Phys. A **656**, 3 (1999).

[18] C. Iliadis, J. M. D'Auria, S. Starrfield, W. J. Thompson, and M. Wiescher, Astrophys. J. Suppl. Ser. **134**, 151 (2001).

[19] C. Iliadis, A. Champagne, J. José, S. Starrfield, and P. Tupper, Astrophys. J. Suppl. Ser. **142**, 105 (2002).

2012 LVD STATUS REPORT

The LVD Collaboration

N.Yu.Agafonova[7], M.Aglietta[8], P.Antonioli[1], V.V.Ashikhmin[7], G.Badino[8], G.Bari[1], R.Bertoni[8], E.Bressan[1], G.Bruno[5], V.L.Dadykin[7], R.I.Enikeev[7], W.Fulgione[8], P.Galeotti[8], M.Garbini[1], P.L.Ghia[2], P.Giusti[1], F.Gomez[8], E.Kemp[3], V.B.Korchaguin[7], A.S.Mal'gin[7], B.Miguez[3], A.Molinario[8], C.Morello[8], R.Persiani[1], I.A.Pless[6], A.Porta[8], A.Romero[8], V.G.Ryasny[7], O.G.Ryazhskaya[7], O.Saavedra[8], G.Sartorelli[1], M.Selvi[1], I.R.Shakiryanova[7], V.P.Talochkin[7], G.C.Trinchero[8], M.Ventura[4], C.Vigorito[8], V.F.Yakushev[7], A.Zichichi[1]

[1] *University of Bologna and INFN-Bologna, Italy*
[2] *Laboratoire de Physique Nucléaire et de Hautes Energies (LPNHE), Universités Paris 6 et Paris 7, CNRS-IN2P3, Paris, France*
[3] *University of Campinas, Campinas, Brazil*
[4] *INFN-LNF, Frascati, Italy*
[5] *INFN-LNGS, Assergi, Italy*
[6] *Massachusetts Institute of Technology, Cambridge, USA*
[7] *Institute for Nuclear Research, Russian Academy of Sciences, Moscow, Russia*
[8] *INFN-Torino, INAF-OATO, Torino and University of Torino, Italy*

Abstract

The Large Volume Detector (LVD) at the INFN Gran Sasso National Laboratory (LNGS), Italy, is an underground neutrino observatory mainly designed to study core-collapse supernovae. The experiment has been monitoring the Galaxy since June 1992 with increasing active mass up to the final configuration $M = 1$ kt that has been reached on January 2001. No burst candidate has been found over about 7000 days of live-time, the resulting 90% c.l. upper limit to the rate of gravitational stellar collapses in the Galaxy (D $<$ 20 kpc) is 0.12 y^{-1}.
Since July 2005 LVD has taken part to the Supernovae Early Warning System (SNEWS), the network of SN neutrino observatories whose main goal is to provide the astronomical community with a prompt alert for the next galactic core-collapse supernova explosion.
Since 2006 LVD has acted as a far monitor for the Cern Neutrinos to Gran Sasso (CNGS) high energy, wide band ν_μ beam, set up at Cern and sent towards the LNGS. During 2012 LVD measured the CNGS neutrino time of flight establishing a new limit on the difference between the neutrino speed and the light velocity that was an order of magnitude lower than previous direct measurements.

1 The LVD experiment

The Large Volume Detector (LVD), located in the hall A of the INFN Gran Sasso National Laboratory, Italy, is made of 1000 tons of liquid scintillator arranged in a modular geometry. The major goal of LVD is to search for neutrinos from Gravitational Stellar Collapses (GSC) in our Galaxy [1].

The detector is a three-dimensional array of 840 scintillator counters, 1.5 m^3 each. The whole array is split into three identical parts (towers) with independent power supply, trigger and data acquisition. In turn, each tower consists of 35 cluster of 8 counters (modules). Each counter is viewed from the top by three photomultipliers (PMTs).

The main neutrino reaction in LVD,[1] in the standard collapse model, is $\bar{\nu}_e p \rightarrow e^+ n$, which gives two detectable signals: the prompt one, due to the e^+, followed by the signal from the (n,p) capture ($E_\gamma = 2.2$ MeV) with a mean delay of 185 ± 5 μs [2].
The trigger logic is optimized for the detection of both products of the inverse beta decay and is based on the three-fold coincidence of the PMTs of a single counter. Each PMT is discriminated at two different thresholds resulting in two possible levels of coincidence between a counter's PMTs: H and L, corresponding respectively to $\mathcal{E}_H \simeq 4$ MeV and $\mathcal{E}_L \simeq 500$ keV.

[1] LVD is also sensitive to $\overset{(-)}{\nu}_i + e^- \rightarrow \overset{(-)}{\nu}_i + e^-$ scattering; $(\nu_e + \bar{\nu}_e)$ c.c. interactions and $\overset{(-)}{\nu}_i$ n.c. interactions with carbon.

[2] Neutrons can also be captured by Fe nuclei with the emission of gammas (sum of E_γ=10,17 MeV, average N_γ=1.7).

The iron support structure of the detector can also act as target for neutrinos and antineutrinos. The products of the interaction can escape from iron and be detected in the liquid scintillator [a].
The observable signal in LVD, in different reactions and due to different kinds of neutrinos, besides providing astrophysical information on the nature of the collapse, is sensitive to intrinsic ν properties. We have studied [2] how neutrino oscillations affect the signal detected by LVD and also evaluated the impact on the signal of the astrophysical parameters of the supernova explosion mechanism, such as the total energy emitted in neutrinos, the star distance, the neutrino–sphere temperatures and the partition of the energy among the neutrino flavors.
However, being aware of the fact that the astrophysical parameters of the supernova mechanism are up to now not well defined, to compute the detector sensitivity expressed in terms of source distance or emitted neutrino flux we adopted the following conservative values for the astrophysical parameters [4], [5]: average $\bar{\nu}_e$ energy $\langle E_{\bar{\nu}_e} \rangle$=14 MeV; total radiated energy $E_b = 2.4 \cdot 10^{53}$ erg and average non-electron neutrino energy 10% higher than $\bar{\nu}_e$ [6]. Concerning neutrino oscillations we conservatively assumed direct mass hierarchy.

[a] LVD is sensitive to gravitational stellar collapses also in the case of rotating collapsar model, developed by V.S. Imshennik, thanks to the $(\nu_e + Fe)$ reaction [3]

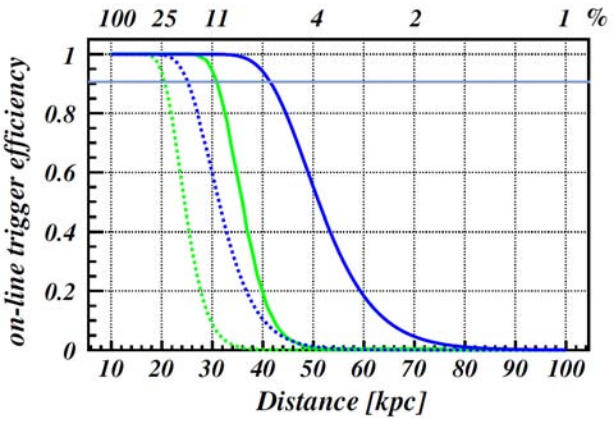

Figure 1: *On-line trigger efficiency versus distance (lower scale) and percentage of SN1987A-like signal at 10 kpc (upper scale) for E_{cut}=7-10MeV (light green and dark blue lines, respectively) and M=300t (dotted) and 1000t (continuous) for LVD stand alone.*

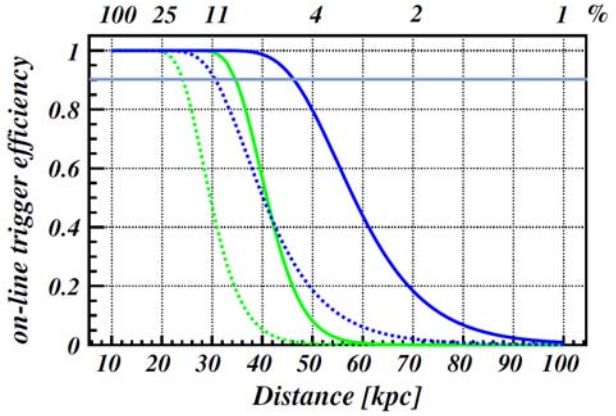

Figure 2: *Same as figure 1 for LVD in the SNEWS.*

Taking into account Poisson fluctuations in the cluster multiplicity, we derived [8] the trigger efficiency shown in figure 1 as a function of the distance (lower scale) for LVD working stand-alone (the trigger efficiency, as a function of neutrino luminosity in terms of percentage of SN1987A one is shown in the upper scale). The trigger efficiency for LVD working in the SNEWS network [7] is shown in figure 2.

2 Supernova physics

2.1 Monitoring the Galaxy

LVD has been taking data since June 1992 with increasing mass configurations, enough to monitor the whole Galaxy ($D \leq 20$ kpc)[3]. In figure 3 we show sensitive mass and duty cycle of the experiment during the period 1992-2012. The average LVD duty cycle, when the sensitive mass is greater than 300 t, is greater than 92%. The search for ν burst candidates is performed by studying the temporal sequence of triggers, looking for clusters and it is widely discussed in [8]. For each cluster, with multiplicity m and

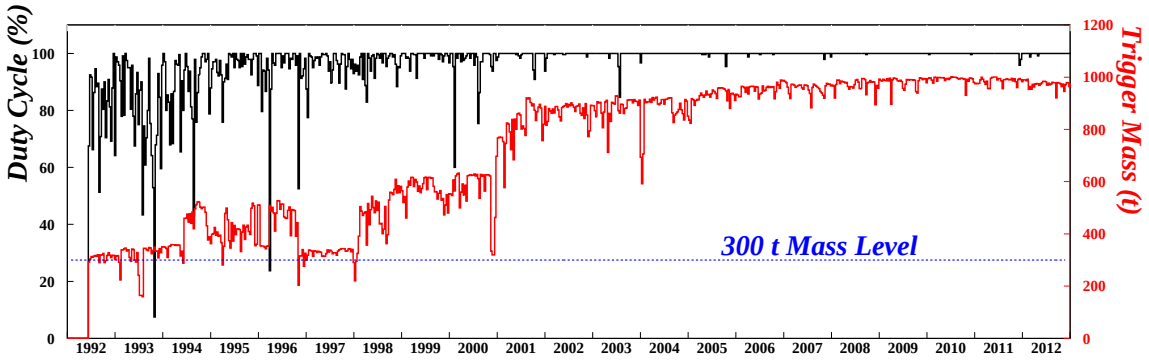

Figure 3: *LVD sensitive mass and duty cycle during 1992-2012.*

duration Δt, the imitation frequency F_{im} is calculated as a function of the background rate. A complete analysis of each detected cluster with $F_{im} \leq 1$ y^{-1} is performed, to test its consistency with a ν burst through the study of the topological distribution of pulses inside the detector. Additional information will come from the study of: *a)* the energy spectrum of the events in the cluster; *b)* the time distribution of the events in the cluster and *c)* the time distribution of delayed low energy pulses.

No candidates have been found since 1992, see details in table 1. Since the LVD sensitivity is higher than what is expected from GSC models (even if the source is at a distance of 20 kpc and for soft neutrino energy spectra), the resulting 90% c.l. upper limit to the rate of gravitational stellar collapses in the Galaxy ($D \leq 20$ kpc) is 0.12 y^{-1}

[3]The results of this search have been periodically updated and published in the ICRC and Neutrino Conference Proceedings, since 1993 till 2011. [9].

Table 1: LVD run.

Run	start	end	days	up (%)	mass (t)
1	6-6-1992	5-31-1993	285	60	310
2	8-4-1993	3-11-1995	397	74	390
3	3-11-1995	4-30-1997	627	90	400
4	4-30-1997	3-15-1999	685	94	415
5	3-16-1999	12-11-2000	592	95	580
6	12-12-2000	3-24-2003	821	98	842
7	3-25-2003	2-4-2005	666	> 99	881
8	2-4-2005	5-31-2007	846	> 99	936
9	5-31-2007	4-30-2009	699	> 99	967
10	5-1-2009	3-27-2011	696	> 99	981
11	3-27-2011	12-31-2012	645	> 99	979
Σ	6-6-1992	12-31-2012	6959		744

2.2 The Supernova On-line Monitor and SNEWS

The first, and unique, observation of ν's from gravitational stellar collapse was driven by optical observation (SN1987A), but, since the probability of such an event for a stellar collapse in our Galaxy is only of 20%, the detector capabilities of identifying a ν burst in the absence of an "external trigger" must be carefully demonstrated. In the presence of an electromagnetic counterpart, on the other hand, the prompt identification of the neutrino signal could alert the worldwide network of observatories allowing study of all aspects of the rare event from its onset.
The SNEWS (SuperNova Early Warning System) [7] project is an international collaboration including several experiments sensitive to a core-collapse supernova neutrino signal in the Galaxy and neighbourhood. The goal is to provide the astronomical community with a prompt and reliable alert of the occurrence of a Galactic supernova event, generated by the coincidence of two or more active detectors. In July 2005, after a few years of tuning, the charter members of SNEWS (i.e., LVD, Super-K and SNO[4]) together with the newly joined Amanda/IceCube, started the effective operation of the network (subscribe at *http://snews.bnl.gov* to get your own SN alert !). Since 2009 also Borexino joined the network.
Since 2001 a fast and reliable on-line ν-burst monitor has been implemented, the algorithm is based on the search for clusters of triggers within a fixed time window, Δt=20 s. The candidate is simply characterized by its multiplicity m, i.e. the number of pulses detected in Δt. All the other characteristics of the cluster are left to a subsequent independent analysis. The search for burst candidates is performed, on-line, simultaneously for two values of the energy threshold: $E_{cut} = 7$ MeV ($f_{bk} = 0.2$ Hz) and $E_{cut} = 10$ MeV ($f_{bk} = 0.03$ Hz). The chosen imitation frequencies, F_{im}, below which the detected cluster will be an on-line candidate supernova event, is 1 per 100 year working stand-alone while

[4]At present the SNO experiment is decommissioned.

it is relaxed to 1 per month working in coincidence with other detectors (SNEWS), and 1 per day for monitoring task. The corresponding detection efficiency are shown in figure 1 and 2, details are discussed in [8].

3 CNGS beam monitor

The Cern Neutrinos to Gran Sasso (CNGS) project is a high energy, wide band ν_μ beam set up at Cern and sent towards the LNGS. Its main goal is the observation of the ν_τ appearance, through neutrino flavour oscillation. As shown in [10], due to its large area and active mass, LVD can act as a beam monitor, detecting the interaction of neutrinos inside the detector and the muons generated by the ν interaction in the rock upstream the detector. The monitor capabilities have been confirmed during CNGS runs since 2006 [11]. The CNGS events in LVD can be subdivided into two main categories:

- ν_μ charged current (CC) interactions in the rock upstream the LNGS; they produce a muon that can reach LVD and be detected,
- ν_μ CC and neutral current (NC) interactions in the material (liquid scintillator and iron of the support structure) of LVD.

A full Montecarlo simulation has been developed including the generation of the neutrino interaction products, the propagation of the muon in the Gran Sasso rock and the response of the LVD detector. The details of the simulation are described in [10]. The resulting number of expected events, at the nominal intensity 4.5 10^{19} p.o.t./y is 33400/y, equivalent to 7.422 10^{-16} events per p.o.t. (considering 200 effective days per year it corresponds to $\sim$ 165 CNGS events per day): 78% are muons from the rock, 17% are CC interactions in the detector and 5% are NC.

The LVD events are filtered using a very loose selection cut: we require to have at least one scintillation counter with an energy release larger that 100 MeV. The resulting rate is quite stable, with an average value of about 0.13 Hz, and it is mainly due to cosmic muon events. Among this sample the selection criteria is based on the coincidence of the LVD event time with the beam spill time written in the DB: we search for the CNGS events in the interval $[-15, +25]$ μs around the start time of the beam spill. The background, estimated considering: the 0.13 Hz rate of events among which the CNGS events are searched for, the time window around the beam spill time, 40 μs wide, and the number of useful spills in the DB, is practically negligible.

4 CNGS neutrino time of flight measurement

4.1 *Determination of a time-shift in the OPERA set-up using high-energy horizontal muons in the LVD and OPERA detectors*

As a consequence of the neutrino time of flight measurement performed by OPERA experiment [12], unexpectedly showing evidence for superluminal propagation of ν_μ neutrinos, we studied the sample of cosmic muon events in time coincidence between the LVD and

OPERA detectors, during a calendar time period from mid 2007 until 2012, for a total live time of about 1200 days. In a time-window of 1 μs, and excluding events in time with the CNGS beam spill, we found 306 events. This sample has a time-difference ($t_{LVD} - t_{OPERA}$) distribution peaked at 616 ns with an RMS of 74 ns, as shown in fig. 4. The central value

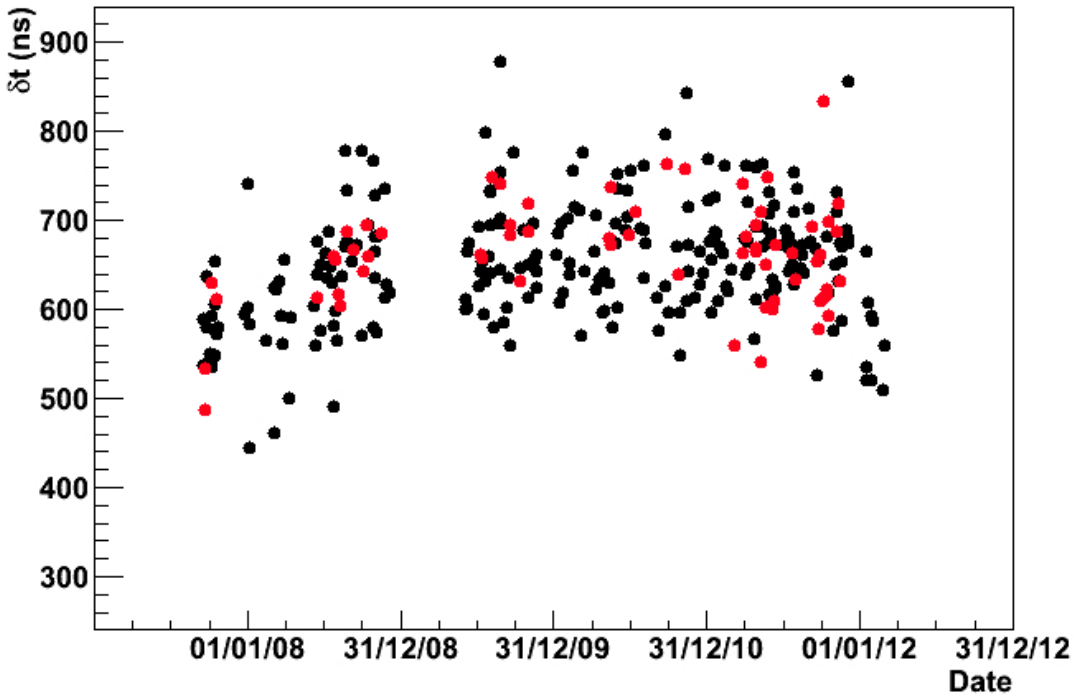

Figure 4: Distribution of $\delta t = t_{LVD} - t_{OPERA}$ for the 306 events inside 1 μs time coincidence. The black (red) dots represent events originated in the Target Tracker (RPC) OPERA sub-system.

of the distribution has the following interpretation: the coincident events are not multiple muons (one per each detector), but single muon events entering horizontally from the OPERA side and going through the LVD detector. Indeed, the OPERA-LVD direction lies along the so-called Teramo valley, where the Gran Sasso mountain profile exhibits small depths even in the horizontal direction. Visual inspection using the event displays of LVD and OPERA detectors confirms this pattern. See in fig. 5 a sketch of the LNGS with the position of the two detectors and the direction of those muons.
The calendar time evolution of the time difference δt for various periods of data-taking shows a variation of the average value in each period, ranging from $\sim$ 580 ns in 2007 up to $\sim$ 670 ns from May 2008 to the end of 2011; then for the 9 events collected in early 2012 it decreases again to $\sim$ 570 ns. The observed variations are larger than the statistical uncertainty estimated for each period.

This behavior corresponds to a negative time shift for OPERA in the calendar period from August 2008 to December 2011 of the same order of the excess leading to a neutrino velocity higher than the speed of light as reported by OPERA [12]. Further checks of the

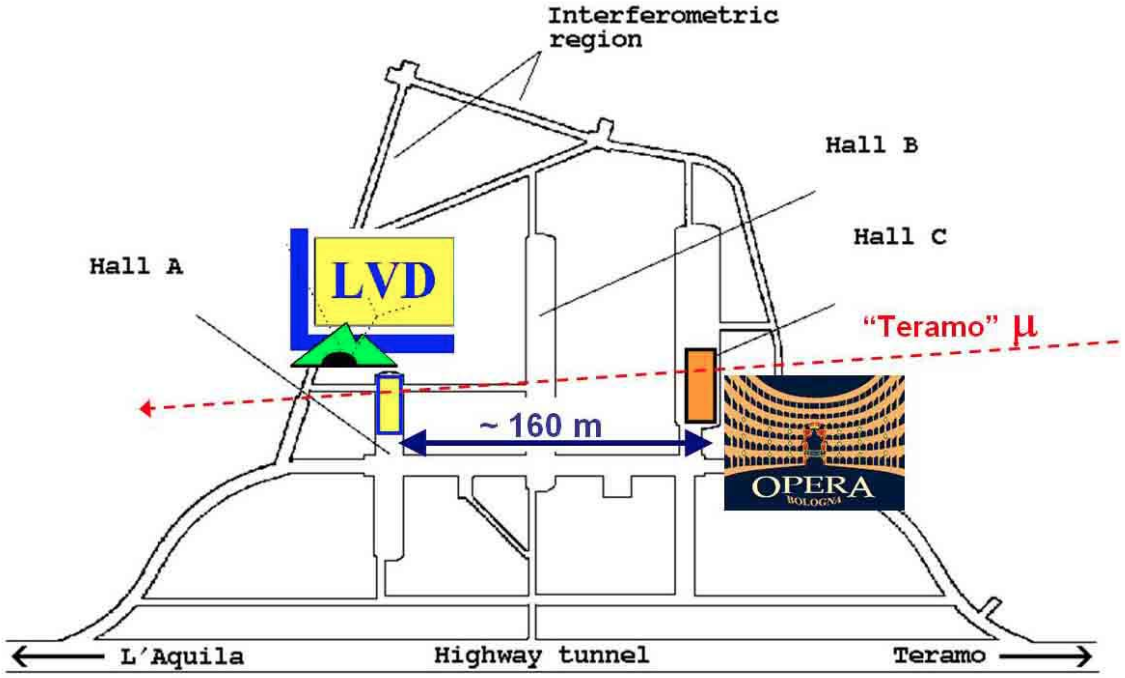

Figure 5: Sketch of the LNGS map with the position of the LVD and OPERA experiments.

OPERA experimental apparatus showed evidence for equipment malfunctionings [13]. A first one was related to the oscillator used to produce the event timestamps, while the second one is linked to the connection of the optical fiber bringing the GPS signal to the OPERA master clock. This allows to conclude that the quantitative effect of this malfunctioning is the negative time shift, δt (A - B), mentioned above. This explains the previous OPERA finding [12] on the neutrino time of flight shorter by 60 ns over the speed of light. The result of this joint analysis was the first quantitative measurement of the relative time stability between the two detectors and provided a check that was totally independent from the TOF measurements of CNGS neutrino events and from the effect presented in [13], pointing to the existence of a possible systematic effect in the OPERA neutrino velocity analysis.

4.2 *Measurement of the Velocity of Neutrinos from the CNGS Beam with the Large Volume Detector*

Moreover to allow a more accurate neutrino time of flight measurement, from May 10^{th} to May 24^{th}, 2012, the CERN-SPS accelerator has been operated with a new beam structure. This structure was made of four batches separated by about 300 ns, with 16 bunches per batch, with a narrow width of $\sim$ 3 ns each, separated by 100 ns. For this occasion, a new High Precision Time Facility (HPTF) has been designed by the Borexino collaboration and installed in the external buildings of the LNGS. A Septentrio PolaRx4 GNSS receiver, synchronized with the 10 MHz frequency of a GPS disciplinated Rubidium clock, provides GPS time and XPPS (10 Hz) output signal. The HPTF is equipped with high precision

(50 ps) Time Interval Counters (TIC) Pendulum CNT-91, to which the triggers of the different LNGS experiments can be connected.
In view of the new neutrino beam, we have modified a subset of the LVD counters, with the aim of improving their timing performances. We have chosen 58 of them (Super-Set, see fig. 6) to maximize the acceptance with respect to CNGS neutrinos while minimizing the number of detectors to be modified. From data taken since 2006 from the CNGS beam we have learnt that the Super-Set counters are involved in 40% of the CNGS events detected by LVD, while representing only less than 7% of the whole array. On the one hand, to avoid time fluctuations in the trigger formation at the single-counter level, we have modified the cabling of the PMTs, by delaying only one of them. The change guarantees that the 3-fold coincidence among the PMTs in every counter is always formed due to the same tube. On the other hand, to perform a measurement of the transit time in each counter, we have equipped them with a LED system. The transit time, denominated δ_{LVD}, is the time between the light generation inside a counter and the formation of the trigger. By means of the LED system, we have measured the behavior of the transit time versus energy for each counter. For each counter, we have best fitted the results with a power-law of the form:

$$\delta_{LVD}\left(E_m\right) \,=\, P_1 \,\cdot\, E_m^{P_2} \,+\, k \tag{1}$$

where E_m is the energy release measured by the ADC, while P1, P2 and k are free parameters of the fit, for each counter.
The trigger of the array has been upgraded too. An independent fast trigger logic has been implemented by extracting the coincidence of the triggered counters from discriminators, with the trigger sent to the HPTF. The trigger has been connected to one of the TIC, this being stopped by the XPPS signal. This provides a high precision time difference, δ_{TIC}, between the LVD trigger and the absolute GPS time. Thanks to this improvement, the absolute time accuracy of LVD is of the order of few nanoseconds.
Finally a new, indipendent, high precision geodesy measurement has been performed. The CNGS-LVD baseline, namely the distance between the center of the BFCTI.400344 intensity monitor at CERN and the LVD Super-Set upstream entry wall (taken as the LVD reference), is found to be 731291.87±0.04 m. The corresponding time-of-flight at speed of light, when including the 2.2 ns contribution due to Earth's rotation, is $tof_c = 2439329.32 \pm 0.13\,\mathrm{ns}$.

We have found 190 events in total, consistent with the $1.89 \cdot 10^{17}$ protons on target (p.o.t.) delivered during the bunched-beam run. For the measurement of the neutrino velocity, we have used only events involving at least one of the Super-Set counters. We have found 79 of them out of 190, i.e., 40% as expected from the Super-Set geometry. To limit the sources of systematic uncertainties, we have applied quality cuts to them. First we have required the non-saturation of ADC of the triggering counter, as the saturation would not allow a precise measurement of the δ_{LVD} term in (1). Second, because the number of photoelectrons for energy releases E<30 MeV is too low to guarantee that the counter is triggered by direct (i.e., fast) light, we have selected only events where the energy release associated to the triggering counter is above a certain value.

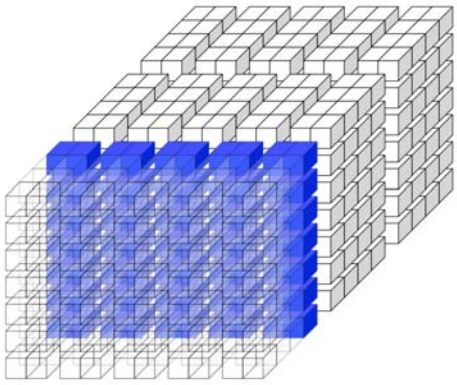

Figure 6: Schema of LVD counters. The blue ones represent the Super-Set, see text.

We have tested different cuts, between 30 and 100 MeV. The r.m.s. of the distribution of δT_{batch} becomes stable for E>50 MeV, this value being our final choice. The described quality cuts reduce the sample to 48 events, that have been used for the final analysis. The systematic uncertainties associated to the measurement of δt are summarized in Table 2. The baseline between LVD and CERN is known with an uncertainty lower than 0.3 ns. In fact, neutrino-induced muons responsible for events in the Super-Set can be generated as far as several hundreds of meters from LVD. This makes shorter the actual neutrinos baseline, while part of the distance is travelled by the produced muons of different energy. This effect has been investigated through a Monte Carlo simulation and has a negligible impact on the measurement. Constant delays at CERN give an additional uncertainty of 1.5 ns. The uncertainty due to the system time inter-calibration has been measured and it is 1.1 ns.

Also, the delay between the proton extraction time and the recording of the BCT waveforms by a digitizer has been measured, with an uncertainty of 1.0 ns. The variable correction δ_{LVD} (energy and counter dependent) introduces a further systematic uncertainty, 0.4 ns, evaluated through the propagation of the one associated to the energy measurement. Finally, the last three terms in Table 2 are related to the constant corrections in the absolute time calibration of the Super-Set counters. They account for the unknown time delay between trigger and LED light generation, 2.6±1.5 ns; the uncertainty associated to the optical fiber length, 0.5 ns, and the difference between the detector response to LED light and to particle ionization, 1.1 ± 0.6 ns (the scintillator decay time is τ=3.32 ns [14]).

Systematic uncertainties	ns	Error dist.
Baseline (< 10 cm)	< 0.3	Gauss.
Const. corr. at CERN	2.0	Gauss.
BCT calibration	1.0	Gauss.
Time link calibration	1.1	Gauss.
GPS syncronization accuracy	1.0	Gauss.
PMT transit time correction	0.4	Gauss.
Absolute transit time cal.	1.5	Flat
Optical fiber length	0.5	Gauss.
Fluorescence lifetime	0.6	Exp.
Total systematic	± 3.2	

Table 2: Sources of systematic uncertainty in the measurement.

By quadratically summing up all these contributions, we obtain a total systematic uncertainty of 3.2 ns.
The distribution of δt for the 48 events is shown in figure 7 compared with the superposition of all the peaks of the waveforms correlated to detected events. The mean value of the measured distribution is:

$$\delta t = -0.3 \pm 0.6_{stat} \pm 3.2_{sys} \text{ ns} \tag{2}$$

The corresponding 99% confidence limit on the speed of neutrino is:

$$-3.3 \cdot 10^{-6} < (v_\nu - c)/c < 3.5 \times 10^{-6} \tag{3}$$

These values are an order of magnitude lower than previous direct measurements.
By using the average neutrino beam energy, $< E_\nu >= 17$ GeV, a limit is found on the relativistic mass of neutrino:

$$m_{\nu_\mu} < 44\ MeV/c^2\ (99\%\ C.L.) \tag{4}$$

This result has been published in Physical Review Letters and indicated among Editors' Suggestions.

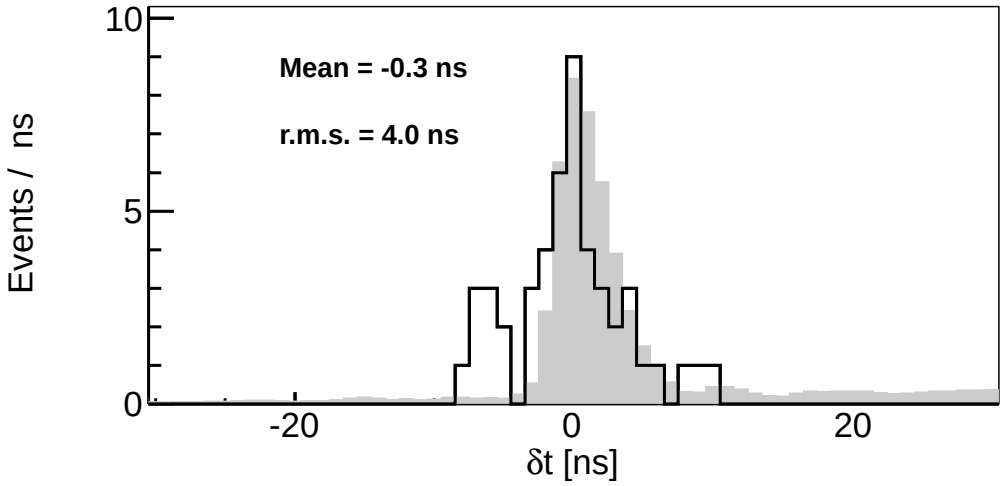

Figure 7: Distribution of δt, the difference between the time-of-flight of neutrino and the time-of-flight at speed of light, for each of the 48 selected events, compared with the superposition of all the peaks of the waveforms correlated to detected events (grey).

5 List of publications in 2012

- *Determination of a time-shift in the OPERA set-up using high-energy horizontal muons in the LVD and OPERA detectors*, Eur. Phys. J. Plus, 127-6, 71 (2012)
- *Measurement of the Velocity of Neutrinos from the CNGS Beam with the Large Volume Detector*, Phys. Rev. Lett., 109-7, 070801 (2012)

6 PhD thesis

- *Detection of neutrino bursts from gravitational stellar collapses in present and future detectors*, A.Molinario, PhD.Thesis, Universita' di Torino.
- *Neutron Background studies for direct dark matter searches in the Gran Sasso Underground Laboratory*, G.Bruno, PhD.Thesis, Universita' dell'Aquila.

References

[1] LVD Collaboration, Il Nuovo Cimento **A105** (1992) 1793

[2] N. Yu. Agafonova *et al.*, *Study of the effect of neutrino oscillations on the supernova neutrino signal in the LVD detector*, Astropart. Phys. **27**, 254-270 (2007) [arXiv: hep-ph/0609305].

[3] V.S.Imshennik, O.G.Ryazhskaya, Astronomy Let. Vol 30, N1, 2004, pp14-31; O.G.Ryazhskaya, Physics-Uspekhi 49(10) 1017-1027(2006)

[4] G. Pagliaroli, F. Vissani, M. L. Costantini, and A. Ianni, Astropart. Phys. **31**, 163 (2009)

[5] M.L. Costantini, A. Ianni and F. Vissani, Phys. Rev. D **70** (2004) 043006.

[6] M.T.Keil, G.G.Raffelt and H.T.Janka, Astrophys. J. **590** (2003) 971.

[7] P. Antonioli *et al.*, New Journal of Physics **6** (2004) 114; http://hep.bu.edu/∼snnet/

[8] N. Yu. Agafonova *et al.*, *On-line recognition of supernova neutrino bursts in the LVD detector*, Astropart. Phys. **28**, 516-522 (2008) [arXiv:0710.0259].

[9] LVD Collaboration, Proceedings of the 32nd ICRC, 2011 and reference therein.

[10] M. Aglietta et al., *CNGS beam monitor with the LVD detector*, Nuclear Instruments and Methods in Physics Research **A 516**, 96 (2004).

[11] N. Yu. Agafonova et al., *First CNGS events detected by LVD*, Eur. Phys. J. **C 52**, 849-855 (2007) [arXiv:0710.1536 hep-ex].

[12] T. Adam *et al.* [OPERA Collaboration], arXiv:1109.4897 [hep-ex].

[13] OPERA Internal Note 143, 2012, report to the SPSC and LNGS-SC, March 2012.

[14] I.R. Barabanov et al., e-Print: arXiv:0803.1577 [physics.ins-det]

OPERA

N. Agafonova[1], A. Aleksandrov[2], O. Altinok[3], A. Anokhina[4], S. Aoki[5], A. Ariga[6], T. Ariga[6], D. Autiero[7], A. Badertscher[8], A. Bagulya[9], A. Bendhabi[10], A. Bertolin[11,*], C. Bozza[12], T. Brugière[7], R. Brugnera[13,11], F. Brunet[14], G. Brunetti[15,16,7], S. Buontempo[2], A. Cazes[7], L. Chaussard[7], M. Chernyavskiy[9], V. Chiarella[17], A. Chukanov[18], N. D'Ambrosio[19], F. Dal Corso[11], G. De Lellis[20,2], P. del Amo Sanchez[14], Y. Déclais[7], M. De Serio[21], F. Di Capua[2], A. Di Crescenzo[20,2], D. Di Ferdinando[16], N. Di Marco[22,a], S. Dmitrievski[18], M. Dracos[23], D. Duchesneau[14], S. Dusini[11], T. Dzhatdoev[4], J. Ebert[24], O. Egorov[25], R. Enikeev[1], A. Ereditato[6], L. S. Esposito[8], J. Favier[14], T. Ferber[24], R. A. Fini[21], D. Frekers[26], T. Fukuda[27], A. Garfagnini[13,11], G. Giacomelli[15,16], M. Giorgini[15,16,b], C. Göllnitz[24], J. Goldberg[28], D. Golubkov[25], L. Goncharova[9], Y. Gornushkin[18], G. Grella[12], F. Grianti[29,17], A. M. Guler[3], C. Gustavino[19,c], C. Hagner[24], K. Hamada[27], T. Hara[5], M. Hierholzer[24], A. Hollnagel[24], K. Hoshino[27], M. Ieva[21], H. Ishida[30], K. Jakovcic[31], C. Jollet[23,*], F. Juget[6], M. Kamiscioglu[3], K. Kazuyama[27], S. H. Kim[32,d], M. Kimura[30], N. Kitagawa[27], B. Klicek[31], J. Knuesel[6], K. Kodama[33], M. Komatsu[27], U. Kose[13,11], I. Kreslo[6], H. Kubota[27], C. Lazzaro[8], J. Lenkeit[24], I. Lippi[11], A. Ljubicic[31], A. Longhin[13,11,e], P. Loverre[34], G. Lutter[6], A. Malgin[1], G. Mandrioli[16], K. Mannai[10], J. Marteau[7], T. Matsuo[30], V. Matveev[1], N. Mauri[15,16,e], E. Medinaceli[16], F. Meisel[6], A. Meregaglia[23,*], P. Migliozzi[2], S. Mikado[30], S. Miyamoto[27], P. Monacelli[22], K. Morishima[27], U. Moser[6], M. T. Muciaccia[35,21], N. Naganawa[27], T. Naka[27], M. Nakamura[27], T. Nakano[27], D. Naumov[18], V. Nikitina[4], K. Niwa[27], Y. Nonoyama[27], S. Ogawa[30], N. Okateva[9], A. Olchevski[18], M. Paniccia[17], A. Paoloni[17], B. D. Park[32,f], I. G. Park[32], A. Pastore[35,21], L. Patrizii[16], E. Pennacchio[7], H. Pessard[14], K. Pretzl[6], V. Pilipenko[26], C. Pistillo[6], N. Polukhina[9], M. Pozzato[15,16], F. Pupilli[22], R. Rescigno[12], T. Roganova[4], H. Rokujo[5], G. Romano[12], G. Rosa[34], I. Rostovtseva[25], A. Rubbia[8], A. Russo[20,2], V. Ryasny[1], O. Ryazhskaya[1], O. Sato[27], Y. Sato[36], A. Schembri[19], W. Schmidt-Parzefall[24], H. Schroeder[37], L. Scotto Lavina[20,2,g], A. Sheshukov[18], H. Shibuya[30], G. Shoziyeov[4], S. Simone[35,21], M. Sioli[15.16], C. Sirignano[12], G. Sirri[16], J. S. Song[32], M. Spinetti[17], L. Stanco[11], N. Starkov[9], M. Stipcevic[31], T. Strauss[8,h], P. Strolin[20,2], S. Takahashi[27], M. Tenti[15,16], F. Terranova[17], I. Tezuka[36], V. Tioukov[2], P. Tolun[3], A. Trabelsi[10], T. Tran[7], S. Tufanli[3,h], P. Vilain[38], M. Vladimirov[9], L. Votano[17], J. L. Vuilleumier[6], G. Wilquet[38], B. Wonsak[24] V. Yakushev[1], C. S. Yoon[32], T. Yoshioka[27], J. Yoshida[27], Y. Zaitsev[25], S. Zemskova[18], A. Zghiche[14] and R. Zimmermann[24].

1. INR-Institute for Nuclear Research of the Russian Academy of Sciences, RUS-117312 Moscow, Russia
2. INFN Sezione di Napoli, I-80125 Napoli, Italy
3. METU-Middle East Technical University, TR-06531 Ankara, Turkey

4. SINP MSU-Skobeltsyn Institute of Nuclear Physics of Moscow State University, RUS-119992 Moscow, Russia
5. Kobe University, J-657-8501 Kobe, Japan
6. Albert Einstein Center for Fundamental Physics, Laboratory for High Energy Physics (LHEP), University of Bern, CH-3012 Bern, Switzerland
7. IPNL, Université Claude Bernard Lyon 1, CNRS/IN2P3, F-69622 Villeurbanne, France
8. ETH Zurich, Institute for Particle Physics, CH-8093 Zurich, Switzerland
9. LPI-Lebedev Physical Institute of the Russian Academy of Sciences, RUS-117924 Moscow, Russia
10. Unité de Physique Nucléaire et des Hautes Energies (UPNHE), Tunis, Tunisia
11. INFN Sezione di Padova, I-35131 Padova, Italy
12. Dipartimento di Fisica dell'Università di Salerno and INFN, I-84084 Fisciano, Salerno, Italy
13. Dipartimento di Fisica dell'Università di Padova, I-35131 Padova, Italy
14. LAPP, Université de Savoie, CNRS/IN2P3, F-74941 Annecy-le-Vieux, France
15. Dipartimento di Fisica dell'Università di Bologna, I-40127 Bologna, Italy
16. INFN Sezione di Bologna, I-40127 Bologna, Italy
17. INFN - Laboratori Nazionali di Frascati dell'INFN, I-00044 Frascati (Roma), Italy
18. JINR-Joint Institute for Nuclear Research, RUS-141980 Dubna, Russia
19. INFN - Laboratori Nazionali del Gran Sasso, I-67010 Assergi (L'Aquila), Italy
20. Dipartimento di Scienze Fisiche dell'Università Federico II di Napoli, I-80125 Napoli, Italy
21. INFN Sezione di Bari, I-70126 Bari, Italy
22. Dipartimento di Fisica dell'Università dell'Aquila and INFN, I-67100 L'Aquila, Italy
23. IPHC, Université de Strasbourg, CNRS/IN2P3, F-67037 Strasbourg, France
24. Hamburg University, D-22761 Hamburg, Germany
25. ITEP-Institute for Theoretical and Experimental Physics, RUS-117259 Moscow, Russia
26. University of Münster, D-48149 Münster, Germany
27. Nagoya University, J-464-8602 Nagoya, Japan
28. Department of Physics, Technion, IL-32000 Haifa, Israel
29. Università degli Studi di Urbino "Carlo Bo", I-61029 Urbino, Italy
30. Toho University, J-274-8510 Funabashi, Japan
31. IRB-Rudjer Boskovic Institute, HR-10002 Zagreb, Croatia
32. Gyeongsang National University, ROK-900 Gazwa-dong, Jinju 660-300, Korea
33. Aichi University of Education, J-448-8542 Kariya (Aichi-Ken), Japan
34. Dipartimento di Fisica dell'Università di Roma "La Sapienza" and INFN, I-00185 Roma, Italy
35. Dipartimento di Fisica dell'Università di Bari, I-70126 Bari, Italy
36. Utsunomiya University, J-321-8505 Tochigi-Ken, Utsunomiya, Japan
37. Fachbereich Physik der Universität Rostock, D-18051 Rostock, Germany
38. IIHE, Université Libre de Bruxelles, B-1050 Brussels, Belgium
a. Now at INFN - Laboratori Nazionali del Gran Sasso, I-67010 Assergi (L'Aquila), Italy
b. Now at INAF/IASF, Sezione di Milano, I-20133 Milano, Italy
c. Now at Dipartimento di Fisica dell'Università di Roma "La Sapienza" and INFN, I-00185 Roma, Italy
d. Now at Pusan National University, Geumjeong-Gu Busan 609-735, Korea
e. Now at INFN - Laboratori Nazionali di Frascati dell'INFN, I-00044 Frascati (Roma), Italy
f. Now at Asan Medical Center, 388-1 Pungnap-2 Dong, Songpa-Gu, Seoul 138-736, Korea
g. Now at SUBATECH, CNRS/IN2P3, F-44307 Nantes, France
h. Now at Albert Einstein Center for Fundamental Physics, Laboratory for High Energy Physics (LHEP), University of Bern, CH-3012 Bern, Switzerland

Abstract

The OPERA neutrino detector at the underground Gran Sasso Laboratory (LNGS) was designed to perform the first detection of neutrino oscillations in appearance mode through the study of $\nu_\mu \to \nu_\tau$ oscillations. The apparatus consists of a lead/emulsion-film target complemented by electronic detectors. It is placed in

the high-energy long-baseline CERN to LNGS beam (CNGS) 730 km away from the neutrino source. Runs with CNGS neutrinos were successfully conducted in 2007, 2008, 2009, 2010 and 2011 for a total luminosity of 14.2×10^{19} p.o.t. (*proton on target*). In 2012 a new CNGS run has been conducted, accumulating 3.86×10^{19} p.o.t.. After a brief description of the beam and of the experimental apparatus we report on the data and related analysis results.

1 Introduction

The solution of the long-standing solar and atmospheric neutrino puzzles has come from the hypothesis of neutrino oscillations. This implies that neutrinos have non vanishing and non-degenerate mass eigenstates, and that their flavor eigenstates involved in weak interaction processes are a superposition of the mass eigenstates.

Several experiments carried on in the last decades with solar and reactor neutrinos, as well as with atmospheric and accelerator neutrinos, contributed to build-up our present understanding of neutrino mixing. Atmospheric neutrino oscillations have been studied mainly by the Kamiokande, MACRO, Super-Kamiokande and SOUDAN2 experiments. Long baseline experiments with accelerator neutrinos (K2K and MINOS) confirmed the oscillation scenario first pointed out by the Super-Kamiokande experiment supporting the $\nu_\mu \to \nu_\tau$ oscillation channel for atmospheric neutrinos, while the CHOOZ and Palo Verde reactor experiments excluded the $\nu_\mu \to \nu_e$ channel as the dominant one.

However, the direct appearance of a different neutrino flavor is still an important open issue. This is the main goal of the OPERA experiment [1, 2] that uses the long baseline (L=730 km) CNGS neutrino beam from CERN to LNGS. The challenge of the experiment is to measure the appearance of ν_τ from ν_μ oscillations in an almost pure muon-neutrino beam. This requires the detection of the short-lived τ lepton ($c\tau = 87.11$ μm) produced in the charged-current interaction of a ν_τ. This sets two conflicting requirements: a large target mass needed to have sufficient statistics and an extremely high accuracy detector technique to observe the short-lived τ lepton.

The τ is identified by the detection of its characteristic decay topologies either in one prong (electron, muon or hadron) or in three prongs. The τ track is measured with a large-mass active target made of 1 mm thick lead plates (target mass and absorber material) inter-spaced with thin nuclear emulsion films (high-accuracy tracking devices). This detector is historically called Emulsion Cloud Chamber (ECC). Among past applications it was successfully used in the DONUT experiment for the first direct observation of the ν_τ.

The OPERA detector [2] is made of two identical Super Modules (SM) each consisting of a target section of about 625 tons made of lead/emulsion-film ECC modules (hereafter called "bricks"), of a scintillator tracker detector (TT) needed to trigger the read-out and pre-localize neutrino interactions within the target, and of a muon spectrometer (Figure 1). A single SM has longitudinal dimensions of about 10 m. The detector is equipped with an automatic machine (the Brick Manipulator System, BMS) that allows the on-line removal of bricks from the detector. Ancillary facilities exist for the handling, the development and the scanning of the emulsion films. The film scanning is performed with two independent types of scanning microscopes: the European Scanning Sytem (ESS) in

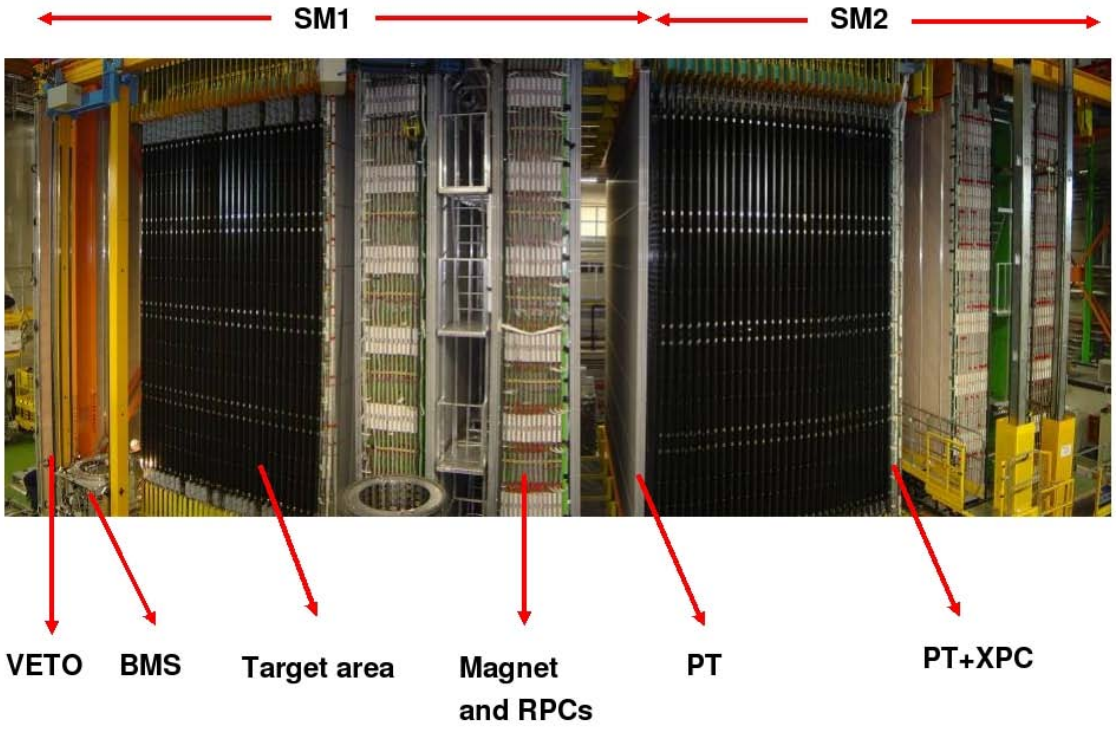

Figure 1: Fish-eye view of the OPERA detector. The upper horizontal lines indicate the position of the two identical supermodules (SM1 and SM2). The "target area" is made of walls filled with ECC bricks interleaved with planes of plastic scintillators (TT). Arrows also show the position of the VETO planes, the drift tubes (PT), the RPC with diagonal strips (XPC), the magnets and the RPC installed between the magnet iron slabs. The Brick Manipulator System (BMS) is also visible. See [2] for more details.

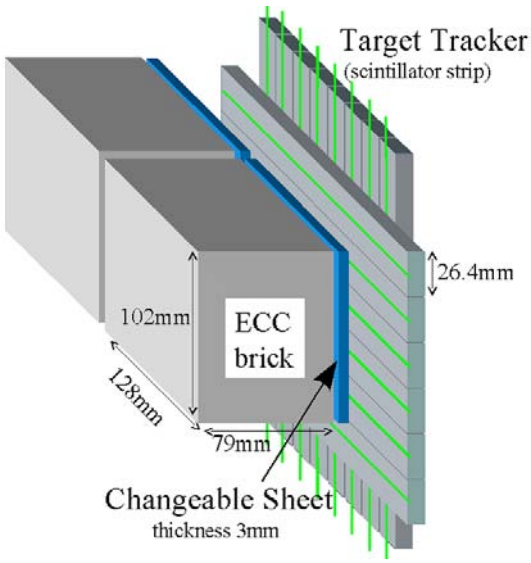

Figure 2: Schematic view of two bricks with their Changeable Sheet and target tracker planes.

Europe and the S-UTS in Japan.

A target brick consists of 56 lead plates of 1 mm thickness interleaved with 57 emulsion films [4]. The plate material is a lead alloy with a small calcium content to improve its mechanical properties [5]. The transverse dimensions of a brick are 12.8 $\times$ 10.2 cm^2 and the thickness along the beam direction is 7.9 cm (about 10 radiation lengths). The construction of more than 150,000 bricks for the neutrino target has been accomplished by an automatic machine, the Brick Assembly Machine (BAM) operating underground in order to minimize the number of background tracks from cosmic-rays and environmental radiation. The production lasted from March 2007 to June 2008 with an average rate of 650 assembled bricks/day. At the end of mass production the BAM had assembled 146621 bricks (June 2008). A few thousand more have been produced at the beginning of 2009. The bricks have been inserted in the detector target by BMS and housed in a light support structure placed between consecutive TT walls. The support structure has been designed with the requirement of minimizing the material along the neutrino beam direction in order to reduce to the 0.1% level the number of interactions in regions not instrumented with emulsion films or scintillators. In order to reduce the emulsion scanning load the use of Changeable Sheets (CS) [6], successfully applied in the CHORUS experiment, was extended to OPERA. Tightly packed doublets of emulsion films are attached to the downstream face of each brick and can be removed without opening the brick. Charged particles from a neutrino interaction in the brick cross the CS and produce a trigger in the TT scintillators. Following this trigger the brick is extracted and the CS developed and analyzed in the scanning facilities at LNGS and in Nagoya. The information of the CS is used for a precise prediction of the position of the tracks in the most downstream films of the brick, hence guiding the so-called *scan-back* vertex finding procedure. The brick, CS and TT layout [6] is schematically shown in Figure 2.

Figure 3: Left: Two of the six chains of the film development facility at the LNGS external laboratory. Right: The European CS Scanning Station at LNGS.

CNGS Performance in 2008-2011 Runs		
Year	POT/Year	neutrino int.
2008	1.74×10^{19}	1698
2009	3.53×10^{19}	3557
2010	4.09×10^{19}	3912
2011	4.75×10^{19}	4210
2012	3.86×10^{19}	3260

Table 1: CNGS beam performance in 2008-2012 Runs: The first column indicates the intensity of the beam integrated over each year, the second column gives the number of neutrino interactions in the OPERA target for each year. The total integrated luminosity obtained by OPERA is 18×10^{19} POT (*protons on target*) and represents 80 % of the luminosity foreseen in the Proposal.

2 Real time detection of CNGS Beam

The CNGS neutrino beam was designed and optimized for the study of $\nu_\mu \rightarrow \nu_\tau$ oscillations in appearance mode, by maximizing the number of charged current (CC) ν_τ interactions at the LNGS site. For a detailed description of the CNGS beam we refer to [2]. After the beam commissioning run in 2006, the CNGS run started on September 2007 at rather low intensity. The first event inside the OPERA target was observed on October 3^{rd}.Longer runs took place in 2008, 2009, 2010, 2011 and 2012. On December 2012 the last CNGS neutrinos were delivered to LNGS. A long shutdown is foreseen at CERN for 2013 and 2014 for the upgrade of LHC. The global CNGS performance during the 2008 to 2012 runs is summarized in table 1. A first ν_τ interaction candidate was found in 2010 [10]. A second ν_τ interaction candidate was found in 2011 and presented in 2012 [17] (Fig.5). A third ν_τ interaction candidate was found in 2012 and officially presented in a seminar at LNGS on March the 26th 2013 (Fig.6). The three candidate events found, together with a conservative background estimation, mostly due to charm candidates with undetected muon, give a significance of 3.5 sigma for the direct detection of $\nu_\mu \rightarrow \nu_\tau$ oscillations

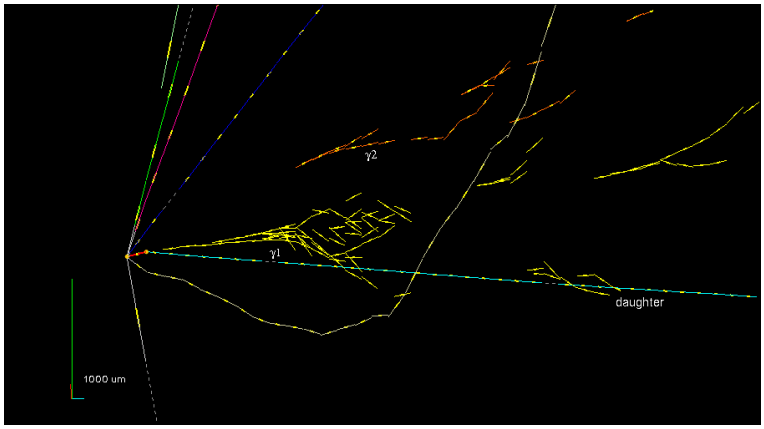

Figure 4: The first OPERA tau candidate (see [10] for details).

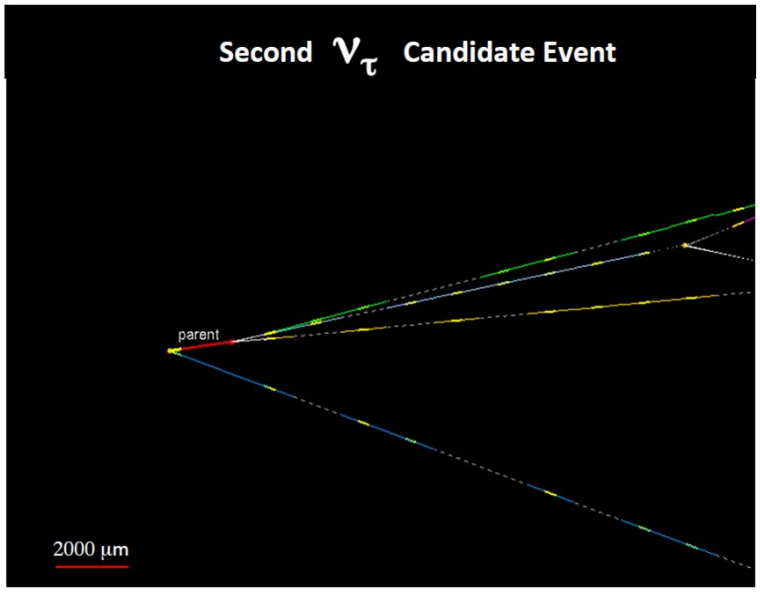

Figure 5: The second OPERA tau candidate (see [17] for details).

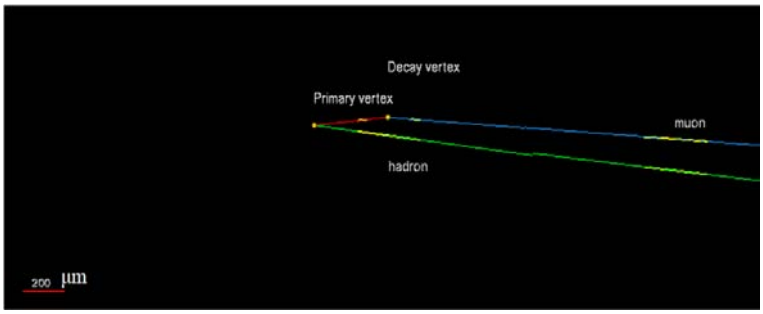

Figure 6: The third OPERA tau candidate; in this candidate event the short track is seen to decay leptonically into one muon which stops in the spectrometer.

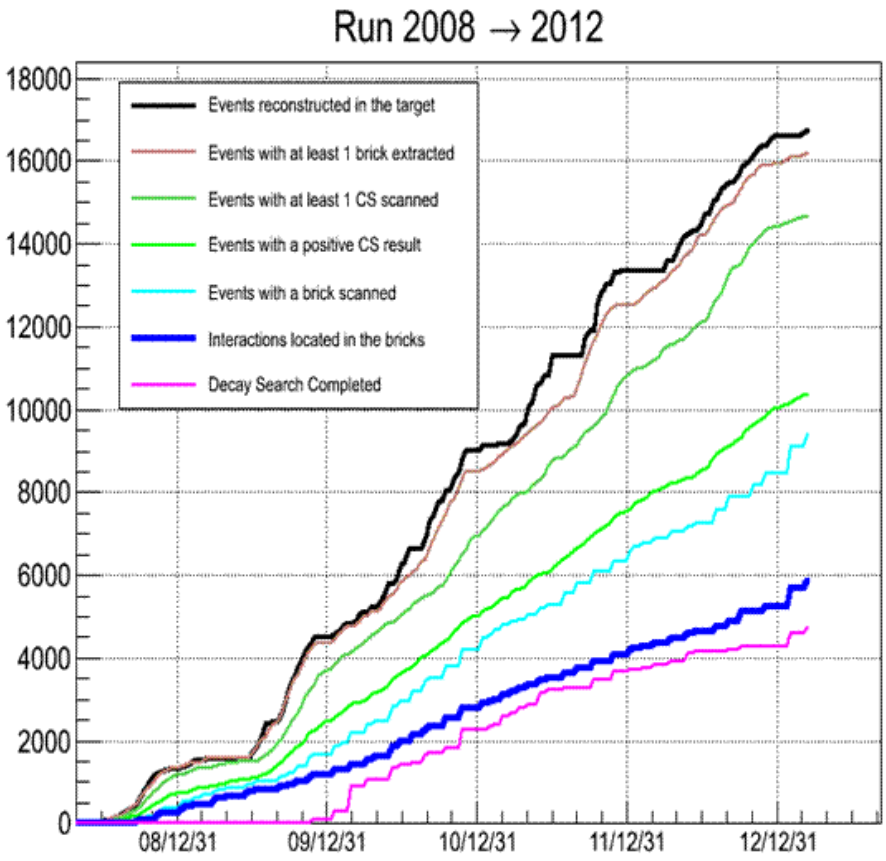

Figure 7: Run 2008 - 2012

3 Emulsion scanning and analysis

In Figure 7, the analysis status of the neutrino interactions is shown. The upmost line reports the interactions reconstructed in the target, the second one from above the events with at least one brick extracted. The brick extraction is the starting point of the analysis. The subsequent lines report the scanning of changeable sheets: the upper curve shows the events with a CS scanned while the other reports the events with a positive result after the interface emulsion film analysis. The last but one line shows the number of located events in the brick. The progress in the decay search is shown in the last curve.

In autumn 2011 we have defined an optimal strategy in order to maximize the efficiency on the short term analysis, i.e. in view of the 2012 summer conferences. We have started from the following considerations: the analysis of first bricks in the probability map provides about 80% of the overall location efficiency; the increase of scanning load due to the analysis of *second* bricks is much larger than the gain in efficiency achieved; the sample of events without a muon in the final state is enriched with ν_τ, since only 18% of the τ decay into a muon; a muon momentum cut at 15 GeV does not significantly affect the efficiency while reducing of about 25% the analysis sample. The above considerations

have motivated the following priorities for the 2010 and 2011 run analysis. For the 2010 run, we give priority to the analysis of all the first predicted bricks of the 0μ sample and of the 1μ sample with a momentum cut at 15 GeV. For the 2011 run we give priority to the analysis of the 0 mu sample with brick probability larger than 50%. It is worth stressing that the 2008 and 2009 runs have been analyzed without any of the above cuts.

The Changeable Sheet analysis has been improved. A likelihood approach is systematically applied to events with a muon in the final state and it is selecting about 40% of the charged-current events without any visual inspection. Moreover, we are currently applying an automatic selection also in the 0μ channel, i.e. for the events without any muon in the final state. Tracks validated via the likelihood approach are used as input in a vertexing algorithm. If a vertex is defined by the measured tracks, the brick is developed, thus achieving a fraction of 40% of the events without any muon in the final state validated without visual inspection.

5844 events show a vertex located within the bricks; 4725 have the decay search completed. In this analyzed sample 50 topological charm candidates and 19 electron neutrino candidates were found. As said before, three candidate tau neutrino events have been found. Relating to the BG studies of tau, studies of the hadron interactions are in progress using ECC bricks exposed to the test beam of 2, 4 and 10GeV/c at CERN and KEK. The features of daughter charged particle multiplicity, emitted angle, momentum, Pt and the probability of associating nuclear fragments are investigated and compared with Monte Carlo simulation.

4 ν_e search

A dedicated procedure was set up in order to make a systematic search for electron neutrinos. For the 505 events (recorded in 2008 and 2009) with the decay search completed and without any muon in the final state, all the charged tracks are considered and projected onto the changeable sheet. If a cluster of tracks is found around the projected point, the track is further checked along its trajectory to assess its possible electromagnetic nature. By this selection, 19 events were identified as ν_e, event. In parallel, BG studies for the misidentification of the electron pair conversion as a single electron is being carried out by using electron pairs detected in CC events. The expected BG is only 0.2 events among the current sample. The event energy was estimated by using the hit information of TT. The observed number 19 is consistent with the expectation of 1.4 oscillated ν_e, plus 19.4 prompt beam ν_e,. In order to improve the S/N ratio, we set the threshold at 20GeV, 4 events remain after this cut (E $<$ 20GeV). The observed number is again consistent with the expectation of 1.1 oscillated and 4.2 prompt beam ν_e. We have a possibility to span the region and to reach the point indicated by recent reactor experiments with full statistics and improved efficiencies and contribute to the global fit. First results of a search for $\nu_\mu \rightarrow \nu_e$ oscillations with the OPERA experiment at the Gran Sasso Underground Laboratory have been published [15]. The experiment searched for the appearance of ν_e in the CNGS neutrino beam using the data collected in 2008 and 2009, corresponding to an integrated intensity of 5.25×10^{19} pot. The observation of 19 candidate events is compatible with the non-oscillation expectation of 19.8 $\pm$ 2.8 events. The current result on

the search for the three flavor neutrino oscillation yields an upper limit $sin^2(\theta_{13}) < 0.44$ (90% C.L.). OPERA limits the parameter space available for a non-standard e appearance suggested by the results of the LSND and MiniBooNE experiments. It further constrains the still allowed region around $\Delta m^2_{new} = 5 \times 10^{-2} eV^2$. For large Δm^2_{new} values, the 90% C.L. upper limit on $sin^2(\theta_{new})$ reaches 7.2×10^{-3}. Various improvements are expected for the future. The statistics will be increased by a factor of 3.4 by completing the analysis of the collected data. The reconstructed energy resolution will be improved when the calorimetric measurement in the TT will be complemented by following the hadron tracks and the electron showers in the downstream bricks. With the increase in sample size and the improvements in the analysis, the effect of a possible statistical underfluctuation of the background will be reduced and OPERA should then be able to access the parameter region comparable to its sensitivity below $sin^2(\theta_{new}) = 5.0 \times 10^{-3}$.

5 neutrino velocity measurement

The OPERA neutrino experiment at the underground Gran Sasso Laboratory has measured the velocity of neutrinos from the CERN CNGS beam over a baseline of about 730 km. The measurement is based on data taken by OPERA in the years 2009, 2010 and 2011. Dedicated upgrades of the CNGS timing system and of the OPERA detector, as well as a high precision geodesy campaign for the measurement of the neutrino baseline, allowed reaching comparable systematic and statistical accuracies. An arrival time of CNGS muon neutrinos with respect to the one computed assuming the speed of light in vacuum of (6.5 $\pm$ 7.4 (stat) $^{+8.3}_{-8.0}$ (sys)) ns was measured corresponding to a relative difference of the muon neutrino velocity with respect to the speed of light (v-c)/c = (2.7 $\pm$ 3.1 (stat) $^{+3.4}_{-3.3}$ (sys)) $\times 10^{-6}$.

The above result, obtained by comparing the time distributions of neutrino interactions and of protons hitting the CNGS target in 10.5 μs long extractions, was confirmed by a test performed at the end of 2011 using a short bunched beam allowing to measure the neutrino time of flight at the single interaction level. These results were obtained by taking into account the corrections for instrumental effects discovered after the originally reported neutrino velocity anomaly.

In spring 2012 CERN provided two weeks of a short bunch proton beam dedicated to the neutrino velocity measurement. The OPERA neutrino experiment at the underground Gran Sasso Laboratory used an upgraded setup compared to the 2011 measurements, improving the measurement time accuracy. An independent timing system based on the Resistive Plate Chambers was exploited providing a time accuracy of 1 ns. Neutrino and anti-neutrino contributions were separated using the information provided by the OPERA magnetic spectrometers. The new analysis profited from the precision geodesy measurements of the neutrino baseline and of the CNGS/LNGS clock synchronization. The neutrino arrival time with respect to the one computed assuming the speed of light in vacuum is found to be (0.6 $\pm$ 0.4 (stat.) $\pm$ 3.0 (syst.)) ns for ν_μ and (1.8 $\pm$ 1.4 (stat.) $\pm$ 3.2 (syst.)) ns for $\bar{\nu}_\mu$, respectively. This corresponds to a limit on the muon neutrino velocity with respect to the speed of light of $1.77 \times 10^{-6} < (v-c)/c < 2.27 \times 10^{-6}$ at 90% C.L. [16]. This new measurement confirms with higher accuracy the revised OPERA

result.

References and list of publications

[1] R. Acquafredda *et al.* [OPERA Collaboration], "First events from the CNGS neutrino beam detected in the OPERA experiment,"New J. Phys. **8** (2006) 303 [arXiv:hep-ex/0611023].

[2] R. Acquafredda *et al.* [OPERA Collaboration] "The OPERA experiment in the CERN to Gran Sasso neutrino beam", JINST 4:P04018,2009.

[3] N. Agafonova *et al.* [OPERA Collaboration] "The Detection of neutrino interactions in the emulsion/lead target of the OPERA experiment", JINST 4:P06020,2009.

[4] T. Nakamura *et al.*, "The Opera Film: New Nuclear Emulsion For Large-Scale, High-Precision Experiments," Nucl. Instrum. Meth. A **556** (2006) 80.

[5] A. Anokhina *et al.* [OPERA Collaboration], "Study of the effects induced by lead on the emulsion films of the OPERA experiment," JINST **3** P07002 (2008).

[6] A. Anokhina *et al.* [OPERA Collaboration], "Emulsion sheet doublets as interface trackers for the OPERA experiment," JINST **3** (2008) P07005

[7] L. Arrabito *et al.*, "Track reconstruction in the emulsion-lead target of the OPERA experiment using the ESS microscope," JINST **2** (2007) P05004

[8] K. Kodama *et al.*, "Momentum measurement of secondary particle by multiple Coulomb scattering with emulsion cloud chamber in DONuT experiment," Nucl. Instrum. Meth. A **574** (2007) 192.

[9] M. Guler *et al.*, OPERA proposal, CERN/SPSC 2000-028, SPSC/P318, LNGS P25/2000.

[10] N. Agafonova *et al.* [OPERA Collaboration], "Observation of a first ν_τ candidate in the OPERA experiment in the CNGS beam," Phys. Lett. *B691* , 138 (2010).

[11] N. Agafonova, *et al.* [OPERA Collaboration], "Measurement of the atmospheric muon charge ratio with the OPERA detector," Eur. Phys. J. *C67* , 25 (2010).

[12] N. Agafonova *et al.* [OPERA Collaboration], "Study of neutrino interactions with the electronic detectors of the OPERA experiment." New J. Phys. *13* , 053051 (2011)

[13] N. Agafonova *et al.* [OPERA Collaboration], "Search for ν_μ -ν_τ oscillation with the OPERA experiment in the CNGS beam." New J. Phys. *14* , 033017 (2012)

[14] N. Agafonova *et al.* [OPERA Collaboration], "Momentum measurement by the Multiple Coulomb Scattering method in the OPERA lead emulsion target." New J. Phys. *14* , 013026 (2012)

[15] N. Agafonova *et al.* [OPERA Collaboration], "Search for ν_μ -ν_e oscillation with the OPERA experiment in the CNGS beam." arXiv 1303.3953, sub. to JHEP

[16] T. Adam *et al.* [OPERA Collaboration], "Measurement of the neutrino velocity with the OPERA detector in the CNGS beam using the 2012 dedicated data." JHEP *1301* , 153 (2013)

[17] M. Nakamura [for the OPERA Collaboration], "Results from OPERA." Neutrino 2012, to be published in Nuclear Phys. B.

THEORY GROUP

The LNGS theory group is organized in the following five working subgroups (or IS, from *Iniziative Specifiche*): PI12, PI21, CT51, FA51, PD51. The coordinators are indicated in bold face in the members list. The research topics concern five main areas: astroparticle physics (mainly FA51); compact stellar objects and dense hadronic matter (CT51); cosmology, large scale structures and dark matter (PD51); computer simulations of gauge theories (PI12); particle physics phenomenology (mainly PI21). There is a tradition of collaboration between the LNGS theory group and several experimental groups. In this report, we briefly describe the activities of the theory group in 2012.

Members of the group: R. Aloisio, Z. Berezhiani, V. Berezinsky, P. Blasi, M. Crisostomi, G. Di Carlo, G. Di Panfilo A.F. Grillo, C. Lujan-Peschard, E. Luzio, A. Maiezza, **M. Mannarelli**, M. Mitra, G. Pagliaroli, L. Pilo, N. Rossi, F. Tortorici, F.L. Villante, F. Vissani.

Updated information can be found at: `http://theory.lngs.infn.it/index.html`

Lattice QCD (PI12)

Member: **G. Di Carlo**.

In collaboration with V. Azcoiti, E. Follana, M. Giordano (Universidad de Zaragoza, Spain) and A. Vaquero (The Cyprus Institute, Cyprus),

Scientific work

The research activity has been focused on the study of the sign problem and topology in lattice field theories: non-zero baryonic density QCD, so-called Aoki phase and models with θ-term.

We performed extensive simulations of QCD in the Aoki phase with Wilson fermions in order to clarify the actual situation about the possible existence of other phases in this region of parameter space and the related issues about the symmetries of the spectral density of the Hermitian Wilson operator. The results, pointing towards the existence of a complex phase structure inside the Aoki phase, have been published in [1].

We completed the study on universality in presence of a θ term using numerical methods we developed in the past years; the behavior of the topological order parameter as a function of θ has been used to characterize the critical behavior of the $\theta = \pi$ theory in three different lattice realizations of the $O(3)$-CP(1) model, relevant for the testing of

the Haldane conjecture. A behavior compatible with the $O(3)$ model being in the same universality class of the Weiss-Zumino-Witten model has been found. These results have been published in [2].

Publications in journals

[1] V. Azcoiti, G. Di Carlo, E. Follana and A. Vaquero, Nucl. Phys. B **870**, 138 (2013) [arXiv:1208.0761 [hep-lat]].

[2] V. Azcoiti, G. Di Carlo, E. Follana and M. Giordano, Phys. Rev. D **86**, 096009 (2012) [arXiv:1207.4905 [hep-lat]].

Fundamental Interactions and Gauge Theories (PI21)

Members: **Z. Berezhiani**, G. Di Panfilo, A. Maiezza, L. Pilo, N. Rossi and F.L. Villante. In collaboration with F. Nesti (Univ. L'Aquila), A. Gazizov (DESY Zeuthen), A. Dolgov, G. Fiorentini (Univ. Ferrara), I.I. Tkachev (INR, Moscow), O.V. Kancheli (ITEP, Moscow), D. Comelli (INFN-Ferrara), and others.

Scientific work

The research activity has been focused on the following topics:

i) Neutron Oscillations. Present experiments do not exclude that the neutron n transforms into some invisible degenerate twin n' from a parallel world, so called mirror neutron, with an appreciable probability. These transitions, which violate baryon number by 1 unit, are actively studied by monitoring neutron losses in ultra-cold neutron traps, where they can be revealed by their magnetic field dependence. We reanalyzed experimental data acquired by the group of A.P. Serebrov at Institute Laue-Langevin, Grenoble, and find a dependence at more than 5σ away from the null hypothesis (see Fig. 1). This anomaly can be interpreted as oscillation $n \to n'$ with a timescale of few seconds, in the presence of a mirror magnetic field $B' \sim 0.1\,\mathrm{G}$ at the Earth. If confirmed by future experiments, the phenomenon of neutron – mirror neutron oscillation will have a number of deepest consequences in particle physics, cosmology and astrophysics [1].

ii) Spectral modification of the UHECR by Neutron Oscillations. We show that the effect of fast $n - n'$ oscillation brings remarkable modifications of the ultrahigh-energy cosmic ray spectrum at $E > 10$ EeV (see Fig. 2) which is testable by the present Pierre Auger Observatory (PAO) and Telescope Array (TA) detector, and the future JEM-EUSO experiment. In particular, the baryon non-conservation during UHECR propagation at large cosmological distances shifts the beginning of the GZK cutoff to lower energies, while in presence of mirror sources it may enhance the spectrum at $E > 100$ EeV. As a consequence, one can expect a significant reduction of the diffuse cosmogenic neutrino flux.

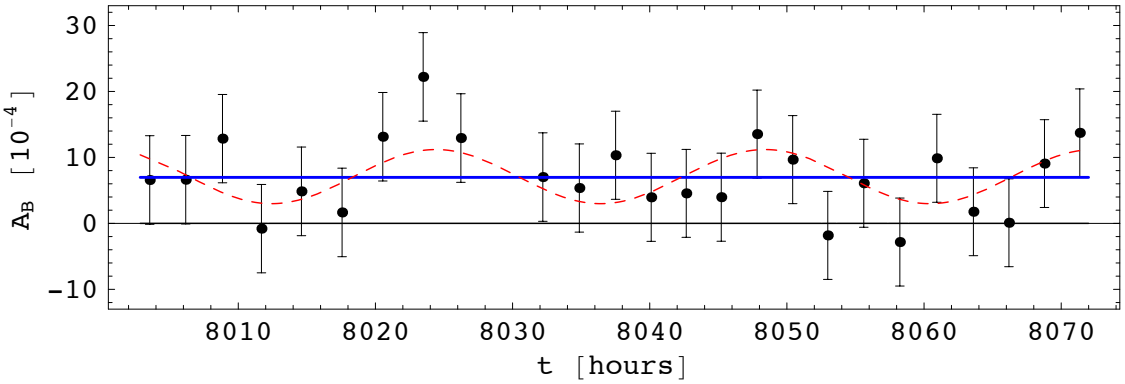

Figure 1: Values of directional asymmetry A_B between the neutron counts between the magnetic field configurations directed vertically up and down, at $B = 0.2$ G. These data, based on 400 measurements by Serebrov's group with the UCN storage time of 300 s in the trap of 190 l volume, yield a constant fit $A_B = (6.96 \pm 1.34) \times 10^{-4}$ with χ^2dof $= 0.87$. The periodic fit favors a 24 h period.

Another consequence is the possible correlation of super GZK cosmic rays with distant sources like BL Lacs [6].

Other works are related to alternative theories of gravity [4]-[8], to direct violation of CP in left-right symmetric theories [9], to solar Be and CNO neutrino fluxes and their detection capabilities [12, 3] to the impossibility of superluminal OPERA neutrinos [10, 7], to tests of new and old physics in primordial nucleosynthesis [3, 2, 4]

Conferences, seminars and other activities

Int. Workshop: "Lithium in the Cosmos", February 27 - 29, 2012, Institut d'Astrophysique de Paris, France (F.L. Villante, poster)

Nat. Workshop: "Incontri di Fisica dell'Alte Energie (IFAE 2012)", Apr. 11-13, 2012, Ferrara, Italy (F. Villante, convener of session)

Int. Workshop: "Hot topics in Modern Cosmology", SW6, May 7 - 12, 2012, Cargese, France (Z. Berezhiani, member of the Organizing committee; Z. Berezhiani and L. Pilo, talks)

"*CORTONA 2012*, Convegno Informale di Fisica Teorica", May 30 - 31, 2012, Cortona, Italy (A. Maiezza and L. Pilo, talks)

Int. Workshop: "Neutrino Oscillation Workshop NOW 2012", Sept. 9-16, 2012, Conca Specchiulla, Otranto, Italy (Z. Berezhiani, talk; F.L. Villante, convener of session)

Int. Workshop: "The Physics of the Sun and the Solar Neutrinos: 3rd", October 8-10, 2012, LNGS, Italy (F.L. Villante, member of the Organizing committee)

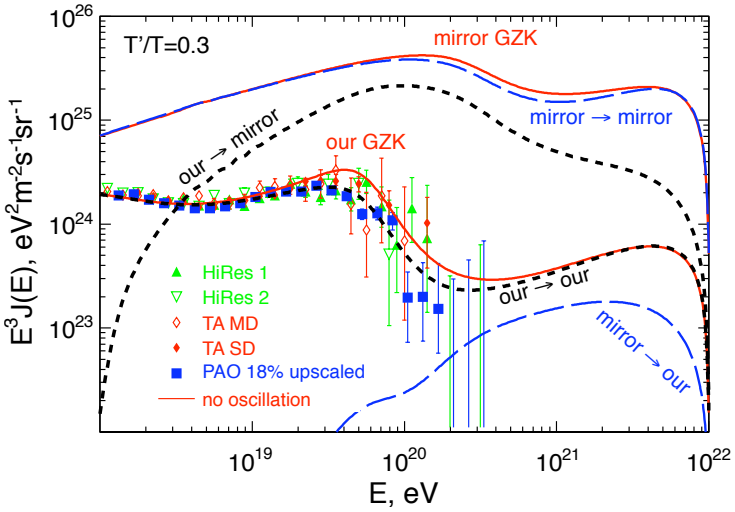

Figure 2: The red solid curves marked as *our GZK* and *mirror GZK* show the expected spectra of the ordinary and mirror cosmic rays in the absence of n–n' oscillation. The generation functions in two sectors are taken identical, with $\gamma_g = 2.4$. We also show experimental results of HiRes, TA and PAO (the latter are 18% upscaled in energy). The black short-dash curves show the spectra of cosmic rays originated from ordinary sources that escape to mirror sector due to n–n' oscillation (*our*→*mirror*) and that remain in our sector (*our*→*our*). Observe that the latter curve nicely fits the PAO data, better then the standard GZK prediction (*our GZK*). The blue long-dash curves show mirror and ordinary cosmic ray fluxes originated from mirror sources of the same intensity.

Int. Workshop: "Understanding the TeV Scale Through LHC Data, Dark Matter, and Other Experiments", 22 Oct. – 11 Nov. 2012, Galileo Galilei Institute, Florence, Italy (Z. Berezhiani, participant and seminar speaker; G. Di Panfilo, participant)

Int. School: "IDAPP: 2nd meeting", Oct 29-31, 2012, Ferrara, Italy (F.L. Villante, invited lecture)

Mini Workshop: "Sasha Fest", A. Dolgov 70 Anniversary, Oct. 31, 2012, Ferrara, Italy (Z. Berezhiani, invited lecture)

Publications in journals and conference proceedings

[1] Z. Berezhiani and F. Nesti, "Magnetic anomaly in UCN trapping: signal for neutron oscillations to parallel world?," Eur. Phys. J. C **72**, 1974 (2012)

[2] Z. Berezhiani and A. Gazizov, "Neutron Oscillations to Parallel World: Earlier End to the Cosmic Ray Spectrum?," Eur. Phys. J. C **72**, 2111 (2012)

[3] Z. Berezhiani, A. Dolgov and I. Tkachev, "BBN with light dark matter," JCAP **1302**, 010 (2013) [arXiv:1211.4937 [astro-ph.CO]].

[4] Z. Berezhiani and O.V. Kancheli, "Spontaneous breaking of Lorentz-invariance and gravitons as Goldstone particles," Procs. Int. Workshop *'Low Dimesion Physics and Gauge Principles', Matinyan Festschrift*, Eds. V.G. Gurzadyan et al., World Scientific, Singapore, 2012, pp. 58-79

[5] D. Comelli, M. Crisostomi, F. Nesti and L. Pilo, "Spherically Symmetric Solutions in Ghost-Free Massive Gravity," Phys. Rev. D **85**, 024044 (2012)

[6] D. Comelli, M. Crisostomi, F. Nesti and L. Pilo, "FRW Cosmology in Ghost Free Massive Gravity," JHEP **1203**, 067 (2012) [Erratum-ibid. **1206**, 020 (2012)]

[7] D. Comelli, M. Crisostomi, F. Nesti and L. Pilo, "Degrees of Freedom in Massive Gravity," Phys. Rev. D **86**, 101502 (2012)

[8] D. Comelli, M. Crisostomi and L. Pilo, "Perturbations in Massive Gravity Cosmology," JHEP **1206**, 085 (2012) [arXiv:1202.1986 [hep-th]].

[9] S. Bertolini, J.O. Eeg, A. Maiezza and F. Nesti, "New physics in ϵ' from gluomagnetic contributions and limits on Left-Right symmetry," Phys. Rev. D **86**, 095013 (2012)

[10] P. Alvarez Sanchez, N. Rossi *et al.*, "Measurement of CNGS muon neutrino speed with Borexino," Phys. Lett. B **716**, 401 (2012)

[11] M. Mannarelli, M. Mitra, F. L. Villante and F. Vissani, "Non-Standard Neutrino Propagation and Pion Decay", JHEP **1201**, 136 (2012)

[12] G. Ranucci, N. Rossi *et al.*, "Recent results on solar neutrinos," PoS HQL **2012**, 052 (2012).

[13] F. L. Villante, A. Ianni, F. Lombardi, G. Pagliaroli and F. Vissani, "A method to extract the CNO solar neutrino signal in ultrapure liquid scintillator detectors", J. Phys. Conf. Ser. **375**, 042035 (2012).

[14] C. Broggini, L. Canton, G. Fiorentini and F. L. Villante, "The cosmological 7Li problem from a nuclear physics perspective", JCAP **1206**, 030 (2012)

[15] C. Broggini, L. Canton, G. Fiorentini, F. L. Villante, "Reducing the space for a nuclear physics solution of the cosmic 7Li problem". Mem. S.A.It. Suppl. **22**, 189 (2012).

Cosmology and Dark Matter (PD51)

Members: Z. Berezhiani, M. Crisostomi, M. Mitra, L. Pilo and **F.L. Villante**.

In collaboration with L. Canton and C. Broggini (INFN-Padova), A. Serenelli (UAM-Barcellona), D. Comelli (INFN-Ferrara), A. Riotto (CERN and INFN-Padova), A. Drago (University of Ferrara), D. Blas (IPT, Lausanne).

Scientific work

The research activity has been focused on the following topics:

i) Modifications of gravity. We have studied modification of gravity at large distances. We focused our activity on both the internal consistency of such models and on their phenomenological implications. In particular, the Stuckelberg formulation that requires an additional non dynamical, God given metric is compared with an alternative approach where the extra metric is dynamical. The physically important cases of spherically symmetric solutions and cosmological FRW solutions are discussed. The bottom line is that the formulation of massive gravity with two dynamical metrics works better than the Stuckelberg one. However, compared with GR, massive gravity is less predictive at the scale of the solar system due to strong coupling.

ii) Big Bang Nucleosynthesis. The primordial abundance of ^{7}Li as predicted by Big Bang Nucleosynthesis (BBN) is more than a factor 2 larger than what observed in metal poor halo stars. In [4] we analyzed the possibility that this discrepancy originates from incorrect assumptions about the nuclear reaction cross sections relevant for BBN. In order to do this, we introduced an efficient method to calculate the response of the ^{7}Li primordial abundance to an arbitrary modification of the nuclear reaction rates. We applied our approach to the various possible ^{7}Be destruction channels and we improved with respect to previous analysis by introducing a better description of the nuclear processes. As a results of this, the parameter space for a nuclear physics solution of the ^{7}Li puzzle is considerably reduced.

iii) Neutrino phenomenology. Motivated by the initial findings of the OPERA experiment, we discussed the hypothesis that neutrino propagation does not obey Einstein special relativity. Under a minimal set of modifications of the standard model Lagrangian, we considered the implications of non standard neutrino propagation on the description of neutrino interactions and, specifically, on the pion decay process. We have shown that all the different dispersion relations which were proposed to explain the erroneous OPERA results, imply huge departures from the standard expectations. The decay channel $\pi^+ \to e^+\nu_e$ becomes significantly larger than in the standard scenario, and may even dominate over $\pi^+ \to \mu^+\nu_\mu$. Moreover, the spectral distribution of neutrinos produced in the decay processes and the probability that a pion decays in flight in neutrinos show large deviations from the standard results.

Conferences, seminars and other activities

Int. Workshop: "The Physics of the Sun and the Solar Neutrinos: 3rd", Oct. 8-10, 2012, LNGS, Italy (F. L. Villante, member of the Organizing committee).

Int. Workshop: "Neutrino Oscillation Workshop (NOW2012) ", Sept. 9-16, 2012, Conca Specchiulla (LE), Italy (F. L. Villante, convener of the session "Oscillations at low energy"; Z. Berezhiani, talk).

Int. Workshop: "Lithium in the Cosmos", February 27 - 29, 2012, Institut d'Astrophysique de Paris, France (F. L. Villante, poster).

Int. School: "IDAPP: 2d meeting", October 29-31, 2012, Ferrara, Italy (F. L. Villante, invited lecture; M. Crisostomi, talk).

Nat. Workshop: "Incontri di Fisica dell'Alte Energie (IFAE 2012)", April 11-13, 2012, Ferrara, Italy (F. L. Villante, convener of the session: "Neutrino Physics").

Invited seminar at Laboratoire de Physique Theorique d'Orsay, Universite Paris XI-Sud-Orsay, November 21, 2012, Paris, France (L. Pilo, talk)

"*CORTONA 2012*, Convegno Informale di Fisica Teorica" May 30 - June 1, 2012, Cortona, Italy (L. Pilo and M. Crisostomi, talks).

Int. Workshop: "Hot topics in Modern Cosmology", SW6, May 7-12, 2012, Cargese, France (Z. Berezhiani, member of the Organizing committee; Z. Berezhiani and L. Pilo, talks)

University of Geneve, Sept. 3, 2012, Geneve, Switzerland (L. Pilo, seminar)

Scuola Normale Superiore di Pisa, Gen. 19, 2012, Pisa, Italy (L. Pilo, seminar)

Int. Workshop: "Understanding the TeV Scale Through LHC Data, Dark Matter, and Other Experiments", Oct. 22 - Nov. 11, 2012, Galileo Galilei Institute, Florence, Italy (Z. Berezhiani, talk)

Mini Workshop: "Sasha Fest", A. Dolgov 70 Anniversary, Oct. 31, 2012, Ferrara, Italy (Z. Berezhiani, invited lecture)

Publications in journals, proceedings and preprints

[1] M. Mannarelli, M. Mitra, F. L. Villante and F. Vissani, "Non-Standard Neutrino Propagation and Pion Decay", JHEP **1201**, 136 (2012)

[2] C. Broggini, L. Canton, G. Fiorentini and F. L. Villante, "The cosmological 7Li problem from a nuclear physics perspective", JCAP **1206**, 030 (2012)

[3] F. L. Villante, A. Ianni, F. Lombardi, G. Pagliaroli and F. Vissani, "A method to extract the CNO solar neutrino signal in ultrapure liquid scintillator detectors", J. Phys. Conf. Ser. **375**, 042035 (2012).

[4] C. Broggini, L. Canton, G. Fiorentini, F. L. Villante, "Reducing the space for a nuclear physics solution of the cosmic 7Li problem". Mem. S.A.It. Suppl. **22**, 189 (2012).

[5] K. Scholberg and F. L. Villante, "Neutrino oscillations at low energies", to be published on Nucl. Phys. B Proc. Suppl.

[6] D. Comelli, M. Crisostomi, F. Nesti, L. Pilo, "Degrees of Freedom in Massive Gravity" Phys.Rev. D **86**, 101502 (2012).

[7] D. Comelli, M. Crisostomi, L. Pilo, "Perturbations in Massive Gravity Cosmology", JHEP **1206**, 085 (2012).

[8] D. Comelli, M. Crisostomi, F. Nesti, L. Pilo, "FRW Cosmology in Ghost Free Massive Gravity", JHEP **1203**, 067 (2012), Erratum-ibid. **1206**, 020, (2012).

[9] D. Comelli, M. Crisostomi, F. Nesti, L. Pilo, "Spherically Symmetric Solutions in Ghost-Free Massive Gravity", Phys.Rev. D **85** 024044 (2012).

[10] Z. Berezhiani and F. Nesti, "Magnetic anomaly in UCN trapping: signal for neutron oscillations to parallel world?," Eur. Phys. J. C **72**, 1974 (2012)

[11] Z. Berezhiani and A. Gazizov, "Neutron Oscillations to Parallel World: Earlier End to the Cosmic Ray Spectrum?," Eur. Phys. J. C **72**, 2111 (2012)

[12] Z. Berezhiani, A. Dolgov and I. Tkachev, "BBN with light dark matter," JCAP **1302**, 010 (2013)

[13] Z. Berezhiani and O.V. Kancheli, "Spontaneous breaking of Lorentz-invariance and gravitons as Goldstone particles," Procs. Int. Workshop *'Low Dimesion Physics and Gauge Principles', Matinyan Festschrift*, Eds. V.G. Gurzadyan et al., World Scientific, Singapore, 2012, pp. 58-79

Theoretical Astroparticle Physics (FA51)

Members: R. Aloisio, **V. Berezinsky**, P. Blasi, M. Mitra, F. Vissani

In collaboration with V. Dokuchaev (INR, Moscow), Yu. Eroshenko (INR, Moscow), A. Gazizov (DESY Zeuthen), S. Grigorieva (INR, Moscow), M. Kachelriess (Trondheim Univ. Norway) and A. Vilenkin (Tufts University, USA).

Scientific work

The work covered the following fields: ultra-high energy (UHE) cosmic rays, UHE neutrinos, neutrinos from SN and SNRs, properties of neutrinos and cosmology. Two particular results may be emphasized: In the work [8], the model of neutrinoless double-beta decay

with with dominant contribution by the exchange of virtual sterile neutrino is developed. It is demonstrated that this neutrino has a mass upper bound about 10 GeV. In another work [5] the concept of the bright phase connected with explosion of the first stars (Pop III stars) is put forward. SN explosions of these stars may explain reionization observed by WMAP, production of heavy metals needed for the next generation stars and production of cosmic magnetic fields. It is demonstrated that diffuse UHE neutrino flux with characteristic energies a few PeV can be detected by IceCube in agreement with two PeV neutrinos detected by IceCube, after [5] was published.

The first calculations of the structure of a collisionless shock in the presence of neutral material, and the consequences for particle acceleration in supernova remnants (SNRs) and the testing of SNRs as the sources of Galactic CRs was presented in a series of papers [12, 13, 14]. The possibility to use atomic Balmer lines to measure the cosmic ray acceleration efficiency is presented for the first time in a self-consistent manner. In another paper [15], a physically motivated model was presented for the spectral breaks observed by PAMELA and CREAM in the spectra of protons and helium nuclei as due to self-generation of turbulence during propagation of cosmic rays in the Galaxy.

Publications in journals, proceedings and preprints

[1] R. Aloisio, V. Berezinsky and A. Gazizov, Astropart. Phys. **39-40**, 129 (2012) [arXiv:1211.0494 [astro-ph.HE]].

[2] R. Aloisio, V. Berezinsky and A. Gazizov, J. Phys. Conf. Ser. **337**, 012042 (2012) [arXiv:1105.1111 [astro-ph.HE]].

[3] R. Aloisio, D. Boncioli, A. F. Grillo, S. Petrera and F. Salamida, JCAP **1210**, 007 (2012) [arXiv:1204.2970 [astro-ph.HE]].

[4] V. Berezinsky, Nucl. Phys. **B** (Proc. Suppl.) 243, 229 (2012) [arXiv:1102.3591 [astro-ph.HE]].

[5] V. Berezinsky and P. Blasi, Phys. Rev. D **85**, 123003 (2012) [arXiv:1111.5461 [astro-ph.HE]].

[6] Z. Berezhiani and A. Gazizov, "Neutron Oscillations to Parallel World: Earlier End to the Cosmic Ray Spectrum?," Eur. Phys. J. C **72**, 2111 (2012)

[7] M. Mannarelli, M. Mitra, F. L. Villante and F. Vissani, "Non-Standard Neutrino Propagation and Pion Decay", JHEP **1201**, 136 (2012)

[8] M. Mitra, G. Senjanovic and F. Vissani, Nucl. Phys. B **856**, 26 (2012) [arXiv:1108.0004 [hep-ph]].

[9] R. Aloisio, arXiv:1207.2089 [astro-ph.HE].

[10] R. Aloisio, arXiv:1211.0497 [astro-ph.HE].

[11] R. Aloisio, arXiv:1211.2004 [astro-ph.HE].

[12] P. Blasi, G. Morlino, R. Bandiera, E. Amato and D. Caprioli, Astrophys. J. **755**, 121 (2012) [arXiv:1202.3080 [astro-ph.HE]].

[13] G. Morlino, R. Bandiera, P. Blasi and E. Amato, Astrophys. J. **760**, 137 (2012) [arXiv:1210.4296 [astro-ph.HE]].

[14] G. Morlino, P. Blasi, R. Bandiera, E. Amato and D. Caprioli, arXiv:1211.6148 [astro-ph.HE].

[15] P. Blasi, E. Amato and P. D. Serpico, Phys. Rev. Lett. **109**, 061101 (2012) [arXiv:1207.3706 [astro-ph.HE]].

Conferences, seminars and other activities

Int. Symposium: "Future directions in UHECR", 13 - 16 Feb. 2012, CERN (R. Aloisio, talk)

Vulcano Workshop "Frontier Objects in Astrophysics and Particle Physics", 26 May - 2 June, 2012, Vulcano, Italy (R. Aloisio, talk)

9th Workshop "Science with new generation gamma ray experiments", 20-22 June, 2012, Lecce, Italy (R. Aloisio, talk)

Int. Symposium: "Future directions in UHECR", 13 - 16 Feb. 2012, CERN (V. Berezinsky, talk)

Ginzburg conference, May 28 - June 2, 2012, Moscow (V. Berezinsky, talk)

GGI workshop "What is nu?", 12 - 30 June, 2012, Florence, Italy (V. Berezinsky, talk)

Int. Conference: "100 Years Cosmic Rays", 5-8 August, 2012, Bad Saarow, Germany (V. Berezinsky, talk)

Astrophysics and high energy physics (CT51)

Members: C. Lujan-Peschard, **M. Mannarelli**, G. Pagliaroli, and F. Vissani.

In collaboration with M.L. Costantini, F. Nesti, G. Senjanovic, F.L. Villante, A. Ianni, F. Lombardi, L. Tolos, C. Manuel, J. Soto, M. Escobedo, R. Anglani, M. Ruggieri, G. Colucci, R. Casalbuoni, R. Gatto.

Scientific work

The scientific achievements concern several aspects of gravitational waves physics [1, 2, 3, 4, 5, 6, 7], neutrino physics [8, 9, 10, 11, 12, 13] and superfluid properties of interest

for compact stars [14, 15]. The S5 LIGO data have been fully analyzed for gravitational wave search [2]; the analysis of various sources, including intermediate mass binary black holes [5] as well as compact binary merging [6], has been carried out. The investigation of the properties of neutrinos was pursued aiming at various goals in connection with neutrinoless double beta decays and heavy sterile neutrinos [10, 11]. The analysis of pion decays has been investigated [9] in connection with the superluminal neutrino propagation claim, reaching the conclusion that the non-standard neutrino propagation would have lead to a large and observable effect on the pion decay. The feasibility of the study of the strangeness content of the proton by the neutrinos produced from pion decay has been studied [13] and its influence on one of the structure functions has been parameterized. The properties of superfluid phonons have been studied in [14, 15], where it was shown that for ballistic phonons a sizable contribution to the shear viscosity might be due to interactions of phonons with the boundary.

Conferences, seminars and other activities

DESY center, Hamburg, Germany (G. Pagliaroli, seminar)

Int. Symposium: "European Week of Astronomy and Space Science (EWASS 2012)" Roma. (G. Pagliaroli, talk)

Int. Workshop: "Neutrino Oscillation Workshop NOW 2012", 9-16 Sept. 2012, Conca Specchiulla, Otranto, Italy (G. Pagliaroli, talk)

Int. Workshop: "The Physics of the Sun and the Solar Neutrinos: 3rd", October 8-10, 2012, LNGS, Italy (G. Pagliaroli, talk)

University of Barcelona, Gen 16, 2012 Barcelona, Spain (M. Mannarelli, seminar)

Int. Conference: "Conference in honor of Roberto Casalbuoni's 70th Birthday", Sept 21, 2012, GGI, Florence, Italy (M. Mannarelli, talk)

Int. Conference: "Xth Quark Confinement and the Hadron Spectrum", Oct. 8-12, 2012, TUM Campus Garching, Munich, Germany (M. Mannarelli, talk)

KM3NeT general meeting: "High Energy Neutrino Astronomy: Highlights", Feb 22, LNS Catania (F. Vissani, talk)

Mini-Workshop: "LNGS results on the neutrino velocity topic", March 18, 2012, LNGS (F. Vissani, talk)

Nat. Workshop: "Incontri di Fisica dell'Alte Energie (IFAE 2012)", April 11-13, 2012, Ferrara, Italy (F. Vissani, talk)

Int. Workshop: "New Frontiers in nuclear astrophysics", June 18-22, 2012, Castiglion

Fiorentino, Italy (F. Vissani, two talks)

Int Workshop: "Exploring the Non-thermal Universe with Gamma Rays", Nov. 6-9, 2012, Barcelona, Spain (F. Vissani, talk)

LNF Frascati, Nov. 22, 2012 (F. Vissani, seminar)

Orca meeting, Dec. 3-10, 2012, LNS Catania (F. Vissani, talk)

Publications in journals and proceedings

[1] T. Accadia *et al.* [Virgo Collaboration], Class. Quant. Grav. **29**, 025005 (2012) [arXiv:1108.1598 [gr-qc]].

[2] J. Abadie *et al.* [The LIGO Scientific and The Virgo Collaboration], Phys. Rev. D **85**, 022001 (2012) [arXiv:1110.0208 [gr-qc]].

[3] T. Accadia *et al.* [VIRGO Collaboration], JINST **7**, P03012 (2012).

[4] J. Abadie *et al.* [LIGO Scientific and Virgo Collaborations], Phys. Rev. D **85**, 122007 (2012) [arXiv:1202.2788 [gr-qc]].

[5] J. Abadie *et al.* [LIGO Scientific and Virgo Collaborations], Phys. Rev. D **85**, 102004 (2012) [arXiv:1201.5999 [gr-qc]].

[6] J. Abadie *et al.* [LIGO and Virgo Collaborations], Phys. Rev. D **85**, 082002 (2012) [arXiv:1111.7314 [gr-qc]].

[7] J. Abadie *et al.* [LIGO Scientific and Virgo Collaborations], Phys. Rev. D **85**, 122001 (2012) [arXiv:1112.5004 [gr-qc]].

[8] F. L. Villante, A. Ianni, F. Lombardi, G. Pagliaroli and F. Vissani, J. Phys. Conf. Ser. **375**, 042035 (2012).

[9] M. Mannarelli, M. Mitra, F. L. Villante and F. Vissani, JHEP **1201**, 136 (2012) [arXiv:1112.0169 [hep-ph]].

[10] M. Mitra, G. Senjanovic and F. Vissani, Nucl. Phys. B **856**, 26 (2012) [arXiv:1108.0004 [hep-ph]].

[11] M. Mitra, G. Senjanovic and F. Vissani, arXiv:1205.3867 [hep-ph].

[12] F. Vissani and F. Aharonian, Nucl. Instrum. Meth. A **692**, 5 (2012) [arXiv:1112.3911 [astro-ph.HE]].

[13] G. Pagliaroli, C. Lujan-Peschard, M. Mitra and F. Vissani, arXiv:1210.4225 [hep-ph].

[14] M. Mannarelli, C. Manuel and L. Tolos, arXiv:1201.4006 [cond-mat.quant-gas].

[15] M. Mannarelli, C. Manuel and L. Tolos, arXiv:1212.5152 [cond-mat.quant-gas].

Other activity in INFN, University and research organizations

Z. Berezhiani organized the Int. Workshop SW6 "Hot Topics in Modern Cosmology" in Cargese, is coordinator of the L'Aquila unit of PRIN biennal grant 20084ZCK5J-004 "Astroparticle Physics", is scientific Coordinator of the Russian Science and Education Ministry biennial Grant N. 14.U02.21.0913 "Physics of solar, reactor and geo-neutrinos" at JINR, Dubna (2012-2013), teaches Theoretical Physics (Quantum Field Theory), Gauge Theories, Relativity and Cosmology at the University. of L'Aquila, is member of the Doctorate Collegium of the Physics Dept. University of L'Aquila.

V. Berezinsky is a member of Int. Advisory Board of JEM-EUSO. He was a member of Int. Advisory Committees of many conferences.

M. Mannarelli is the scientific secretary of the LNGS and of the CFA and co-organizer of the LNGS seminars, teaches Weak and Strong Interactions II at the University of L'Aquila.

L. Pilo is member of the Doctorate Collegium of the Physics Dept. and of the Doctorate Commission, University of L'Aquila and teaches Weak and Strong Interactions I at the University of L'Aquila.

F.L. Villante is a member of the scientific board of the CFA, has been convener of the "Int. Neutrino Oscillation Workshop (NOW 2012)", of the Nat. Workshop: "Incontri di Fisica delle Alte Energie (IFAE 2012), member of the organizing committee of the Int. Workshop: "The Physics of the Sun and the Solar Neutrinos: 3rd", teaches Astrophysics at the University of L'Aquila.

F. Vissani is co-organizer of the LNGS seminars, observer in Comm.II on behalf of Comm.IV, referee for the INFN National Permanent Committees II on non-accelerator physics and IV on theoretical physics, LNGS representative in the Italian Physics Society, INFN representative in the Scientific Advisory Committee of ApPEC/ASPERA, member of the scientific committee for the ICRANet-INFN agreement, member of the scientific council of the Groupement de Recherche Neutrino (CEA and IN2P3), coordinator of the CFA, lecturer of two PhD neutrino courses, one at the University of Milan and one at the University of Catania.

THE PIERRE AUGER EXPERIMENT

D. Boncioli[a], A. di Matteo[a], A.F. Grillo[b],
S. Petrera[a], V. Rizi[a]
for the Auger Collaboration

[a] INFN and Dipartimento di Fisica, Università dell'Aquila - Italy
[b] LNGS-INFN - Italy

Abstract

The Pierre Auger Project is an international Collaboration involving over 400 scientists from 17 countries, with the objective of studying the highest energy cosmic rays. Recent results from the Collaboration as well as further developments in the detector are presented in this report.

1 Introduction

Ultra-high energy cosmic rays are of intrinsic interest as their origin and nature are unknown. It is quite unclear where and how particles as energetic as $\simeq 10^{20}$ eV are accelerated. Over 40 years ago it was pointed out that if the highest energy particles are protons then a fall in the flux above an energy of about $\times\ 10^{19}$ eV is expected because of energy losses by the protons as they propagate from distant sources through the CMB radiation. At the highest energies the key process is photo-pion production in which the proton loses part of its energy in each creation of a Δ resonance. This is the Greisen-Zatsepin-Kuzmin (GZK) effect. It follows that at 10^{20} eV any proton observed must have come from within about 50 Mpc and on this distance scale the deflections by intervening magnetic fields in the galaxy and intergalactic space are expected to be so small that point sources should be observed. Despite immense efforts in the period since the prediction, the experimental situation remains unclear. The main problem in examining whether or not the spectrum steepens is the low rate of events which, above 10^{20} eV, is less than 1 per km^2 per century so that the particles are only detectable through the giant air showers that they create.

These showers have particle footprints on the ground of $\simeq$ 20 km^2 and suitably distributed detectors can be used to observe them. Also the showers excite molecules of atmospheric nitrogen and the resulting faint fluorescence radiation, which is emitted isotropically, can be detected from distances of several tens of kilometers.

The Pierre Auger Observatory has been developed by a team of over 400 scientists from 17 countries. The Observatory comprises about 1600 10 m$^2\times$ 1.2 m water-Cherenkov

detectors deployed over 3000 km^2 on a 1500 m hexagonal grid. This part of the Observatory (the surface detector, SD) is over-looked by 24 fluorescence telescopes in 4 clusters located on four hills around the SD area which is extremely flat. The surface detectors contain 12 tonnes of clear water viewed by 3 × 9" hemispherical photomultipliers. The fluorescence detectors (FD) are designed to record the faint ultra-violet light emitted as the shower traverses the atmosphere. Each telescope images a portion of the sky of 30° in azimuth and 1°-30° in elevation using a spherical mirror of 3 m^2 effective area to focus light on to a camera of 440 × 18 cm^2 hexagonal pixels, made of photomultipliers complemented with light collectors, each with a field of view of 1.5° diameter.

An important feature of the design of the Observatory was the introduction of the hybrid technique as a new tool to study airshowers. It is used here for the first time. The hybrid technique is the term chosen to describe the method of recording fluorescence data coincident with the timing information from at least one surface detector. Employing these two complementary observation methods provides the Auger Observatory with high quality information about angular reconstruction, determination of the core position of the shower and of the types of particles in the primary cosmic rays. Comparing results from the different types of detectors also helps scientists reconcile the two sets of data and produce the most accurate results about the energy of primary cosmic rays.
During 2012 a substantial effort has started to physically motivate the continuation of data taking beyond 2015 (official date of end of operations of the Observatory) and the proposal of technical improvements which could make this extension possible. This effort will be finalized in definite proposals during 2013.

2 Recent results from the Pierre Auger Cosmic Ray Observatory

The energy spectrum of ultra-high energy cosmic rays at energies greater than 2.5×10^{18} eV has been derived using data from the surface detector array of the Pierre Auger Observatory [1]. The spectrum obtained with the surface detector array, updated using data until the end of December 2010, is combined with the hybrid one to obtain a spectrum measurement over a wide energy range with the highest statistics available and wa updated in [2]. The combined energy spectrum scaled with E^3 is shown in Fig. 1.

The atmospheric depth, X_{max} , at which the longitudinal development of a shower reaches its maximum in terms of the number of secondary particles is correlated with the mass of the incident cosmic ray particle. With the generalization of Heitler's model of electron- photon cascades to hadron-induced showers and the superposition assumption for nuclear primaries of mass A, the average depth of the shower maximum, $\langle X_{max}\rangle$, at a given energy E is expected to follow [3]

$$\langle X_{max}\rangle = \alpha(\ln E - \ln\langle A\rangle) + \beta \tag{1}$$

where $\ln\langle A\rangle$ is the average of the logarithm of the primary masses. The coefficients α and β depend on the nature of hadronic interactions, most notably on the multiplicity, elasticity and cross-section in ultra-high energy collisions of hadrons with air, see e.g. [4].

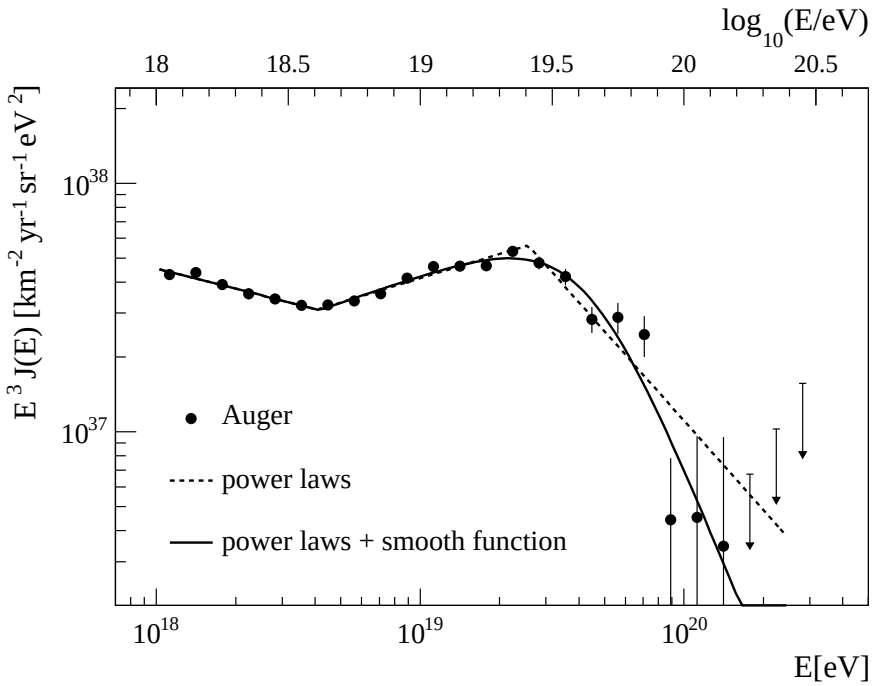

Figure 1: The combined energy spectrum [2] is fitted with two functions (see text). The systematic uncertainty of the flux scaled by E^3 due to the uncertainty of the energy scale of 22% is indicated by arrows.

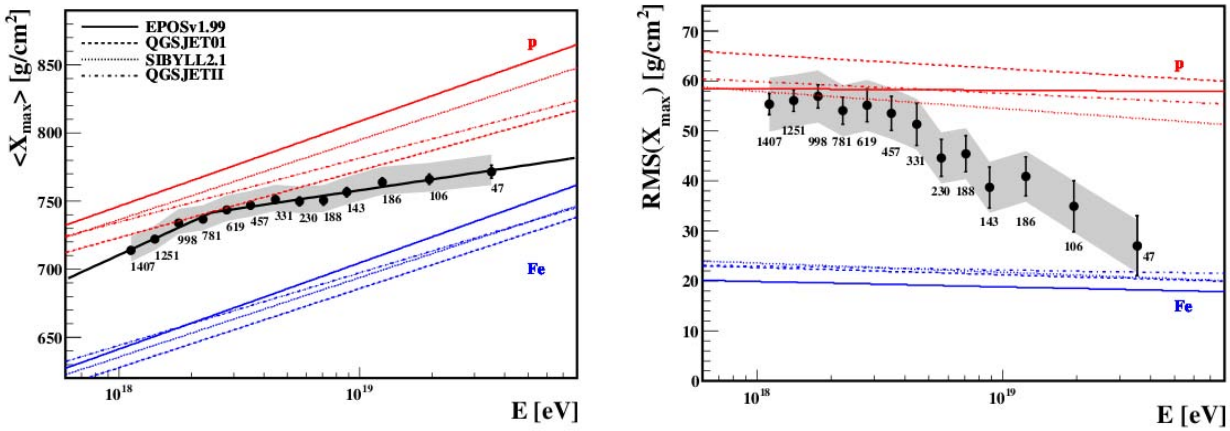

Figure 2: Measurements of X_{max} (left) and its RMS (right) as a function of energy [5].

The results of such measurements were updated in [5] and are reported in Fig. 2.

The shape of the distribution of X_{max} was also analyzed. The tail of the Xmax distribution is sensitive to the proton-air cross-section [12]. The analysis is restricted to the energy interval 10^{18} to $10^{18.5}$ eV, where the shape of the X_{max} distribution is compatible with there being a substantial fraction of protons. The proton-air cross-section is derived in a two-step process. Then we convert the proton-air production cross-section into the total, and the inelastic, proton-proton cross- section using a Glauber calculation that

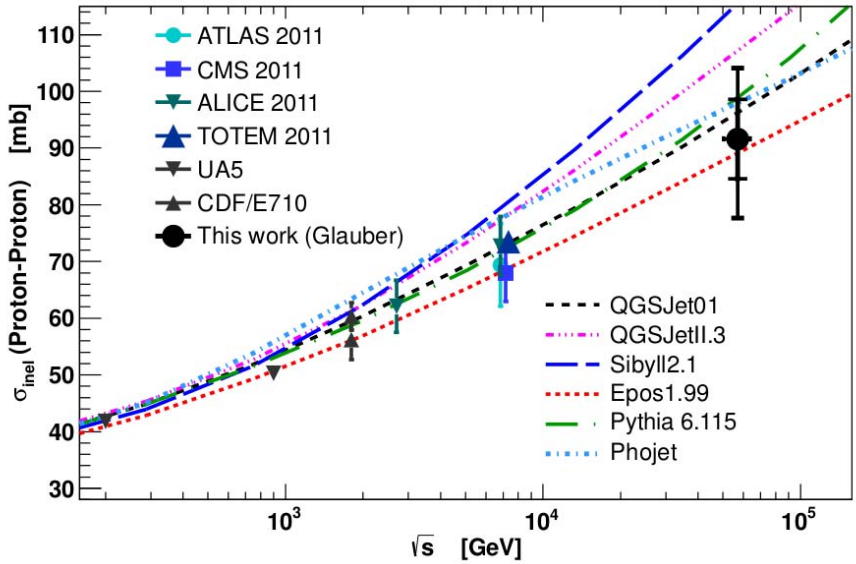

Figure 3: Comparison of derived pp to model predictions and accelerator data [6].

includes intermediate inelastic screening corrections. The corresponding average center-of-mass energy of a proton interacting with a nucleon is 57 TeV, significantly above the reach of the Large Hadron Collider. In Fig. 3 we compare our inelastic cross-section result to accelerator data and to the cross-sections used in the hadronic interaction models.

Between January 2004 and December 2009 the Pierre Auger Observatory has detected 69 cosmic rays events with energy in excess of 55 EeV. Their arrival directions are reported in [7]. This data set is more than twice as large as the one analyzed in [8]. The evidence for anisotropy has not strengthened since the analysis reported in [8].
A knowledge of CR composition is important for deciding which of several source scenarios is more likely. The trajectories of highly charged nuclei are expected to undergo large deflections due to the Galaxy's magnetic fields. While a correlation of arrival directions with nearby matter on small angular scales is plausible for protons above 55 EeV, it is puzzling if the CR are heavy nuclei. If the particles responsible for the measured excesses for example around Centaurus A at E >55 EeV are heavy nuclei with charge Z, the proton component of the sources should lead to excesses in the same regions at energies E/Z. In [9] the lack of anisotropies in the directions of the excesses at energies above E_{th}/Z is reported, setting constraints on the allowed proton fraction at the lower energies.

The study of large scale anisotropies at EeV energies would help in establishing whether the origin of UHECRs is galactic or extragalactic in this energy range. A thorough search for large scale anisotropies in the distribution of arrival directions was developed [10]. Upper limits on dipole and quadrupole amplitudes are derived under the hypothesis that any cosmic ray anisotropy is dominated by such moments in this energy range. These upper limits provide constraints on the production of cosmic rays above 10^{18} eV, since they allow us to challenge an origin from stationary galactic sources densely distributed

in the galactic disk and emitting predominantly light particles in all directions.

A search for ultra-high energy cosmic ray multiplets was performed in the data gathered be- tween 1st January 2004 and 31st December 2010 by the Pierre Auger Observatory with energy above 20 EeV. The largest multiplet found was one 12-plet. The probability that it appears by chance from an isotropic distribution of events is 6%. Thus, there is no significant evidence for the existence of correlated multiplets in the present data set [15].

Although the primary goal of the SD is to detect UHECRs, it can also identify ultra-high energy neutrinos. Neutrinos of all flavours can interact at any atmospheric depth through charged or neutral currents and induce a "downward-going" (DG) shower. In addition, tau neutrinos can undergo charged current interactions in the Earth crust and produce a tau lepton which, after emerging from the Earth surface and decaying in the atmosphere, will induce an "Earth-skimming" (ES) upward-going shower. Even if tau neutrinos are not expected to be produced at the astrophysical source, approximately equal fluxes for each neutrino flavour should reach the Earth as a result of neutrino oscillations over cosmological distances. Neutrino candidate events must be identified against the overwhelming back- ground of showers initiated by standard UHECRs (protons or nuclei) and, in a much smaller proportion, photons. A search has been performed [11] for highly inclined extensive air showers produced by the interaction of neutrinos of all flavours in the atmosphere (downward-going neutrinos), and by the decay of tau leptons originating from tau neutrinos interactions in the Earths crust (Earth-skimming neutrinos). No candidate neutrinos have been found in data up to 2010 May 31. Upper limits on the neutrino flux from point- like sources have been derived as a function of the source declination [11].

2.1 Atmospheric measurements

The light profiles recorded with the fluorescence telescopes must be corrected for UV attenu- ation along light paths of up to 40 km. To estimate the attenuation of light by molecules, aerosols, and clouds, regular atmospheric measurements are performed at the Observatory using UV laser shots, radiosonde launches, optical observations, and cloud measurements in the mid-infrared.
The Global Data Assimilation System (GDAS) is a global atmospheric model predicated on meteorological measurements and numerical weather predictions. GDAS provides altitude-dependent profiles of the main state variables of the atmosphere like temperature, pressure, and humidity. The reconstructions of air showers measured at the Pierre Auger Observatory have used a set of monthly mean profiles as the standard atmospheric description until recently. These profiles are averages from meteorological radio soundings performed at the site of the observatory over several years. The mean profiles describe the local conditions reasonably well, but cannot describe short-term variations in the atmosphere [13].

To provide high-resolution atmospheric data for interesting air showers, we have also implemented an automatic online monitoring system which can be used to trigger dedi-

cated atmospheric mea- surements a few minutes after the air showers are detected. This rapid monitoring trigger was commissioned in early 2009 and has been integrated into the regular monitoring schedules of several of the atmospheric monitoring subsystems.The online reconstruction has produced reliable data which have been used to trigger dedicated observations of the atmosphere [14].

2.2 Radio detection

An intense activity is also going on searching for signals of UHECRs using radio detection methods, both at the VHF (AERA,EASIER) frequencies and microwave (AMBER, MIDAS, FDWave, EASIER).
The emission of electromagnetic radiation from air showers in the MHz frequency regime was first observed by Jelley and co-workers in 1965 [17]. It was found that air showers emit an electromagnetic pulse in the direction of the shower propagation. The observation of the wavefront with an array of individual antennas at different positions with respect to the shower axis should allow a reconstruction of the properties of the air shower and the corresponding primary cosmic ray.
The Auger Engineering Radio Array (AERA) is a radio detector situated at the Pierre Auger Observatory. AERA will instrument a sensitive area of 20 km^2 with 160 detector stations and is thus the first detector with sufficient collecting area to make possible the measurement of radio signals of air showers beyond 10^{18} eV [16].

3 Activity of the L'Aquila - Gran Sasso Group

The group developed a Monte Carlo code (*SimProp*) for the propagation of UHECR Nuclei in extragalactic space during 2011, being this the argument of D. Boncioli PhD thesis (PhD obtained in December 2011). The code is based on the kinetic approach by R. Aloisio et al. [18] and has been developed in collaboration with F. Salamida (now at Paris-Orsay) and R. Aloisio (Arcetri,LNGS). The code has been tested by comparison with results of other Monte Carlo simulations as well as with the results obtained by directly solving the kinetic equation for the propagation of UHECR. The code has been used for the study of physical observables and a paper [19] was published in 2012. The simulation code is also available for downloading upon request to SimProp-dev@aquila.infn.it.

A. di Matteo developed his Thesis during 2012 concerning some enhancements of the original version of *SimProp*: stochastic propagation of protons and the consequent production of photons and neutrinos during the propagation of UHECR Nuclei in extragalactic space.

Outputs of the simulation code *SimProp* have been used for several physical analyses. A global fit strategy of Auger data (spectrum and composition) with respect to the parameters of a basic model of UHECR production by extragalctic sources have been performed. The results are compatible with independent approaches.

A work about the interpretation of the mean depth of cosmic ray air shower maximum and its dispersion has been developed within the l'Aquila-Gran Sasso group [20]. This allows the parametrization of those two observables as functions of the first two moments of the *ln(A)* distribution. The application of the parameterization to Pierre Auger Observatory data allows one to study the energy dependence of the mean $\ln A$ and of its variance under the assumption of selected hadronic interaction models, and in principle it applies to data of any UHECR experiment. This approach has become a full Auger paper, in publication in 2013.

Concerning the activity of atmospheric monitoring, the activity of the group has mainly regarded the analysis of the data taken by the Raman Lidar system in coincidence with a lateral scattering facility in Lamar (Colorado) and the preparation of its final installation in Malargue, which has been cosiderably delayed by custom problems and will be finalized in 2013. This has mainly required dismounting the system in Colorado, the developement of HV power supply and of a standalone acquisition system based on low consumption single board computers.

4 List of Publications

1. P. Abreu *et al.* [Pierre Auger Collaboration], "Constraints on the origin of cosmic rays above 10^{18} eV from large scale anisotropy searches in data of the Pierre Auger Observatory", Astrophys.J. 762 (2012) L13
   arXiv:1212.3083 [astro-ph.HE]

2. P. Abreu *et al.* [Pierre Auger Collaboration], "Results of a self-triggered prototype system for radio-detection of extensive air showers at the Pierre Auger Observatory", JINST 7 (2012) P11023
   arXiv:1211.0572 [astro-ph.HE]

3. P. Abreu *et al.* [Pierre Auger Collaboration], "A search for point sources of EeV neutrons", Astrophys.J. 760 (2012) 148
   arXiv:1211.4901 [astro-ph.HE]

4. P. Abreu *et al.* [Pierre Auger Collaboration], "Large scale distribution of arrival directions of cosmic rays detected above 10^{18} eV at the Pierre Auger Observatory", Astrophys.J.Suppl. 203 (2012) 34
   arXiv:1210.3736 [astro-ph.HE]

5. P. Abreu *et al.* [Pierre Auger Collaboration], "Antennas for the Detection of Radio Emission Pulses from Cosmic-Ray induced Air Showers at the Pierre Auger Observatory", JINST 7 (2012) P10011
   arXiv:1209.3840 [astro-ph.IM]

6. P. Abreu *et al.* [Pierre Auger Collaboration], "Search for point-like sources of ultra-high energy neutrinos at the Pierre Auger Observatory and improved limit on the

diffuse flux of tau neutrinos", Astrophys.J. 755 (2012) L4
arXiv:1210.3143 [astro-ph.HE]

7. P. Abreu *et al.* [Pierre Auger Collaboration], "The Rapid Atmospheric Monitoring System of the Pierre Auger Observatory", JINST 7 (2012) P09001
arXiv:1208.1675 [astro-ph.HE]

8. P. Abreu *et al.* [Pierre Auger Collaboration], "Measurement of the proton-air cross-section at $\sqrt{s} = 57$ TeV with the Pierre Auger Observatory", Phys.Rev.Lett. 109 (2012) 062002
arXiv:1208.1520 [hep-ex]

9. P. Abreu *et al.* [Pierre Auger Collaboration], "A search for anisotropy in the arrival directions of ultra high energy cosmic rays recorded at the Pierre Auger Observatory", JCAP 1204 (2012) 040
arXiv:1210.3602 [astro-ph.HE]

10. P. Abreu *et al.* [Pierre Auger Collaboration], "Description of Atmospheric Conditions at the Pierre Auger Observatory using the Global Data Assimilation System (GDAS)", Astropart.Phys. 35 (2012) 354-361
arXiv:1111.2472 [astro-ph.HE]

11. P. Abreu *et al.* [Pierre Auger Collaboration], "Search for signatures of magnetically-induced alignment in the arrival directions measured by the Pierre Auger Observatory", Astropart.Phys. 35 (2012) 354-361, arXiv:1111.2472 [astro-ph.HE]

12. P. Abreu *et al.* [Pierre Auger Collaboration], "The Lateral Trigger Probability function for the ultra-high energy cosmic ray showers detected by the Pierre Auger Observatory", Astropart.Phys. 35 (2011) 266-276, Erratum-ibid. 35 (2012) 681-684
arXiv:1111.6645 [astro-ph.HE]

References

[1] J.Abraham *et al.* [The Pierre Auger Collaboration], Phys. Lett. **B685**, 239-246 (2010), arXiv:1002.1975 [astro-ph.HE]

[2] F. Salamida for the Pierre Auger Collaboration, Proc. 32th ICRC (Beijing, China) 2011, arXiv:1107.4809.

[3] W. Heitler, Oxford University Press, 1954;
J. Matthews, Astropart. Phys. **22** (2005), 387

[4] T. Wibig, Phys. Rev. D **79**, 094008;
R. Ulrich *et al.* for the Pierre Auger Collaboration, Proc. 32th ICRC (Beijing, China) 2011

[5] P. Facal San Luis *et al.* for the Pierre Auger Collaboration, Proc. 32th ICRC (Beijing, China) 2011

[6] N. Kalmykov and S. Ostapchenko, Phys. Atom. Nucl. 56, 346 (1993).

[7] P.Abreu *et al.* [The Pierre Auger Collaboration], Astropart. Phys. **34**, 314-326 (2010). ([arXiv:1009.1855])

[8] Pierre Auger Collaboration [J. Abraham et al.], Science 318 (2007) 938.
Astropart. Phys. 29 (2008) 188.

[9] Pierre Auger Collaboration [J. Abraham et al.], JCAP 1106 (2011) 022 and arXiv:1106.3048 [astro-ph.HE].

[10] P. Abreu *et al.* [Pierre Auger Collaboration], Astrophys.J. 762 (2012) L13, arXiv:1212.3083 [astro-ph.HE]

[11] P. Abreu *et al.* [Pierre Auger Collaboration], Astrophys.J. 755 (2012) L4, arXiv:1210.3143 [astro-ph.HE]

[12] P. Abreu *et al.* [Pierre Auger Collaboration], Phys.Rev.Lett. 109 (2012) 062002, arXiv:1208.1520 [hep-ex]

[13] P. Abreu *et al.* [Pierre Auger Collaboration], Astropart.Phys. 35 (2012) 354-361, arXiv:1111.2472 [astro-ph.HE]

[14] P. Abreu *et al.* [Pierre Auger Collaboration], JINST 7 (2012) P09001, arXiv:1208.1675 [astro-ph.HE]

[15] P. Abreu *et al.* [Pierre Auger Collaboration], Astropart.Phys. 35 (2012) 354-361, arXiv:1111.2472 [astro-ph.HE]

[16] P. Abreu *et al.* [Pierre Auger Collaboration], JINST 7 (2012) P10011, arXiv:1209.3840 [astro-ph.IM]

[17] J. V. Jelley et al., Nature 205 (1965) 327328.

[18] R. Aloisio, V. Berezinsky and S. Grigorieva, arXiv:0802.4452.
R. Aloisio, V. Berezinsky and S. Grigorieva, arXiv:1006.2484.

[19] R. Aloisio et al., JCAP 1210 (2012) 007, arXiv:1204.2970 [astro-ph.HE]

[20] P. Abreu *et al.* [Pierre Auger Collaboration], JCAP 1302 (2013) 026, arXiv:1301.6637 [astro-ph.HE]

The Pierre Auger Collaboration

P. Abreu[61], M. Aglietta[50], M. Ahlers[91], E.J. Ahn[79], I.F.M. Albuquerque[15], I. Allekotte[1], J. Allen[83], P. Allison[85], A. Almela[11, 8], J. Alvarez Castillo[54], J. Alvarez-Muñiz[72], R. Alves Batista[38], M. Ambrosio[43], A. Aminaei[55], L. Anchordoqui[92], S. Andringa[61], T. Antičić[22], C. Aramo[43], F. Arqueros[69], H. Asorey[1], P. Assis[61], J. Aublin[28], M. Ave[72], M. Avenier[29], G. Avila[10], A.M. Badescu[65], K.B. Barber[12], A.F. Barbosa[13 ‡], R. Bardenet[27], J. Bäuml[33], C. Baus[35], J.J. Beatty[85], K.H. Becker[32], A. Bellétoile[31], J.A. Bellido[12], S. BenZvi[91], C. Berat[29], X. Bertou[1], P.L. Biermann[36], P. Billoir[28], F. Blanco[69], M. Blanco[28], C. Bleve[32], H. Blümer[35, 33], M. Boháčová[24], D. Boncioli[44], C. Bonifazi[20], R. Bonino[50], N. Borodai[59], J. Brack[77], I. Brancus[62], P. Brogueira[61], W.C. Brown[78], P. Buchholz[39], A. Bueno[71], L. Buroker[92], R.E. Burton[75], M. Buscemi[43], K.S. Caballero-Mora[72, 86], B. Caccianiga[42], L. Caccianiga[28], L. Caramete[36], R. Caruso[45], A. Castellina[50], G. Cataldi[47], L. Cazon[61], R. Cester[46], S.H. Cheng[86], A. Chiavassa[50], J.A. Chinellato[16], J. Chudoba[24], M. Cilmo[43], R.W. Clay[12], G. Cocciolo[47], R. Colalillo[43], L. Collica[42], M.R. Coluccia[47], R. Conceição[61], F. Contreras[9], H. Cook[73], M.J. Cooper[12], S. Coutu[86], C.E. Covault[75], A. Criss[86], J. Cronin[87], A. Curutiu[36], R. Dallier[31, 30], B. Daniel[16], S. Dasso[5, 3], K. Daumiller[33], B.R. Dawson[12], R.M. de Almeida[21], M. De Domenico[45], S.J. de Jong[55, 57], G. De La Vega[7], W.J.M. de Mello Junior[16], J.R.T. de Mello Neto[20], I. De Mitri[47], V. de Souza[14], K.D. de Vries[56], L. del Peral[70], O. Deligny[26], H. Dembinski[33], N. Dhital[82], C. Di Giulio[44], J.C. Diaz[82], M.L. Díaz Castro[13], P.N. Diep[93], F. Diogo[61], C. Dobrigkeit [16], W. Docters[56], J.C. D'Olivo[54], P.N. Dong[93, 26], A. Dorofeev[77], J.C. dos Anjos[13], M.T. Dova[4], D. D'Urso[43], J. Ebr[24], R. Engel[33], M. Erdmann[37], C.O. Escobar[79, 16], J. Espadanal[61], A. Etchegoyen[8, 11], P. Facal San Luis[87], H. Falcke[55, 58, 57], K. Fang[87], G. Farrar[83], A.C. Fauth[16], N. Fazzini[79], A.P. Ferguson[75], B. Fick[82], J.M. Figueira[8, 33], A. Filevich[8], A. Filipčič[66, 67], S. Fliescher[37], B.D. Fox[88], C.E. Fracchiolla[77], E.D. Fraenkel[56], O. Fratu[65], U. Fröhlich[39], B. Fuchs[35], R. Gaior[28], R.F. Gamarra[8], S. Gambetta[40], B. García[7], S.T. Garcia Roca[72], D. Garcia-Gamez[27], D. Garcia-Pinto[69], G. Garilli[45], A. Gascon Bravo[71], H. Gemmeke[34], P.L. Ghia[28], M. Giller[60], J. Gitto[7], C. Glaser[37], H. Glass[79], G. Golup[1], F. Gomez Albarracin[4], M. Gómez Berisso[1], P.F. Gómez Vitale[10], P. Gonçalves[61], J.G. Gonzalez[35], B. Gookin[77], A. Gorgi[50], P. Gorham[88], P. Gouffon[15], S. Grebe[55, 57], N. Griffith[85], A.F. Grillo[49], T.D. Grubb[12], Y. Guardincerri[3], F. Guarino[43], G.P. Guedes[17], P. Hansen[4], D. Harari[1], T.A. Harrison[12], J.L. Harton[77], A. Haungs[33], T. Hebbeker[37], D. Heck[33], A.E. Herve[12], G.C. Hill[12], C. Hojvat[79], N. Hollon[87], V.C. Holmes[12], P. Homola[39, 59], J.R. Hörandel[55, 57], P. Horvath[25], M. Hrabovský[25, 24], D. Huber[35], T. Huege[33], A. Insolia[45], S. Jansen[55, 57], C. Jarne[4], M. Josebachuili[8, 33], K. Kadija[22], O. Kambeitz[35], K.H. Kampert[32], P. Karhan[23], P. Kasper[79], I. Katkov[35], B. Kégl[27], B. Keilhauer[33], A. Keivani[81], J.L. Kelley[55], E. Kemp[16], R.M. Kieckhafer[82], H.O. Klages[33], M. Kleifges[34], J. Kleinfeller[9, 33], J. Knapp[73], R. Krause[37], N. Krohm[32], O. Krömer[34], D. Kruppke-Hansen[32], D. Kuempel[37], N. Kunka[34], G. La Rosa[48], D. LaHurd[75], L. Latronico[50], R. Lauer[90], M. Lauscher[37], P. Lautridou[31], S. Le Coz[29], M.S.A.B. Leão[19], D. Lebrun[29], P. Lebrun[79], M.A. Leigui de Oliveira[19], A. Letessier-Selvon[28], I. Lhenry-Yvon[26], K. Link[35], R. López[51], A. Lopez Agüera[72], K. Louedec[29, 27], J. Lozano Bahilo[71], L. Lu[73], A. Lucero[8, 50], M. Ludwig[35], H. Lyberis[20], M.C. Maccarone[48], C. Macolino[28], M. Malacari[12], S. Maldera[50], J. Maller[31], D. Mandat[24], P. Mantsch[79],

A.G. Mariazzi[4], J. Marin[9, 50], V. Marin[31], I.C. Mariş[28], H.R. Marquez Falcon[53], G. Marsella[47], D. Martello[47], L. Martin[31, 30], H. Martinez[52], O. Martínez Bravo[51], D. Martraire[26], J.J. Masías Meza[3], H.J. Mathes[33], J. Matthews[81], J.A.J. Matthews[90], G. Matthiae[44], D. Maurel[33], D. Maurizio[13], E. Mayotte[76], P.O. Mazur[79], G. Medina-Tanco[54], M. Melissas[35], D. Melo[8], E. Menichetti[46], A. Menshikov[34], S. Messina[56], R. Meyhandan[88], S. Mićanović[22], M.I. Micheletti[6], L. Middendorf[37], I.A. Minaya[69], L. Miramonti[42], B. Mitrica[62], L. Molina-Bueno[71], S. Mollerach[1], M. Monasor[87], D. Monnier Ragaigne[27], F. Montanet[29], B. Morales[54], C. Morello[50], J.C. Moreno[4], M. Mostafá[77], C.A. Moura[19], M.A. Muller[16], G. Müller[37], M. Münchmeyer[28], R. Mussa[46], G. Navarra[50 ‡], J.L. Navarro[71], S. Navas[71], P. Necesal[24], L. Nellen[54], A. Nelles[55, 57], J. Neuser[32], P.T. Nhung[93], M. Niechciol[39], L. Niemietz[32], N. Nierstenhoefer[32], T. Niggemann[37], D. Nitz[82], D. Nosek[23], L. Nožka[24], J. Oehlschläger[33], A. Olinto[87], M. Oliveira[61], M. Ortiz[69], N. Pacheco[70], D. Pakk Selmi-Dei[16], M. Palatka[24], J. Pallotta[2], N. Palmieri[35], G. Parente[72], A. Parra[72], S. Pastor[68], T. Paul[92, 84], M. Pech[24], J. Pękala[59], R. Pelayo[51], I.M. Pepe[18], L. Perrone[47], R. Pesce[40], E. Petermann[89], S. Petrera[41], A. Petrolini[40], Y. Petrov[77], C. Pfendner[91], R. Piegaia[3], T. Pierog[33], P. Pieroni[3], M. Pimenta[61], V. Pirronello[45], M. Platino[8], M. Plum[37], V.H. Ponce[1], M. Pontz[39], A. Porcelli[33], P. Privitera[87], M. Prouza[24], E.J. Quel[2], S. Querchfeld[32], S. Quinn[75], J. Rautenberg[32], O. Ravel[31], D. Ravignani[8], B. Revenu[31], J. Ridky[24], S. Riggi[48, 72], M. Risse[39], P. Ristori[2], H. Rivera[42], V. Rizi[41], J. Roberts[83], W. Rodrigues de Carvalho[72], I. Rodriguez Cabo[72], G. Rodriguez Fernandez[44, 72], J. Rodriguez Martino[9], J. Rodriguez Rojo[9], M.D. Rodríguez-Frías[70], G. Ros[70], J. Rosado[69], T. Rossler[25], M. Roth[33], B. Rouillé-d'Orfeuil[87], E. Roulet[1], A.C. Rovero[5], C. Rühle[34], S.J. Saffi[12], A. Saftoiu[62], F. Salamida[26], H. Salazar[51], F. Salesa Greus[77], G. Salina[44], F. Sánchez[8], C.E. Santo[61], E. Santos[61], E.M. Santos[20], F. Sarazin[76], B. Sarkar[32], R. Sato[9], N. Scharf[37], V. Scherini[42], H. Schieler[33], P. Schiffer[38], A. Schmidt[34], O. Scholten[56], H. Schoorlemmer[55, 57], P. Schovánek[24], F.G. Schröder[33, 8], A. Schulz[33], J. Schulz[55], S.J. Sciutto[4], M. Scuderi[45], A. Segreto[48], M. Settimo[39, 47], A. Shadkam[81], R.C. Shellard[13], I. Sidelnik[1], G. Sigl[38], O. Sima[64], A. Śmiałkowski[60], R. Šmída[33], G.R. Snow[89], P. Sommers[86], J. Sorokin[12], H. Spinka[74, 79], R. Squartini[9], Y.N. Srivastava[84], S. Stanič[67], J. Stapleton[85], J. Stasielak[59], M. Stephan[37], M. Straub[37], A. Stutz[29], F. Suarez[8], T. Suomijärvi[26], A.D. Supanitsky[5], T. Šuša[22], M.S. Sutherland[81], J. Swain[84], Z. Szadkowski[60], M. Szuba[33], A. Tapia[8], M. Tartare[29], O. Taşcău[32], R. Tcaciuc[39], N.T. Thao[93], D. Thomas[77], J. Tiffenberg[3], C. Timmermans[57, 55], W. Tkaczyk[60 ‡], C.J. Todero Peixoto[14], G. Toma[62], L. Tomankova[33], B. Tomé[61], A. Tonachini[46], G. Torralba Elipe[72], D. Torres Machado[31], P. Travnicek[24], D.B. Tridapalli[15], E. Trovato[45], M. Tueros[72], R. Ulrich[33], M. Unger[33], M. Urban[27], J.F. Valdés Galicia[54], I. Valiño[72], L. Valore[43], G. van Aar[55], A.M. van den Berg[56], S. van Velzen[55], A. van Vliet[38], E. Varela[51], B. Vargas Cárdenas[54], G. Varner[88], J.R. Vázquez[69], R.A. Vázquez[72], D. Veberič[67, 66], V. Verzi[44], J. Vicha[24], M. Videla[7], L. Villaseñor[53], H. Wahlberg[4], P. Wahrlich[12], O. Wainberg[8, 11], D. Walz[37], A.A. Watson[73], M. Weber[34], K. Weidenhaupt[37], A. Weindl[33], F. Werner[33], S. Westerhoff[91], B.J. Whelan[86], A. Widom[84], G. Wieczorek[60], L. Wiencke[76], B. Wilczyńska[59 ‡], H. Wilczyński[59], M. Will[33], C. Williams[87], T. Winchen[37], B. Wundheiler[8], S. Wykes[55], T. Yamamoto[87 a], T. Yapici[82], P. Younk[80], G. Yuan[81], A. Yushkov[72], B. Zamorano[71], E. Zas[72], D. Zavrtanik[67, 66], M. Zavrtanik[66, 67], I. Zaw[83 d], A. Zepeda[52 b], J. Zhou[87], Y. Zhu[34], M. Zimbres Silva[32, 16], M. Ziolkowski[39]

[1] Centro Atómico Bariloche and Instituto Balseiro (CNEA-UNCuyo-CONICET), San Carlos de Bariloche, Argentina

[2] Centro de Investigaciones en Láseres y Aplicaciones, CITEDEF and CONICET, Ar-

gentina
[3] Departamento de Física, FCEyN, Universidad de Buenos Aires y CONICET, Argentina
[4] IFLP, Universidad Nacional de La Plata and CONICET, La Plata, Argentina
[5] Instituto de Astronomía y Física del Espacio (CONICET-UBA), Buenos Aires, Argentina
[6] Instituto de Física de Rosario (IFIR) - CONICET/U.N.R. and Facultad de Ciencias Bioquímicas y Farmacéuticas U.N.R., Rosario, Argentina
[7] Instituto de Tecnologías en Detección y Astropartículas (CNEA, CONICET, UNSAM), and National Technological University, Faculty Mendoza (CONICET/CNEA), Mendoza, Argentina
[8] Instituto de Tecnologías en Detección y Astropartículas (CNEA, CONICET, UNSAM), Buenos Aires, Argentina
[9] Observatorio Pierre Auger, Malargüe, Argentina
[10] Observatorio Pierre Auger and Comisión Nacional de Energía Atómica, Malargüe, Argentina
[11] Universidad Tecnológica Nacional - Facultad Regional Buenos Aires, Buenos Aires, Argentina
[12] University of Adelaide, Adelaide, S.A., Australia
[13] Centro Brasileiro de Pesquisas Fisicas, Rio de Janeiro, RJ, Brazil
[14] Universidade de São Paulo, Instituto de Física, São Carlos, SP, Brazil
[15] Universidade de São Paulo, Instituto de Física, São Paulo, SP, Brazil
[16] Universidade Estadual de Campinas, IFGW, Campinas, SP, Brazil
[17] Universidade Estadual de Feira de Santana, Brazil
[18] Universidade Federal da Bahia, Salvador, BA, Brazil
[19] Universidade Federal do ABC, Santo André, SP, Brazil
[20] Universidade Federal do Rio de Janeiro, Instituto de Física, Rio de Janeiro, RJ, Brazil
[21] Universidade Federal Fluminense, EEIMVR, Volta Redonda, RJ, Brazil
[22] Rudjer Bošković Institute, 10000 Zagreb, Croatia
[23] Charles University, Faculty of Mathematics and Physics, Institute of Particle and Nuclear Physics, Prague, Czech Republic
[24] Institute of Physics of the Academy of Sciences of the Czech Republic, Prague, Czech Republic
[25] Palacky University, RCPTM, Olomouc, Czech Republic
[26] Institut de Physique Nucléaire d'Orsay (IPNO), Université Paris 11, CNRS-IN2P3, Orsay, France
[27] Laboratoire de l'Accélérateur Linéaire (LAL), Université Paris 11, CNRS-IN2P3, France
[28] Laboratoire de Physique Nucléaire et de Hautes Energies (LPNHE), Universités Paris 6 et Paris 7, CNRS-IN2P3, Paris, France
[29] Laboratoire de Physique Subatomique et de Cosmologie (LPSC), Université Joseph Fourier Grenoble, CNRS-IN2P3, Grenoble INP, France
[30] Station de Radioastronomie de Nançay, Observatoire de Paris, CNRS/INSU, France
[31] SUBATECH, École des Mines de Nantes, CNRS-IN2P3, Université de Nantes, France
[32] Bergische Universität Wuppertal, Wuppertal, Germany
[33] Karlsruhe Institute of Technology - Campus North - Institut für Kernphysik, Karlsruhe, Germany

[34] Karlsruhe Institute of Technology - Campus North - Institut für Prozessdatenverarbeitung und Elektronik, Karlsruhe, Germany
[35] Karlsruhe Institute of Technology - Campus South - Institut für Experimentelle Kernphysik (IEKP), Karlsruhe, Germany
[36] Max-Planck-Institut für Radioastronomie, Bonn, Germany
[37] RWTH Aachen University, III. Physikalisches Institut A, Aachen, Germany
[38] Universität Hamburg, Hamburg, Germany
[39] Universität Siegen, Siegen, Germany
[40] Dipartimento di Fisica dell'Università and INFN, Genova, Italy
[41] Università dell'Aquila and INFN, L'Aquila, Italy
[42] Università di Milano and Sezione INFN, Milan, Italy
[43] Università di Napoli "Federico II" and Sezione INFN, Napoli, Italy
[44] Università di Roma II "Tor Vergata" and Sezione INFN, Roma, Italy
[45] Università di Catania and Sezione INFN, Catania, Italy
[46] Università di Torino and Sezione INFN, Torino, Italy
[47] Dipartimento di Matematica e Fisica "E. De Giorgi" dell'Università del Salento and Sezione INFN, Lecce, Italy
[48] Istituto di Astrofisica Spaziale e Fisica Cosmica di Palermo (INAF), Palermo, Italy
[49] INFN, Laboratori Nazionali del Gran Sasso, Assergi (L'Aquila), Italy
[50] Osservatorio Astrofisico di Torino (INAF), Università di Torino and Sezione INFN, Torino, Italy
[51] Benemérita Universidad Autónoma de Puebla, Puebla, Mexico
[52] Centro de Investigación y de Estudios Avanzados del IPN (CINVESTAV), México, Mexico
[53] Universidad Michoacana de San Nicolas de Hidalgo, Morelia, Michoacan, Mexico
[54] Universidad Nacional Autonoma de Mexico, Mexico, D.F., Mexico
[55] IMAPP, Radboud University Nijmegen, Netherlands
[56] Kernfysisch Versneller Instituut, University of Groningen, Groningen, Netherlands
[57] Nikhef, Science Park, Amsterdam, Netherlands
[58] ASTRON, Dwingeloo, Netherlands
[59] Institute of Nuclear Physics PAN, Krakow, Poland
[60] University of Łódź, Łódź, Poland
[61] LIP and Instituto Superior Técnico, Technical University of Lisbon, Portugal
[62] 'Horia Hulubei' National Institute for Physics and Nuclear Engineering, Bucharest-Magurele, Romania
[64] University of Bucharest, Physics Department, Romania
[65] University Politehnica of Bucharest, Romania
[66] J. Stefan Institute, Ljubljana, Slovenia
[67] Laboratory for Astroparticle Physics, University of Nova Gorica, Slovenia
[68] Institut de Física Corpuscular, CSIC-Universitat de València, Valencia, Spain
[69] Universidad Complutense de Madrid, Madrid, Spain
[70] Universidad de Alcalá, Alcalá de Henares (Madrid), Spain
[71] Universidad de Granada and C.A.F.P.E., Granada, Spain
[72] Universidad de Santiago de Compostela, Spain
[73] School of Physics and Astronomy, University of Leeds, United Kingdom

[74] Argonne National Laboratory, Argonne, IL, USA
[75] Case Western Reserve University, Cleveland, OH, USA
[76] Colorado School of Mines, Golden, CO, USA
[77] Colorado State University, Fort Collins, CO, USA
[78] Colorado State University, Pueblo, CO, USA
[79] Fermilab, Batavia, IL, USA
[80] Los Alamos National Laboratory, Los Alamos, NM, USA
[81] Louisiana State University, Baton Rouge, LA, USA
[82] Michigan Technological University, Houghton, MI, USA
[83] New York University, New York, NY, USA
[84] Northeastern University, Boston, MA, USA
[85] Ohio State University, Columbus, OH, USA
[86] Pennsylvania State University, University Park, PA, USA
[87] University of Chicago, Enrico Fermi Institute, Chicago, IL, USA
[88] University of Hawaii, Honolulu, HI, USA
[89] University of Nebraska, Lincoln, NE, USA
[90] University of New Mexico, Albuquerque, NM, USA
[91] University of Wisconsin, Madison, WI, USA
[92] University of Wisconsin, Milwaukee, WI, USA
[93] Institute for Nuclear Science and Technology (INST), Hanoi, Vietnam

(‡) Deceased
(a) Now at Konan University
(b) Also at the Universidad Autonoma de Chiapas on leave of absence from Cinvestav
(d) Now at NYU Abu Dhabi

Cosmic Silence

L. Satta[d], D. Capece[a], E. Fratini[a], G. Simone[a], M.A. Tabocchini[a], M. Balata[c], L. Ioannucci[c]

[a] Museo Storico della Fisica e Centro Studi e Ricerche Enrico Fermi, Italy
[b] Ist. Sup. di Sanità, Techn. and Health Dep., and INFN-Roma 1 Gr. coll. Sanità, Italy
[c] INFN - Gran Sasso National Laboratory, Italy
[d] INFN - Frascati National Laboratory, Italy

1 Introduction

Life has evolved on Earth for 3 billion years in the presence of a daily stimulus of ultra-low dose of environmental radiation. Such condition has been "incorporated" in the biology of living organisms that have developed defense mechanisms well preserved during phylogenies. A question arises as to whether the biochemical behavior of living organisms would differ in the absence of radiation (Yang, 1994). To address this scientific question, an ideal experimental design would consist in the twin set-up of a cell or animal culture in a laboratory where environmental radiation is reduced as low as possible, and in a reference laboratory at "reference" environmental level. Using a number of experimental assays, the experimenter would look for the appearance of any differential response in the biological model between the two laboratories. The Gran Sasso National Laboratory (LNGS) of the Istituto Nazionale di Fisica Nucleare (INFN), located under the Gran Sasso d'Italia mountain, offers a unique opportunity to investigate whether a significant reduction in the environmental radiation can change the susceptibility to acute exposures to genotoxic agents. The cover of at least 1400 m of rock gives an excellent shielding against cosmic rays and neutrons. As a matter of fact, cosmic rays are reduced by a factor of 106 [as reported for instance in: The MACRO Collaboration, 1990] and neutrons by a factor of 103 [Rindi et, 1988; Belli et al, 1989]. Our previous works [Satta et al 1995, Satta et al 2002, Carbone et al 2009] on the influence of different environmental radiation have indicated that cell cultures maintained under low radiation environment (LRE) developed a different biochemical behaviour, compared to the cultures in reference radiation environment (RRE). In particular, cells cultured in a low radiation environment (underground LNGS laboratory) are less preserved from DNA damage, induced by chemical and physical agents, and show a reduced Reactive Oxigen Species (ROS) scavenging power. Cosmic Silence Project aim to study exhaustively the biochemical behaviour of living organisms in a reduced radiation environment by means of a very sensitive model.

The reported data are obtained with the hybridoma cell line A11 obtained from a pKZ1 splenocyte harboring the pKZ1 inversion cassette [Hooker et al 2002]. These experiments will define the sensitivity and reproducibility of the assay based on pKZ1 inversion after exposure to environmental radiation in "cosmic silence (underground at LNGS) or in reference conditions (at the ISS in Rome).

2 pKZ1 chromosomal inversion assay

The pKZ1 intrachromosomal recombination assay [Matsuoka et al 1991] is an extremely sensitive assay for studying responses to low doses of DNA damaging agents. After cells are treated with a DNA damaging agent, are examined for cells in which inversions have occurred in the transgene (E. coli lacZ gene) using histochemical staining of transgene (E. coli β-galactosidase) marker expression (Fig. 1). The pKZ1 DNA construct contains an E. coli lacZ reporter transgene in inverse orientation to a chicken β-actin enhancer/promoter (EP) complex (Figure 1, upper part). If DNA recombination is induced, the lacZ gene reorients using V(D)J recombination signals Vk21c and Jk5 to the correct transcriptional orientation with respect to the promoter (Figure 1, lower part). The messenger RNA is therefore appropriately spliced, and a functional gene product can be detected using the chromogenic substrate stain X-gal, which stains blue.

3 Results

The A11 cell line and its clone Pos (at high inversion frequency of the gene pKZ1), kindly donated by Professor Pamela Sykes, Flinders University, Adelaide, Australia, were cultured in parallel at the ISS (reference radiation environment, RRE) and at the LNGS underground laboratory (low radiation environment, LRE). It has been measured: cellular growth, pKZ1 gene inversion, PARP (Poli (ADP-ribose) polymerase) expression, expression of enzymes involved in ROS (Reactive Oxygen Species) scavenging. Cellular growth has been analyzed with cytofluorimetry analysis: cells kept for 1 month in a low radiation environment show a significant increase in the G2-S phase respect to cells kept at reference radiation environment. On the contrary, after 1 month of culture, it has not been found a significant difference in the pKZ1 chromosomal inversion assay between the cells kept at low or at reduced environmental radiation in both cell line (A11 and Pos). One important function of PARP is assisting in the repair of single-strand DNA nicks, and is inactivated by caspase cleavage. It is believed that normal inactivation occurs in systems where DNA damage is extensive and cells go through programmed cell death. Our preliminary data on Western Blot analysis have shown that A11 cells kept for 1 month at LRE do not show PARP expression. Superoxide dismutase (SOD), catalase (CAT), and glutathione peroxidase (GPx) enzymatic activities has been analyzed with real time PCR (polymerase chain reaction). These enzymes are involved in ROS scavenging. For GPx the four isoforms (GPx1, GPx2, GPx3 and GPx4) have been analyzed. It has been found that the enzymatic expression after 1 month of culture is less in cells kept at LRE respect to cells kept at RRE. Particularly interesting are the data on GPx4,

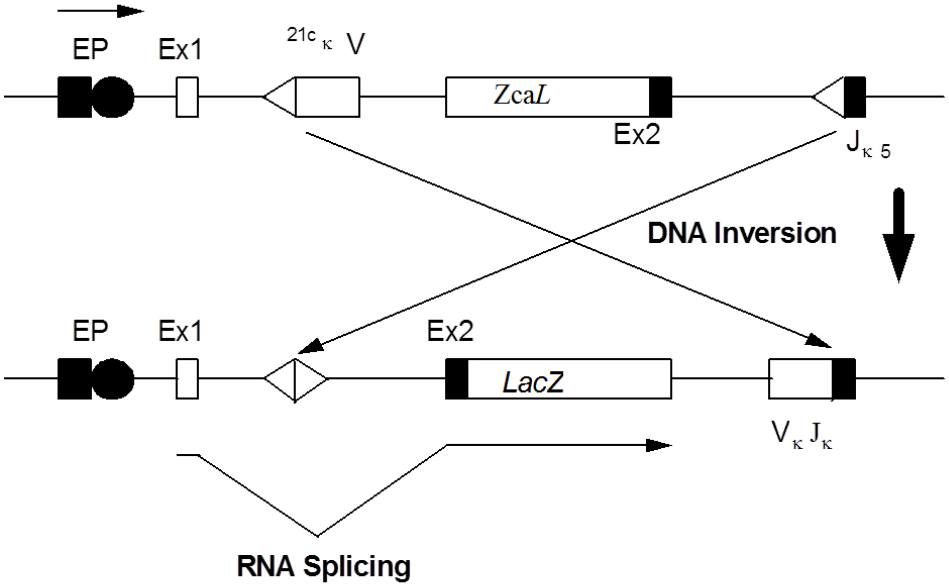

Figure 1: Diagram of the pKZ1 transgene, adapted from (7). LacZ = E.coli β-galactosidase gene in inverse orientation (upper part of figure) with respect to EP (chicken β-actin promoter complex). Vk21c and Jk5 are mouse immunoglobulin recombination signal sequences. Ex1 and Ex2 are chicken -actin exon1 and exon2 splice sites. When an inversion event occurs (lower part of figure) the LacZ gene is now in the correct transcriptional orientation and the message is appropriately spliced.

being this isoform involved in the regulation of the phospholipids oxidation and in one of the apoptosis mechanism.

4 Final Remark

Although the results obtained (and briefly described in the preceding paragraphs) with the A11 transgenic cell line are very promising, one should always keep in mind that there is still a long way to go before reaching the necessary understanding, both experimental and theoretical, of the effects of interactions between background radiation and living matter.

5 Acknowledgements

We are indebted with Dr. M. Belli for the interesting discussions and suggestions through the experiment.

References

[1] Belli P, Bernabei R, D'Angelo S, De Pascale M, Paoluzi L, Santonico R, et al. *Deep underground neutron flux measurement with large BF3 counters.* Nuovo Cimento A (1989) 101:959-966.

[2] Carbone M. C., Pinto M., Antonelli F., Amicarelli F., Balata M., Belli M., Conti Devirgiliis L., Ioannucci L., Nisi S., Sapora O., et al (2009) *The Cosmic Silence Experiment: on the putative adaptive role of environmental ionizing radiation.* Radiat. Environ. Biophys. 48:189-196

[3] Hooker A M, Home R, Morley A A, Sykes P J, (2002) *Dose-dependent increase or decrease of somatic intrachromosomal recombination produced by etoposide.* Mut. Res. 500, 117-124.

[4] The MACRO Collaboration (1990) *Study of penetrating cosmic ray muons and search for large scale anisotropies at the Gran Sasso Laboratory.* Phys Lett B 249:149 - 156

[5] Matsuoka M, Nagawa F, Okazaki K, Kingsbury L, Yoshida K, Muller U, Larue D T, Winer J A, Sakano H, (1991) *Detection of somatic DNA recombination in the transgenic mouse brain.* Science 254, 81-86

[6] Rindi A, Celani F, Lindozzi M, Miozzi S. *Underground neutron flux measurement.* Nucl Inst Meth A (1998)272:871-874

[7] Satta L, Augusti-Tocco G, Ceccarelli R, Esposito A, Fiore M, Paggi P, Poggesi I, Ricordy R, Scarsella G, Cundari E. *Low environmental radiation background impairs biological defence of the yeast Saccharomyces cerevisiae to chemical radiomimetic agents.* Mutat Res (1995) 347 (3-4):129-33

[8] Satta L, Antonelli F, Belli M, Sapora O, Simone G, Sorrentino E, Tabocchini MA, Amicarelli F, Ara C, Cer MP, Colafarina S, Conti Devirgiliis L, De Marco A, Balata M, Falgiani A, Nisi S. *Influence of a low background radiation environment on biochemical and biological responses in V79 cells.* Radiat. Environ. Biophys. (2002) 41 (3):217-24

ERMES
Uranium and tritium groundwater monitoring at INFN-LNGS

W. Plastino[a,b],M. Balata[c], F. Bella[a],A. Cardarelli[c], M. Ciarletti[a,b], L. Copia[a,b], M. De Deo[c], L. Ioannucci[c], S. Nisi[c], G. F. Panza[d,e], A. Peresan[d,e], P. P. Povinec[f]

[a] Dept. of Mathematics and Physics, University of Roma Tre, I-00146 Rome, Italy
[b] INFN, Section of Roma Tre, I-00146 Rome, Italy
[c] INFN, Gran Sasso National Laboratory,I-67010 Assergi (AQ), Italy
[d] Dept. of Mathematics and Geosciences, University of Trieste, Trieste, Italy
[e] Abdus Salam International Centre for Theoretical Physics, Trieste, Italy
[f] Dept. of Nuclear Physics and Biophysics, Comenius University, Bratislava, Slovakia

Abstract

Uranium groundwater anomalies, which were observed in cataclastic rocks crossing the underground Gran Sasso National Laboratory before the L'Aquila earthquake (April 6^{th}, 2009), have been studied versus tritium contents. The radionuclide analysis supports the role of endogenic fluid dynamics for uranium content in groundwater rather than percolation processes, due to meteoric events occurring above the water table of the Gran Sasso aquifer. The uranium anomalies represent a key geochemical signal of a progressive increase of deep fluids fluxes at middle-lower crustal levels associated with the geodynamics of the earthquake. Moreover, the uranium represents a more precise strain-meter than radon as its presence can be modulated during the preparation phase of the earthquake, and only successively released by microfracturing during the main shock and aftershocks.

1 Introduction

Uranium has been frequently analyzed in groundwater, however, mostly for radioecological purposes, or for studying groundwater characteristics [1, 3]. Within the framework of the National Institute of Nuclear Physics (INFN) project Environmental Radioactivity Monitoring for Earth Sciences (ERMES), environmental radioactivity measurements have been carried out inside the Gran Sasso National Laboratory (INFN-LNGS), specifically for radon [4, 5], radiocarbon [6], tritium [7] and later also uranium [8, 10]. These

measurements confirmed different chemical-physical and fluid dynamical characteristics of groundwater. The uranium groundwater monitoring was included in the project with the aim to study possible pattern for radon sources in groundwater. Moreover, uranium was tested as a potential strain indicator of geodynamic processes occurring before an earthquake, rather than the consolidated scheme for radon release due to stress-strain processes in rocks [8, 9].

2 Experimental

Groundwater samples were collected weekly in four sites located inside the LNGS-INFN. They were taken from pipes inserted into the rock up to a depth ranging from 3 m to 6 m. Collected groundwater sample was stored in 1l cleaned polyethylene bottles, after 5 min of water flushing at maximum flow. The analysis has been primarily carried out at site E3dx, because this is the nearest site to cataclastic rocks, as well as for a better characterization of water-rock interactions through the main overthrust fault, which separates water masses belonging to two distinct flow paths [8].

Tritium measurements of the groundwater samples collected at site E3dx were carried out by liquid scintillation counting of electrolytically pre-enriched samples in order to improve the sensitivity of the analysis [7, 11]. The enrichment procedure consisted of the primary distillation, an electrolytic run, the neutralization, a secondary distillation and the final preparation of the scintillation mixture [12, 13]. The first distillation of the samples removed impurities and allowed obtaining negligible conductivity. In order to avoid isotopic fractionation the distillation was brought to dryness. Subsequently 1.5 g of Na_2O_2 was dissolved in each distilled sample in order to homogenize the conductivity and to permit electrolysis. The enrichment run took place in a batch of twenty almost identical cells, each equipped with a stainless steel anode and an iron cathode. Each cell was filled with 500 ml of groundwater sample. The cells were put in a refrigerator, (operating temperature - 2 ℃) in order to control and to minimize evaporation loses during the run. The value of the total charge for reducing the starting mass from 500 g to about 16 g was typically 2.95 Ah g^{-1}. A LabVIEW program was developed to control current and voltage levels, and to check the temperature in the refrigerator. An external alarm was set to switch off the current supply in case of a sudden rise in the temperature.

In order to avoid damaging of the glassware, a neutralization of the samples by adding CO_2 and adjusting the pH of the samples to 7-8 was carried out in advance of the second distillation. This method increased the tritium recovery converting the hydrogen of NaOH into water. During the second distillation, when the tritium level (especially in the spikes) was quite high, it was fundamental to provide hydraulic guards in order to avoid cross contamination between blanks, samples and spikes. Then, 10 ml of the enriched sample were mixed with 10 ml of scintillation cocktail (Ultima Gold LLT®) in 20 ml PE, shaking each vial by hand, and counting in the Wallac 1220 Quantulus liquid scintillation spectrometer (LSS) located in the INFN-LNGS [14]. A typical run consisted of two tritium standards, two background water samples, two spiked samples before the enrichment, two blank water samples (background water that has gone through the whole enrichment procedure), three enriched spike samples and 15 unknown groundwater samples [13]. The

LSS has a thermostatic system to keep the samples at a constant temperature in order to avoid variations in the efficiency of LSS. A measurement run was divided for each sample in three cycles of five repetitions each. Total counting time was about 600 min for ordinary samples and background water samples, and 450 min for standard and spike samples. The uncertainty assessment of the results obtained with LSS was carried out following the procedure described in [15].

The uranium isotopes and their isotopic ratios in the groundwater samples from site E3dx were measured by means of ICP-MS as this technique has been frequently used for uranium analysis in groundwater [16, 19]. All samples and reagents used for ICP-MS measurements were diluted with ultra-pure de-ionized water produced by coupling a Millipore Milli-RX unit with a Millipore Milli-QElement. Only ultra-pure grade acids supplied by Carlo Erba Reagenti (Italy), and purified acids obtained from a quartz sub-boiling purification system (DuoPur, Milestone, Italy) were used. For the determination of the uranium isotopic ratios the isotopic standard IRMM-3184 supplied by the European Commission Joint Research Centre- Institute for Reference Material and Measurements was used. Moreover, a 1,000 mg l^{-1} standard solution of U (AccuTrace Reference Standard, USA) was used to prepare all the calibrating solutions for the determination of the U concentrations.

The measurements of the U concentration were done by means of an inductively coupled plasma-quadrupole mass spectrometer (model 7500a, Agilent Technologies®). The instrument was equipped with an ASX500 CETAC autosampler. One minute 2 % HNO_3 rinses were carried out between samples in order to avoid cross contamination due to memory effect in the sample introduction line. The water samples, collected in one liter polyethylene bottles, were filtered by 0.45 μm nylon membrane filters with polypropylene housing [20], and acidified with 2.5 % ultra pure nitric acid. The U concentration was evaluated in quantitative mode using an external calibration curve built with four standard levels between 0.2 and 2 ng g^{-1} . A 100 ng g^{-1} Bi solution was added as internal standard to correct possible signal instability and drift. The uncertainties of the reported values are purely statistical, i.e. results of three instrumental replicates. They were calculated with a coverage factor equal to 1.

Before the uranium isotopic ratio determination was done, a pre-concentration was adopted: 50 mL of water sample were treated according to [20]. The samples were acidified with 2.5 % ultra pure nitric acid, and evaporated to dryness. The residue was dissolved in 5 ml of 2.5 % HNO_3 solution. The U concentration in the final solution for isotopic measurements was around 10 ng g^{-1}. The dead time of the ICP-MS detector was set at 5 ns; it was determined through a set of measurements of U standard solutions with different U concentrations [21].

All isotopic measurements were carried out on a double focusing mass spectrometer (Element2, Thermo Fischer Scientific, USA) equipped with an ASX520 CETAC auto sampler. The instrument was equipped with a cyclonic spray chamber working at room temperature and a concentric Teflon nebulizer with 200 μl min^{-1} flow. The ^{235}U presence in the samples was analyzed with good precision. The minor isotope ^{234}U was detectable but with a rather large uncertainty (20 %) because of its very low concentration.

It is well known from literature that some polyatomic ionic species such as PbO^{2+} and PbN^{2+} can give isobaric interferences in the U isotope range mass [22]. An interference

test was performed preparing a lead solution at 10 ng g^{-1} in 2.5 % nitric acid. The signal of the masses of interest was comparable to background. Because the lead concentration in the analyzed groundwater samples was lower than 1 ng g^{-1} the interference could be excluded.

The uranium hydride formation was taken into account detecting the signals of the ions $^{238}U_1H^+$ and $^{238}U^+$ in a uranium standard solution. Their ratio, in agreement with [22], was about 5×10^{-5}. The combined uncertainty of the uranium isotopic ratio was calculated following the EURACHEM/CITAC procedure [23]. Within the uncertainties all the measured uranium isotopic ratios did not show significant differences with respect to the natural composition [24]. For assurance of good quality data the certified reference material IAEA-381 [25] has been analyzed regularly.

3 Results and Discussion

The uranium groundwater monitoring started on June 2008 with the aim of better defining the Rn groundwater transport processes through the cataclastic rocks [4], as well as to check its contribution to the neutron background at the INFN-LNGS [26]. The U measurements carried out between June 2008 and December 2012 at sites E1, E4, E3 and E3dx show some peak structures supposed to be induced mainly by geodynamical processes through the main fault, crossing the deep underground (INFN-LNGS), as a result of chemical interactions with endogenic fluids. Therefore, in order to test this hypothesis, new analyses of selected water samples from E3dx, which is orthogonal to the main fault in the E4 direction into the cataclastic rocks, have been carried out.

A seismic swarm affected the area under investigation from October 2008 to April 2009, before the main shock which occurred at 01:33 UT on April 6th, 2009 (M_w 6.3, M_l 5.9) [9]. The main shock was followed by a period of relatively intense seismic activity, associated with aftershocks occurrence. A further moderate size swarm occurred in the second half of 2010, NW of the main shock epicentral area at a distance of about 30 km. The main event of this swarm was an earthquake with M_l 3.6 on August 31^{st} 2010, accompanied by three earthquakes with magnitude M_l 3.0, and by about 80 additional events with $M_l \geq 2.0$, which occurred within a small area of 5 km radius, from July to November 2010. Hence, the swarm is characterized by a quite large number of events, although having fairly small magnitudes [10].

These are the main periods of seismic activity that can be identified during the monitoring period nearby the Gran Sasso National Laboratory. The first five selected E3dx water samples were those that showed the highest uranium concentrations before the first swarm (three samples), and the second swarm (two samples). The last sample of September 26^{th}, 2011 was chosen in a time period more than 1 year after the last swarm.

The ^3H data support the hypothesis that the contribution due to percolation processes were linked with meteoric events before the seismic swarm, particularly the snow melting during the spring-summer time did not affect the groundwater dynamics through possible mixing with younger surface water. The highest ^3H value was recorded in the water sample taken in the time period far away from seismic swarms at a moment of maximum water table recharge of the Gran Sasso aquifer [10].

4 Conclusions

The uranium groundwater anomalies were observed in cataclastic rocks crossing the underground Gran Sasso National Laboratory during the seismic swarm and before the main shock, which occurred on 6^{th} April, 2009 in L'Aquila. They are most likely associated with geodynamic processes occurring before the earthquake, and can be used as a possible strain meter in domains where continental lithosphere is subducted.

This analysis supports the hypothesis that the uranium anomalies represent a key geochemical signal of the progressive increase of deep fluids fluxes at middle-lower crustal levels associated with the geodynamics of the earthquake.

References

[1] Grabowski P, Bem H (2012) J Radioanal Nucl Chem. doi:10.1007/s10967-011-1558-0

[2] Killiari T, Tsiaili A, Pashalidis I (2010) J Radioanal Nucl Chem 284:553-556

[3] Landstetter C, Kaltzlberger C (2009) J Radioanal Nucl Chem 282:467-471

[4] Plastino W, Bella F (2001) Geophys Res Lett 28:2675-2678

[5] Plastino W (2006) In: Povinec PP, Sanchez-Cabeza JA (eds) Radionuclides in the environment, vol 8. Elsevier, Amsterdam, pp 335-341

[6] Plastino W, Kaihola L, Bartolomei P, Bella F (2001) Radiocarbon 43:157

[7] Plastino W et al (2007) Radiat Meas 42:68-73

[8] Plastino W et al (2010) J Environ Radioact 101:45-50

[9] Plastino W et al (2011) J Radioanal Nucl Chem 288:101-107

[10] Plastino W et al. (2013) J Radioanal Nucl Chem 295:585-592

[11] Neary MP (1997) Radioact Radiochem 8:23-35

[12] Hut G (1986) Nucl Instr Meth Phys Res B17:490-492

[13] Florkowski T (1981) Methods of low-level counting and spectrometry. International Atomic Energy Agency, Vienna, pp 335-353

[14] Schnhofer F, Kralik C (1999) Radioact Radiochem 10:14-17

[15] Rozanski K, Grning M (2003) Accred Qual Assur 8:359-366

[16] Oliveira OP, Sarkis JES (2002) J Radioanal Nucl Chem 253:345-350

[17] Gonzales ER et al (2005) J Radioanal Nucl Chem 263:457-465

[18] Pointurier F et al (2008) J Radioanal Nucl Chem 276:505-511

[19] Kelly DG et al (2008) J Radioanal Nucl Chem 278:807-811

[20] Eaton AD, Cresceri LS, Rice RW, Greenberg AB (2005) Standard methods for the examination of water and wastewater, 21st edn. American Water Works Association, Denver

[21] Nelms SN et al (2001) J Anal At Spectrom 16:333-338

[22] Boulyga SF, Becker JS (2002) J Anal At Spectrom 17:1143-1147

[23] Ellison SLR, Rosslein M, Williams A (2000) Lancet 355:712-715

[24] Becker S (2007) Inorganic mass spectrometry. Wiley, New York

[25] Povinec PP et al (2002) J Radioanal Nucl Chem 251:369-374

[26] Plastino W et al (2009) J Radioanal Nucl Chem 282:809-813

TELLUS Experiment. Method for Signal Conditioning and Data Acquisition System, based on Variable Amplification and Feedback Technique

V. Sgrigna[a], L. Conti[b], D. Zilpimiani[c]

[a] Dipartimento di Matematica e Fisica, Università Roma Tre, Rome, Italy.
[b] Facoltà di Ingegneria, Università Telematica Internazionale UNINETTUNO and INFN, Rome, Italy.
[c] Institute of Geophysics, Georgian Academy of Sciences, Tbilisi, Georgia.

Abstract

In many space and ground-based applications of interest for the TELLUS Experiment the amplitude and frequency content of analog signals to be detected is a priori unknown and can lie in a very large range of values [1-5]. This is a particularly challenging problem to be managed, especially when the data acquisition and signal analysis must be carried out in extreme environments where large data processing resources are requested together with a low power consumption and high efficiency of the device. The method is specifically useful when power spectrum of measured signals exhibits a very large variability in the different frequency bands making particularly difficult the runtime signal analysis of the phenomena under study. The method proposed within the TELLUS Experiment is of particular interest in two applications. The first being an analysis of multi-channel analog signals constituted by several frequency components each one of which exhibits very different amplitudes that need to be simultaneously registered by the acquisition system. The second application further enhances the specific characteristics of the method when, in addition to manage multichannel analysis, we should treat multiparameter data (i.e. data relating to signals of different nature associated with parameters or fields different from each other) [6].

1 Description of the method

The method is based on three (conditioning, acquisition and processing) interconnected modules, performing the following three main functions of data analysis procedures as

illustrated in figure 1:

1. to perform a signal conditioning consisting into a pre-amplification of the analog input signal, before it is sub-divided into a fixed number of frequency channels, at each one of which is applied a different tunable amplification defined as a function of weights estimated by a calibration procedure.

2. to sum up the conditioned channel signals, to digitize the resulting signal by a single analog-to-digital converter (ADC), and then performing an appropriate spectrum analysis.

3. to execute the calibration procedure mentioned in item 1), accomplished on the basis of the spectrum analysis on the output signal of the ADC (with the aim at optimizing separately the amplification of each frequency channel) and then reconstructing the spectrum of the initial input signal.

The method may be applied to any analog signal $S(t)$ to reconstruct its spectrogram (i.e. the spectrum $S(\omega)$ as a function of time) through the continuous optimization of the differential amplification of each individual signal frequency band, so that all the spectral amplitudes of the various frequency bands are made comparable between them. Once known the amplification gains (that in general vary over time), the true $S(\omega)$ spectrum can be reconstructed. The possibility to vary the gain of each frequency channel separately allows exploiting the resolution of a single ADC. The change in amplification, through a calibration procedure, optimizes the dynamic resolution of the ADC sampling in all frequency bands without "wasting bits" [7]. This flexibility of the method is particularly useful for signals in which the spectral content varies considerably from one frequency band to another. It follows that the actual dynamic resolution of digitization procedure, achieved by the proposed method, is higher than the static one of the ADC. Concerning the configuration it must be underlined that the subdivision into modules, shown schematically in Figure 1, is to be understood only as an example, since the functional units can be placed and grouped in different configurations depending on the application needs or technological requirements. The functional scheme described for each module may be constructed through both physical devices (hardware) and with processing and control algorithms (software). All modules can be installed on a single electronic board or on separated interconnected units. In the basic scheme (described below) the method is applied to an analog input signal and outputs its spectrogram. However, it is possible to exploit the modularity of the method to achieve different architectures. In particular, in case you want to simultaneously analyze more analog input signals, it is possible an architecture consisting of a single processing module that handles simultaneously many subsystems. Each subsystem will consist of a conditioning module and an acquisition module and will be able to acquire separately several incoming analog signals. The single processing module will analyze all the various signals simultaneously and in parallel outgoing return all the spectra of the input signals.

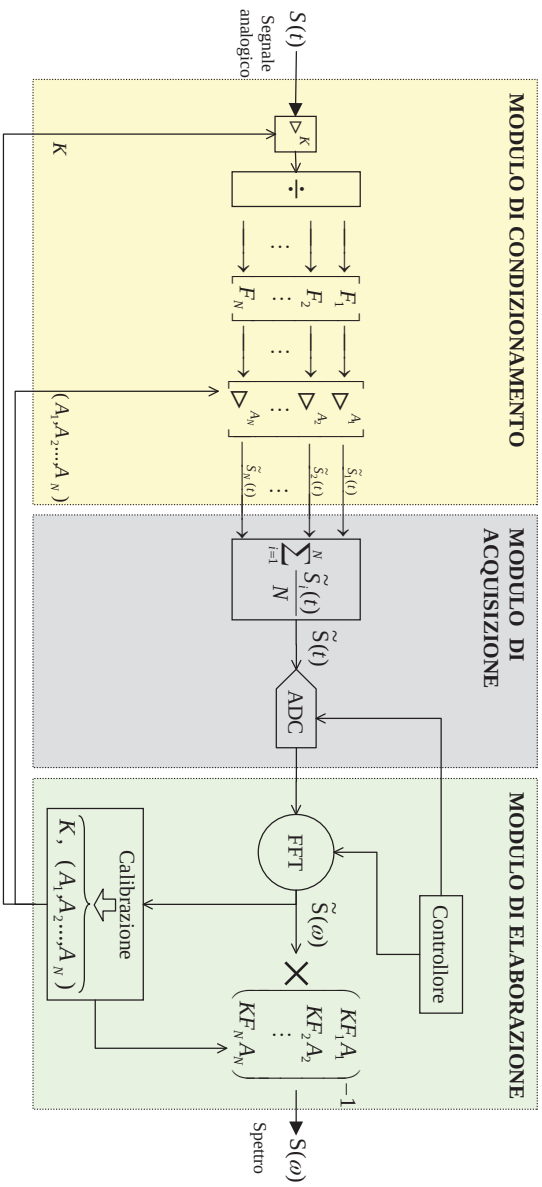

Figure 1: Schematic representation of the conditioning, acquisition and processing modules.

2 Conclusions.

Within the TELLUS Experiment we have developed the design scheme of three interconnected modules for the conditioning, digitizing, and processing of an input analog signal (generally a priori unknown and that can be measured in a large variety of different phenomena on the ground, in space or in the laboratory) designed to determine with great accuracy the spectrum of the signal. The method consists in dividing the investigated analog input signal into different frequency bands and in making each of the different channel amplitudes comparable with one other, with an appropriate calibration process (by assigning to each channel a suitable weight), and digitizing all the channels with a single analog-digital converter. The weights are determined on the basis of the spectral contents of the input signal. This approach optimizes the performances of the ADC by maximizing its dynamic range [8]. The method exploits all its versatility when applied to signal with a large variable spectral content in different frequency bands. The output of the processing module produces the optimized spectrograms of the analog input signal e.g. the spectra as a function of time.

References

1. Parrot, M., 2002, The micro-satellite DEMETER, J. Geodyn., 33, 535-541.

2. Sgrigna, V., Conti, L., Zilpimiani, D., 2012, Tellus Experiment. A Multi-instrument Payload for the investigation of the Topside Ionosphere, LNGS Annual Report 2011, INFN, LNGS/EXP-01/12, 2012, ISBN: 978-88-907304-8-1, pp. 221-228.

3. Sgrigna, V., Carota, L., Conti, L., Corsi, M., Galper, A., Koldashov, S.V., Murashov, A.M., Picozza, P., Scrimaglio, R., Stagni, L., 2005, Correlations between earthquakes and anomalous particle bursts from SAMPEX/PET satellite observations, J. Atm. Solar-Terrestrial Phys., 67, 1448-1462.

4. Sgrigna, V., Altamura, F., Ascani, S., Battiston, R., Bencardino, R., Blasko, S., Buzzi, A., Casolino, M., Conti, L., Lucidi, S., Minori, M., Papi, A., Picozza, P., Rossi, S., Stagni, C., Zilpimiani, 2007, First data from the EGLE space experiment onboard the ISS, Microgravity and Sci. Technology, XIX-2, 45-49.

5. Sgrigna, V., and Conti, L., 2012, A Deterministic approach to Earthquake Prediction, Int. J. Geophysics, Vol. 2012, Article ID 406278, 20 pages, doi:10.1155/2012/406278.

6. Proakis J., 1995, Digital Communications, 3rd ed. Singapore: McGraw-Hill.

7. Hadji-Abdolhamid A. and A. Johns D., 2003, A 400-MHz 6-bit ADC with a partial analog equalizer for coaxial cable channels, Proceedings of the 29th European Solid-State Circuits Conference, ESSCIRC '03, 16-18 Sept. 2003, Estoril, Portugal, 0-7803-7995-0, pp. 237-240, DOI: 10.1109/ESSCIRC.2003.1257116.

8. Johns D.A. and Martin K. W., 1997, Analog integrated circuit design, J. Wiley and Sons Inc., ISBN 0471144487.

THE VIP EXPERIMENT

S. Bartalucci[a], S. Bertolucci[b], M. Bragadireanu[a,c]
M. Cargnelli[d], A. Clozza[a], C. Curceanu (Petrascu)[a],
S. Di Matteo[e], J-P. Egger[f], C. Guaraldo[a], M. Iliescu[a],
T. Ishiwatari[d], M. Laubenstein[g], J. Marton[d], E. Milotti[h], D. Pietreanu[a,c],
K. Piscicchia[a], M. Poli Lener[a], T. Ponta[a,c], A. Rizzo[a], A. Romero Vidal[a],
A. Scordo[a], D.L. Sirghi[a,c], F. Sirghi[a,c], L. Sperandio[a],
O. Vazquez Doce[a], E. Widmann[d], J. Zmeskal[d]

[a] INFN, Laboratori Nazionali di Frascati, CP 13, Via E. Fermi 40, I-00044, Frascati (Roma)-Italy
[b] CERN, CH-1211, Geneva 23-Switzerland
[c] "Horia Hulubei" National Institute of Physics and Nuclear Engineering, Str. Atomistilor no. 407, P.O. Box MG-6, Bucharest - Magurele-Romania
[d] The Stefan Meyer Institute for Subatomic Physics, Boltzmanngasse 3, A-1090 Vienna-Austria
[e] Institut de Physique UMR CNRS-UR1 6251, Université de Rennes1, F-35042 Rennes-France
[f] Institut de Physique, Université de Neuchâtel, 1 rue A.-L. Breguet, CH-2000 Neuchâtel-Switzerland
[g] INFN, Laboratori Nazionali del Gran Sasso, S.S. 17/bis, I-67010 Assergi (AQ)-Italy
[h] Dipartimento di Fisica, Università di Trieste and INFN– Sezione di Trieste, Via Valerio, 2, I-34127 Trieste-Italy

Abstract

The Pauli exclusion principle (PEP) and, more generally, the spin-statistics connection, is at the very basis of our understanding of matter and Nature. The PEP spurs, presently, a lively debate on its possible limits, deeply rooted in the very foundations of Quantum Mechanics and Quantum Field Theory. Therefore, it is extremely important to test the limits of its validity. The VIP (VIolation of the Pauli exclusion principle)experiment at LNGS established a new limit on the probability that PEP is violated by electrons, using the very clean method of searching for PEP forbidden atomic transitions in copper. Presently an upgraded VIP setup is under test, to be installed at LNGS to improve by an additional factor of 100 on the PEP violation probability.

1 Introduction

The Pauli Exclusion Principle (PEP), which plays a fundamental role in our understanding of many physical and chemical phenomena, from the periodic table of elements, to the electric conductivity in metals and to the degeneracy pressure which makes white dwarfs and neutron stars stable, is a consequence of the spin-statistics connection [1]. Although the principle has been spectacularly confirmed by the huge number and accuracy of its predictions, its foundation lies deep in the structure of quantum field theory and has defied all attempts to produce a simple proof [2]. Given its basic standing in quantum theory, it seems appropriate to carry out precise tests of the PEP validity and, indeed, mainly in the last 15-20 years, several experiments have been performed to search for possible small violations[3, 4, 5, 6, 7, 8, 9, 10, 11]. Moreover, many (if not all) of these experiments are using methods which are not obeying to the so-called Messiah-Greenberg superselection rule [12]. The indistinguishability and the symmetrization (or antisymmetrization) of the wave-function should be checked independently for each particle, and accurate tests were and are being done.

The VIP (VIolation of the Pauli Exclusion Principle) experiment, has the goal to improve the limit on the probability of the violation of the PEP for electrons, (P $<$ 1.7 x 10^{-26} established by E. Ramberg e G. A. Snow: *Experimental limit on a small violation of the Pauli principle*, Phys. Lett. **B 238** (1990) 438) by three-four orders of magnitude (P $<10^{-29\div-30}$), exploring a region where new theories might allow for a possible PEP violation.

The experimental method, originally described in [13] consists in the introduction of electrons into a copper strip, by circulating a current, and in the search for X-rays resulting from the forbidden radiative transition that occurs if one of the new electrons is captured by a copper atom and cascades down to the 1s state already filled by two electrons with opposite spins. The energy of this transition would differ from the normal K_α transition by about 300 eV (7.729 keV instead of 8.040 keV) [14] providing an unambiguous signal of the PEP violation. The measurement alternates periods without current in the copper strip, in order to evaluate the X-ray background in conditions where no PEP violating transitions are expected to occur, with periods in which current flows in the conductor, thus providing "fresh" electrons, which might violate PEP. The rather straightforward analysis consists in the evaluation of the statistical significance of the normalized subtraction of the two spectra in the region of interest.

The experiment is being performed at the LNGS underground Laboratories, where the X-ray background, generated by cosmic rays and natural radioactivity, is reduced.

2 The VIP experimental setup

The first VIP setup was realized in 2005, using the CCD (Charge Coupled Devices)as X-ray detectors [15, 16, 17, 18, 19], and consists as main elements of a copper cylinder, 4.5 cm in radius, 50 μm thick, 8.8 cm high, surrounded by 16 equally spaced CCDs of type 55.

The CCDs were at a distance of 2.3 cm from the copper cylinder, grouped in units of

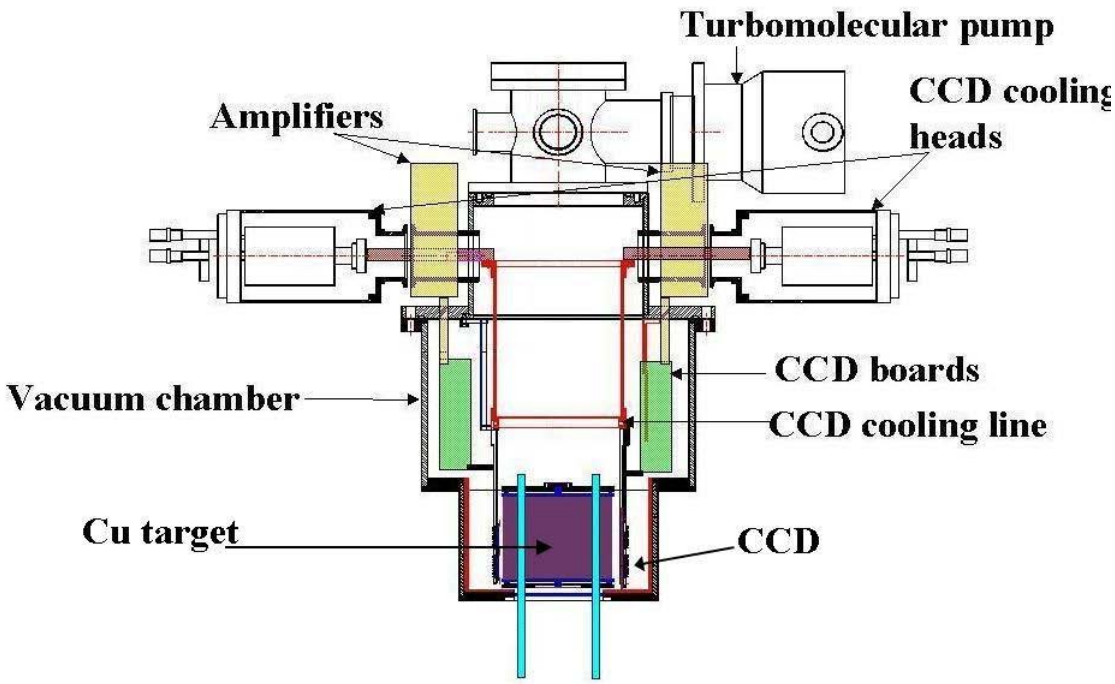

Figure 1: *The VIP setup. All elements af the setup are identified in the figure.*

two chips vertically positioned. The setup was enclosed in a vacuum chamber, and the CCDs were cooled to about 165 K by the use of a cryogenic system. A schematic drawing of this setup is shown in Fig. 1.

The DAQ alternated periods in which a 40 A current is circulated inside the copper target with periods without current, referred as background.

This was installed at the LNGS Laboratory in Spring 2006 and was taking data in this configuration until Summer 2010 (presently, see below, we are working on an improved version of the setup). The setup was surrounded by layers of copper and lead (as seen in the picture) to shield the setup against the residual background present inside the LNGS laboratory, see Fig. 2.

3 VIP results

3.1 VIP analyses results

Until summer 2010 the VIP experiment was in data taking, alternating periods of "signal" (I=40 A) with periods without signal (I=0 A). Data analyses were performed (energy calibration, sum of spectra, subtraction of background) and the probability of violation of PEP for electrons obtained (upper limit):

$$\frac{\beta^2}{2} < 4.7 \times 10^{-29} \tag{1}$$

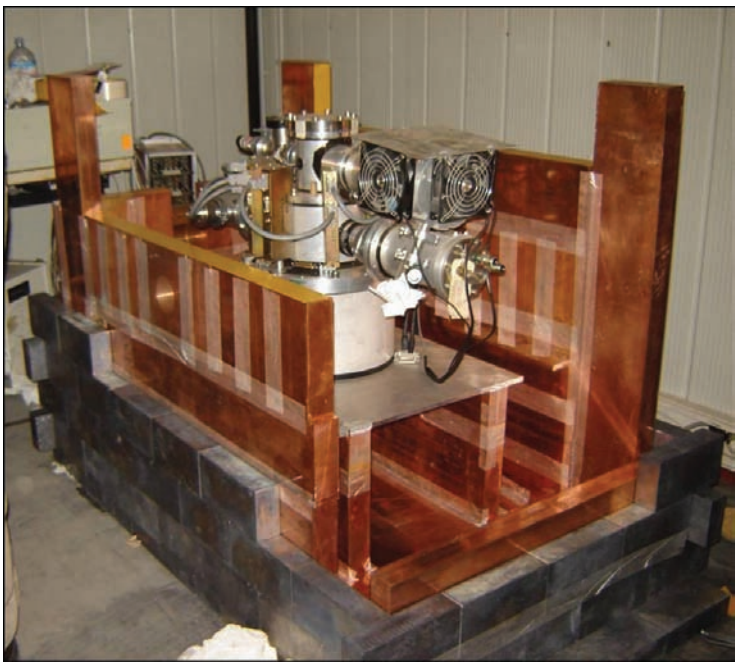

Figure 2: The VIP setup at the LNGS laboratory during installation.

3.2 Discussion of the results

We are attempting an interpretation of our results in the framework of quon-theory, which turned out to be a consistent theory of *small* violations of PEP. The basic idea of quon theory [20] is that (anti)commutators, are replaced by weighted sums

$$\frac{1-q}{2}\left[a_i, a_j^+\right]_+ + \frac{1+q}{2}\left[a_i, a_j^+\right]_- = a_i a_j^+ - q a_j^+ a_i = \delta_{i,j} \tag{2}$$

where $q = -1$ ($q = 1$) gives back the usual fermion (boson) commutators. The statistical mixture in equation (2) also shows that the PEP violation probability is just $(1 + q)/2$ and thus our best experimental bound on q is

$$\frac{1+q}{2} < 4.7 \times 10^{-29} \tag{3}$$

A consistent interpretation of the VIP results can thus be based on quon theory; however here we note that is not easy to devise tests of PEP, because of many conceptual difficulties, presented in our published papers (see list at the end).

4 Future perspective of the VIP setup

The VIP setup used CCD detectors, which are excellent X-ray detectors, but very slow. We plan to switch to a new type of detectors for precision X-rays measurements, the triggerable Silicon Drift Detectors (SSD) which have a fast readout time ($\simeq 1\mu$s) and large collection area (100 mm^2). These detectors were successfully used in the SIDDHARTA

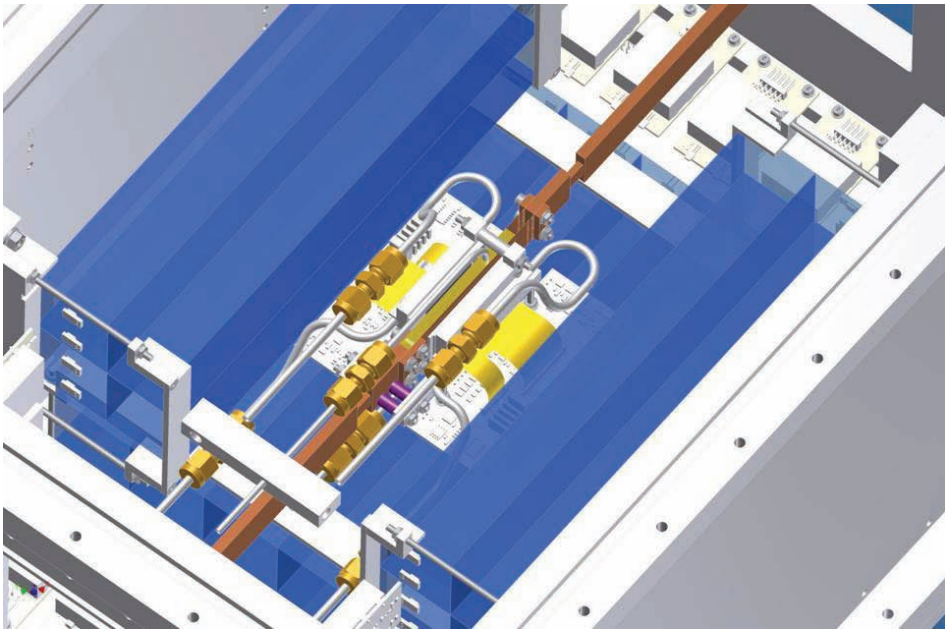

Figure 3: The VIP setup experiment using SDD detectors and an external veto-system.

experiment at LNF-INFN for measurements of the kaonic atoms transitions at the DAΦNE accelerator of LNF-INFN [21]; using a proper trigger system a background rejection factor of the order of 10^{-4} was achieved in SIDDARTHA. We built a new setup, much more compact, with higher current circulating and with a veto system against background coming from outside. A schematic layout of the new setup is shown in Fig. 3.

In 2012 we plan to proceed with VIP upgraded setup installation, debug and testing at LNGS.

We then expect to gain a factor of 2 orders of magnitude in the limit of PEP vilation in a data taking of 3-4 years. We are, as well, considering to extend the scientific program towards a feasibility study of limits on parameters of the collapse model (as a solution of the measurement problem, put initially forward by Ghirardi, Rimini and Weber) by measurements of X rays spontaneously emitted in the continuous spontaneous localization (CSL) model [22], [23] .

5 Acknowledgements

The VIP Collaboration wishes to thank all the LNGS laboratory staff for the precious help and assistance during all phases of preparation, installation and data taking. The support from the HadronPhysics FP6, HadronPhysics2 and HadronPhysics3 FP7, from EU COST 1006 Action and MIUR PRIN2008 2008LX2X28-004 projects is acknowledged.

6 List of Publications

1. C. Curceanu (Petrascu) *et al.* (The VIP Collaboration), A glimpse into the Pandora box of the quantum mechanics: The VIP exclusion principle violation and

spontaneous collapse models put at test, AIP Conf. Proc., 136-145 (2012).

2. C. Curceanu (Petrascu) *et al.* (The VIP Collaboration), Experimental tests of Quantum Mechanics: from Pauli Exclusion Principle Violation to spontaneous collapse models, Journal of Physics, Conference Series, Vol. 361 (2012).

3. C. Curceanu (Petrascu) *et al.* (The VIP Collaboration), Experimental tests of quantum mechanics: Pauli Exclusion Principle Violation and spontaneous collapse models, AIP Conference Proceedings, 1424, 397-406 (2012).

4. C. Curceanu, J.D. Gillaspy, R.D. Hilborn, Resouce Letter SS-1: The Spin Statistics Connection, American Journal of Physics, Vol. 80, Issue 7, 561-577 (2012).

References

[1] W. Pauli, *Phys. Rev.* **58**, (1940), 716.

[2] R. P. Feynman, R. B. Leighton and M. Sands *The Feynman Lectures on Physics*, Addison-Wesley, Reading, MA (1963).

[3] R. Arnold, *et al.*, *Eur. Phys. J. A***6** (1999) 361.

[4] H.O. Back, *et al.*, *Eur. Phys. J. C***37** (2004) 421.

[5] A. Barabash, *Found. of Phys.* **40** (2010) 703.

[6] A.S. Barabash,*et al.*, *JETP Lett.* **68** (1998) 112.

[7] P. Belli, *et al.*, **460** (1999) 236.

[8] G. Bellini, *et al.*, *Phys. Rev. C* **81** (2010) 034.

[9] R. Bernabei, *et al.*, *Phys. Lett. B* **408** (1997) 439.

[10] R. Bernabei, *et al.*, *Eur. Phys. J. C* **62** (2009) 327.

[11] Y. Suzuki, *et al.*, *Phys. Lett. B* **311** (1993) 357.

[12] A.M.L. Messiah, O.W. Greenberg, *Phys. Rev.* **136** (1964) B248.

[13] E. Ramberg and G. A. Snow, *Phys. Lett. B* **238** (1990) 438.

[14] S. Di Matteo, L. Sperandio, VIP Note, IR-04, 26 April 2006; The energy shift has been computed by P. Indelicato, private communication.

[15] J. L. Culhane, *Nucl. Instrum. Methods A* **310** (1990) 1.

[16] J.-P. Egger, D. Chatellard and E. Jeannet, *Particle World* **3**, (1993) 139.

[17] G. Fiorucci, *et al. Nucl. Instrum. Methods A* **292** (1990) 141.

[18] D. Varidel, *et al.Nucl. Instrum. Methods A* **292** (1990) 147

[19] R. P. Kraft, *et al.Nucl. Instrum. Methods A* **372** (1995) 372.

[20] O. W. Greenberg *Phys. Rev. Lett.* **64** (1990) 705.

[21] C. Curceanu *et al. Eur Phys* **J A31** (2007) 537-539; M. Bazzi *et al. Phys. Lett.* **B681** (2009) 310; M. Bazzi *et al. Phys. Lett.* **B704** (2011) 113; Bazzi *et al. Phys. Lett.* **B697** (2011) 199; Bazzi *et al. Phys. Lett.* **B714** (2012) 40.

[22] Q. Fu *Phys. Rev* **A56** (1997) 1806.

[23] G.C. Ghirardi, A. Rimini and T. Weber *Phys. Rev.* **D34** (1986) 470: ibid. (1987) 3287: *Found. Phys.* **18** (1988) 1.